UNIONE EUROPEA
FONDO SOCIALE EUROPEO

A.D. MDLXII

Sede Amministrativa
Università degli Studi di Sassari
Dipartimento di Scienze della Natura e del Territorio

Sede Consorziata
Università degli Studi di Napoli
Dipartimento di Scienze della Terra, dell'Ambiente e delle Risorse

Indirizzo

Scienza e Tecnologia dei Minerali e delle Rocce di Interesse Industriale

XXVII CICLO

MINERALOGICAL AND GEOTECHNICAL CHARACTERIZATION OF STRUCTURALLY COMPLEX FORMATIONS INVOLVED IN THE SLOW MOVING LANDLIDES AFFECTING THE SOUTHERN APENNINE

CARATTERIZZAZIONE MINERALOGICA E GEOTECNICA DELLE FORMAZIONI STRUTTURALMENTE COMPLESSE COINVOLTE NEI LENTI MOVIMENTI DI VERSANTE DELL'APPENNINO MERIDIONALE

Direttore
Prof. Marco Curini Galletti

PhD Student
Dott.ssa Mara Cesarano

Tutor
Prof. Piergiulio Cappelletti

Co-tutors
Prof. Calcaterra D., Prof. De Vita P.,
Dott. Fiore S., Prof. Ramondini M.,
Prof. de' Gennaro M.

TABLE OF CONTENTS

ABSTRACT

Slow-moving landslides affect several areas in the Apennine chain (Italy). They involve sedimentary rocks that are weathered in the more surficial parts. The occurrence of weathering-related clay minerals (e.g. smectites) able to trap high amounts of water, is generally considered a predisponding factor for these landslides. The main goal of this research is to verify this statement, carrying out a mineralogical-geotechnical characterization of clayey rocks occurring in the Termini-Nerano slow-moving landslide (Massalubrense, Italy).

The mineralogical composition of soils involved in the landslide was evaluated on several drill-core samples from the studied area, by using quantitative X-ray powder diffraction analyses, calibrated through chemical bulk rock analyses. Clay separates allowed to determine the composition of the clay fraction. The results confirm that the total amount of clays, and specifically the smectite amount in mixed layers I/S, could have played a role in the landslide development. However, relationships between mineralogical composition and weathering zones in the soil have not been observed.

Geotechnical analyses attested that the mechanical behavior of the material involved in the landslide depends on the amount of granulometric clay fraction in the samples, but, differently from what expected, no correlations were observed between this behavior and the measured amounts of smectite or mixed layers I/S.

Key words: *slow-moving landslides, mineralogical analyses, geotechnical tests, structurally complex formations, Southern Apennines, Italy.*

RIASSUNTO

Le frane a cinematica lenta sono particolari movimenti di versante che avvengono in diverse zone dell'Appennino Meridionale, e coinvolgono rocce sedimentarie particolarmente alterate, contenenti silicati. La presenza di minerali associati a profili di alterazione supergenica (es. smectite) favorirebbe l'innesco di questi fenomeni franosi, per la loro capacità di adsorbire elevati quantitativi di acqua. L'obiettivo del presente lavoro è verificare tale assunzione attraverso la caratterizzazione mineralogico-geotecnica dei terreni argillosi coinvolti nella frana di Termini Nerano (Massalubrense, Italia).

La composizione mineralogica dei materiali coinvolti nella frana è stata valutata su campioni estratti da sondaggi eseguiti nell'area di studio, mediante analisi diffrattometriche ai raggi X (su tal quale e frazione argillosa), calibrate attraverso analisi chimiche. I risultati confermano che la quantità delle fasi argillose, in particolare di smectite presente in strati misti I/S, potrebbe aver influenzato lo sviluppo del fenomeno franoso, anche se la composizione mineralogica delle rocce non è in questo caso direttamente correlabile ad una presenza di orizzonti di alterazione nel sottosuolo.

Analisi geotecniche hanno confermato che il comportamento meccanico del materiale dipende dalla quantità granulometrica di frazione argillosa che presenta, ma non dalla quantità di smectite o strati misti I/S che contiene.

Parole chiave: *Lenti Movimenti di Versante, analisi mineralogiche, analisi geotecniche, formazioni strutturalmente complesse, Sud Appennino, Italia.*

INTRODUCTION

The subject of this PhD-thesis is the characterization of a slow-moving landslide, which in the past underwent paroxysmal evolution. The aim of the study is to verify whether it is possible to correlate mineralogical features and geotechnical parameters of the clayey materials involved in these phenomena.

Slow-moving landslides are down-slope movements of soils and rocks characterized by slow rate of displacement. External events, such as long duration rainfalls and earthquakes, can trigger paroxysmal events, increasing velocity of the moving mass and consequently making it more dangerous. These landslides are usually associated with highly weathered part of slopes, constituted by rock generally called "structurally complex formations" and defined, according to Esu (1977), as highly tectonized clayey formations, provided with a pervasive scaly structures. The author (Esu, 1977) subdivided them into two groups, on the basis of their lithological complexity.

As a matter of fact, it is generally assumed that highly weathered rocks are characterized by great amount of expandable clays which seems to be directly related to the shear strength of rock material. In fact the presence of expandable clays (e.g. smectite) should favor the water absorption in the rocks, thus promoting the decrease of their shear strength (Taylor & Cripps, 1987).

In geotechnical engineering, the relationship between the amount of water in a soil and its mechanical behavior is evaluated by the Atterberg Limits. The latter represent a basic measure of the critical water contents of a fine grained soil, at which the physical properties of the material changes (e.g. the water content at the transition from the plastic to liquid state). These measures are generally used to obtain indirect information about the mineralogical nature of the analyzed material, through, for example, the so called Casagrande chart, which allow to determine the types of clays occurring in a rock by comparing Plastic index (IP) and Liquid Limit (W_L).

Bearing this in mind, the main aim of this thesis was to test the benefits and the limits of the empirical mineralogical-geotechnical correlation, carrying out direct mineralogical analyses on the same samples analyzed to determine the geotechnical properties, and comparing the results.

The work was conducted on samples extracted from three boreholes drilled within the 1963 Termini Nerano landslide, occurred in the Sorrento peninsula, and involving three different villages: Termini, Nerano and Marina del Cantone, where several infrastructures where damaged. The paroxysmal phenomenon was triggered by a long duration rainfall.

The material mainly involved in the landslide consists of a Miocene aged flysh, called "*Arenarie di Termini*" Formation, which in turn is made up of sandstones, more or less rich in calcareous clasts and clays, and has the typical characteristics of the above cited "structurally complex formations".

XRPD analyses on several samples were carried out to directly evaluate the mineralogical composition of the material involved in the landslide. Specific analyses on clay fraction were also performed to deeply investigate the nature of

possible expandable clays occurring in the rock. Geotechnical analyses (Atterberg Limits, shear tests, specific gravity tests and grain size distribution analyses) instead, allowed to evaluate the physico-mechanical properties of the landslide. The results were compared and discussed on the basis of the previous studies on Termini Nerano landslide and of other studies on slow-moving landslides in southern Italy.

CHAPTER 1

LANDSLIDES: TYPES AND PROCESSES

Landslides are defined as *movements of a mass of rock, debris or earth down slope* (Cruden, 1991).

In 1978 Varnes followed by Cruden & Varnes (1996), proposed an accurate description of landslide features (Fig. 1.1). In Table 1.1 a description of each part is reported (Cruden & Varnes, 1996).

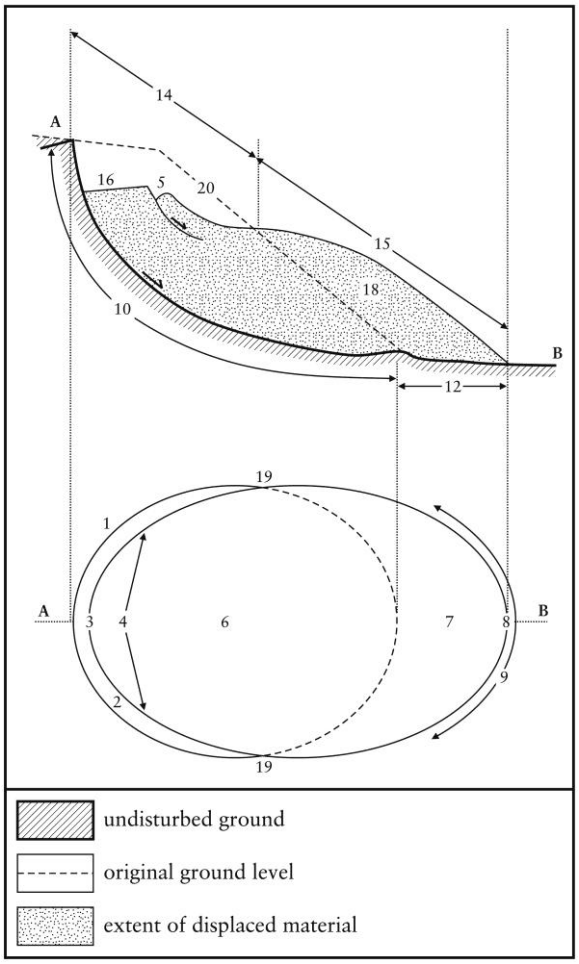

Figure 1.1 Landslide features (Cruden & Varnes, 1996).

Table 1.1 Definitions of landslide features (Varnes, 1978; Cruden & Varnes, 1996).

ID Number	Name	Definition
1	Crown	Practically undisplaced material adjacent to highest parts of main scarp
2	Main Scarp	Steep surface on undisturbed ground at upper edge of landslide caused by movement of displaced material (13) way from undisturbed ground; it is visible part of surface of rupture (10)
3	Top	Highest point of contact between displaced material (13) and main scarp (2).
4	Head	Upper parts of the landslide along contact between displace material and main scarp (2)
5	Minor Scarp	Steep surface on displaced material of landslide produced by differential movements within displaced material.
6	Main body	Part of displaced material of landslide that overlies surface of rupture between main scarp (2) and toe surface of rupture (11)
7	Foot	Portion of landslide that has moved beyond toe of surface of rupture (11) and overlies original ground surface (20)
8	Tip	Point on toe (9) farthest from top (3) of landslide.
9	Toe	Lower, usually curved margin of displaced material of a landslide, most distant from main scarp (2)
10	Surface of rupture	Surface that forms (or that has formed) lower boundary of displaced material (13) below original ground surface (20).
11	Toe Surface of rupture	Intersection (usually buried) between lower part of surface of rupture (10) of a landslide and original ground surface (20).
12	Surface of separation	Part of original ground surface (20) now overlain by foot (7) if landslide.
13	Displaced material	Material displaced from its original position on slope by movement in landslide; it forms both depleted mass (17) and accumulation(18)
14	Zone of depletion	Area within which displaced material (13) lies below original ground surface (20).
15	Zone of accumulation	Area within which displaced material lies above original ground surface (20)
16	Depletion	Volume bounded by main scarp (2), depleted mass (17) and original ground surface (20).
17	Depleted mass	Volume of displaced material that overlies surface of rupture (10) but underlies original ground surface (20).
18	Accumulation	Volume of displaced material (13) that lies above original ground surface (20).
19	Flank	Undisplaced material adjacent to sides of surface of rupture; compass directions are preferable in describing flanks, but if left and right are used, they refer to flanks as view from crown.
20	Original ground surface	Surface of slope that existed before landslide took place.

LANDSLIDE CLASSIFICATION

Several kinds of landslide classifications have been proposed in the years, in which different types of parameters are considered. In 1985, Sassa proposed a landslides classification on the basis of the geotechnical parameters of the involved material (e.g. granulometric features, type of shear stress). Pearson & Costa (1987) focused their attention on the rheological features of water flows (e.g. flow velocity and sediment concentration). Hutchinson (1988) based the classification on the main geotechnical and morphological parameters of the material involved in the movement.

The most complete classification of landslides was firstly proposed by Varnes in 1978, and lately revisited by Cruden & Varnes (1996).
This classification considers several parameters:

- Material
- Water content
- Type of movement
- Landslide activity
- Rate of movement

A description of these parameters is reported below.

MATERIAL: according to the Cruden & Varnes classification (1996) the material involved in a landslide can be subdivided in two main groups: rock and soil.
Rock is defined as *hard or firm mass that was intact and in its natural place before the initiation of movement, or soil, an aggregate of solid particles, minerals or rocks, that either was transported or was formed by the weathering of rock in place.*
Soil is subdivided into two other categories: earth and debris. In case of earth, more than 80% of material consists of particles whose size is smaller than 2 mm. In case of soil, a variable range of material, from 20 to 80% is characterized by particles whose size is larger than 2 mm, whereas the remainder is smaller.

WATER CONTENT: considering the Cruden & Varnes classification (1996) the material involved into the landslides is classified on the basis of its amount of water:

- *Dry: no moisture visible*
- *Moist: contains some water but no free water; the material may behave as a plastic solid but does not flow*
- *Wet: contains enough water to behave in part as a liquid, has water flowing from it, or supports significant bodies of standing water*
- *Very wet: contains enough water to flow as a liquid under low gradients.*

TYPE OF MOVEMENT: the kinematics of a landslide is the most important parameter for its classification. Cruden & Varnes (1996) defined:
Fall: the movement starts with the detachment of soil or rock from a steep slope along a surface on which little or no shear displacement takes place. The involved material descends mainly through the air by falling, bouncing or rolling.

Specifically, free falls usually happen when the slopes angle exceeds 76°, rolling usually happens when slope angle is below 45° are reached, bouncing happens when the slope angle is lower than 45°. The rate of movement varies from very rapid to extremely rapid.

Topple: this movement is defined as a forward rotation out of the slope of a mass of soil or rock around a point axis below the center of gravity of the displaced mass. Toppling is sometimes driven by the gravity exerted by material upslope of the displaced mass, as well as by water or ice leak into cracks in the rock mass. The rate of movement varies from extremely slow to extremely rapid. Flexural topple occurs if the rock mass is characterized by the presence of one preferred discontinuity.

Slide: a slide is a down-slope movement of soil or rock mass, occurring mainly on surfaces of rupture or on relatively thin zones of intense shear strain. It is possible to distinguish between rotational slide and transitional slide, on the basis of the surface of rupture shape.
Specifically, a *rotational slide* moves along a surface of rupture that is circular or cycloidal concave. In this case the displaced mass may move along the surface with little internal deformation. If the movement extends for a considerable distance along the slope, which is perpendicular to the direction of motion, the surface of rupture may be roughly cylindrical.
Rotational slides usually occur in homogeneous material. The rotation in the rotational slides tends to restore the displaced mass to equilibrium.
In case of *translational slides* the mass displaces along a planar or undulating surface of rupture, sliding out over the original ground surface. Translational slides generally are relatively shallower than rotational slides. In the case of translational landslides the movement continues unchecked if the surface of the separation is particularly inclined.

Spread: this kind of movement is an extension of a cohesive soil or rock mass combined with a general subsidence of the fractured mass of cohesive material into softer underlying material. The surface of rupture is not a surface of intense shear. Spreads may result from liquefaction or flow of softer materials. The cohesive materials usually subside, translate, rotate, disintegrate, or liquefy and flow.

Flow: a flow is a spatially continuous movement in which surfaces of shear are short-lived, closely spaced, and usually not preserved. The distribution of velocities in the displacing mass resembles the one which characterizes viscous liquid. The lower boundary of the displaced mass can be a surface along which an appreciable differential movement has taken place or a thick zone of distributed shear. The differentiation of slide and flow depends on the water content, as well as the mobility and the evolution of the movement. An evolution from slide movement to flow is possible if the amount of water increases, as well as the

cohesion decreases. The transition also occurs when slide encounters steeper slopes.

On the basis of the involved material, Varnes (1978) and Hungr et al. (2001) distinguished the following types of flows: rock flow, rock avalanche, debris flow, debris avalanche and earth flow. Specifically, rock flow is a flow movement in bedrock (Varnes, 1978); rock avalanche is an extremely rapid, massive, flow-like movement involving fragment of rock from a large rock slide or rock fall (Hungr et al., 2001); debris flow is a very rapid to extremely rapid flow of saturated non plastic debris in a step channel (Hungr et al., 2001); debris avalanche is a very rapid to extremely rapid shallow flow of partially or fully saturated debris on a steep slope without confinement in a established channel (Hungr et al., 2001); earth flow is a rapid or slower intermittent flow like movement of plastic clayey earth (Hungr et al. 2001).

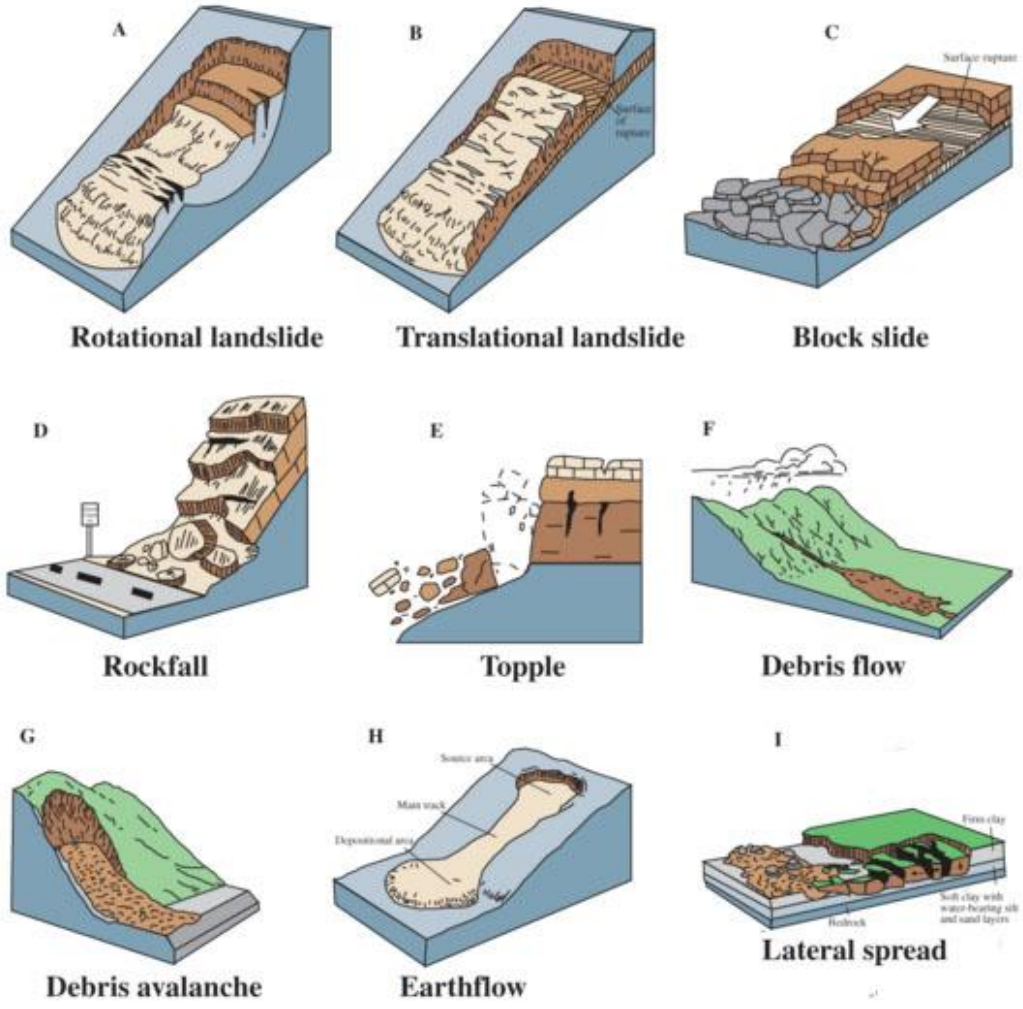

Figure 1.2 Landslide types of movements (Cruden & Varnes, 1996).

On the basis of what written above, each landslide can be classified considering both the type of movement and the involved material (Table 1.2).

Table 1.2 Classification of Slope Movements (Cruden & Varnes, 1996).

	Type of material		
Type of movement	Bedrock	Predominantly Coarse Soil	Predominantly Fine Soil
Fall	Rock Fall	Debris Fall	Earth Fall
Topple	Rock Topple	Debris Topple	Earth Topple
Slide	Rock Slide	Debris Slide	Earth Slide
Spread	Rock Spread	Debris Spread	Earth Spread
Flow	Rock Flow	Debris Flow	Earth Flow

LANDSLIDE ACTIVITY: the state of activity as well as the distribution of activity and the style of activity gives information about the age and the repetition of movements of landslides.
Specifically, the state of activity describes what is known about the timing of movement, the distribution of activity describes where the landslide is moving and the style of activity indicates the manner in which different movements contribute the landslide (Cruden & Varnes, 1996).
On the basis of the *state of activity,* landslides are classified in:

Active: when landslides are currently moving, including first time movements and reactivations.

Reactived: when landslides are again active after having been inactive. They usually move on pre-existing shear surfaces characterized by about residual strength as defined by Skempton (1970), or ultimate strength as defined by Krahn & Morgenstern (1979). The shear strength of the rupture surface allows to distinguish reactive slides from active which are characterized by peak values.

Suspended: this term is used to describe landslides that have moved within the last annual cycle of season but that are not moving at present (Varnes, 1978).

Inactive: landslides whose last movement has been dated one annual cycle of season before. Inactive slides are defined "dormant", if the movement remains apparent, and "abandoned" if the river that erodes the toe of the moving slope changes course, as defined by Hutchinson (1973). Inactive slides are defined "stabilized", if the toe of the slope has been protected against erosion by natural or artificial remedial measures. Ancient landslides are inactive landslides, which remain visible in the landscape for thousands of years after they have moved.

Relict: they are currently inactive landslides, developed under different geomorphic and climatic conditions.

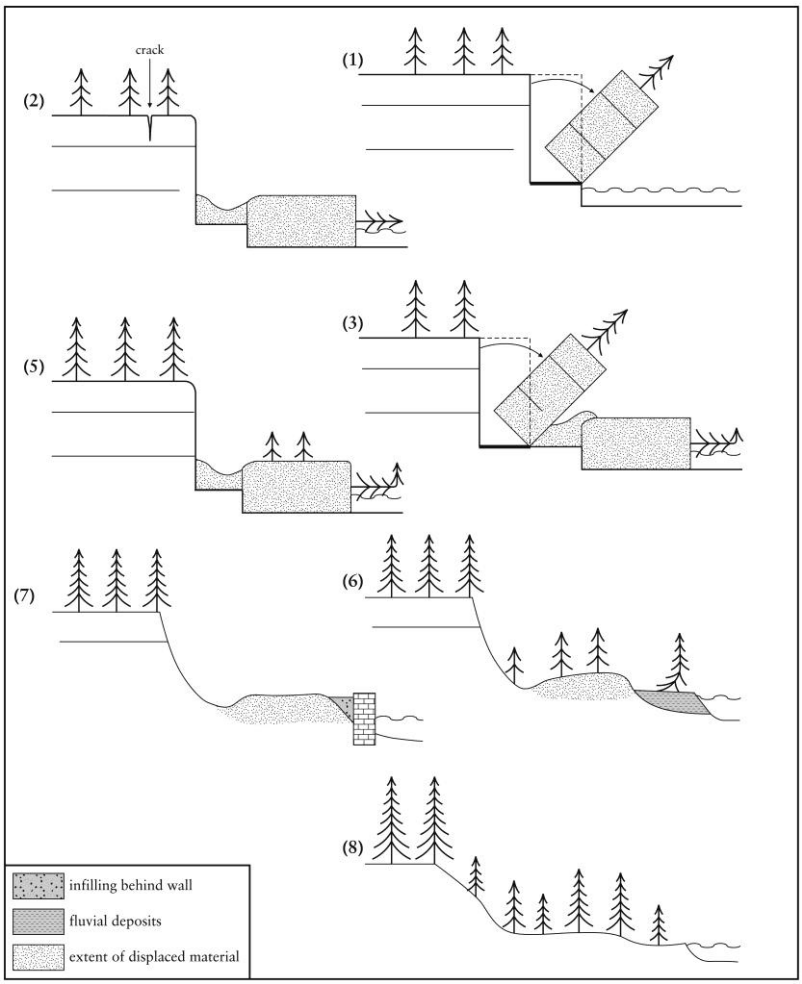

Figure 1.3 Landslide state of activity: 1) active slide; 2) suspended slide; 3) re-activated slide; 5) dormant slide; 6) abandoned slide; 7) stabilized slide; 8) relict slide. After WP/WLI (1993).

On the basis of the *distribution of activity*, landslides are classified as:

Advancing: if the surface of rupture is extending in the direction of movement.

Retrogressive: when the surface of rupture is extending in the direction opposite to the movement of the displaced material.

Widening: when the surface of rupture is extending at one or both lateral margins of the landslide.

Enlarging: when the rupture surface of the landslide is extending in two or more directions.

Diminishing: when the volume of an active slide decreases with time.

Confined: if there is a scarp, but not a visible rupture surface at the foot of the displaced mass.

Moving: when the displaced material continues to move without any visible change in the rupture surface as well as in volume of the displaced material.

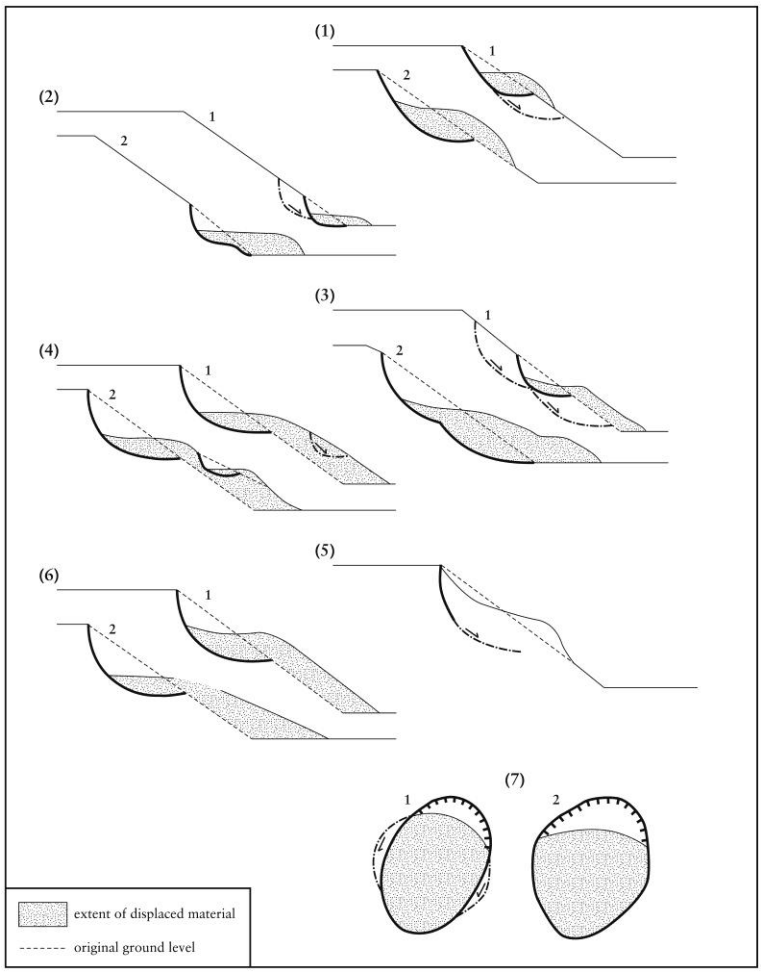

Figure 1.4 Landslide distribution of activity: 1) advancing slide; 2) retrogressive slide; 3) enlarging slide; 4) diminishing slide; 5) confined slide; 6) moving slide; 7) widening slide. After WP/WLI (1993).

On the basis of the *style of activity*, landslides are classified in:
Complex: the landslide exhibits at least two types of movement (e.g. falling, toppling, sliding, etc.) in sequence.
Composite: the landslide simultaneously exhibits at least two types of movement in different parts of the displacing mass.

Successive: the landslide is the same as a nearby, earlier landslide, but does not share displaced material or rupture surface with it.

Single: the landslide is a single movement of displaced material.

Multiple: the landslide shows repeated development of the same type of movement.

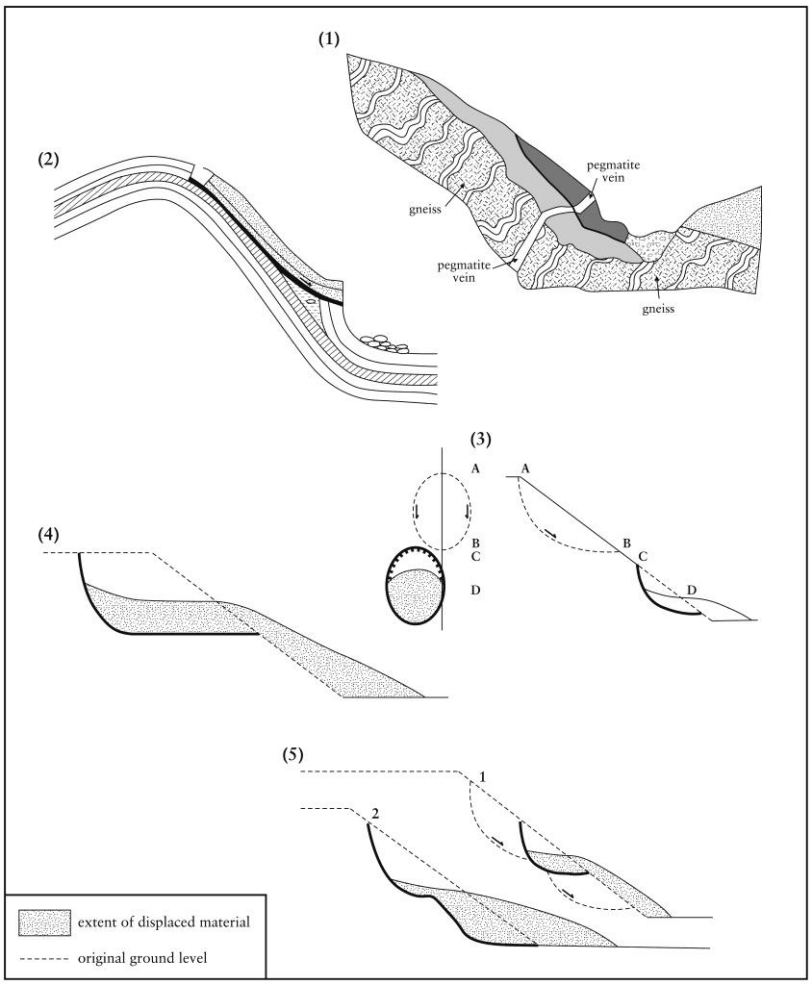

Figure 1.5 Landslide style of activity: 1) complex slide; composite slide; 3) successive; 4) single slide; 5) multiple slide. After WP/WLI (1993).

RATE OF MOVEMENT: the rate of movement represents the most important parameter in the landslides hazard evaluation. A first velocity scale was proposed by Varnes in 1978, successively revisited in 1996 as shown in Figure 1.6.
In this scale, seven classes are established: from extremely low (15 mm/year) to extremely rapid >5 m/s. For each class, a description of the entity of the damage is reported. In fact, small rapid debris avalanche can cause total destruction as well as loss of life. Vice versa, large slope movements, characterized by low velocity, can have less serious effects, only damaging infrastructures or buildings. This means that velocity can influence the risk related to a landslide more than the amount of the involved material.

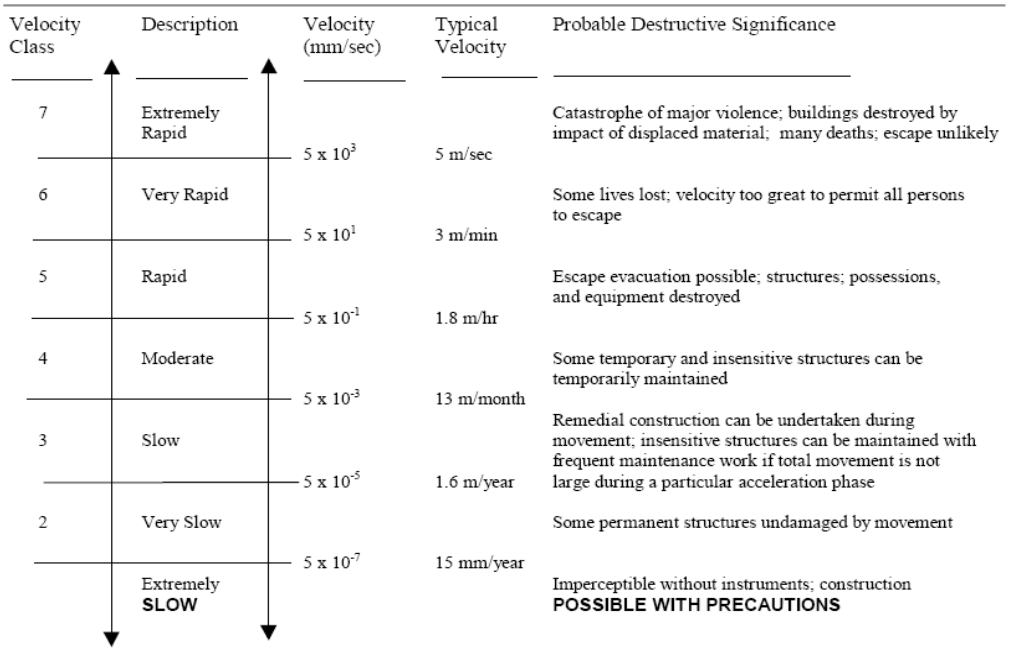

Figure 1.6 Landslide velocity classes (Cruden & Varnes, 1996).

MAIN TRIGGERING FACTORS

Cruden & Varnes (1996) also gave information about the main causes of landslides. After the authors, the main causes for triggering landslides are:

- Increased shear stress: it can be related to removal of lateral support, imposition of surcharges, transitory stresses resulting from explosion or earthquakes and finally uplift or tilting of the land.
- Low strength: it may be associated with the presence of discontinuities within soil or rock mass as well as water infiltrations.
- Reduced material strength: this phenomenon mainly affects clays, which are considered particularly prone to weathering processes. Rocks can be disintegrated because of cycles of freezing and thawing.

Successively Highland & Bobrowsky (2008) subdivided the main causes for landslides triggering in two main categories: natural causes and human causes.

- Natural causes are water, seismic activity and volcanic activity. Saturation of slopes because of rainfall events, snowmelt, changes in ground water levels can cause the decreasing of shear strength of involved material. Earthquakes in landslide-prone areas increase the likelihood that landslides will occur because of ground shaking and consequently liquefaction phenomenon, or dilation of soil material which favours the water infiltration. Volcanic eruption can also cause landslides because the lava melts snow rapidly by triggering typical phenomenon called *lahar*. In addition landslides, rockslides and debris avalanches can affect young volcanic edifices, which are unconsolidated as well as characterized by weak structures.
- Human causes: the most common are the artificial modification of drainage pattern, the vegetation removal and the destabilization of slopes.

- Also building activity in landslide-prone areas favours landslide triggering.

Table 1.3 Landslide causes (Cruden & Varnes, 1996).

Geological causes	
1	Weak materials
2	Sensitive materials
3	Weathered materials
4	Sheared materials
5	Jointed or fissured materials
6	Adversely oriented mass discontinuity (bedding, schistosity, etc)
7	Adversely oriented structural discontinuity (fault, uncoformity, contact, etc)
8	Contrast in permeability
9	Contrast in stiffness (stiff, dense material over plastic materials)
Geomorphological causes	
1	Tectonic or volcanic uplift
2	Glacial rebound
3	Fluvial erosion of slope toe
4	Wave erosion of slope toe
5	Glacial erosion of slope toe
6	Erosion of lateral margins
7	Subterranean erosion (solution, piping)
8	Deposition loading slope or its crest
9	Vegetation removal (by forest fire, drought).
Physical causes	
1	Intense rainfall
2	Rapid snow melt
3	Prolonged exceptional precipitation
4	Rapid drawn down (of floods and tides)
5	Earthquakes
6	Volcanic eruption
7	Thawing
8	Freeze and thaw weathering
9	Shrink and swell weathering
Human causes	
1	Excavation of slope or its toe
2	Loading of slope or its crest
3	Drawdown (of reservoirs)
4	Deforestation
5	Irrigation
6	Mining
7	Artificial vibration
8	Water leakage from utilities

SLOW-MOVING LANDSLIDES IN THE SOUTHERN APENNINES

The geological and geomorphological features of Southern Apennines (Italy) favour the occurrence in the chain of particular types of landslides called "Slow-moving landslides". In fact, these phenomena are widely diffused in flyschoid rocks that are characteristic of this mountain chain.

Slow-moving landslides usually start as slow roto-translational slides (Cruden & Varnes, 1996), and evolving into fast flows after triggering events such as long duration rainfalls and earthquakes.

These are considered as a very dangerous natural hazard, because of their wide distribution and also because of the damages that cause to structures and infrastructures (Picarelli & Russo, 2004; Cascini et al., 2005; Mansour & Morgenstern, 2011). The displacement rate is so slow (some mm to 1/2 m per year), that very long term monitoring is required for a satisfactory evaluation of the kinematics (Mansour & Morgenstern, 2011), but long duration rainfalls and earthquakes can steeply increase the Slow Moving Landslides rate of movement from few mm (to some 1/2 mm per year), up to 50 cm/hour - 5 m/day, making them more dangerous.

The paroxysmal activation of large Slow-moving landslides in Southern Apennine is associated to both rain-falls and earthquakes (Calcaterra et al. 2007). Examples of earthquakes-triggered landslides are the Calitri (province of Avellino) and Bisaccia (province of Avellino) landslides, whereas the Moio della Civitella (province of Salerno) and Agnone (province of Isernia) landslides represent two examples of rainfall triggered landslides.

Calitri and Bisaccia landslides were both triggered by the earthquake, occurred in Irpinia (province of Basilicata) in 1980. Although this earthquake represents one of the most destructive events that affected Southern Italy (Cotecchia & Del Prete, 1984; Carrara et al., 1986; Cotecchia, 1986), by some authors the destructive power of the related landslides has been locally considered higher (Picarelli & Urcioli, 1993).

The Calitri landslide, located along the left valley side of the Ofanto River (Avellino province, Southern Italy), is classified as a deep-seated slow moving slide; its main scarp developed in correspondence of the old town, whereas a shallow mudslide involves the middle-lower portion of the slope, going down to the Ofanto River (Calò, 2009). In the same area, other earthquakes triggered several other landslides in the past (Martino & Scarascia Mugnozza, 2005) (Table 1.4).

Table 1.4 Synthesis of seismic events triggering landslides for Calitri town (By Martino & Scarascia Mugnozza, 2005).

Year*	E.I.	E.E.M.	L.I.	Damage and ground effects	L.A.	Causalities
1561	IX-X	6.4	VII	Collapse of the Castle Tower and of the *Chiesa Madre di S. Canio* cathedral; damage to all houses.	Unrep.	0
1688	XI	6.7	VIII	Damage of residential buildings; failures at the Castel.	Poss.	Unrep.
1689	Und.	Und.	Und.	Collapse of the residential buildings; damaged by previous foundation instabilities	Poss.	6
1692	Und.	Und.	Und.	Collapse of the residential buildings failures at the S. Canio cathedral; destruction of the Castle	Poss.	few
1694	X-XI	6.9	XI	Collapse of the Castle Tower and of the *Chiesa Madre di S. Canio* cathedral; all residential buildings were damaged.	Poss.	Castle inhabitants
1805	VI-VII	Und.	Und.	Ground cracks (Vallone Monaci) and gas exhalations	Unrep.	0
1840	N.E.	N.E.	N.E.	Damage to the S. Canio Cathedral due to foundation instabilities.	Rep.	Unrep.
1851	X	6.4	VI	Damage to buildings a well as ground effects were not reported.	Unrep.	Unrep.
1882	N.E.	N.E.	N.E.	Demolition of the S. Canio Cathedral because of failure appearing after its 1840 restoration and reconstruction.	Rep.	Unrep.
1893	N.E.	N.E.	N.E.	Demolition of the S. Michele Arcangelo Church, located in the Torre district, because of foundation damage.	Rep.	Unrep.
1910	XIII-IX	5.7	IX	Damage to residential buildings due to fall of ruins from the Castle wall.	Unrep.	40
1923	VI-VII	4.7	IV-V	Damage to buildings as well as ground effects were not reported.	Unrep.	Unrep.
1930	X	6.7	VIII	Damage to buildings as well as ground effects were not reported.	Unrep.	0
1951-1952	N.E.	N.E.	N.E.	Damage and destruction of structures in the Torre district due to landslide movements.	Rep.	1
1980	X	6.9	VIII	Landslide activation; destruction of buildings all along the Torre street, De Sanctis street and Matteotti Main street; damage all over the Torre and Piano S. Michele districts; ground cracks in the sorts field plain and mobilization of an earth flow from the sports field plain of the	Rep.	12

Notes: E.I.= Epicentral intensity; E.E.M.=Equivalent epicentral magnitude; L.I.=Local intensity; L.A.= Landslides activation; Und=Undefined; N.E.=No earthquake; Unrep.= Unreported; Rep.=Reported; Poss.= Possible.

The 1980 Calitri landslide, which represents the last event affecting the town, caused the formation of a great number of cracks as well as failures in several areas along the slope (Martino & Scarascia Mugnozza, 2005). Geological surveys in the area (in 2005 and 2009) detected a deep slow moving slide, which is subject to temporary accelerations (Martino & Scarascia Mugnozza, 2005).
The town of Bisaccia is located 24 km north of the epicenter of the Irpinia 1980 earthquake (Parise & Wasowski, 1999). Here, a deep seated gravitational movement was reactivated by this seismic event (Parise & Wasowski, 1999). The mass movement occurred in correspondence of two valleys called V*allone dei Corvi* and *Vallone Ferrelli*, already affected by seismic-induced landslides before the 1980 event. Landslides have been recorded here from 1954 to 1995. Few differences characterize the landslides in the mentioned areas: flow landslides mainly affected *Vallone Ferrelli*, whereas rotational slides, and subordinately complex landslides, prevailed in the *Vallone dei Corvi* (Parise & Wasowski, 1999).

Moio della Civitella is a small village located in Cilento (Salerno province), characterized by frequent reactivations of dormant landslides after pluviometric events. The largest slope movement, directly involving the inhabited areas and the communication routes of Moio della Civitella and the near village of Pellare, derived from an ancient phenomena and is actually considered dormant (Calò, 2009).
The Agnone landslide (Calcaterra et al., 2006; 2007; 2008), located into the Isernia province was triggered after an intense pluviometric rainfall in July 2003. The movement occurred in *Vallone S. Antonio*, and started as a roto-translational slide and evolved into an earth flow (Cruden & Varnes, 1996). Further reactivations, connected to other rainfall events as well as snowmelt, were recorded between 2003 and 2005.

CHAPTER 2

CLAY MINERALS

Clay minerals are hydrous aluminium silicates belonging to the phyllosilicates group. Although they have different chemical composition and physical properties, all clay minerals are characterized by very small size (< 2 μm), and platy morphology (Moore & Reynolds, 1997).

ORIGIN OF CLAY MINERALS

Most of clay minerals derive from the interaction of aqueous solutions with rocks. They are formed and transformed by processes of dissolution and recrystallization (Velde, 1995).

Three main factors control the clay minerals formation:

I. The amount of water: the ratio "water/solid" controls the rate of the reactions. Specifically the greater the renewal, the more amount of dissolution will occur (Velde, 1995).

II. The temperature: most of the clays structures are stable on the earth surface, at low environment temperature. If the temperature exceeds 50-80°C, the clays become instable and start to change into other minerals or other clay minerals, characterized by different structures that are stable at higher temperatures (Velde, 1995).

III. The time: this parameter, associated to the temperature changes, plays an important role. The higher the temperature, the faster the reaction (Velde, 1995).

Stable clay minerals originate from the accumulation of in sedimentary basins of clay-rich materials, through processes that usually last several million years.

Weathering, deposition or sedimentation and hydrothermal alteration are generally considered the main processes responsible for clay minerals genesis (Moore & Reynolds, 1997).

Weathering: "Weathering" phenomenon is generally considered to be constituted by two main processes: physical disintegration and chemical decomposition. These processes are complementary. Physical disintegration of a rock increases the surface area of particles that are exposed to the environment elements (e.g. water), and consequently accelerates the chemical decomposition of the constituting minerals (Taylor & Spears, 1970; Taylor & Cripps, 1987).
As considered by Taylor & Cripps (1987), weathering processes have the major effects near the ground surface. The water percolating in the ground, deriving from rain, has a chemical composition different from the underground pore water, and consequently favours the occurrence of reactions with minerals, and when it

reacts with clays produces swelling processes. Swelling processes represent the results of stress relief, intraparticle swelling of expandable clay minerals and inter-particle (osmotic) swelling between clay minerals (Taylor & Cripps, 1987). This process usually proceeds until the equilibrium between ionic concentration of soil water and double layers water-strata is attained (Taylor & Cripps, 1987).
Weathering process can produce a progressive transformation of rocks into assemblages of only Fe and Al oxy-hydroxides. This is the reason why under tropical or equatorial climates, where the reactions proceeded for long periods of time, Fe and Al are inert components, whereas silica, calcium and magnesium are dissolved and leached from the rock (Taylor & Cripps, 1987).
Although weathering processes under temperate climate are not as aggressive as those occurring under tropical environment, several mineral reactions occur.
Taylor & Cripps (1987) assumed that a typical soil profile is made of two parts:

- One is characterized by reactions between minerals and meteoric solutions under the effect of the temperature
- The other one is characterized by reactions between clay minerals and the solutions.

It means that the transformation of primary mineral phases in more stable assemblages (e.g. kaolinite and Fe-oxy-hydroxides) depends on the local features of an area. Considering that the weathering processes under temperate climates also depend on the mineralogical and chemical features of the parent rock, if weathering is not as aggressive as in tropical or equatorial climates, it derives that clay properties can change from point to point in the soil profile (Taylor & Cripps, 1987).

Deposition and sedimentation: Fine grained sediments rich in clay minerals are very abundant (Velde, 1995). Their great distribution is mainly related to the grain size of particles as well as to their chemistry.
Clay minerals occurring in sedimentary rocks can have two origins: detrital or authigenic. Specifically, detrital clays are inherited from another environment to the one in which they are found (Velde, 1995). During transport and temporary deposition, clays are affected by physical and chemical modifications as ion exchange or fixation.
Most of the fine grain sediment reaching the open sea is supplied by rivers. The great part of this clay sized material, is transported no further than the shallow shelf environments of the continental platform (Velde, 1995). The deposition of clay size particles from all types of water bodies occurs mainly by settling from suspension (Velde, 1995). In static water the rate of settling is governed by particle size on the base of Stoke's low. Without taking in consideration other factors, the bigger the particle size the faster the settling.
In the world deserts as well as in semi-arid areas, erosion and entrainment of clay particles are due to the wind action. Into glacial environments, ice is responsible of clay size minerals transport.
Authigenic clays are formed in situ through direct precipitation from solution, reaction of amorphous materials and precursor minerals (Velde, 1995). Although authigenic clay minerals are not as abundant as detrital, they have been often

studied because they give information about specific geochemical process occurring in the place of formation.

Diagenesis: After several sedimentation cycles of deposition, diagenesis processes occur. The most important type of diagenesis for silicates is called burial diagenesis. As detrital sedimentation proceeds in a basin, silicates are subjected to two major changes: increase of temperature and expulsion of water.
First of all, sediments buried in a basin become progressively hotter as the burial process proceeds. Secondary, compaction produces an escape of water from sediments, with a consequent precipitation of salts.
In the case of clay-rich sediments, the combined increase of temperature and escape of water promotes the formation of silicates-dominated sediments (Velde, 1995).
The geothermal gradients of sedimentary basins range between 20°-50°C/km, on a scale of millions years (Velde, 1995). Higher temperatures promote metamorphism processes. As written above, temperature and time can influence clay minerals formation. For example if the heating period lasts less than one or two million years no metamorphic minerals are produced. Effects on clays are possible for temperatures higher than 100°C.
It is worth to note that different geological settings are characterized by different thermal regime. It means that for the same burial depths, different temperatures can be reached, and consequently different reactions can occur. This is the reason why clay minerals can give indication on the temperature at the time of formation (geothermometers).
To explain how clay minerals can be used ad indicators of temperature and time of burial, Velde (1995) showed the case of deposition of material eroded from a mountain of recent formation (Fig. 2.1).

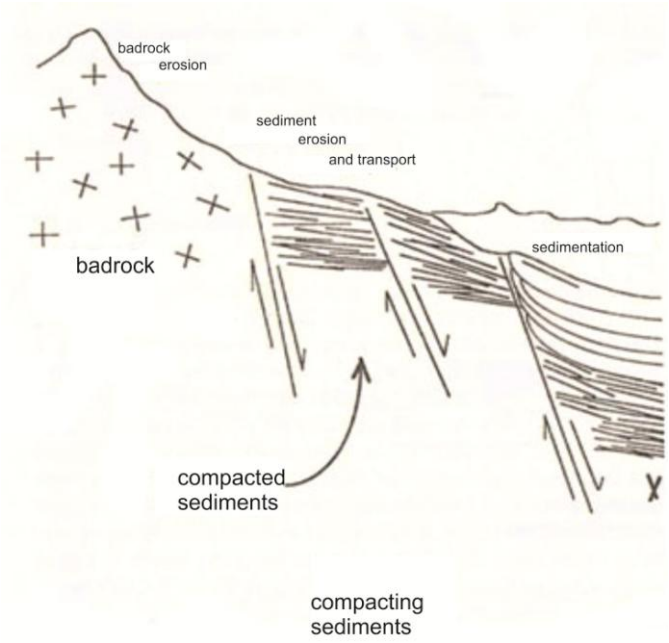

Figure 2.1 Passive continental margin sedimentation setting where source area and sedimentation are linked (Velde, 1995).

Compaction of clay rich sediments occurs in the first kilometer of burial. The density of these sediments increases as well as the water content decreases. At the same time, changes in the water chemistry occur whereas, mainly in correspondence of the first kilometer, only few significant changes in mineralogy of silicates are detectable. In fact the thermal gradient is not high, ranging between 25° and 45°C/km, hampering an increase of material temperature.
In correspondence of the second kilometer of burial, the temperature increases enough and some reactions become visible on a large scale.
In the last kilometer, mineral reactions depend on the amount of water against the amount of solids, on burial temperature, and on burial rate. At this depth other minerals and materials start to interact with clays in sediments. The influence of carbonates as well as the reduction of the oxidation state of iron oxides becomes the major factors in diagenetic mineralogy. Also in this zone the interaction between layers can give out fluids influencing sand layer clay mineralogy (Velde, 1995).

Formation of clay mineral in hydrothermal environments: Hydrothermal alteration promotes clay mineral formation through the circulation of hot water in the Earth's crust. The interaction of hot water and rocks promotes the formation of temporary zonal patter of new clay minerals (Inoue, 1995).

GENERAL STRUCTURAL FEATURES OF CLAY MINERALS

Clay minerals structures are mainly characterized by covalent ionic bonds. About half of the atoms in the structure are represented by oxygen and among the cations silicon and aluminium are the major constituents (Moore & Reynolds, 1997).
Two typical structural units are recognised in the clay minerals, called *Tetrahedral* and *Octahedral* (Fig. 2.2). In tetrahedral sheet Si^{4+} represents the dominant cations, even frequently it is substituted by Al^{3+} and rarely by Fe^{3+}. Each cation is surrounded by four oxygens. The ratio between the number of cation (T) and oxygen (O) is T_2O_5.

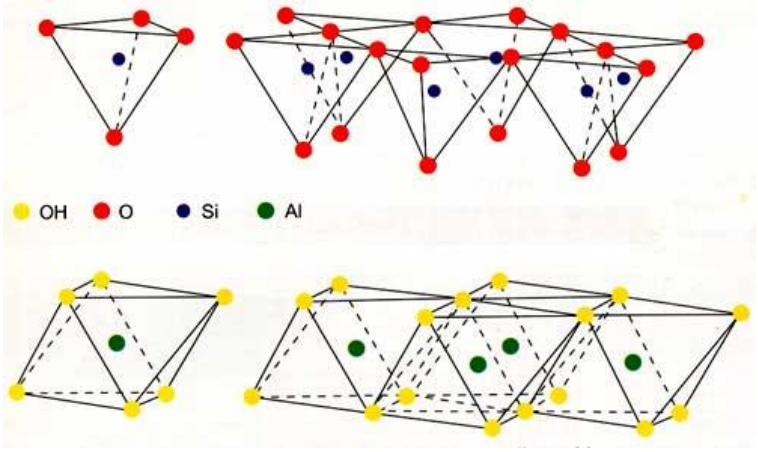

Figure 2.2 a) Tetrahedral sheet; b) Octahedral sheet.

As written in Moore & Reynolds (1997), octahedral sheets can be thought as two planes of closets-packed oxygen ions with cations occupying the resulting

octahedral sites between the two planes. The central cation (Al^{3+}, Fe^{2+}, Mg^{2+}) are surrounded by six oxygens. If the octahedral layer contains divalent ions in all the possible sites, it is known as trioctahedral mineral, whereas if it contains trivalent ions in two of every three possible sites, it is known as a dioctahedral mineral. Trioctahedral minerals are constituted by the so called brucite like sheets $Mg(OH)_2$. The cation-to-anion ratio is 1:2 and all three octahedral sites around each hydroxyl must be filled to have electrical neutrality (Moore & Reynolds, 1997).
Dioctahedral minerals are constituted by gibbsite like sheets $Al(OH)_3$. The cation to anion ratio is 1:3 and to reach electrically neutrality only two Al^{3+} are needed instead of three Mg^{2+} ions (Moore & Reynolds, 1997).

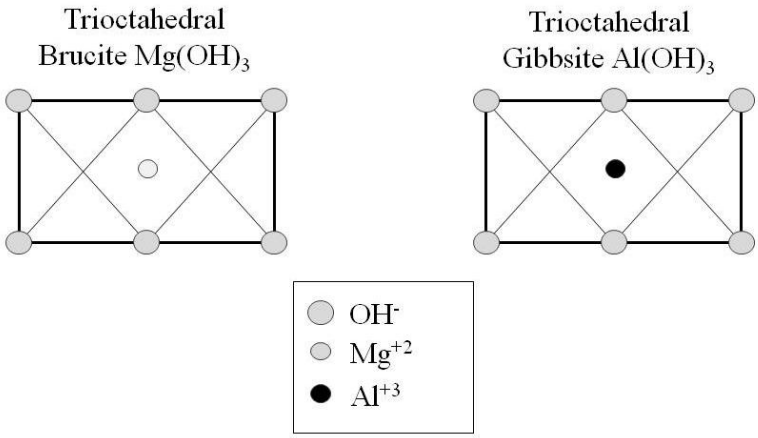

Figure 2.3 Gibbsite and brucite structures.

Tetrahedral and octahedral sheets are characterized by a constant thickness which is called "thickness of the fundamental sheet structure". Specifically, the tetrahedral layers thickness is about 3.4 Å, whereas it is thinner for octahedral layers.

Tetrahedral and octahedral linking, can be give the following structures:

- Tetrahedral + octahedral layers = 7 Å unit layer - 1:1 structure;
- Two tetrahedral + octahedral layers = 10 Å unit layer - 2:1 structure;
- Two tetrahedral + two octahedral layers = 14 Å unit layer - 2:2 structure.
- The repeated distance from one type of unit layer to the next or layer thicknesses represents the main tool in identifying clay mineral species.

CLAY MINERAL PROPERTIES

As defines by Moore & Reynolds (1997), the structures of clay minerals directly or indirectly influence their properties. They also represent the results of the interaction between these minerals and other substances, mainly water. The nature of water, the type and also the size of ions which water contains in solution, the character and distribution of electric charges on the clay mineral surface influence the properties of these minerals. The most important clay minerals properties are listed below:

- Charge
- Electric double layers
- Cation exchange capacity
- Interaction of water with clay mineral surfaces
- Surface area

Charge: Clay minerals as well as clay-sized minerals have electric charges on their surfaces (Moore & Reynolds, 1997), which influences ion-oxygen capacities, the dispersion/flocculation behaviours, and the transport of solutes. It also governs the rates of chemical weathering and the erodibility of the minerals (Moore & Reynolds, 1997). The total electric charge on particles is the sum of permanent and variable charge (Fig. 2.4).
The permanent charge, also defined as layer charge, derives from the substitution of a cation for another in the structure of the mineral, when the valence charge of the first is lower than that of the second. These types of substitution occur because assembled tetrahedral and octahedral sheets may be electrically neutral or negatively charged (Moore & Reynolds, 1997).
The variable charge, located at the edges of minerals particles where structural patterns end as broken bonds, is consider as the final result of the interaction between the broken bonds and H^+ or OH^- .

Electric Double Layer: The external surface of clay minerals tends to attract swarms of cations, because of the presence of anions O^{2-} or OH^-. Within the layers of water which are attracted with rigidly held, cations usually concentrate in a volume near the surface of clay minerals and in turn attract anions, by less rigid held. The anions in turn attract cation, until electrical neutrality is achieved. Neutrality can be reached only in suspensions dilutes enough in clay mineral particles (Moore & Reynolds, 1997). The double layers interaction between particles can vary from a particle pair to particle pair on the basis of the different van der Waals attraction (Moore & Reynolds, 1997). In fact if the surrounding fluid contains a number of divalent or trivalent cations that is not sufficient to neutralize the clay mineral surface, the immobile layer is thinner and particles can get closer to one another particles (Moore & Reynolds, 1997). On the other hand, univalent cations from a thicker immobile layer, keeping particle apart by a respectable distance making it more difficult for the Waals forces to be effective. In this case, clay minerals particles remain discrete entities and because of their small size, remain in suspension (Moore & Reynolds, 1997).

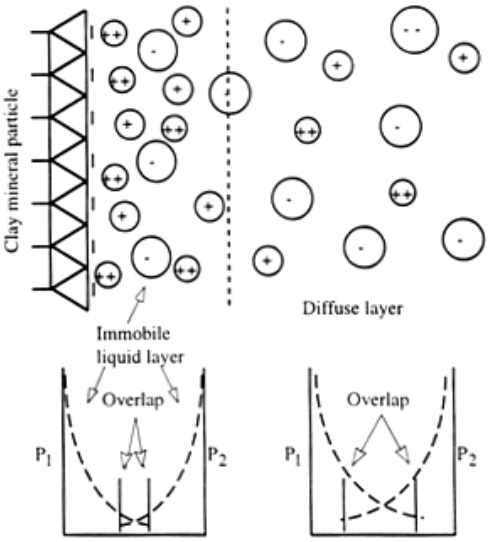

Figure 2.4 Electrical double layer (Moore & Reynolds, 1997). The negative surface of the clay mineral attracts oppositely ions from the liquid in which the particle is immersed. This band of relatively tightly held positive ions attract a less tightly distinguishable band of anions, which in turn attracts an even less distinguishable band of cations.

Cation Exchange Capacity: The cation exchange capacity (CEC) is a measure of the capacity of clay to exchange cations. It is a very important property of clay surfaces, representing their chemical activity and their interaction with ions in aqueous solution (Velde, 1995). It is a dynamic process controlled by the *law of mass action*. In most of the cases, cations are attracted to the (001) surfaces, whereas anions to the edges of particles. Clay minerals, in fact, are characterized by a big surface area, especially the (001) surface.
Mainly in the case of expandable clays, cations can be exchanged in contact with a solution rich of other cations. In this case, cations in the fluid and those on the (001) surface interchange at specific rate in dependence of temperature, concentration, pH as well as size and charge of the cations, the energy of hydration of the cations, and the amount and distribution of the layer charge of the clay minerals (Moore & Reynolds, 1997). The CEC can also be defined as the measure of the concentration of unfixed cations in the diffuse layers (interlayers and surface layers), which depends on the magnitude of the total layer charge (structural plus surface), which in turn varies with pH (Moore & Reynolds, 1997).

Interaction of Water with Clay Mineral Surfaces: The interaction with water is an important topic to take in consideration (Velde, 1995; Moore & Reynolds, 1997).
It is worth to note that some clay minerals tend to swell in contact with water. In addition the influence of the clay mineral layer charge extends only a few water layers away from the surface. Water forms "coordination sphere" or shell around most cations, which are more tightly held by some cations than others (Moore & Reynolds, 1997). Swelling or expansion happen exclusively along the 001 or c* direction, and no variation occur in *a* and *b* dimensions of crystals. The crystallographic integrity is maintained. Water in the interlayer space of expandable clay minerals is controlled by three factors: the polar nature of the water molecules, size and charge of cations and the value and localization of the charge on the adjacent silicate layers. During diagenesis water is released,

carrying with it cations and anions in solution, representing one of the primary driving factors in diagenetic changes (Moore & Reynolds, 1997).

Specific Surface Area: specific surface areas SSA, represents the ratio of the surface area of material to either its mass or volume (Holtz & Kovacs, 1981).

SSA= surface area/volume (Eq. 2.1)

It is an important parameter to quantify interaction processes as mineral dissolution and sorptive interactions in soils and sediments (Macht et al., 2011).
The clay particle thickness depends upon the magnitude of the forces of attraction between the layers. The variation in SSA is due to different thickness of the particles (Fig. 2.5); specifically, the thinner the particles, the higher the SSA.
Swelling clay minerals exhibit internal surfaces in their interlayer spaces (Macht et al. 2011).

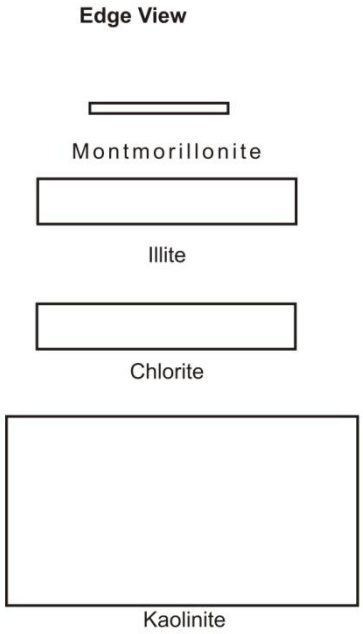

Figure 2.5 Average values of relative sizes, thicknesses and specific surfaces of the common clay minerals (modified by Holtz & Kovacs, 1981).

CLAY MINERALS CLASSIFICATION

Several types of clay minerals classification have been proposed in the years. First of all it is possible to subdivide clay minerals on the basis of layer type: 1:1 or 2:1 (Bailey, 1980b).
As written in the previous chapter 1:1 layer types consist of repeated pairs of a tetrahedral and octahedral sheet whereas 2:1 later types consist of repeated stacks of an octahedral sheet sandwiched between 2 tetrahedral sheets. Moore & Reynolds (1997) proposed that within each subdivision it is possible to make a further distinction between the trioctahedral or dioctahedral character of the layer (Tab.2.1).

1:1 LAYER TYPE

The 1:1 layer type is usually characterized by very small layer charge. Tetrahedral cation sites are all occupied by Si^{4+} and the octahedral sites by Al^{3+} and Mg^{2+} (Moore & Reynolds, 1997).
Dioctahedral and trioctahedral varieties of 1:1 layer silicates are possible.

Serpentine: $Mg_6Si_4O_{10}(OH)_8$. Mg3Si2O5(OH)4 Serpentine minerals are usually larger in particle size than other clay minerals. They can be found as:

- silky asbestos fibres and as smaller fibres in more massive or splintery material (chrysotile)
- platy material (lizardite and amesite)
- iron rich variety berthierite.

Serpentine minerals are characterized by *modulated* structures, consisting of a series of alternating waves with a wavelength of 30-100 Å (antigorite).

Table 2.1 Classification of phyllosilicates with emphasis on clay minerals.

Layer type	Group	Subrgoup	Species
1:1	Srp-Kln	Srp(Tr)	Ctl, , atg, lz, brt, odn
		Kln (Di)	Kln, dck, nct, hly
2:1	Tlc-prl	Tlc(Tr)	
		Prl(Di)	
	Sme	Tr sme	Sap, hct
		Di sme	Mnt, bei, ntn
	Verm	Tr vrm	
		Di Vrm	
	Ilt	Tr ilt	
		Di ilt	Ilt, gln
	Mc	Tr micas	Bt, phl, lpd
		Di micas	Ms, pg,
	Brittle mc	Di brittle mc.	Mrg
	Chl	Tr, Tr chl	Common name based on Fe^{2+}, Mg^{2+}, Mn^{2+}, Ni_{2+}
		Di, Di chl	Dnb
		Di, Tr chl	Sud, ckt
		Tr Di chl	Not known examples
2:1 Sepiolite-palygorskite	Inverted ribbons, with variable charge		

Notes: Srp=serpentinit, kln= kaolinite; ctl=chrysotile, brt= berthierite, atg=antigorite, lz= lizardite, odn=odinite, dck=dickite, nct=nacrite, hly=halloysite, prl= pyrophyllite, sme= smectite, mnt= montmorillonite, bei=beidellite, ntn= nontronite, sap= saponite, hct= hectorite, vrm= vermiculite, ilt=illite, gln=glauconite, bt= biotite, pg= paragonite, ms=muscovite, mrg=margarite, phl=phlogopite, lpd=lepidolite, dnb=donbassite, sud= sudoite, ckt= cookeite, chl=chlorite, mc=micas.

Berthierite: $(Fe^{2+}_3Mg_{0.75}Al_2)(Si_{2.5}Al_{1.5})O_{10}(OH)_8$. Berthierite mineral is commonly present in unmetamorphosed sedimentary iron formation and can form as flint clay. It can be find in shallow marine environment rich in iron (Moore & Reynolds, 1997).

Odinite: $(Fe^{3+}_{1.6}Mg1.6Al1.1\ Fe^{2+}_{0.6})(Si_{3.6}Al_{0.4})O_{10}(OH)_8$. Odinite's composition is similar to berthierite. The main difference is the higher presence of ferric iron relatively to ferrous iron in the first than the second. It usually forms on continental shelves and into reef lagoons (Moore & Reynolds, 1997).

Kaolin: $Al_2Si_2O_5(OH)_4$ Kaolin minerals are: kaolinite (in various degrees of disorder, dioctahedral), dickite (trioctahedral), nacrite, 7 Å halloysite and 10 Å halloysite.
Kaolinite as well as the two halloysites, are single-layers structures, whereas dickite and nacrite are double-layer polytypes (Moore & Reynolds, 1997). Kaolinite is characterized by the presence of two Al^{3+} and lower amount of Fe^{3+}.
It always represents the product of diagenetic processes as well as of hydrothermal alteration. In addition sedimentary and lacustrine deposits of kaolinite have also been reported. However, kaolinite stable structure always represents the final product of alteration processes.
Dickite has been defined as high temperature polytype of kaolinite, characterized by minor structural variation. Several doubts exist on the relationship between halloysite and kaolinite. A layer of water, about 2.9 Å thick, gives to halloyasite the 10 Å spacing. This water can spontaneously leave the mineral structure, or after heating or under the effect of vacuum. Vice versa, kaolinite structure doesn't swell in contact with water.

Allophane and imogolite: $r Al_2O_3/s.SiO_2/t.H_2O$. These minerals have been classified as 1:1 minerals considering both their chemical and structural features. They mainly occur in volcanic ash as well as in soils deriving from basalts. They seem chemically distinguishable one from another but there is not general agreement on this point, because there are some materials that are intermediate between allophone and imogolite, and hydrous oxides of Al, Fe and Si. The ratio of SiO_2 to Al_3O_3 is usually 1.3 to 2.0 for allophone. Imogolite does not seem to vary as much. It gives a ration of SiO_2 to Al_3O_3 of 1.05 to 1.15 (Moore & Reynolds, 1997).

Pyrophillite: $Al_2Si_4O_{10}(OH)_2$. This mineral is characterized by the presence of Al in the octahedral site and Si in the tetrahedral site. The unit layer structure has two tetrahedral sheets and one octahedral sheet, and a resulting total thickness of 9.6 Å.

Talc: $(R^{2+})_3Si_4O_{10}(OH)_2$. This mineral appears characterized by the presence of three divalent ions in the octahedral site with a small number of trivalent ions in the octahedral and tetrahedral sites. Two tetrahedral layers and one octahedral

sheet give a 9.6 Å thick unit layer structure. Significant Fe and Mg substitution occurs.

2:1 LAYER TYPE (high charge ~1)

For these minerals the charge imbalance is between 0.8 and 1.0. An interlayer between the layer units strongly blinds the mineral into a coherent unit. These are dioctahedral in low temperatures environments. Potassium is the most common interlayer cation (Moore & Reynolds, 1997). Considering that the charge is usually less than 1.0 per unit cell, which characterizes the mica structures, this group of phyllosilicates is called "*mica-like minerals group"*. In addition true micas have different composition and also are found in rocks deriving from high temperature environments.

The trioctahedral subgroup: $(K,Na)_{x+y}(Mg,Fe^{2+},R^{3+})_{3-y}R^{+}_{y}(Si_{4-}xAl_x)O_{10}(OH)_2$. The main species of this subgroup are phlogopite, biotite and annite. Mg dominates the octahedral sites in phlogopite, whereas Fe dominates octahedral sites in annite. Both Fe and Mg occur sub-equally in biotite (Moore & Reynolds, 1997). Rarely Fe^{3+} is found as well as substitution of Si^{4+} in the tetrahedral sites. In all the other cases Al^{3+} occurs instead of Fe^{3+}. In addition Fe^{2+} and Mg^{2+} represent the most common cations in the octahedral sites whereas Mn^{2+}, Li^{+}, Al^{3+} and Fe^{3+} are found occasionally. The interlayer spaces in pseudo-12-fold coordination are sites for K^{+}, Na^{+}, NH_4^{+} and Ca^{2+} (Moore & Reynolds, 1997).

The dioctahedral subgroup: $(K,Na)_{x+y}[(Al,Fe^{3+})_{2-y}(Mg,Fe^{2+})_y]_y(Si_{4-}xAl_x)O_{10}(OH)_2$. Muscovite and paragonite are the main species characterizing this subgroup. The main difference between these two minerals is represented by the presence of K as interlayer cation in the muscovite and Na as interlayer cation in the paragonite. Si-rich varieties can also be found. They are called phengite and celadonite. Phengite mineral is characterized by a Si:Al ratio in tetrahedral sites of about 3.5:0.5, whereas in celadonite Al is almost absent.

2:1 LAYER TYPE (low charge <1)

Illite, glauconite, smectite, vermiculite and chlorite belong to 2:1 layer type group. They are considered transitional one to another (Moore & Reynolds, 1997), and frequently occur as interstratified clays.
Illite and glauconite are almost always dioctahedral, whereas smectite and vermiculite form both dioctahedral and trioctahedral species (Moore & Reynolds, 1997).

Illite: $K_{0.8-0.9}(Al,Fe,Mg)_2(Si,Al)_4O_{10}(OH)_2$. Illite is defined as an aluminous phyllosilicate with 10 Å unit layer, characterized by some substitution of Fe^{3+}, Mg and Fe^{2+} in the octahedral site, and Al^{3+} for Si in the tetrahedral site. These substitutions generate the greatest part of the layer charge imbalance. Si content is usually low (less than 3.50 a.p.f.u.).

The characteristic green color, visible in hand specimen, is given by the high iron content. The illite structure always occurs interlayered to iron rich smectite. Illite shows Si, Mg and H_2O amounts generally higher than those occurring in the muscovite. In addition illite has less tetrahedral Al and less interlayer K than muscovite (Moore & Reynolds, 1997). Pure illite, as well as interstratified illite, is a characteristic mineral of sedimentary rocks. Illite in sedimentary rocks can occur as a recycled phase, deriving from pedogenesis, weathering or sedimentary processes. Illite can also have a hydrothermal or metamorphic origin.

Glauconite: $K_{0.8}(Fe, Mg, Al)_2(Si,Al)_4O_{10}(OH)_2$. Considering the AIPEA Committee this name should be restricted to Fe rich dioctahedral micas, with tetrahedral Al or Fe^{3+} usually greater than 0.2 atoms per formula unit, and octahedral R^{3+} greater than 1.2 a.p.f.u. (Moore & Reynolds, 1997).

Smectite: is the name of a group of minerals both dioctahedral and trioctahedral (Moore & Reynolds, 1997), whose main feature is the ability to expand and contract, maintaining two dimensional crystallographic integrity. This property is related to the relatively small layer charge that characterizes this group of minerals. A charge of 0.7 to 0.2 allows the layers to absorb hydrated cations and polar molecules between the 10 Å sheets (Velde, 1995). When water as well as other polar organic compounds (e.g. ethylene glycol) enters in the interlayer space, expansion takes place (Moore & Reynolds, 1997). In fact, with water as well as the other polar organic compound, the interlayer cations pull them into the interlayer space. Usually interlayer distance for swelling minerals is greater than the 10 Å unit because of the presence of hydrated cations. The normal basal spacing is 12.5 Å for a mono-hydration state (one water layer) and 15.2 Å for double-hydration state.
Although it is easier to find smectite as a discrete mineral than illite, in most of the cases smectite constitutes the end member of composite phases called mixed layers clays.
Smectite usually represents the product of the alteration of volcanic glass with relatively high silica content (Moore & Reynolds, 1997). In addition the nature of smectite minerals is closely related to other associated interstratified minerals and to primary minerals from which it derives (Moore & Reynolds, 1997). Montmorillonite, beidellite and nontronite belong to smectite dioctahedral groups, whereas saponite belongs to the smectite trioctahedral group.
Beidellite, whose chemical formula is $M_{0.n}(Al,Mg)_2(Si,Al)_4O_{10}(OH)_2xH_2O$ where $n<0.5$, is an aluminous mineral characterized by the presence of two tetrahedral layers dominated by Si ions. For beidellite minerals, Al substitution represents the major source of charge imbalance. The octahedral layer is mainly aluminous (Velde, 1995).
Montmorillonite has chemical formula $M_{0.n}(Al,Mg,Fe^{2+})_2Si_4O_{10}(OH)_2xH_2O$, and represents an aluminous mineral characterized by two tetrahedral layers which are almost exclusively occupied by silicon. The charge imbalance comes from divalent ion substitutions, Fe or Mg, for the trivalent aluminum ions in the octahedral site (Velde, 1995).

Nontronite (chemical formula is $M^{0.n}(Fe^{3+},Fe^{2+}Al)_2(Si,Fe^{3+})_4O_{10}(OH)_2xH_2O$) is a ferric mineral characterized by low number of Al substitution and occasionally Mg ions in the octahedral site. These substitutions, as well as some substitutions of ferric iron in the tetrahedral site for Si^{4+}, produce the interlayer charge (Velde, 1995).

Saponite, whose chemical formula is $M_{0.n}(Mg,Al)_{3.0-2.5}(Si,Al)_4O_{10}(OH)_2nH_2O$, is characterized by the introduction of divalent ions in the octahedral site and consequently by the occurrence of vacant sites, which produce a positive charge in the layer. Because of this positive charge balance, it is necessary a compensation into the interlayer site.

Vermiculite: $M_{0.x}(Mg,Fe,Al)_{<3}(Si,Al)_4O_{10}(OH)_2nH_2O$. Vermiculite has been often described as a high charge smectite. The main difference between these two types of clays is represented by the fact that vermiculite does not expand (or contract) fully, as smectite does when hydrating (or heating).

As reported in Moore & Reynolds (1997) vermiculite seems to be a member of three different series:

- biotite - trioctahedral vermiculite - trioctahedral smectite series
- muscovite - dioctahedral vermiculite - dioctahedral smectite series
- chlorite - vermiculite series

For this characteristic, in clay size specimens, vermiculite may be both trioctahedral and dioctahedral, whereas in macroscopic varieties, it is trioctahedral with platy morphology like that the trioctahedral micas (Velde, 1995).

Chlorite: As reported by Moore & Reynolds (1997), chlorite ideally consists of:

- a negatively charged 2:1 layer→ $[(R^{2+}, R^{3+})_3(Si_{4-x}R^{3+}_x)O_{10}OH_2]^-$
- a positively charged interlayer octahedral sheet→ $[(R^{2+}, R^{3+})_3OH_6]^+$.

In low temperature environments, chlorite minerals are strictly trioctahedral. Dioctahedral substitutions usually occur with trivalent ions (Al and Fe^{3+}) into up to half of the octahedral sites for the normal divalent ions (Velde, 1995). Substitutions of trivalent ions (Al^{3+}) also occur in the tetrahedral site. They compensate for a proportion of the trivalent ion substitution into the octahedral site (Velde, 1995).

The chlorite composition represents the result of several types of complex, simultaneous ionic substitutions. The basic structure of chlorites is characterized by the presence of two layers of silica tetrahedrons which are linked by an octahedral layer, and by an interlayer substitution between the 10 Å layers of the basic structure (Velde, 1995). Specifically, the interlayer ions between the 10 Å layers are well organized hydroxyl-complexes of divalent and divalent-trivalent ions.

Chlorite can be found:

- In shales at the highest grade of diagenesis;
- In soil;
- On the surface of sandstones, as neoformation minerals, where they may be the alteration product of odinite or berthierite;
- As replacement of carbonate grains in carbonate rocks;

- In geothermal and low temperature hydrothermal system.

The chlorites in sandstones can be distinguished as diagenetic or detritical on the basis of the morphology. Chlorite is also found in high concentrations in Mg-rich evaporate sequences. In this case it may be a replacement or it may be primary (Moore & Reynolds, 1997).

Chlorite's name derives from Greek *chloros* which means "green". Chlorite usually gives the green color to the rocks affected by metamorphism in the green schist facies.

MIXED LAYERS

Środoń et al. (1999) defined mixed layer clays as *intermediate products of reactions involving pure end-members, coming from natural environments ranging from surface to low-grade metamorphic and hydrothermal conditions.* They are usually constituted by two components. Interstratifications of more than two components seem to be rare.

Moore & Reynolds (1997) considered mixed-layering, interlayering and interstratifications, as *clay minerals formed of two or more kinds of inter-grown layers, not physical mixtures.*

The periodicity in the c* direction, which usually characterizes clay minerals, is preserved if the crystal contains identical layers as well as interlayer.

In case of differences in layer type as well as interlayer material, the periodicity is not preserved, and the phenomenon known as interstratification occurs.

The formation of mixed layers appears to be driven by the time, the increase of temperature and pressure, fluid movements and shearing phenomena, associated with faults.

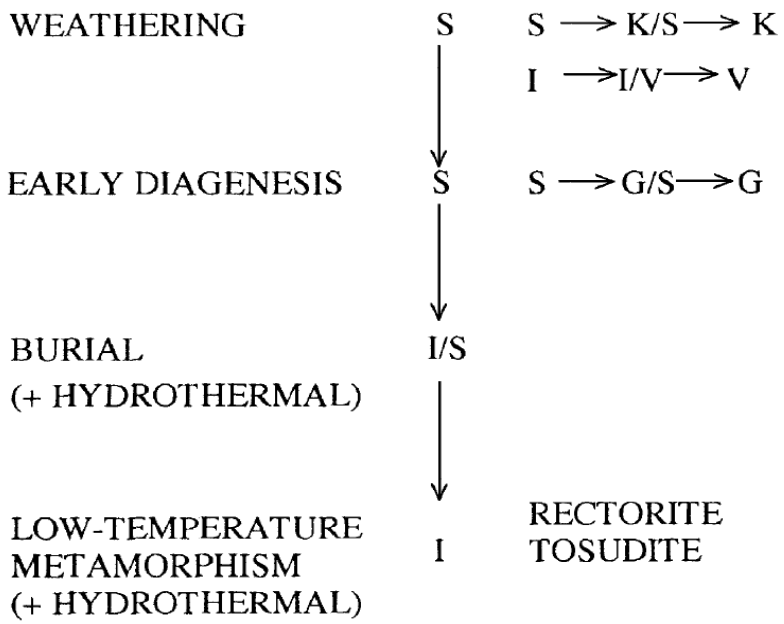

Figure 2.6 Summary of the occurrences of mixed layers at different stages of the rock cycle. S=smectite, K=Kaolinite, V=vermiculite, G= glauconite. The arrows highlight the direction of the alteration process (Srodon, 1999).

THE MIXED LAYER ORDERING

Mixed layer members are found stacked in random, partially regular, or regular sequences (Moore & Reynolds, 1997).
The *grade of ordering "R"* (Reichweite) of mixed layer is defined as the probability that one type of layer occurs next to another (Reynolds, 1980).
Specifically:

- R0 is used to identify mixed layers characterized by random ordering (ABABBAAAABAABABA…).
- R1 is used to identify mixed layer characterized by short range of ordering (ABABABABABABA...).
- R3 is used to identify mixed layer characterized by long range of ordering (BAAABAAABAAABAAAB…).

The grade of ordering can also give information about the grade of diagenesis. Specifically, for example, in the case of mixed layer I/S, the higher the R value, the higher the illitization process and consequently the higher the diagenesis.

Illite/smectite: Mixed layer represents the most common clay component of sedimentary rocks (Środoń, 1980).
The mixed layer I/S arrangements vary from random (R0), to short-range (R1) ordered, and then to long-range (R3) (Bauluz, 2007).
The series involving dioctahedral clay minerals is:

Smectite→mixed layer illite/smectite→ illite.

Hower at al. (1976) studied the illitization process and wrote the illitization reaction as:

$$K+Al+smectite \rightarrow illite+Na+Ca+Fe+Mg+Si+H_2O$$

Three of the most evident variables driving the smectite-to-illite transition are:

- the time ,
- the temperature,
- the availability of K.

Specifically, a temperature variation can derive from burial and geothermal gradient, hydrothermal fluids, or intrusion of igneous bodies.
Środoń & Eberl (1984) also verified that the porosity of the rocks can promote the illitization process. In situations where rocks that are more or less permeable have been compared, it appears that the smectite to illite transition had developed more in most permeable rocks.
Time is also important factor in the diagenetic change from smectite to illite. Sediments of Miocene age, buried less than 200 m, contain smectite but no illite (Środoń & Eberl, 1984).
In general, both time and temperature control the kinetics of the reaction. Although usually young rocks have not changed as much as the old, Moore & Reynolds (1997) affirmed that, in the case of an instantaneous diagenesis, all the occurring smectite is comprehensively illitized. In this case, the degree of sediment illitization is a function of depth, and consequently, of temperature.

To explain how the illitization of smectite happens, Moore and Reynolds (1977) proposed three different models:

- *MacEwan crystallite model*
- *Fundamental particle model*
- *Two solid solution model*

MacEwan crystallite model: smectite and illite layers are considered intimately interlayered, stacked either randomly or regularly into a fixed sequence.
This sequence, acting as coherent unit, scatters X-rays. The repeated distance is developed along c*, and the division between the layers occurs in the center of the octahedral sheet. The transition from a smectite to an illite layer derives from an in place remodeling of the chemistry and the structure, without solid-state transformations (Moore & Reynolds, 1997).

Fundamental particle model: the particles independently develop an epitaxial overgrow. They are stacked together in a group of particles that diffract X-rays. Formation of fundamental particles by direct precipitation, rather than by a rearrangement of the structure of precursor minerals, represents a tenet of this model called dissolution-crystallization model.
Some proofs that attest the occurrence of the dissolution-crystallization model are changes in morphology and polytype as the proportion of illite increases (Moore & Reynolds, 1997).

Two solid solution model: Inoue (1987), studying hydrothermally altered silicatic volcanic glass, identified three phases. Each of them appeared to be characterized by distinct morphology. Two of them appeared as solid solution whereas the third showed little variation in chemical composition.
Specifically they characterized the first solid solution as a smectite undergoes to K-fixation, the second as maturing illite, and the third as a phase showing less than 5% expandable layers (Moore & Reynolds, 1997).
In general, for mixed layer I/S originated by burial diagenesis process, the amount of smectite tends to decrease with depth, whereas the amount of illite increases. This was described as the "smectite to illite reaction series". The intermediate stages of the reaction are expressed by the appearance of mixed layer minerals of illite/smectite compositions. For this reason when evaluating the grade of ordering of a mixed layer I/S, it is possible to obtain information about the grade of diagenesis of the analyzed material. The higher the amount of illite (the lower the amount of smectite), the higher is the grade of ordering (from R0 to R3), consequently the deeper the diagenesis process.

However, not all clay mineral reactions take place at the same rates: some changes occur over short burial distances, whereas others, in the same rock, change over kilometers.
As Velde (1995) affirmed, the rate of the sedimentation in a given basin often changes during its history. Some basins have a sedimentation rate which

progressively decreases with time. This has an effect on the mineralogy of each layer in the rocks of the basin.

Kaolinite/smectite: these mixed layers are generally not easy to detect (Delveaux et al., 1990; Hughes et al., 1993; Cuadros et al., 1994). They often form in temperate to tropical climate and are consequently found in the corresponding paleosoils (Hughes et al., 1993). Their formation is related to a wide range of chemical environments, spanning from acidic (e.g. acid clays from Japan) to alkaline, as detected by Robinson & Wright (1987). No occurrence of K/S originating from kaolinite has been recorded. The diagenetic illitization of kaolinite is responsible of the formation of discrete illite crystals, instead of mixed layer K/S.

Chlorite/smectite: Bettison & Mackinnon (1997) defined the chlorite/smectite mixed layer as a product of diagenesis and low temperature metamorphism of intermediate to mafic volcanic rocks. The transition from smectite to chlorite, via corrensite (regularly interlayer), occurs with the presence of mixed layer C/S, with variable percentages of expandable layers (Bettison & Schiffman, 1988; Bevins et al., 1991). This transition should be not directly related to an increase in metamorphic conditions, whereas water/rock ratios and the mode of occurrence of phyllosilicates represents an important factors in controlling the structure of the stable layer silicate (Alt et al., 1986; Shau & Peacor, 1992; Schiffman & Staudigel, 1995).
As in case of mixed layer I/S, also in this case, the reaction mechanism can be determined through the layer transition boundaries. In general, during the transformation processes, the amount of smectite decreases as the amount of chlorite increases (Inoue, 1987; Inoue & Utada, 1991; Schiffman & Staudigel, 1995).
Moore & Reynolds (1997) revealed the occurrence of mixed layers C/S in a great variety of geological environments:

- contact metamorphic zones of shales,
- old carbonate sequences,
- Lake Superior iron ores,
- hydrothermal alteration and weathering product of ophiolitic rocks and dolomites,
- sediments containing sufficient Mg subjected to burial diagenesis.

CHAPTER 3

RELATIONSHIPS BETWEEN SLOW-MOVING LANDSLIDES AND MINERALOGY OF THE STRUCTURALLY COMPLEX FORMATIONS

STRUCTURALLY COMPLEX FORMATIONS: ESU (1977) CLASSIFICATION

Slow-moving landslides are often related to particular types of flyschoid materials widespread in Southern Italy. The characteristic heterogeneity as well as the anisotropy of these materials makes them complex from a mechanical point of view. In 1977, Esu classified complex material involved in landslides, by introducing the term "Structurally complex formations" and subdivided them on the basis of their lithology in two main groups (Figure 3.1).

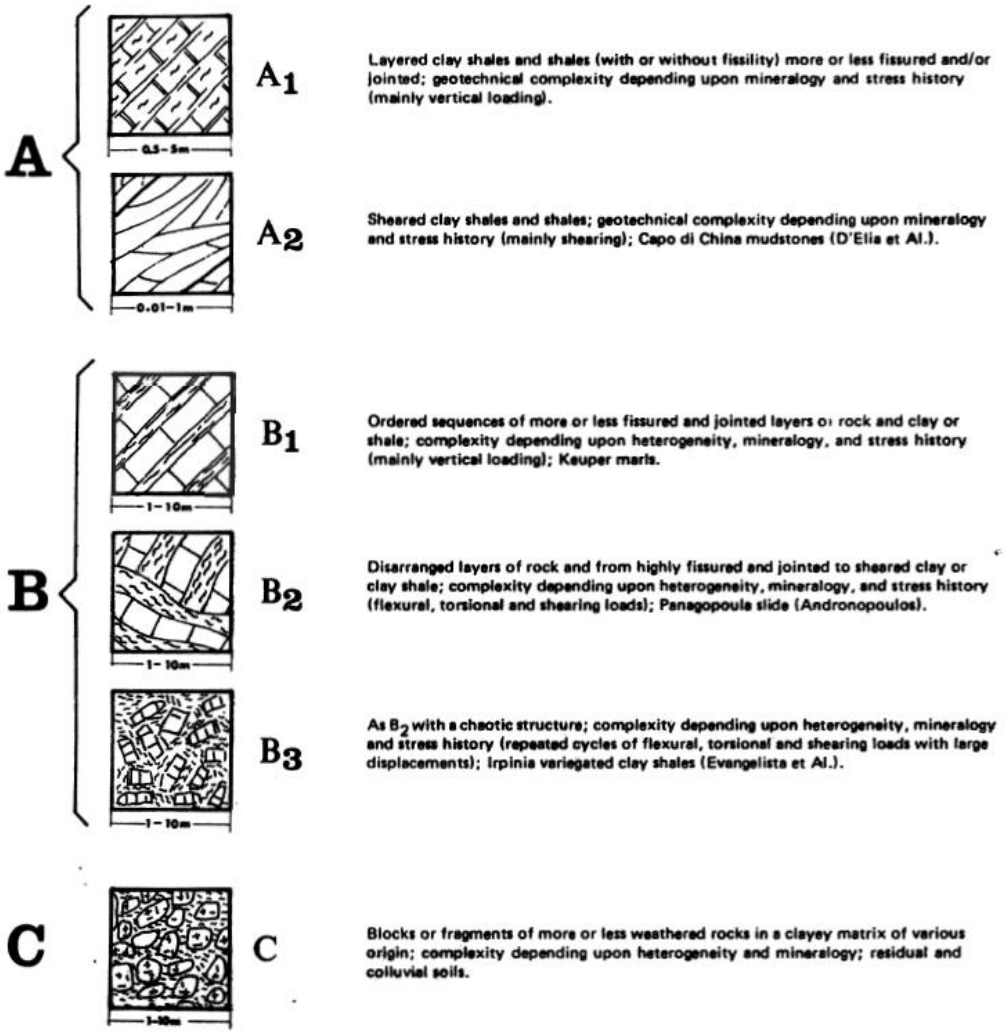

Figure 3.1 Structurally complex formations (from Esu, 1977).

- A: Lithologically homogeneous materials having singenetic or superimposed structures
- B: Materials constituted by at least two components, characterized by marked differences in their mechanical properties. These components can form separate domains with an ordered and clearly recognizable arrangement, or can be randomly assembled; in most cases one of the constituents is a clay, whereas the other one is a rock.

The characteristic heterogeneity of structurally complex formations makes the slopes more prone to landslides, especially in the case of areas characterized by interbedded soft and hard rocks. The case of the Vajont-Monte Toc landslide represents a clear example of this situation.
The tragedy of Vajont and the great number of deaths spurred numerous investigations on the conditions triggering slope collapse. The failure occurred along bands of clay within the limestone mass, at depths between 100 and 200 m below the surface (Hendron & Patton, 1985). Considering the Kilburn & Petley (2003) interpretation, these clay beds, 5 – 15 cm thick, represented planes of weakness. The catastrophic collapse was related by the authors (Kilburn & Petley, 2003) to the self-accelerating rock fracture, common in crustal rocks at loads around 1 – 10 MPa, and readily catalyzed by circulating fluids.
Although landslides can be associated to several types of triggering events, the clay component of the involved material is considered crucial in their development (Summa et al., 2010). The presence of "expandable clay" (e.g. smectite) can promote shrinkage and swelling phenomena, because of their property to adsorb and retain water, mainly during the transition from the dry season (summer), to the cold and rainy season (winter). As considered by Cruden & Varnes (1996), the increase of water pore pressure can be responsible of a decreasing of the shear strength and for this reason represents a crucial factor to the onset of slope instability.
In 1987, Taylor and Cripps proposed a model showing that weathering acts on clay soils by forming several "weathering zones". As shown in the Figure 3.2, the transition from the deeper to the more surficial zones is governed by an increase of material degradation. Slow moving landslides are usually considered to be related with the more weathered and surficial parts of structurally complex formation slopes.

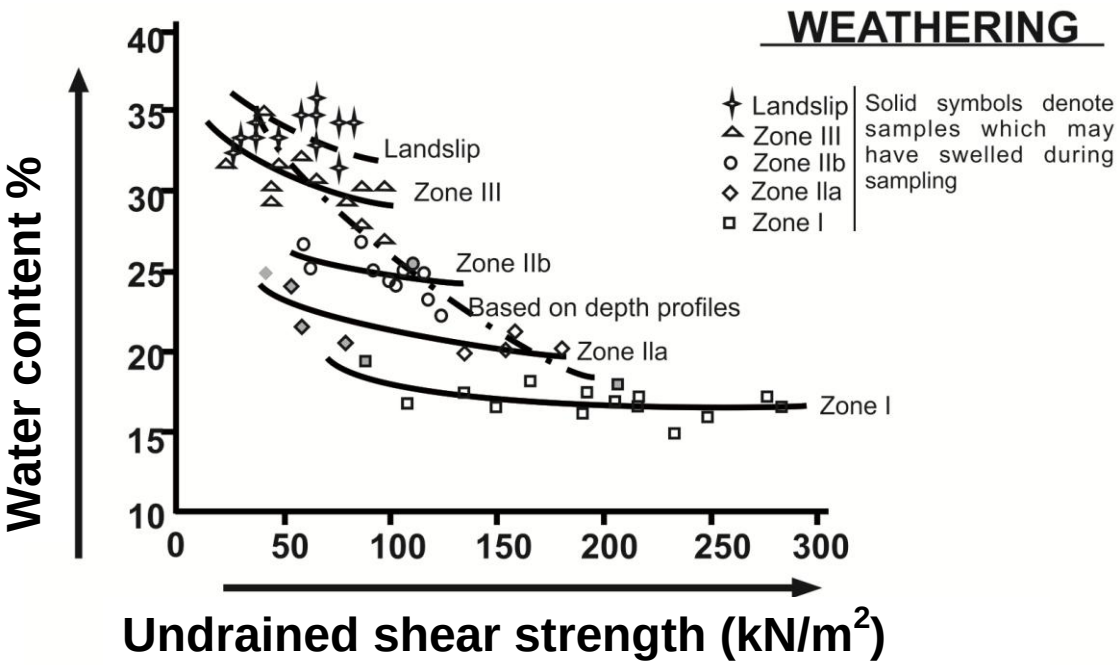

Figure 3.2 Weathering zones from Taylor & Cripps (1987) modified.

PREVIOUS STUDIES ON SLOW-MOVING LANDSLIDES IN SOUTHERN ITALY

A key problem in landslides investigation is represented by geotechnical and mineralogical properties of the involved material (Summa et al., 2010). As reported below, several authors in the past analyzed slow moving landsides by considering both these features.

BISACCIA LANDSLIDE (AVELLINO PROVINCE, SOUTHERN ITALY)

At Bisaccia, a reactivation of previous landslide occurred in 1980 after the Irpinia-Basilicata earthquake.

Bisaccia movements mainly occur in correspondence of two deeply valleys *Vallone Corvi* and *Vallone Ferrelli,* located respectively at the east side and the west side of the Bisaccia village. Although these two valleys have similar geomorphic setting, *Vallone Ferrelli* is characterized by higher grade of activity (Fig. 3.4).

Geological setting: Bisaccia is built on the top of a hill characterized by relatively competent cap rock (Parise & Wasowski, 1999). The area is characterized by the presence of two main lithologies: *Argille Varicolori* of Late Cretaceous-Paleogene age and *Marne di Toppo Capuana* of Tortonian age (Fiorillo et al., 2006). *Argille Varicolori* are characterized by a wide spectrum of lithologies including marly clays, clayey marls, calcarenites and clay-shales, with interbedded blocks of sandstones, calcarenites and calcareous marls (Fiorillo et al., 2006) *Marne di Toppo Capuana* are characterized by interbedded greenish-gray marls, silts and thin sandstone layers (Di Nocera et al., 1995).

Figure 3.3 Landslide-inventory map of Bisaccia (modified after Fiorillo et al., 2006).

Mineralogical and geotechnical analyses: Several analyses have been carried out by several authors in the studied area (Fenelli & Picarelli, 1990; Di Maio & Onorati 2000a,b), to obtain information about the main geotechnical and mineralogical features of the involved material (e.g. Grain size distribution, Atterberg limits., Specific Surface termination, Compressibility test, Direct shear test, Ionic diffusion test, Triaxal tests). Although no specific mineralogical analyses have been carried out on the material involved in this phenomenon, geotechnical analyses put in evidence a behavior similar to the Norway quick clays, *Active clays* (see 6th chapter " Results") which are mainly constituted by montmorillonite (Maggiò, 2003). Quick clays are defined as glaciomarine clays whose structure collapses completely at remolding and whose strength reduces almost to zero. Most of them were formed in sediments deposited in sea water during the last deglaciation and are rich of salts (Rankka et al. 2004).
The authors (Maggiò & Pellegrino, 2002; Maggiò, 2003) observed that the clays involved in the Bisaccia landslide were subjected to salt leaching, because weathering acted by washing the sediments, generating an increase of the pore water, which promoted the lack of counterbalancing charge from salts. This phenomenon was responsible of clay particle repulsion and realignment into an extremely weak and unstable structure.
The consequently reduction in strength made the slope prone to landslides.

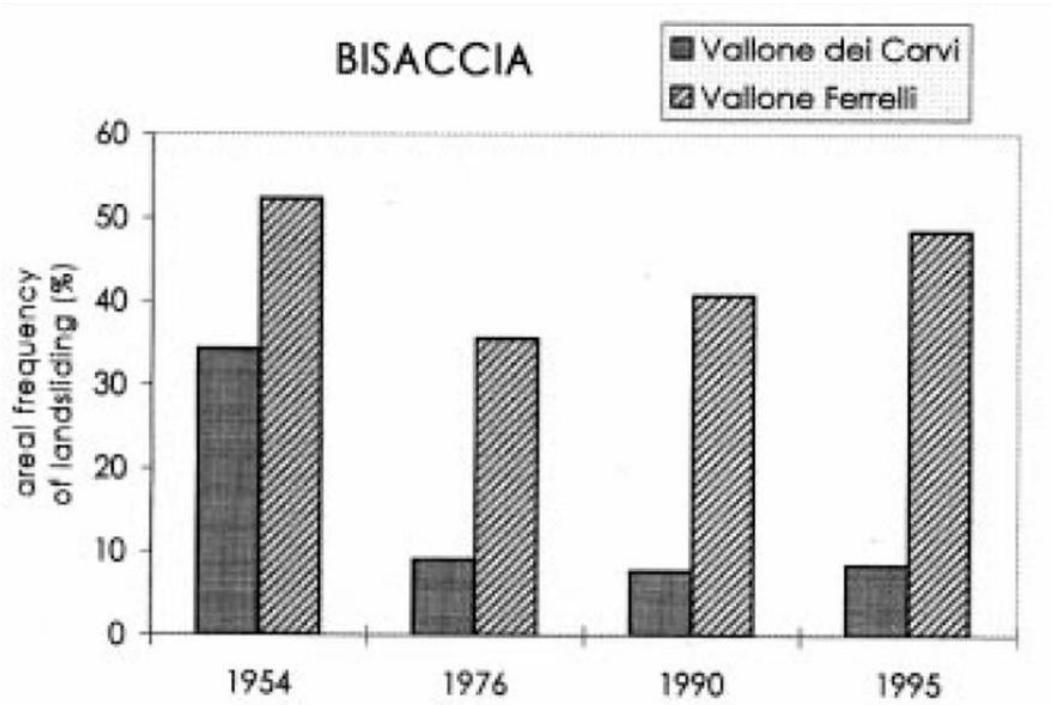

Figure 3.4 Areal frequency of active landsliding in Vallone Corvi and Vallone Ferrelli (Bisaccia area). Modified from Parise & Wasowski (1999).

Ground stabilization activity: If salt is added to these clays, they regain strength rapidly, because of the property of clay particles to form complexes one to another. Consequently, salt intrusions were artificially carried out in the area in correspondence of an experimental field around the main landslide with the aim to invert the leaching process described above and to increase the clay strength (Maggiò & Pellegrino, 2002).

AGNONE LANDSLIDE (ISERNIA PROVINCE, SOUTHERN ITALY)

A huge reactivation of the pre-existing Agnone landslide occurred in 2003 after intense rainstorms and snow-melt between *Colle Lapponi* and *Piano Ovetta*. This landslide was classified as a complex movement consisting a roto-translational slide which evolved in an earth flow. The landslide caused several damage to rural buildings and the local road network.

Geological setting: the area affected by the Agnone landslide is characterized by the presence of a structurally complex formation known as Agnone Flysch, of Upper Miocene Age (Calcaterra et al., 2008). The lower part of the Agnone Formation crops out in the landslide area and it is mainly constituted by an interbedding of marly clays, clayey marls, as well as silty-sandy clays and sands.

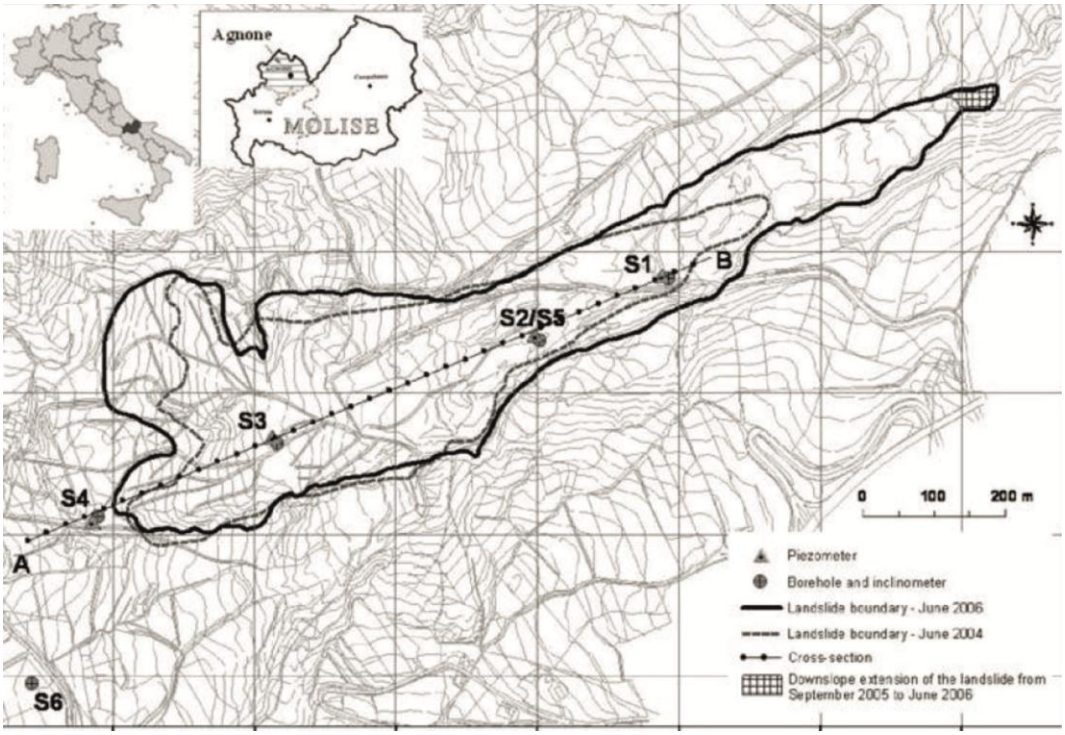

Figure 3.5 Plane view of the Colle Lapponi landslide (modified from Calcaterra et al., 2008).

Mineralogical and geotechnical analyses: geological survey, in situ geotechnical monitoring and mineralogical and geotechnical laboratory tests were performed. Moreover, during 2006, 26 boreholes were drilled and Casagrande piezometers and inclinometers were installed.

Thanks to topographical survey, surficial displacements ranging between 20 and 76 cm have been measured. Field activity in the toe zone allowed to verify that between September 2005 and June 2006, an extension of about 70 m of the landslide occurred (Calcaterra et al. 2008). As a whole the landslide was characterized by intermittent movement at the time of the survey.

XRPD analyses carried out on selected samples evidenced the occurrence of mixed layer I/S in the landslide material. On the basis of the mineralogical variations between the samples, in the local stratigraphy, three main grades of weathering were distinguished, which were correlated with the sliding surfaces (Calcaterra et al., 2007).

The main geotechnical parameters (e.g. Specific gravity, liquid limit, plastic limit, plastic index, γ_{sat}, γ_{dry}) were evaluated on different material involved in the landslide. On the basis of the obtained results, the authors considered that the particular mineralogical composition of the material involved in the analyzed material was decisive in the development of the landslide.

CHAPTER 4

THE TERMINI NERANO LANDSLIDE

The Termini Nerano landslide, object of this research, is located in Italy, in the Campania region, Massa Lubrense municipality. Considering the kinematic features of this phenomenon, it represents a clear example of slow-moving landslide.

The 1963 event was firstly analyzed by Cotecchia & Melidoro (1966), and no further analyses have been later carried out. A description of the main features of the analyzed area is reported here below.

GEOLOGICAL SETTING

The Termini Nerano landslide is located in the Southern Apennines.

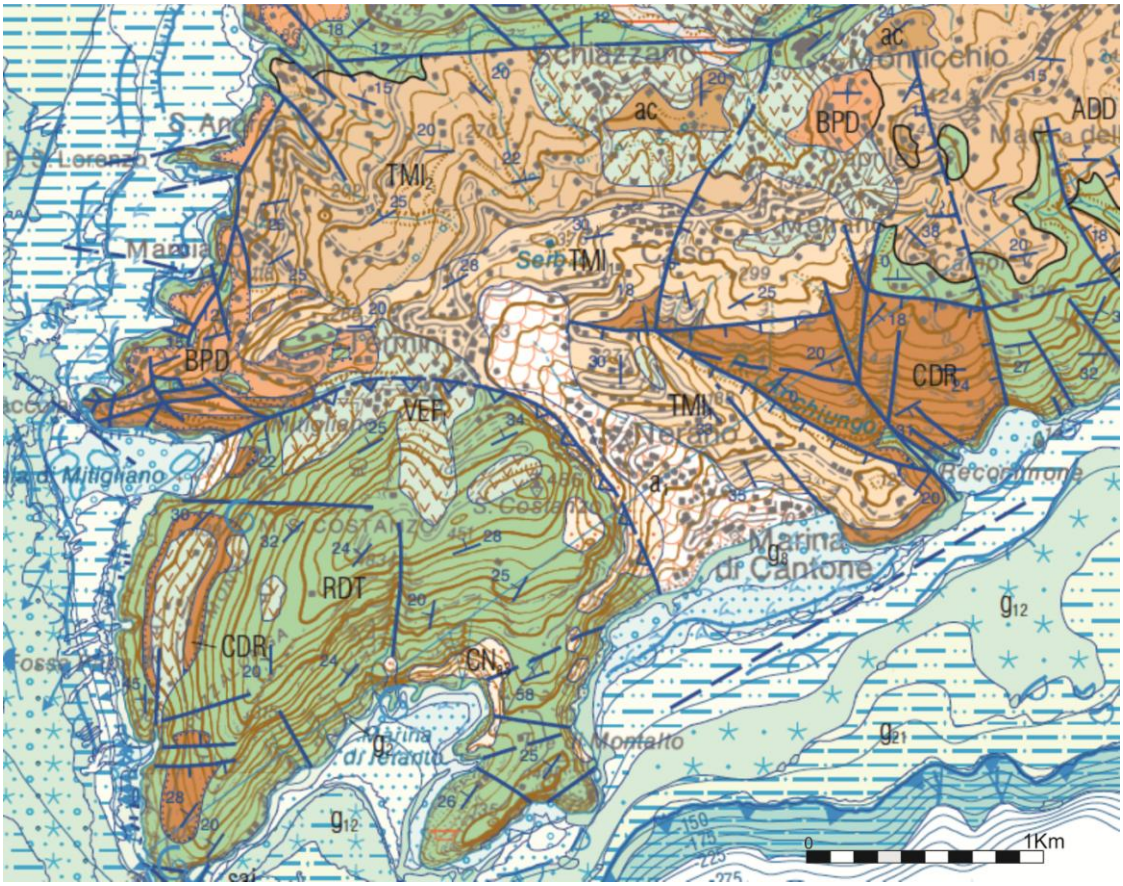

Figure 4.1 Exeprt from sheet N° 446. TMI= Termini sandstone, CDR= Recommone calcarenite, RDT= Radiolitidi limestone, a_1 = landslide deposits, BPD= Punta del Capo breccias, VEF= Vesuvian Phlegrean Synthem.

The Southern Apennine is an Adriatic-verging fold and thrust belt, derived from the deformation of the African passive margin (Pescatore et al., 1999) occurred during the Oligocene Early Miocene age (Pescatore et al., 1999). Its structural

setting represents the result of compressive and extensive tectonic events (Bonardi et al., 2009).

Different and sometimes opposite models have been proposed by several authors for the paleogeographic restoration of the Southern Appenines (Selli, 1962; Scandone, 1967; Ogniben, 1969; D'Argenio et al. 1973, 1975; Sgrosso, 1986, 1988, 1996, 1998; Mostardini & Merlini, 1986; Patacca & Scandone, 2007; Mazzoli *et al.* 2008). The simplest has been proposed by Mostardini and Merlini (1986). The authors recognized six paleogeographic domains, from west to east: Tyrrhenian Basin, Apenninic Platform, Apulia Basin and Outer Apulia Platform which corresponds to the present Southern Apennines foreland. Selli (1962) and Scandone (1967) proposed a different restoration, considering that the Lagonegro Units derive from an oceanic realm located in the west side of the Apenninic Platftorm together with the Ligurian (= North Calabrian), Sicilide and Molise Units. Sgrosso (1986, 1988, 1996 1998) proposed a more complex paleogeographic restoration by considering five platforms and five basins existing during Mesozoic and Paleogene age, between the internal oceanic basin and the Apulia Platform (= Outer Apulia Platform of Mostardini & Merlini, 1986).

Following recent views, the chain architecture can be considered as a complex duplex system with enclosed several tectonic units of the Adria plate (Bonardi et al., 2009). The Southern Apennine tectonic units include Mesozoic-Tertiary shallow water to slope- facies carbonates, which are part of the Apennine and Apulian carbonate platforms, and a pelagic basin succession also known as Lagonegro succession (Mazzoli et al., 2008; Bonardi et al., 2009; Vitale et al., 2010).

The studied area is located on the southern side of the Sorrento Peninsula, within the municipality of Massa Lubrense in the area of Termini, Nerano and Marina del Cantone villages.

Most of the outcropping terrains belong to the *Monti Lattari-Picentini* tectonic unit, which is a part of Apennines Carbonate platform. The *Monti Lattari Picentini* unit was subdivided in 10 formations (Iannace et al., in press.): *Dolomia Superiore, Calcari a palaeodasycladus*, *Calcari e dolomite con selce dei Monti Mai*, *Calcari oolitici ed oncolitici*, *Calcari con cladocoropsis e clypeina*, *Calcari con requienie e gasteropodi*, *Calcari con Radiolitidi, Calcareniti di Recommone*. *Arenarie di Termini*. *Brecce di Punta del Capo* belong to Syn-orogenic Unit.

Here below, the main charcateristics of the lithologies outcropping in the study area are reported.

Calcari con Radiolitidi (RDT): this formation is constituted by alternating gray dolostones, limestones and rare intrabasinal. Between *Punta del Capo* and Massalubrense, medium bedded intensively bioturbated, up to pseudobrecias, vacuolar calcareous and dolomitic lithofacies, with greenish marly matrix, are present. The formation is about 1100 m thick and indicates proximal to distal open platform environment, with local intra-platform scarps.

Age: Upper Aptian p.p. – Santonian

Calcareniti di Recommone **(CRD):** this formation mainly outcrops in proximity of *Punta Vaccola* in the Reccomone area and is mainly constituted by bioclastic and glauconitic calcarenites with ostreids, pectinids and Miogypsina sp. The thickness of this formation ranges between a few meters to some tens of meters. In the upper part, calcarenites become arenaceous with grains of quartz and white mica. Gradually the formation passes to the overlaying sandstones through increase in the silico-clastic fraction and reduction in the carbonatic fraction.
Age: Burdugalian (?)-Serravallian (?).

Arenarie di Termini **(TMI):** this formation indicates a deepening siliciclastic platform environment. Its thickness reaches 160-220 m
The *Arenarie di Termini* formation is subdivided in two members: *Membro delle Arenarie di Termini* and *Membro delle Arenarie di Nerano.*

- ✓ *Membro delle Arenarie di Nerano*: it represents the lower level of the *Arenarie di Termini* formation and consists of greyish coarse-grained, medium to thick-bedded arkosic sandstones, more or less rich in calcareous clasts. The thickness of this member reaches about 60-70 m.
  Main fossil contents: Neogloboquadrina continuosa (BLOW), Globorotalia praemenardii CUSHMAN & STAINFORTH, Globorotalia scitula (BRADY), Paragloborotalia siakensis (LEROY), Globoquadrina dehiscens dehiscens (CHAPMAN, PARR & COLLINS), Globigerina falconensis BLOW, Globigerinoides trilobus (REUSS) Globigerinoides bisphericus TODD.Age: Serravallian.

- ✓ *Membro delle Arenarie di Marciano*: this member grades into middle-fine-grained, grayish, thin to medium-bedded, arkosic sandstones, with frequent centimetric sized siltite and pelitepe layers. In the upper part slumping and olistoliths of Sicilide terrains are recognizable. This member results about 100-150 m thick.
  Age: Seravallian (?)

Brecce di Punta del Capo (BPD): it has been defined as a syn-orogenic unit mainly constituted by breccias and conglomerates, with yellowish sandy conglomeratic matrix and up to decameter-sized clasts, which consists of Miocene calcarenites and Cretaceous limestones, unconformable on the underlying rocks. Breccias and conglomerates deposited in an up-thrust basin, located on the Miocene and Cretaceous terrains, occur. The thickness of this formation can reach about 300 m. The formation closes the stratigraphic succession.

HISTORICAL LANDSLIDES IN THE STUDIED AREA

The study area has been affected by several landslides before the 1963 event.

The oldest phenomenon is dated to 1910 as reported by Cotecchia & Melidoro in 1966. The subsequent event occurred in the eastern part of the Termini village in 1936.

In 1939, several reactivactions have been recorded. Little lakes located near an area called *"Pozzo del Prete"* were associated to these phenomena.
Between the end of December 1940 and January 1941, a wide landslide occurred, as a consequence of intense and long-duration rainfalls. The phenomenon destroyed the Termini-Capo d'Arco road, few houses and the S. Croce church.
Between 1954 and 1955 the stabilization of the slope was made up by using gabions, deep drainages, and a surface drainage network (Cotecchia & Melidoro, 1966).
The surrounding areas have been affected in the course of time by some rock-falls as the one happened in 1973 along *Mt. San Costanzo*.
The last reactivation of the slow moving landslide occurred in 1963. The phenomenon is described in detail here below.

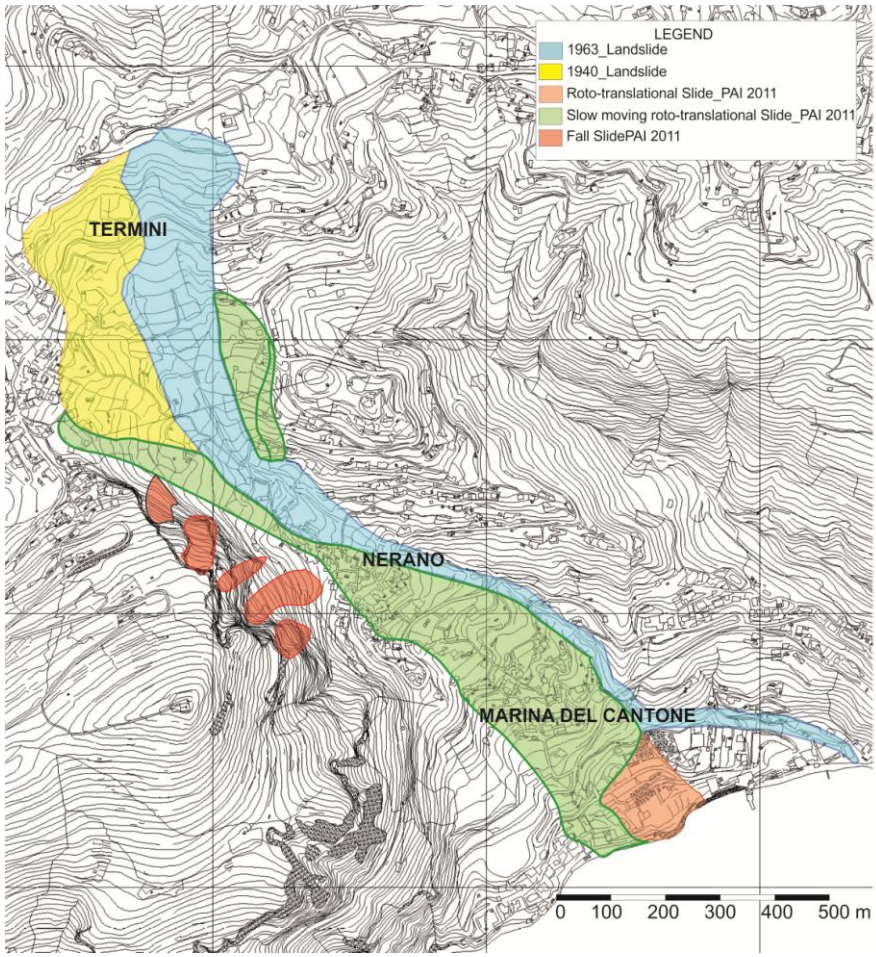

Figure 4.2 Excerpt from Landslides Invetory maps IFFI project, PAI 2011 (*Piano Stralcio per l'Assetto Idrogeologico*/hydro-geomorphological risk management plan).

1963 LANDSLIDE: MAIN FEATURES

The last historical event recorded in the Termini Nerano area occurred in 1963. The triggering event was represented by a long-duration rainfall.

The movement started on 19th February of the 1963 after about four rainy days (Fig. 4.3), and went on until 25th February.

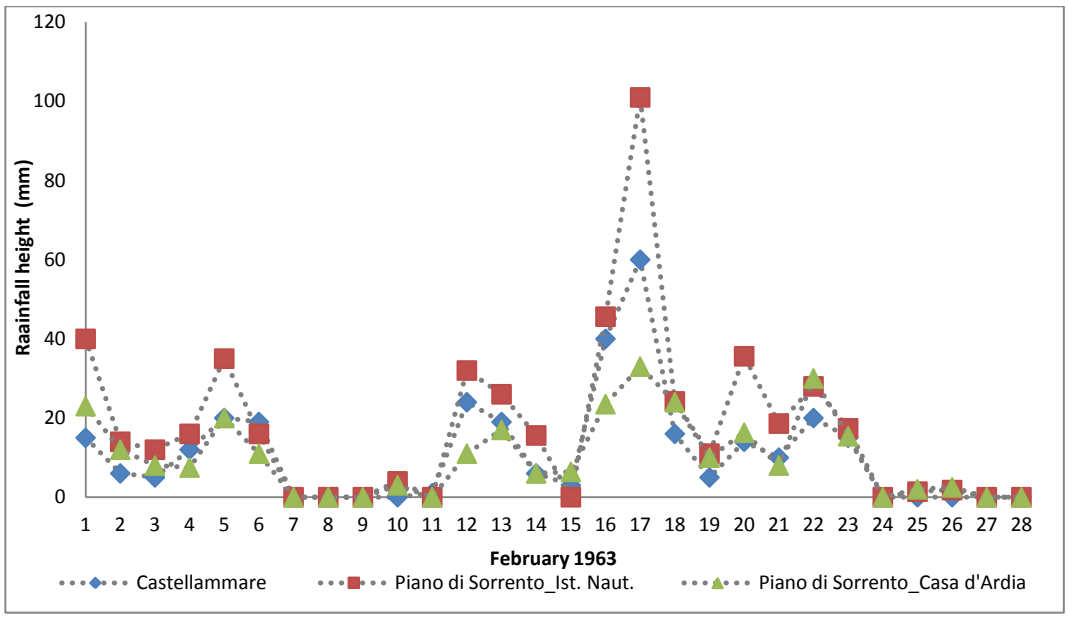

Figure 4.3 Daily rainfalls values recorded at the rain gauge stations surrounding the analyzed area.

The Termini Nerano landslide can be defined as complex movement (Cotecchia & Melidoro, 1966; Cruden & Varnes, 1996), which started as roto-translational landslide and evolved in a fast flow, overlapping the material deposited during the 1940 event. The total landslide length has been estimated in about 1900 m, from the crown zone to the shore in correspondence of the Marina del Cantone village. As reported by Cotecchia & Melidoro (1966), the 1963 phenomenon involved about $1x10^6$ m^3 of material characterized by alternance of shales and sandstones belonging to the *Membro delle Arenarie di Nerano*.

Figure 4.4 View of 1963 Termini Nerano landslide (After Cotecchia & Melidoro, 1966).

The authors also reported information about rates of movement (Table 4.1).

Table 4.1 Rates of movement of 1963 Termini Nerano landslide (after Cotecchia & Melidoro, 1966).

Reached distance (m)	Rate of movement (m/h)	Slope angles (°)
400	9	12
50	3	17
150	7	14
700	27	10

Seismic analyses, carried out in the area after the event, showed that the deepest slip surface occurred at about 25 m of depth (Cotecchia & Melidoro, 1966).
Mineralogical and chemical analyses have been also carried out on a set of three samples collected on the studied area after the 1963 event. By XRPD (X-ray powder diffraction) analysis, illite and quartz were considered as the main phases occurring in the samples. The main results obtained by X-ray fluorescence analysis are listed (Table 4.2).
Dubious geotechnical analyses were also carried out on the same samples. (Cotecchia & Melidoro, 1966).

Table 4.2 Whole rock chemical data by Cotecchia & Melidoro (1966)

Sample ID	1	2	3
SiO_2	53.30%	53.62%	48.09%
Al_2O_3	18.33	21.23	15.13
Fe_2O_3	6.25	5.05	}7.63
FeO	2.57	2.17	
MnO	0.28	0.1	-
MgO	3.22	2.86	2.45
CaO	2.18	0.92	8.65
Na_2O	0.51	0.55	1.48
K_2O	4.17	3.51	2.59
H_2O^-	0.5	0.3	1.28
H_2O^+	6.07	6.60	5.73
CO_2	1.47	0.51	6.25
TiO_2	1.14	1.41	0.52
P_2O_5	0.46	0.40	-
SO_3	0.12	0.99	-
Cl	0.07	TR	
$CaCO_3$	3.34	1.16	14.21

Notes: - : not determined
TR: the element occurs in trace.

CHAPTER 5

ANALYTICAL METHODS AND TECHNIQUES

Several analytical methods have been used to obtain a complete investigation and analysis of the area affected by the Termini Nerano landslide, consisting of fieldwork activities, sampling and laboratory testing.

To obtain information about the main landforms of the area, a geological survey has been carried out. Boreholes and geophysical analyses allowed to investigate the subsurface of the landslide area in term of geological and stratigraphical features. Aerial photo analysis allowed to assess the landslide evolution.

A set of 34 borehole samples has been used, for mineralogical and geotechnical analyses.

Rheological analyses have been performed to obtain information about the flow behaviour of the material involved in the landslide.

GEOLOGICAL SURVEY AND SAMPLING STRATEGY

General Outline

A geological survey represents the preliminary activity to recognize the main landforms and, in the case of an area affected by slow moving landslides, to evidence damage to infrastructures and buildings. It also represents a useful tool to plan an in situ investigation campaign giving information about its logistic aspects. The number and the type of boreholes, as well as their location, should be carefully assessed on the basis of the aim of the research, and the characteristics of the investigated area. Continuous core drilling allows to obtain information about the stratigraphy of the area whereas destructive drillcing is usually used to install instruments, such as piezometers and inclinometers. These two devices are both essential when studying an area affected by slow moving landslides, because they supply information about groundwater regimes and slope displacement.

Analytical Details

The geological survey of the area has been carried out on April 2012. Few months later, between July and August 2012, five boreholes have been drilled, three of which with a core drilling technique and two with a destructive technique.

Table 5.1 Main drill core features. CC= continuous core; CD= destructive drilling core.

Locality	ID core	Sampling	Depth (m)	Instrument	Instrument depth (m)
Termini	Sc1	CC	26.00	Inclinometer	25.00
Termini	Sd3	CD	5.00	Piezometer	5.00
Nerano	Sc2	CC	24.00	Inclinometer	23.00
Marina del Cantone	Sc3	CC	30.00	Inclinometer	29.00
Marina del Cantone	Sd1	CD	30.20	Piezometer	30.00

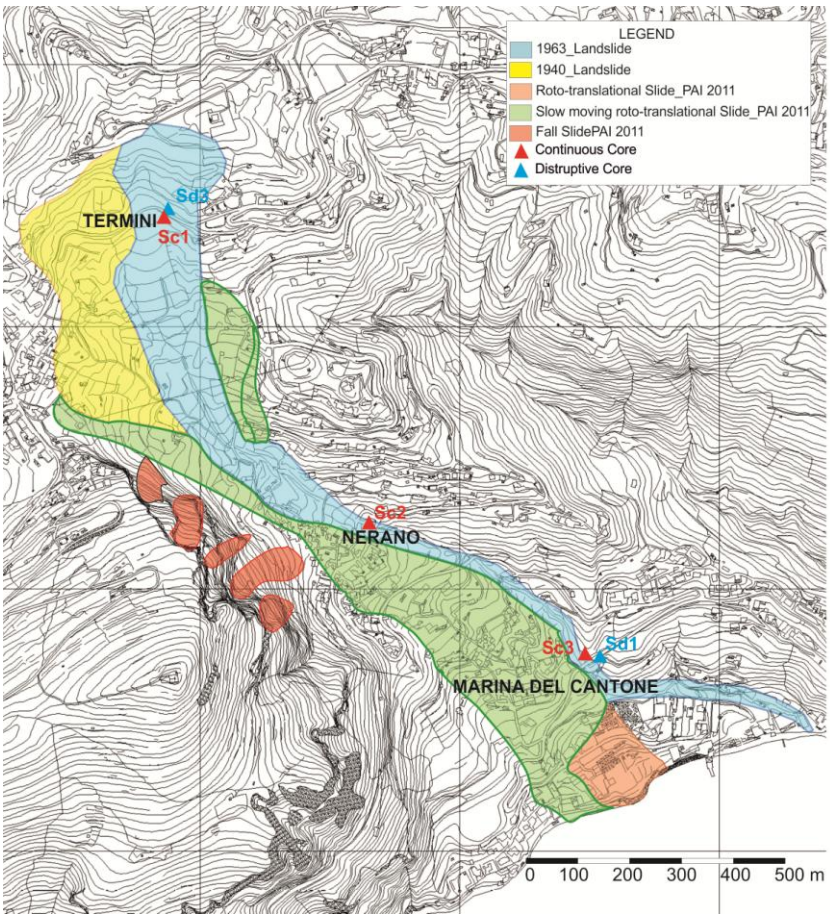

Figure 5.1 Excerpt from sheet No. 446 Sorrento.

To obtain an exhaustive knowledge of the area affected by the Termini Nerano landslide, the boreholes have been drilled in the crown, track and accumulation zones in proximity of Termini, Nerano and Marina del Cantone villages respectively (Fig.5.1). The technical features of the boreholes are reported in Table 5.1.

A CMV MK420 drilling has been used, characterized by a fully hydraulic, self erecting and self propelled equipment, designed to work with a wide range of drilling techniques e.g. micro piles, anchors, tie backs, soil investigation, rock drilling, soil mixing ext. Tronco-conical coring drills have been used (external diameter= 76 mm; length= 1500 mm; weight per linear meter= 12.7 kg)

The continuous boreholes have been carried out by using a single tube core barrel for dry material (external diameter= 101 mm; length=3 m) and a double tube core barrel for lithoid material (external diameter=100 mm; length=3 m). The sampled material has been stored into PVC core boxes.

Figure 5.2 Picture representative of the CMV MK420 machine used to perform the cores (a) and PVC boxes where the extracted material has been collected (c).

To obtain information about the groundwater level, Casagrande piezometers have been installed into destructive boreholes (PVC tube length =2 m) (Fig.5.3).

Figure 5.3 Casagrande piezometers installed in the studied area.

To monitor horizontal displacements, inclinometers have been installed following AGI (Italian Geotechnical Association) 1977 recommendations (Fig.5.4).

Figure 5.4 Inclinometers installation in the studied area.

From Sc1 and Sc2 cores, two undisturbed samples and two environmental samples have been collected, to perform geotechnical and biological analyses (Tab.5.4), by using the MAZIER sampler (external diameter=80mm; length=500 mm). In case of environmental samples, to avoid possible contamination of soil material sterilized steel dies were used as shown in the Figure 5.5.

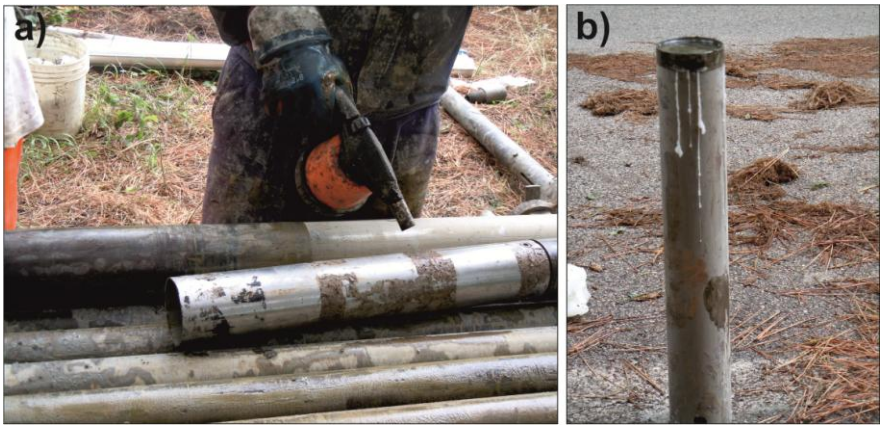

Figure 5.5 Undisturbed sampler. Each sampler tube has been sterilized by fire before sampling, to prevent contamination.

GEOELECTRICAL PROSPECTING

General outline

Geoelectrical prospecting represents a useful geophysical tool for the investigation of landslide areas, giving indirect information on the internal structure of soil and rock masses. This technique allows to reach depths ranging from 3 to 400 m, according to different experimental conditions..

The most common geoelectrical technique is the geoelectrical tomography (Telford *et al.*, 1990; Reynolds, 1997).

The *Apparent resistivity (*ρ) of the geological layers, between two electrodes, is evaluated on the basis of the following relation:

$$\rho = K^* V_{MN} / I_{AB} \quad \text{(Eq. 5.1)}$$

Where

- V_{MN} represents the difference of potential produced by circulation of a current I into the ground.
- I_{AB} represents the current transmitted into the ground by two electrodes A-B.
- k is a geometric factor which depends on the arrangement of the four electrodes.
- ρ is defined as the resistivity of a homogeneous ground which will give the same resistance value for the same electrode arrangement.

Multi-electrodes system is usually used. The obtained data are plotted versus the depth, by drawing isolines of apparent resistivity. The final result is a tomographic image of the subsurface along a selected profile.

In the current work the electrical tomography has been carried out by using the *dipolo-dipolo* array (Fig. 5.6).

This array consists of two current electrodes A-B and two potential electrodes M-N. The A-B distance is given by "δ" which is the same as the distance between M-N. *Dipolo-dipolo* array also considers the "n" factor which represents the ratio of the distance between A and M and "δ".
The "δ" value is initially kept fixed and the n factor is increased from 1 to 2 to 3 until up to about 6 in order to increase the depth investigation. The depth of investigation depends on the distance between the electrodes. Specifically the higher the AB distance the deeper the penetration of the current.

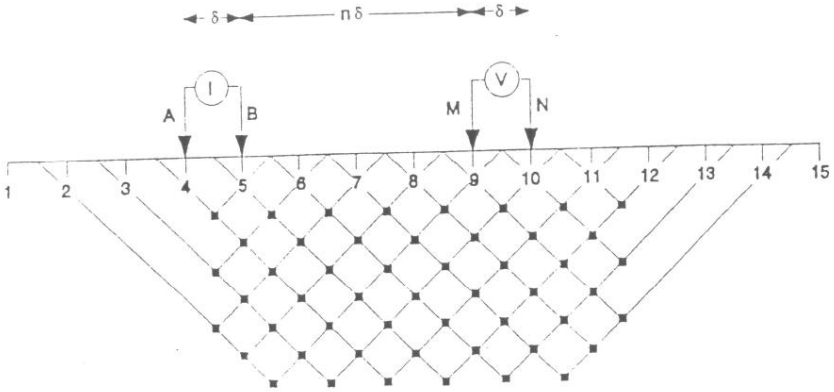

Figure 5.6 Typical *dipolo-dipolo* array.

Analytical details
In April 2013, a geoelectrical survey has been carried out by the G.G.I. s.a.s. company on the investigated area along two main profiles (Fig. 5.7).

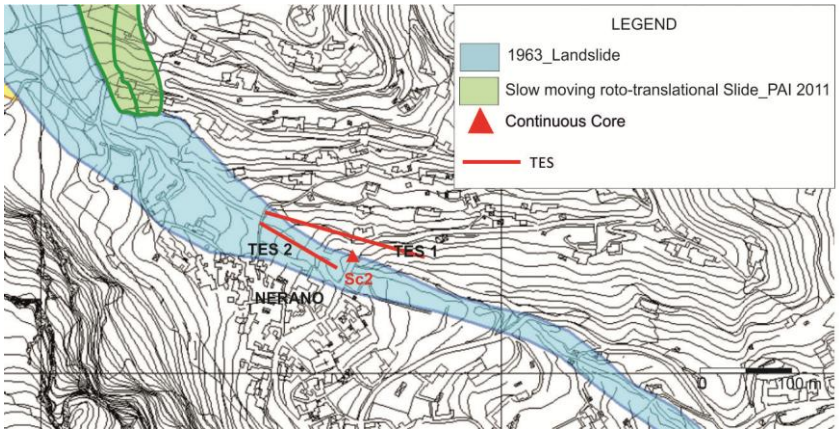

Figure 5.7 Location of two geoelectrical tomography surveys, TES1 and TES2.

The used equipment consisted of:

a) digital geo-resistivity meter for Multi-Electrode Tomography Model A3000-E m.a.e (advanced geophysics instruments) *http://www.mae-srl.it/prodotti/listprodotti/2/20/0*.
b) n°5 microprocessor boxes, for 8 electrodes.
c) n°5 Multi-polar seismic cables, low resistivity conductor.
d) n°40 steel inox electrodes.

The RES2DINV software has been used for the data analysis.

Table 5.2 Main features of the geoelectical tomography urveys.

	TES1	TES2
No. of electrodes	40	40
δ (m)	3	2
Total length (m)	117	78
Reached depth (m)	22	15

AERIAL PHOTOGRAPHIC INTERPRETATION

General outline

Analysis of the geo-morphological evolution of the studied area has been carried out through aerial photograph interpretation.

An aerial photograph represents an instantaneous record of the ground details. The geological interpretation is based on the analysis of color texture, pattern and shape and size of the main landforms. The amount of geological information that can be obtained from aerial photography is mainly dependent on the type of terrain (igneous, metamorphic, or sedimentary), climatic environment, and stage of geomorphic cycle of an investigated area (Ray, 1960).

Black/white aerial photos are commonly used for geological interpretation of the ground surface, land use, and engineering geology. Color infrared film and colored photogram have been recently developed, to take information about the water temperature or the lithological features of an area.

Analytical details

For this study black/white aerial photos were selected from the I.G.M (Military Geographical Institute) database. The available aerial photos were dated at 1955, 1974, 1990, 2003 hence covering a wide temporal range, before and after the 1963 landslide (Table 5.3).

Table 5.3 Aerial photo features.

ID photo	Year	Altitude (m, a.s.l.)	Scale
8823	1955	6000	36000
3004	1974	5900	41000
679	1990	6200	36000
9671	2003	4500	29000

MINERALOGICAL AND CHEMICAL ANALYSES

Mineralogical analyses have been carried out to identify the main mineralogical constituents, which characterize the material involved in the landslide. The quantitative evaluation of these phases has been carried out on drillcore samples

to point out possible variations along vertical profiles of minerals, which may have favoured the development of landslide slip surfaces.

X-RAY POWDER DIFFRACTION ANALYSIS

General outline

X-ray powder diffraction is a standard technique primarily used for the identification of crystalline or poor crystalline phases, forming natural or synthetic materials and mixtures.

X-rays are electromagnetic radiations characterized by a wavelength shorter than light, ranging between 0.1 and 10 Å (Cullity, 1978). They have been used for a variety of applications, and in geology for the mineralogical analysis of the rocks, because of their capability to investigate the fine structure of minerals, through the phenomenon of *X-ray diffraction* (Cullity, 1978).

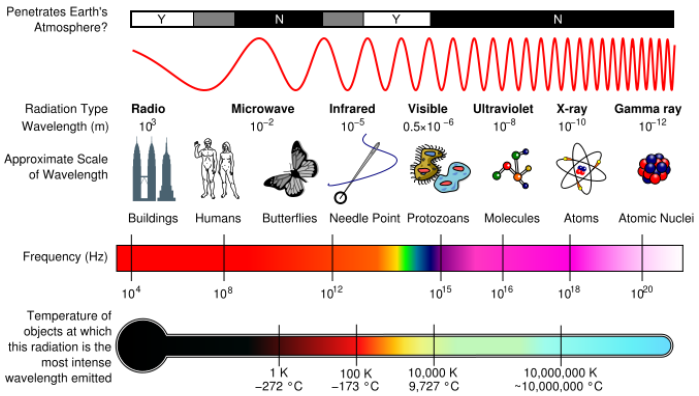

Figure 5.8 The electromagnetic spectrum.

The diffraction phenomenon is due to the existence of certain phase relation between two or more waves (Cullity, 1978). When a radiation beam bits atoms in a crystal structure, each of them re-radiates the beam in all directions. This phenomenon is known as "scattering" (Moore & Reynolds, 1997).

In 1912 Bragg postulated that the diffraction from a crystal can occur whenever the following law is satisfied (Bragg, 1913):

$$n\lambda=2d_{hkl}\sin\theta \quad \text{(Eq. 2)}$$

Where:

- n is an integer
- λ is the X-ray wavelength
- d is the lattice spacing
- θ is the diffraction angle

The Bragg's law defines a very strict relationship between λ and θ for any crystal or mineral structure.

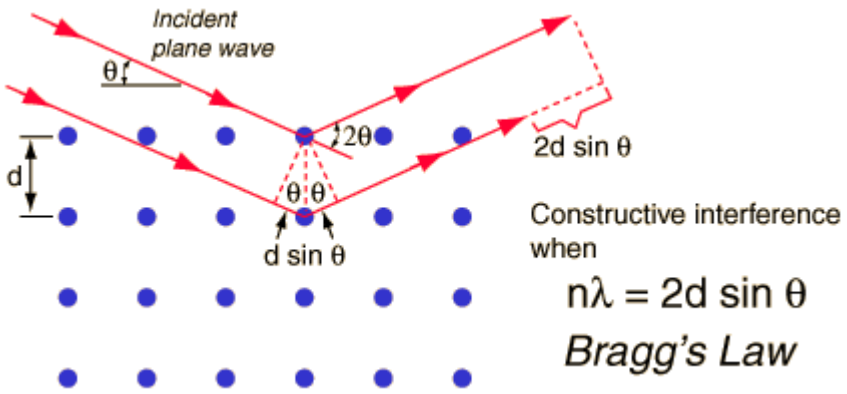

Figure 5.9 Bragg's Law.

The most common technique to apply the Bragg's law to identify unknown minerals in a powder is to use a X-radiation characterized by a specific wavelength, λ, to measure the diffraction angle θ of the radiations diffracted by the powder, and to compare these angles with a database listing the diffraction angles of scheduled mineral phases, which depend by their d-spacing (Cullity, 1978). The instrument which allows to carry out this analysis is called diffractometer.

The most widespread diffractometers are based on the so-called "Bragg-Brentano (semi-) focalizing geometry". Two settings are possible, i.e. θ/θ and θ/2θ types with horizontal or vertical geometry. In θ/2θ diffractometer, both sample and detector move with angular velocities equal to 1:2. In θ/θ diffractometer, the sample does not move, whereas the X-ray tube and the detector rotate with the same angular velocity (Cullity, 1978; Moore & Reynolds, 1997).

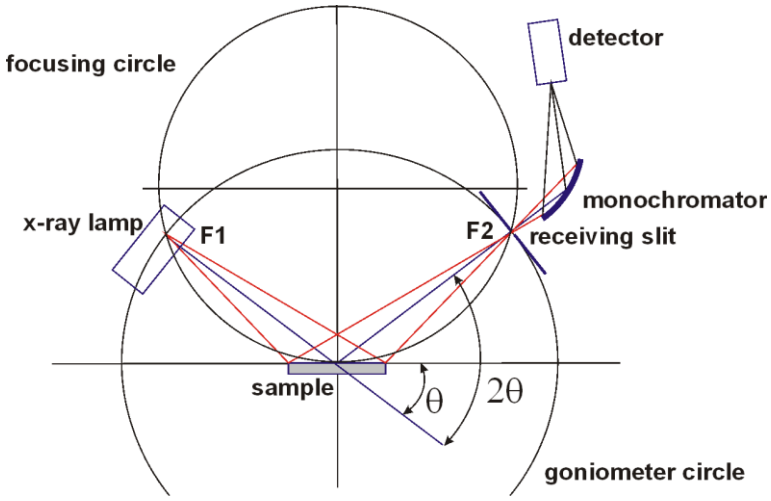

Figure 5.10 Brag- Brentano focalizing geometry. The goniometer or diffractometer circle is defined by the source (f) and receiving slit (G) and has fixed radius. The sample (S) is located in the central part of the diffractometer circle and is tangent to the focusing circle.

Although different geometries are possible, all the instruments are composed of the same basic components:

- X-ray source (X-ray tube)
- collimation system
- goniometer
- sample lodge

- X-ray detector (± radiation monochromator).

The X-ray tube produces a X-ray beam, by streaming electrons across a high voltage potential (15-45 kV). Current is applied to a tungsten filament (cathode) in a vacuum. Electrons are then accelerated into a metal target (anode), producing X-ray radiations. The most common anode materials are Cu and Mo (heavily absorbing sample), Co (for ferruginous samples), Fe, W and Cr.

X-ray powder diffraction (XRPD) analyses are reported on a XY diagram, where the horizontal scale is calibrated in °2θ and the vertical scale shows the intensity of the diffracted X-rays. XRD patterns of a mono- or poly-crystalline matrix are constituted by a sequence of characteristic peaks, with various intensities at specific 2θ positions. Each sequence of peaks is diagnostic for each mineral structure, in agreement with the Bragg's law. Comparing the XRPD pattern of any crystalline mixture, as a rock sample, with the standard minerals of available database, it is possible to identify the mineral compounds by an automated search-match procedure between the measured peaks and the standard ones. Several databases exist, among which worldwide used are the ICDD-PDF (International Centre for Diffraction Data, PDF Powder Diffraction Files) and the ICSD (Inorganic Crystal Structure Database).

When used for rocks, X-ray powder diffraction analysis allows to identify both their qualitative mineralogical composition and the quantitative abundances of minerals constituting the powder. Computational methods, like those based on the intensity peak ratio or on the internal standard reference intensity ratio (RIR), or Rietveld method, allow to evaluate the relative amount of the minerals.

The internal standard method is based on the comparison, in the intensity vs. °2θ diagram, between the intensities of peaks of minerals occurring in the original sample and a single reflection intensity of a mineral that has been previously mixed into the powder in a specific amount.

The so-called RIR method represents an evolution of the internal standard method, and provides an analysis of all the phases in a powder. It is assumed that the sum of all the mineral weight fractions equals 1.0.

The Rietveld method is based on the "whole pattern profile fitting", which consists on the progressive comparison between the experimental XRPD pattern and calculated profiles, obtained varying the scale factors of each phase occurring in the sample, (Snyder & Bish, 1989; Moore & Reynolds, 1997).

Analytical details

For the present work XRPD analysis has been carried out by means of the following instrument:

- Panalytical X'Pert Pro, equipped with RTMS X'Celerator detector (CuKα radiation; 40 kV Tube tension , 40mA) Soller slits 0.04 Rad. The data were collected between 4 and 50÷80°2θ angle by using 0.017°2θ equivalent steps X-Celerator detector RTMS and 60 seconds per degree step size (DiSTAR lab., University of Naples Federico II).

- Philips PW1730 (CuKα radiation; graphite secondary monochromator; 40 kV, 30 mA) with incident and diffracted-beam Soller slits 0.04 Rad. The data were collected between 3-35°2θ angle by using 0.02°2θ steps and 2

seconds per degree step size (DiSTAR lab., University of Naples Federico II).

- Bruker D8 Advance X-Ray diffractometer equipped with incident and diffracted-beam Soller slits a SolX solid-state Si(Li) energy dispersive detector (CuKα radiation, 45 kV, 35mA). The data were collected between 2-70°2θ angle by using 0.02°2θ steps and 2 seconds per degree step size (Indiana University lab.).

- Siemens D5000 powder diffractometer (CuKα radiation; graphite secondary monochromator; 112 kV, 31 mA). The data were collected between 2-70° by using 0.02°2θ steps, and 1 second per degree step size. (IMAA-CNR of Tito Scalo (Potenza, Basilicata)).

Figure 5.11 a) Diffractometer used at University Federico II, Naples; b)Diffractometer used at Indiana University of Bloomington (US).

Qualitative analyses have been carried out on bulk samples and clay fraction by using the Panalytical High Score Plus 3.0 software.
Quantitative analyses have been carried out on bulk samples, by using the Bruker TOPAS software, and tested with chemical analyses, by using the Vb Affina software.
Bruker's TOPAS software has been used to estimate the mineral abundance and unit cell parameters of the major phases. It allows to quantify the amount of phases, controlling the errors affecting the peak position as well as the specimen displacement, the preferred orientation, and crystallite size and strain. Combined RIR and Rietveld methods have been used for the quantitative analyses. An amount of 20 wt.% corundum has been added to the samples as internal standard.
It is worth to note that Topas software usually reaches the best results for the evaluation of materials constituted by strongly crystalline mineralogical phases. In the case of samples composed of poorly crystalline phases, like clay minerals and mixed layer phyllosilicates, TOPAS software evidences some working problems, and overestimates or underestimates the amounts of mineral phases. For this reason, an experimental software named Vb Affina has been used.
Vb Affina is a Microsoft Visual basic 6.0 computer program for the quantitative mineralogical analysis of clayey sediments. It controls the amount of phases by combining chemical analyses (e.g. XRF) and XRPD data (Leoni et al. 2008).

The progressive match of mineralogical and chemical data allows to obtain more accurate results.
A set of 34 samples has been selected from the three boreholes (tab.4) on the basis of two parameters:

1) depth
2) stratigraphy

XRPD analyses have been also carried out on the same material used for the evaluation of the Atterberg limits.
The analyzed samples have been prepared after the procedures described in Moore & Reynolds (1977).
Specifically for bulk samples analysis the material has been disaggregated in an agate mortar to obtain a homogeneous powder (particle size <200μm). An amount of 20 % wt. corundum (α-Al_2O_3, Buehler micropolish, 1 μm grain size) has been added for quantitative analyses. The obtained corundum-specimen mixture has been subsequently micronized (grain size < 10 μm) by using Mc Crone Micronising Mill, with agate cylinders and 10 mL of deionized water for 15 min of grinding time. This technique was used to avoid orientation related problems, primary extinction or crystallite size which usually affect clay minerals (Klug & Alexander, 1974; Bish & Chipera, 1988; Srodon et al., 2001).

Figure 5.12 Agate mortars.

The extraction of the clay fraction has been carried out by using three different techniques, at Department of Earth Sciences, Environment and Resources (DiSTAR) University of Naples Federico II, at Department of Geological Sciences Indiana University, and at IMAA CNR, Tito Scalo (Potenza).
At DiSTAR, the clay fraction has been extracted as here described: about 30 g of crushed material has been placed in a plastic beaker (500 ml), and undergone to ultrasonic probe disaggregation for about 10 minutes by using a Sonoplus HD 2200. The suspension was then energetically mixed by hand, and after one minute the supernatant was transferred in glass beaker (500 ml), and the deposited material displaced in a Petri dish. This procedure was repeated after 5 minutes, 1 hour and 17 hours (Overnight). The overnight suspension was centrifuged using Hettich centrifuge universal 32, in two steps:

- 5 minutes at 5000 rpm → which allows to obtain a fraction ≤ 0.35 μm
- 40 minutes at 8000 rpm → which allows to obtain a fraction ≤ 0.2 μm

After these two steps, the resulting supernatant, representing the fraction <0.2 μm, was recovered and dried, to obtain a more concentrated suspension which was used to produce oriented mounts.

Oriented mounts were prepared following the Moore and Reynolds (1997) procedure, by using the smear glass slide method.

XRPD analyses have been carried out on air dried specimens, Ethylen-glycol solvatation (EG) at 60 °C for 8 hours, and heated at 375 °C for 1 hour (Moore & Reynolds, 1997) samples. This technique allowed to identify the clay minerals fraction, including mixed layers illite smectite (I/S) and mixed layers chlorite smectite (Chl/S) In fact, EG solvation expanded smectite layers from 15 Å to 17 Å, whereas heating the sample at 375°C produces a contraction of the same layers.

A similar procedure was adopted to threat the samples at the Indiana University, with the difference that the sampler was preliminarily disaggregated in a DI (deionized) water solution by using a Waring blender.

At the IMAA-CNR the procedure was slightly different. Crushed material was placed in glass blenders (length = 15.5 cm, internal diameter = 5.5 cm) and mixed with DI water by using a multi position magnetic stirrer. All beakers were allowed to settle the finest part of the sample. After 24 hours the clay fraction occurring in the supernatant was recovered and dried. About 200 mg of the clay fraction were selected and mixed to 1M of $MgCl_2$, by using *GFL 3005* shaker. After Mg-saturation the supernatant was centrifuged for 15 minutes at 4200 rpm. Oriented mounts were prepared after the Moore and Reynolds procedure.

Glycolated oriented samples were also used to obtain information about the grade of ordering of mixed layer (I/S), by considering the distance between the 001/002 and 002/003 reflections of the mixed layer I/S in glycolated patterns (Moore & Reynolds, 1997).

To verify the presence of chlorite and kaolinite, the clay fraction obtained after the method used at IMAA-CNR was heated at 500°C (Thorez, 1975; Moore & Reynolds, 1997) for about two hours. Although these phyllosilicates (kaolinite and chlorite) have different structures, the basal series of chlorite tends to superimpose on the members of the kaolinite *00l* series. The heating process causes dehydroxylation of the hydroxide chlorite sheet, changing the XRD pattern of this phyllosilicate, increasing the 001 reflection and weakening the 002, 003, 004 reflections (Moore & Reynolds, 1997). After heating, kaolinite becomes amorphous under the X-ray (meta-kaolinite), and its diffraction pattern disappears.

Table 5.4. Main sample features.

ID sample	Depth (m)	Lithology
PN1	3.30	Sand
PN2	4.70	Silty clay
PN3	7.00	Marly clay
PN4	8.90	Calcarenitic sandstone
PN5	14.00	Marly shale
PN6	16.50	Marly shale
PN7	18.50	Marly shale
PN8	23.00	Marly shale
PN9	24.90	Marly shale
PR1	3.00	Silty shale
PR2	4.50	Silty shale
PR3	6.00	Clayey silt
PR4	6.60	Calcarenitic sandstone
PR5	9.70	Sandstone
PR6	11.00	Sandstone
PR7	14.45	Calcarenitic sandstone
PR8	16.50	Calcarenitic sandstone
PR9	16.80	Calcarenitic sandstone
PR10	20.00	Calcarenitic sandstone
PR11	22.45	Calcarenitic sandstone
MC1	3.00	Clayey silt
MC2	4.50	Silty shale
MC3	5.20	Silty shale
MC4	7.00	Clayey silt
MC5	9.35	Silty sand
MC6	11.40	Silty sand
MC7	14	Silty shale
MC8	15.20	Clayey silt
MC9	16.90	Sandstone
MC10	18.50	Calcarenitic sandstone
MC11	19.00	Calcarenitic sandstone
MC12	23.00	Calcarenitic sandstone
MC13	25.60	Sandstone
MC14	29.00	Calcarenitic sandstone
SC1	21.00÷21.30	Marly shale
SC2	7.50÷7.85	Clayey silt
SC1*	21.30÷21.55	Marly shale
SC2*	7.85÷8.20	Clayey silt

Notes: PN samples were collected from Sc1 borehole, PR sample, from Sc2 boreholes MC samples from Sc3 borehole; SC1= undisturbed sample selected from the crown zone; SC2= undisturbed sample selected from the sliding zone; SC1* =environmental sample selected from the crown zone; SC2*= environmental sample selected from the sliding zone.

X-RAY FLUORESCENCE (XRF)

General outline

X-ray fluorescence analysis is a powerful analytical tool for the spectrochemical determination of almost all the elements present in a sample. This technique is extremely versatile for applications in many fields of science, research and quality control.

The working principle of XRF analysis is the measurement of wavelength or energy and intensity of the characteristic X-ray photons emitted from the sample, when atoms of any chemical element are irradiated with X-rays.

Considering that the energy is characteristic of each evolved element, their identification is possible as well as determination of their mass or concentration.

Analytical method

X-ray fluorescence analysis has been carried out by using Axios Panalytical instrument, controlled by Super Q 4.0J.L. software, at the DiSTAR and at Department of Earth Sciences and Geo environmental (University of Bari Aldo Moro) . By XRF analyses the weight % of the major elements (SiO_2, TiO_2, Al_2O_3, Fe_2O_3, MnO, MgO, CaO, Na_2O, K_2O and P_2O_5, in wt.%) as well as of trace elements (Rb, Sr, Y, Zr, Nb, Ba, Cr, Ni, Sc, V, La and Ce, in ppm) have been evaluated.

About 4 g of samples have been used, crushed by agate mortar, mixed with polyvinyl alcohol (at 10 % wt.) and oven dried (about 50° C per 48 h). The dried material was and crushed. The obtained powder was located into a metal sampler which was about ½ full of granular boric acid. Finally the sample was pressed at about 18 atm for about 20 seconds.

The bulk chemical evaluation has been carried out also considering the loss on ignition (LOI) parameter. It represent the weight reduction connected to the loss of water and carbon dioxide, obtained by drying the sample at 1100°C (for about two hours), into a muffle furnace.

SCANNING ELECTRON MICROSCOPE (SEM)

General outline

The scanning electron microscope (SEM) is an electronic instrument used for inspecting topographies of sample materials allowing a high-resolved and high-zoomed observation up to enlargements of 1-10 μm. This technique is based on the interaction between an incident electron beam and sample surface. The electron beam is focused and accelerated at high potential, by means of magnetic lenses, on the specimen, and its interaction generates several electromagnetic radiations such as backscattered electrons, secondary electrons, Auger electrons, characteristic X-rays, and visible light.

High-resolution imaging of surface morphology is generated by secondary electrons. The efficiency of production of backscattered electrons is strongly related to the material‘s atomic number. The higher the atomic number the brighter the material image.

For conventional imaging in the SEM, specimen must be electrically conductive, and electrically grounded to prevent the accumulation of electrostatic charge at

the surface, which generate surface artifact. The most used conductive materials are gold and graphite.

Analytical details

Secondary electron imagining by scanning electron microscopy (SEM) has been performed by using a Joel JSM 5310 instrument, at the Interdepartmental Center for Geomineralogical Analyses (CISAG), Federico II University of Naples. The analysis has been carried out on a set of 12 specimens to investigate the morphological characteristics of minerals, occurring in the landslide samples. The specimen were gold-coated and then mounted on a Al "*stub*", using a conductive glue

GEOTECHNICAL ANALYSES

A geotechnical study has been done on the same samples used for mineralogical analyses, to investigate the possible relationship between the clay mineral properties and the geomechanical parameters of the investigated material.

SPECIFIC GRAVITY TEST

General outline

The *specific gravity* is defined as the ratio between the density of a material (mass of a unit volume) and the density of water at 20°C (the mass of the same unit volume) (ASTM D 854-92).

The *Specific gravity of soil* is obtained from the specific gravity of the solid matter of the soil, and is designed G_s (ASTM D 854-92). Each type of soil is characterized by a specific G_s value (Tab. 5.5)

Table 5.5 G_S value for specific type of soils.

Type of soil	G value (kN/m^3)
Inorganic soil	25.48÷27.44
Lateritic soil	26.95÷29.40
Sand particles	25.97 ÷26.17
Inorganic clay	25.48÷27.44
Soil with organic matter or porous particles	<25.48

Specific gravity test is usually applied to crushed material passing the No. 4 sieve (Tab. 5.6) ((ASTM D 854-92).

The apparatus used for specific gravity test is made of:

- Pycnometer
- balance
- drying oven thermometer dessicator
- a system for removing the entrapped air, called vacuum pump.

The specific gravity G_s is evaluated by considering the following equation:

$$G_S = \frac{W_S}{(W_s + W_{bw} + W_{bws})} \quad \text{(Eq.5.3)}$$

Where

- W_s represents the weight of dry soil
- W_{bw} is the weight of the picnometer and water
- W_{bws} is the weight of picnometer,water and immersed soil.

Analytical details

The specific gravity has been carried out on a set of 29 samples at the DiSTAR laboratory of the Federico II Univerity of Naples, following the ASTM 854 procedure.

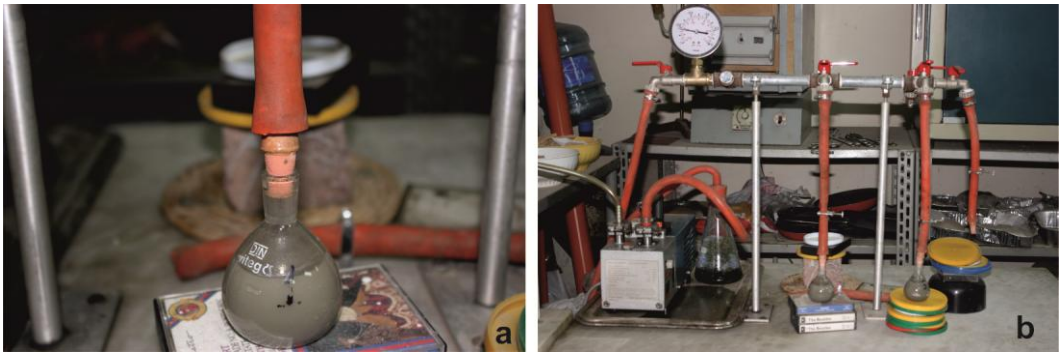

Figure 5.13 Specific gravity test; a) pycnometer; b) vacuu pump and picnometers.

Each sample has been dried to 100°C and crusched by hand, to obtain about 3-4 g of powder passing the No 4 sieve. The specimen has been mixed to dionized (DI) water into a picnometer. A vacuum pump has been used to remove the entrapped air. For each sample two tests have been carried out, and the average value has been considered as the final G_s value.

GRAIN SIZE ANALYSIS AND DISTRIBUTION

General outline

Grain size analysis test allows to determine the relative proportion of different grain sizes particles. It represents an useful tool in the soil classification.

Grain size analysis consists of two steps (ASTM 2217-85):

- Sieve analysis for particles with sizes retained by No. 200 sieve (<0.75 mm).
- Hydrometer analysis for particles with sizes passing through No. 200 sieve (<0.75 mm).

Sieving analyses are usually carried out on dry material. In case of shale soils or sandstones characterized by a high volume of clays, a wet sieving analysis is generally done, to simplify the separation of the various fractions.

The hydrometer analysis is based on the application of the Stokes's Law:

$$V = \frac{2}{9}\frac{(\rho_p - \rho_f)}{\mu} g r^2 \quad \text{(Eq.5.4)}$$

Where:

V is the particles' settling velocity (m/s)

ρ_p is the mass density (kg/m^3)

ρ_f is the mass density of the fluid (kg/m^3)
μ is the the dynamic viscosity (kg/m*s)
g is the gravitational acceleration (m/s^2)
r^2 is the radius of the sphere (m)

Analytical details

Wet sieve analysis has been carried out on a set of 29 samples, at the DiSTAR laboratory of the Federico II University of Naples, on the basis of ASTM procedures. The following set of sieves has been adopted (Tab. 5.6):

Table 5.6 Sieves used for grain size analysis.

ID sieves	sieve sizes (mm)
2"	50.00
1.5"	37.50
1"	25.00
3/4"	19.00
1/2"	12.00
3/8"	9.50
No. 4	4.75
No. 8	2.36
No. 16	1.18
No. 40	0.43
No. 50	0.30
No. 100	0.15
No. 200	0.75

Considering that material used for this study is expected to contain clays, wet sieving analysis was adopted.

Wet sieving process was carried out by sprinkling water through the sieves pile, by using a spray nozzle located above the uppermost sieve.

Figure 5.14 Grain size analysis apparatus; a) sieve; b) graduated glass cylinders; sieve stuck for wet sieve analysis.

Together with finest fraction of the soil, passes through the sieve stack and is collected in a collector, from an outlet located at the base of the sieves pile. The use of plastic rings between the sieves prevents the loss of liquid and sample material. The material collected into the sieves, as well as the material collected into the collector, was dried for 24 h at 100°C and weighted.

Hydrometer analysis has been carried out on the fraction of the soil smaller than 75 µm. The fraction was mixed with distilled water and a dispersing agent (sodium hexametaphosphate to 33% and carbonate sodium to 7%). The obtained suspension was placed into a graduated glass cylinder (1000 mL).

Relative different density was recorded on the basis of the timetable here below, by using a densimeter.

Table 5.7 Timetable for hydrometer analysis.

hour	minute
0.00167	1
0.0333	2
0.0833	5
0.250	15
1	60
2	120
4	240
24	1440
48	2880

ATTERBERG LIMITS

General outline

The Atterberg limits of a fine grained material represent a basic measure of the critical amount of water which changes the physical properties of sample, for example the transition from a plastic behaviour to a liquid behaviour (Fig. 5.15).

- The Shrinkage Limit (W_S) of a soil sample represents the water content below which the soil sample does not decrease its volume anymore as it continues to dry out.
- The Plastic Limit (W_P) of a soil sample represents the lowest water content at which the soil sample behaves like a plastic material.
- The Liquid Limit (W_L) of a soil sample represents the moisture content at which soil sample begins to behave as a liquid material and begins to flow. It is usually determined by using the *Casagrande Cup* (Fig.), but in the last few years this device has been substituted by an automatic device called "fall cone".

Atterberg Limits are extensively used for the identification, description and classification of cohesive sample and as a basis for preliminary assessment of their mechanical properties, through the use of the Casagrande chart, which is a diagram that allows to compare the Plastic Index to the Liquid limit of the analyzed sample (Mitchel & Soga, 2005). The Plastic index (IP) is defined as:

$$IP = W_L - W_P \qquad \text{(Eq.5.5)}$$

The higher the IP value, the higher the plasticity of the sample, and vice versa.

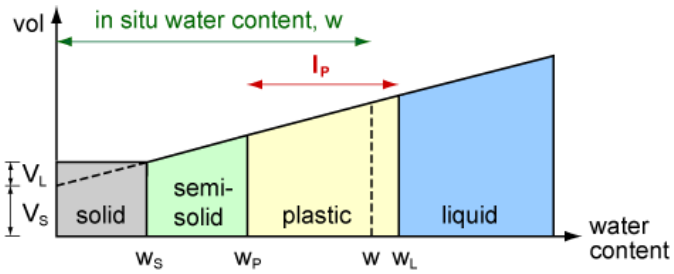

Figure 5.15 Atterberg Limits.

Liquid limit can be determined by using the *Casagrande Cup* or the fall cone method. In recent times, several studies have been verified that the fall cone test has a greater suitability than the *Casagrande Cup* for the Liquid limit determination (Wood, 1985; Brown & Downing, 2001; Rashid, 2005; Reza Emami Azadi & Monfared, 2012). The fall cone method is considered more reliable for determining Liquid limit than Casagrande method, because it allows to do analyses also on silt or sand samples; moreover, it also allows to determine quite satisfactorily the plastic limit of cohesive sample (Reza Emami Azadi & Monfared, 2012), and exceeding the operator dependence which affects the Casagrande cup method (Dragoni et al. 2008; Di Matteo, 2012).

Analytical details

Liquid limit and Plastic limit have been determined on a set of 29 samples, at the laboratory of the DiSTAR of Federico II University of Naples. Calcarenitic sandstones have been excluded.

The Liquid limit W_L has been evaluated with a fall cone, by using the British fall cone apparatus (British Standard Institution1377, 1975), manufactured by *Wykeham Farrance Inc.* with a 30° cone and weighing 0.785 N. The apparatus has a cup were the specimen is disposed (internal diameter=55 mm, height=40 mm).

The tests have been performed in a range of depths of penetration spanning from 4 to 25 mm, considering that the water content corresponding to a cone penetration of 20 mm defines the liquid limit (Di Matteo, 2012). The sample has been prepared by mixing the particle fraction below 75µm with distilled water. The mixture has been placed into the cup. The cone has been released and after a few seconds the measure of the penetration was registered.

The Liquid limit W_L has been evaluated in a linear graph obtained by plotting the moisture content against the corresponding penetration value.

The Plastic limit W_p has been determined according to the Casagrande plastic limit test. It considers the Plastic limit as the gravimetric water content at which a rolled thread of freshly molded sample, with a diameter of 3 mm, just begins to crack (British Standard 1377, 1975).

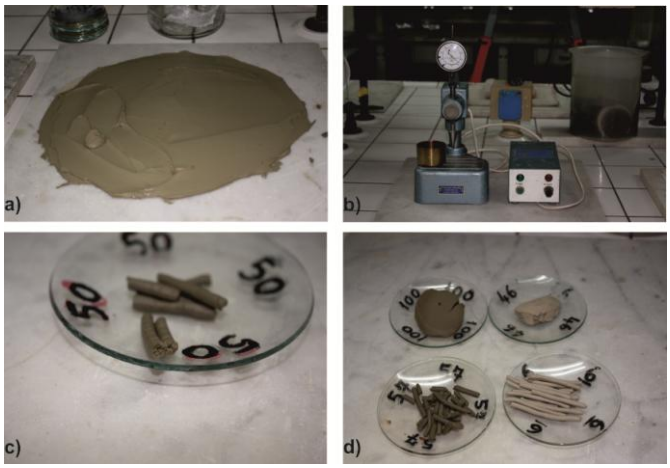

Figure 5.16 Atterberg limits analysis: a) mix powder+ water, used for fall cone analysis; b)fall cone apparatus; c) modeled soil (internal diameter about 3 mm) used to determine W_P; d) modeled material for W_P and specimen used for determining the water amount. The material is wet on the left hand corner, and dry on the right hand corner.

DIRECT SHEAR STRESS TEST

General outline

The direct shear stress laboratory test is used to evaluate the shear strength of a soil material.

The shear strength is defined as the maximum shear stress value that a soil sample can sustain, and represents a measure of the soil sample resistance to the deformation by continuous displacement of its individual soil particles. Shear strength depends upon several parameters like the effective stress, the drainage

conditions, the density of the particles, the rate of strain, and the direction of the strain.

Direct shear test is widely used also to obtain information about the bulk material properties. The test is performed by deforming a specimen at a controlled shear rate on or near a single shear plane, determined by the configuration of apparatus (ASTM 3080-98). In soil mechanics it is performed by using the Casagrande Shear box (Thornton & Zhang, 2003).

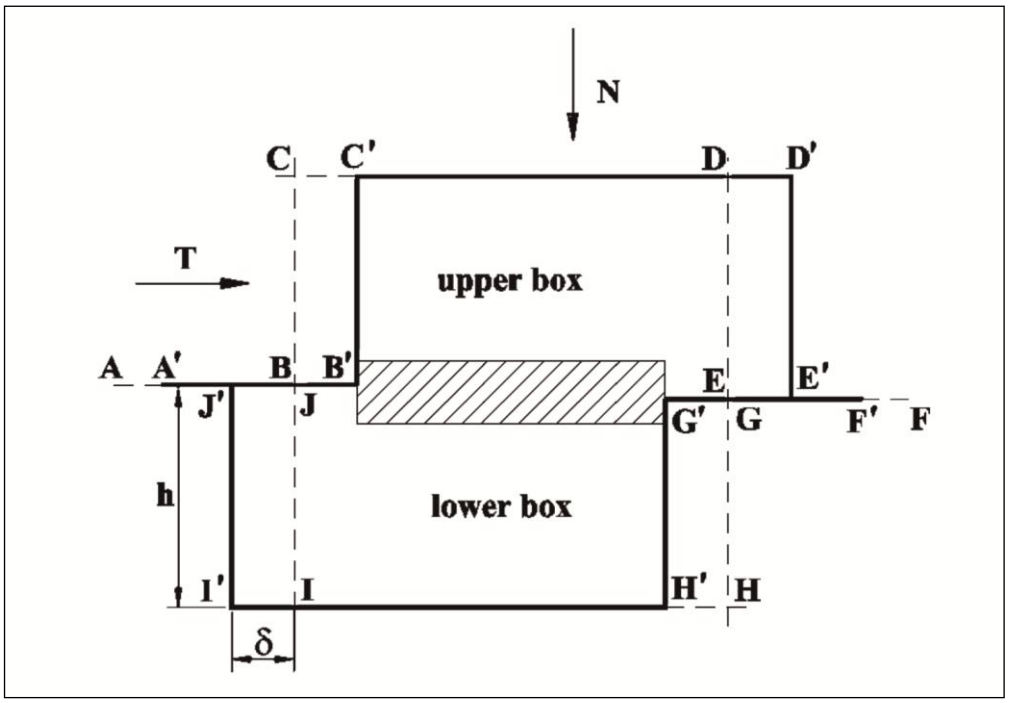

Figure 5.17 Casagrande shear box.

The test is conducted into two steps: consolidation and shear.

A force N is applied on the top surface of the box, then a displacement of the bottom part of the box is imposed at a constant speed, to produce the sample shearing. This has the effect to break the sample along the horizontal shearing plane. The force N is maintained constant during the test, because it is necessary to measure the resistance to the shearing strength (T), and the variation of the height of the sample (dh).

Direct shear tests are available for all kinds of material: cohesionless samples, like sands, or cohesive samples, like normal- or over-consolidated clays.

The maximum shear stress along a sheared surface, obtained during the direct shear test, is called Peak Shear Stress. In the case of clay samples, after very large shear displacements, when clay particles become aligned within a well defined shear zone or slip plane, the so-called "Residual Strength" can be reached.

Analytical details

Direct shear stress analysis has been carried out at the DiSTAR (Department of Earth science, Environment and Resources) of the Federico II University of Naples.

Two undisturbed samples have been analyzed. They were collected during drilling, in correspondence of the crown zone and the track zone of the Termini-Nerano landslide.

The *S277-01 Shear Machine with Data Acquisition* has been used. It consist of:

- Digital shear frame with microprocessor, complete with beam loading device, shear box case with adaptors, transducer/dial gauges supports
- Load cell, 3000 N capacity, complete with cable
- Linear potentiometric vertical transducer 10 mm travel
- Linear potentiometric horizontal transducer 25 mm travel
- Set of 50 kg slotted weights
- Shear box

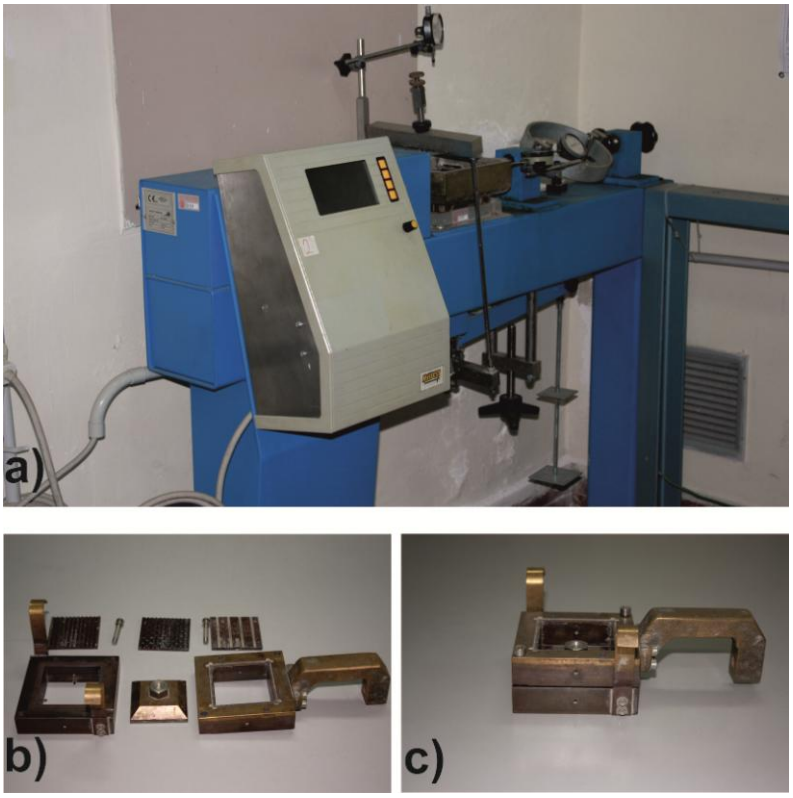

Figure 5.18 Shear test apparatus; a) s277-01 shear maschine; b)-c) shear box.

The shear stress analysis has been carried out on the basis of the procedure ASTM D3080.

Both Peak Shear Strength and Residual Shear Stress have been determined.

The direct shear test has been performed on three specimens 60x60x24 mm, coming from both two undisturbed samples.

The load applied and the induced strain have been recorded at frequent intervals to determine the shear strength parameters: cohesion and friction angle.

Results have been plotted on a (τ-σ) diagram allowing to define the Mohr-Coulomb envelope :

$$\tau = c' + \sigma * tg\varphi' \quad \text{(Eq. 5.6)}$$

Where

τ represents the Shear strength (kPa).

c' represents the cohesion (kPa).
σ represents the normal stress (kPa).
φ represents the friction angle (°).

Table 5.8 Applied load for each test. 435.4 (kPa) (kg/cm^2) corresponds to in situ load; 653.1(kPa) represent 870.8 (kPa) the in situ load; 8.88 represent two times the in situ load.

Test	N (kPa)
1	435.4
2	653.1
3	870.8

REOLOGYCAL ANALYSIS

General outline

Rheology describes the deformation of a body (solids, liquids or gasses) under the influence of a stress.
Ideal solids deform elastically, which means that the energy required for the deformation is fully recovered when the stresses are removed.
Ideal fluids deform irreversibly by flowing. The energy required for the deformation is dissipated within the fluid in the form of heat and cannot be recovered simply by removing the stresses (Schramm, 1998).
Newton described the basic law of viscometry for an ideal liquid (e.g. water) as:

$$\tau = \eta * \gamma \quad \text{(Eq. 5.7)}$$

Where:

- τ represents the shear stress, also considered as the tangential force applied to an area (A) that is the interface between the fluid and the upper plate:

$$\tau = \frac{Fource\ (Newton)}{Area\ (m^2)} = Pa\ (Pascal) \quad \text{(Eq. 5.8)}$$

- γ represents the shear rate, which is the change in velocity within the apparent lamellae gap of the fluid across the gap between the upper and lower plates:

$$\gamma = \frac{dv}{dx} = \frac{m/s}{m} = s^{-1} \quad \text{(Eq. 5.9)}$$

- η represents the viscosity, which is the fluid's resistance to flow:

$$\eta = Pa * s \quad \text{(Eq. 5.10)}$$

Real bodies are neither solids nor ideal fluids (Schramm, 1998). Most of the liquids show a rheological behavior which is located between the liquid and solid.
In general, it is possible to distinguish two main groups: Newtonian and Non Newtonian liquids.

- Newtonian Liquid: the ratio between the shear stress and the shear rate is constant, which means that the viscosity is not affected by changes in shear rate.
- Non Newtonian Liquid:
    - Pseudoplastic flow behavior: the viscosity tends to decrease as the shear rate tends to increase.
    - Dilatant flow behavior: the viscosity tends to increase as the shear rate tends to increase
    - Plastic liquid flow behavior: the viscosity tends to decrease as the shear rate tends to increase. When outside forces are strong enough to overcome the network forces, so when the yield point is overcome, the network collapses and the solid turns into liquid.

Several authors have used the rheological properties of a material to explain the landslide behavior (Malet et al. 2003; 2004; Bonzanigo et al. 2006; Bizjak & Zupančič, 2007; Jeong, 2010).
Rheological characteristics can be useful in establishing the transformation process of the materials into flow-like phenomena (Malet, 2003) on the basis of their yield stress and viscosity.

Analytical details

Rheological analyses have been carried out at the Indiana University in Bloomington (IN)
A rotational Viscoanalyser (ATS Rheosystems/Rheologica Instruments AB*)* has been used (Fig. 5.19)

Figure 5.19 a) Rheometer device; b) and c) enlargements of the sample slot.

A Viscometry Test has been carried out to determine the flow curve of the material or the dependence of its viscosity and stress, time or temperature.
In case of Viscometry Tests, a stress is applied to the sample and the resulting movement of the upper measurement system is detected. The rotational speed depends on the viscosity of the sample, calculated by means of stress and shear rate. For this kind of tests, the shear stress represents the INPUT datum, whereas the shear rate is the OUTPUT datum.
Minimum and maximum stresses have been selected. The former corresponds to the minimum motor torque, whereas the latter corresponds to the maximum

torque. Also the delay time has been set up. It corresponds to the time between the application of stress and the collection of the data. In the following table all parameters set for the analysis are reported.

Table 5.9 Minimum stress, maximum stress and daily time values, used for viscometry test.

Minimum stress (Pa)	Maximum stress (Pa)	Daily time (s)
1.000E+0	1.000E+2	1.000E+0

Soil samples characterized by different water contents, 75 and 100 %, were prepared by adding water to dry powders (particles size below 63 μm). The analyses have been carried out on a set of 15 samples, selected, from surface to the depth of the landslide body, on the basis of their mineralogical and stratigraphic characteristics.

CHAPTER 6

RESULTS

GEOLOGICAL SURVEY AND SAMPLING

GEOLOGY AND STRATIGRAPHY OF THE AREA

Geological survey evidenced that a retrogressive movement, which can be classified as roto-translation slide (Cruden & Varnes, 1996), characterizes the Termini Nerano landslide, and in particular its crown zone. In Figure 6.1 a typical wide counter-sloping landslide terrace can be observed, as well as several cracks on the fresh paved road, near the crown zone.

The stratigraphy of the material involved in the landslide was determined from continuous drillcores (Table 6.1).

Figure 6.1 View of the crown zone; a) typical landslide terrace; b) cracks on the paved road

The drilled material is highly heterogeneous (Fig.6.2), variously characterized by alternating beds of shales, silts, sandstones and calcarenitic-sandstones.
On the basis of the characteristics of the drillcores reported before, and also considering the description of the main lithologies characterizing the studied area, the material involved in the landslide belongs to the *Arenarie di Termini* formation.
As shown in Figure 6.2 it was not possible to correlate the stratigraphy of the three drillcores., although the material belongs to the same formation.
The investigated samples in correspondence of the crown zone are constituted by a sandstone layer immediately after the top soil. It is not well cemented, showing a certain grade of softness, and is interbedded by centimetric shale levels. The transition from this level to the subsequent is well visible. As shown in Figure 6.3 this step is marked by a sudden variation in colour, which changes from ochre (sandstone level) to leaden grey (shale level). Considering the classification of structurally, complex formations proposed by Esu (1977), these soils belong to the B3 category, since they display a very chaotic structure.
The last interval, which continues down to the end of the core (-26.00 m) is constituted by marly clay. Its consistence is higher than that of the overlying intervals. Its structure becomes less chaotic going toward the bottom of the hole, and for this reason it has been classified as B3 down to a depth of -16.00 m,, and as B2 between -16.00 and -26.00 m.

Table 6.1 Stratigraphic sequence of Sc1 borehole in correspondence of the crown zone.

Layer	Depth (m)	Description	Color	Grain size
	0÷0.5	Top soil with roots and calcareous clasts (dmax=8 cm).	Light brown	Coarse to medium coarse sand
	0.5÷3.7	Soft cemented sandstone, with interbedded centimetric silty shale levels.	Yellow. light brown	Fine sand
	3.7÷5	Shales with interbedded greenish marly shale levels.	Leaden gray	Silty shale
	5÷26	Marly clay with calcareous clasts (dmax=4 cm) and glauconitic crystals (from 10 meters) interbedded. Between 8 and 10 meters calcareous layer is present, constituted by gravel and pebbles. The layer is characterized by high consistence.	Leaden gray	Silty shale

The stratigraphic succession analyzed in correspondence of the sliding zone, after few centimetres of top soils is constituted by a leaden gray shale layer, interbedded by marly shale levels. Although its structure can be considered scaly, its chaotic organization makes it more similar to B3 category of the Esu

classification (1977). From a depth of about -5.50 m, a silty shale interval is present. It is characterized by interbedding of calcarenitic sandstones and sandstones and it was classified as B2 (Esu, 1977). From about -10.50 m to a depth of -24.00 m, well cemented calcarenitic sandstones have been recovered.

Table 6.2 Stratigraphic sequence of Sc2 borehole in correspondence of the sliding zone.

Layer	Depth (m)	Description	Color	Grain size
	0÷0.2	Upper soil constituted by pavement road.	Leaden gray	
	0.2÷5.5	Shale with clayey marl layers characterized by highly consistence.	Leaden gray	Silty shale
	5.5÷6.6	Silty shale with interbedded calcareous clasts and clays (d_{max}=4.0 cm). From slightly to highly consistence.	Gray	Clayey silt.
	6.6÷6.7	Highly compact calcarenitic sandstone layer characterized by the presence of calcite veins.	Gray	Sand
	6.7÷8.3	Silty shale with interbedded calcareous clasts and clays (d_{max}=4.0 cm).	Gray	Silty shale
	8.30÷8.35	Sandstone characterized by variable consistence (from slightly to highly consistence).	Gray with yellowish greenish veins.	Sand
	8.35÷9.5	Silty shale with interbedded calcareous clasts and clays (d_{max}=4.0 cm). From slightly to highly consistence.	Gray	Silty shale
	9.50÷9.9	Sandstone slightly cemented collected as little piece of core.	Gray from 9.5 to 9.7 m; yellowish until the bottom	Sand
	9.9÷10.5	Calcarenitic sandstones collected as little piece of core (L_{max}=5 cm).	Gray	Sand
	10.5÷24	Calcarenitic sandstones collected as little piece of core (L_{max}=67 cm).	Gray	Sand

The investigated area in correspondence of the accumulation zone is constituted by an alternance of silty shale levels, differing for their colour (greyish green, reddish brown, brown, bluish green), and for their structure, which can be variable from massive to highly laminated. A sandy interval appears at about -13.00 m, followed by an interval of silty shale and sandstone, which continues until the

bottom of the hole, and is only interrupted by a calcarenitic sandstone layer, at about -19.00 m. This stratigraphic sequence has been classified as B3 from 0.00 to -10.00 m, as B2 from -10.00 m to -17.00 m and B1 from -17.00 m to 30.00 m.

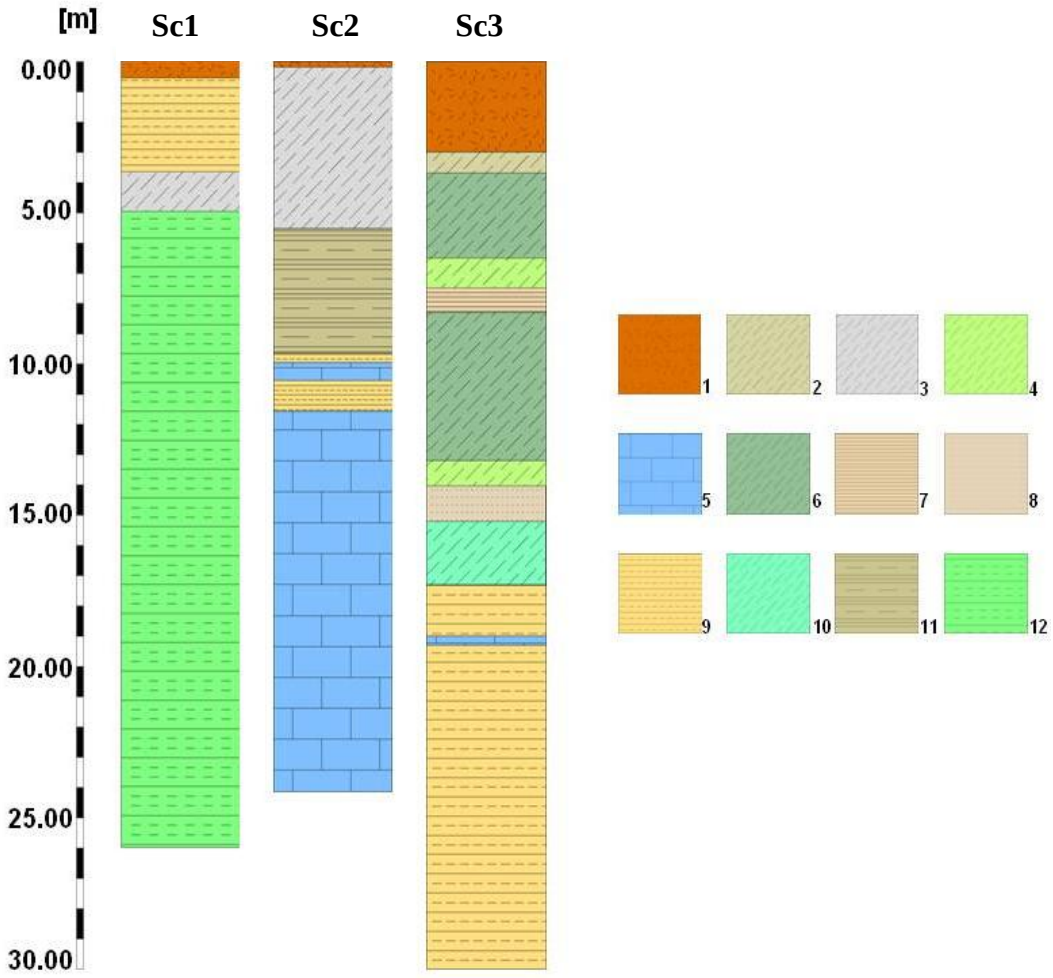

Figure 6.2 Stratigraphic sequences: 1) Top soil; 2)Greyish-green silty shales; 3) Shales; 4)Greenish silty shale; 5) Calcarenitic sandstone; 6)Greyish silty shale; 7) Brownish silty shale ; 8) Silty sand; 9) Sandstone; 10) Bluish-gray silty shale; 11) Greyish clayey silts ; 12) Marly shale with calcareous clasts.

Table 6.3 Stratigraphic sequence of Sc3 borehole in correspondence of the crown zone.

Layer	Depth (m)	Description	Color	Grain size
	0÷1.8	Top Soil constituted by heterometric calcareous clasts (d_{max}=5-6 cm) piece of core (L_{max}=10 cm) and lateritic clasts, sandy gravels and pebbles.	Brown	
	1.80÷3	Top soil constituted by silt, highly compact with calcareous and sandstone clasts (d_{max}=3 cm). and lateritic pieces. It is characterized by low consistence and by highly humidity.	Reddish-brown	Clayey silt.
	3÷3.7	Silty shale with roots and clasts inside. It is characterized by slightly laminar versus massive structure. Highly humid.	Greyish - green and reddish brown.	Clayey silt alternated to sandy silt.
	3.7÷6.5	Silty shale with interbedded stem vegetables and roots and marls. It is characterized by variable consistence form slightly consistence to highly consistence. Highly humid.	Greyish - green and reddish brown.	Clayey silt alternated to sandy silt.
	6.5÷7.5	Silty shale with stem vegetables, roots and marls interbedded. It is characterized by massive to slightly laminar structure. and massive consistence.	Greyish - green and reddish brown.	Clayey silt alternated to sandy silt.
	7.5÷8.2	Silty shale with sandstone and calcareous clasts inside (d_{max}=1-2 cm). It is characterized by massive structure and by high consistence.	Brown	Clayey silt
	8.2÷13.2	Silty shale with sandy silt levels and sandstone and marl clasts interbedded (d_{max}=4-5 cm). It is characterized by highly consistence structure.	Gray, greenish gray.	Silts and shales with sand levels*
	13.2 ÷14.1	Silty shale with calcareous clasts (d_{max}=4-5 cm). It is characterized by a) massive structure slightly laminated and b) by variable consistence.	Greenish gray	Clayey silt
	14.1÷15.1	Sand characterized by massive structure from slightly to highly consistent.	Bluish gray	Silty sand
	15.1÷17.2	Silty shale with centimetric silty sand levels interbedded. It is characterized by massive structure. Highly consistent.	Bluish gray	Silty clay alternated to silty sand.
	17.20÷19	Slightly cemented compact sandstone characterized by massive structure.	Ochre	Fine sand
	19÷19.2	Calcarenitic level	Gray	Sand
	19.2÷3	Slightly cemented compact sandstone characterized by massive structure. From 24-24.30 . 25.50-26 , 26.30-27 and 27.50-28.20 meters depth sandstones blocks have been detected. Fractures are also visible along the carrot.	Ochre and gray at the bottom.	Sand

Notes: **9.30÷9.50 m: Sandy clayey silt. yellowish- green; 10.50÷10.60 m: silty sand bluish green; 11.30÷11.80 m: silty sand with calcareous clasts; 12.40÷12.60 m: silty sand ; 13.10÷13.20 m: silty sand bluish green

GROUND MONITORING LANDSLIDE

Ground monitoring of the landslide has been carried out by using a set of two inclinometers and two piezometers installed in correspondence of the crown and the accumulation zones of the Termini Nerano landslide.

Figures 6.3 and 6.4 show the inclinometer reading related to the boreholes Sc1 and Sc3.

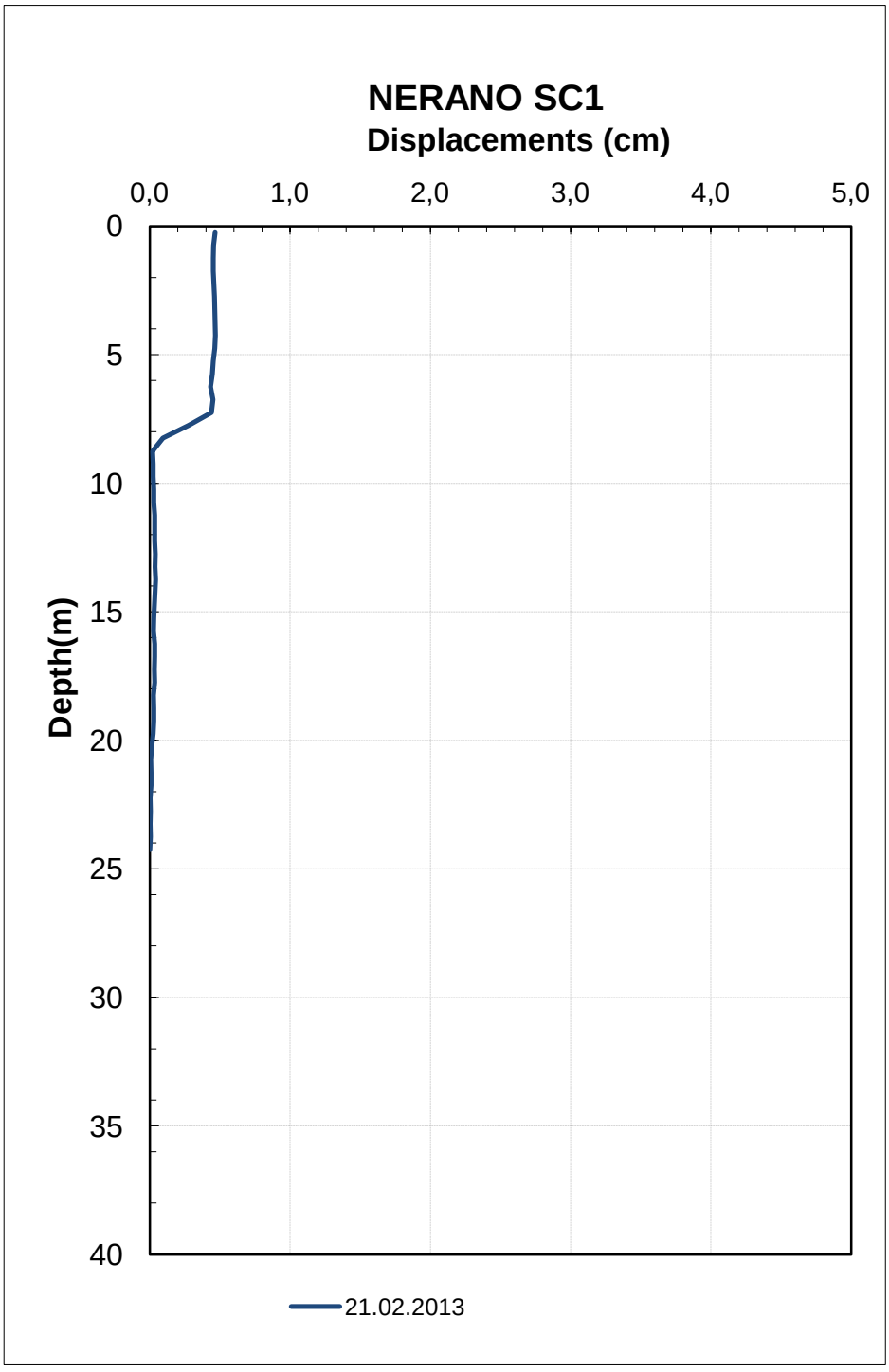

Figure 6.3 Sc1 boreholes inclinometer readings.

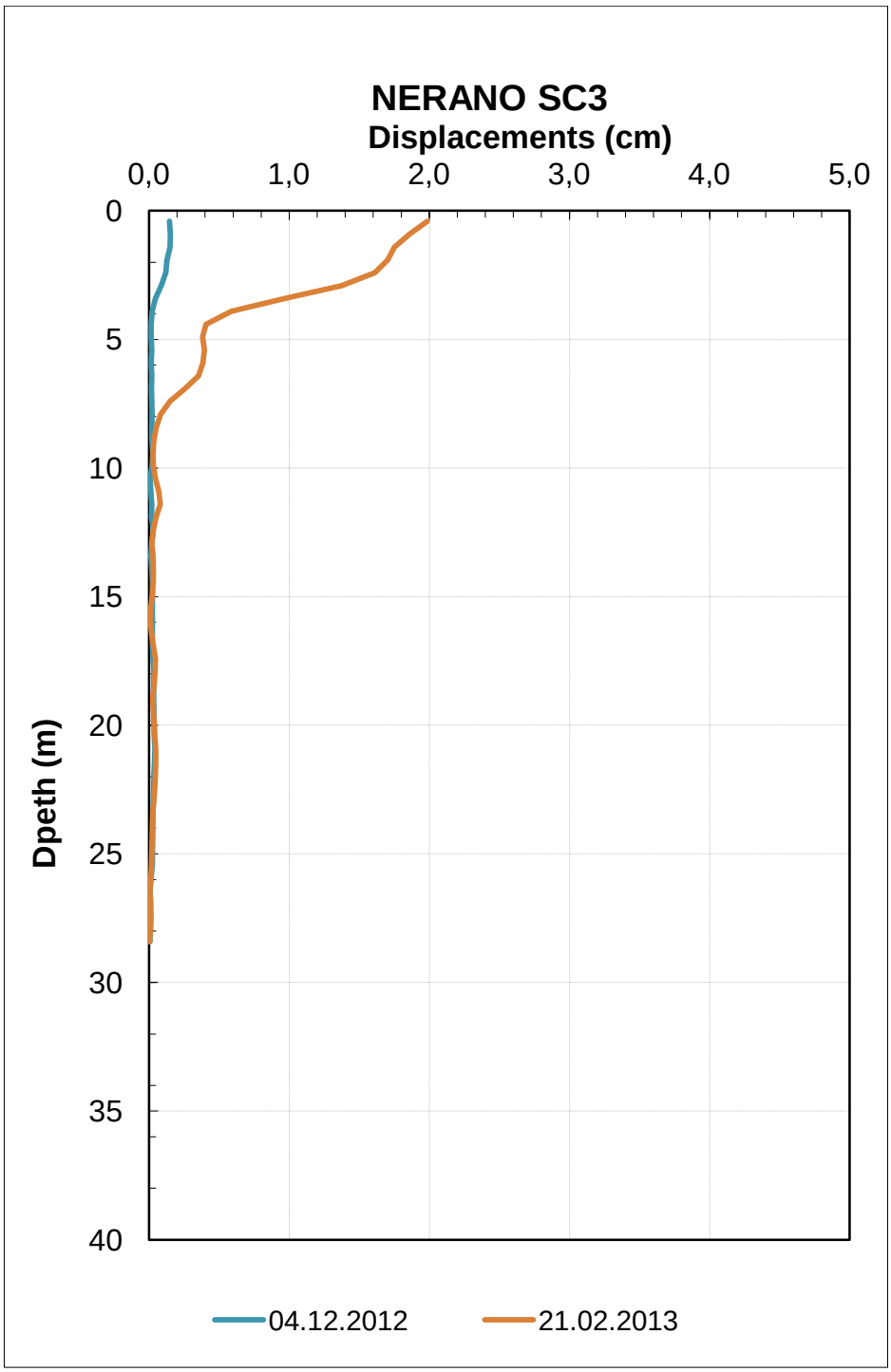

Figure 6.4 Sc3 boreholes inclinometer readings.

A surficial slip surface at a depth of about 8.00 m has been determined in correspondence of crown and accumulation zones.

The water table depth has been investigated in the Sd1 and Sd3 boreholes. Piezometric levels variations have been measured during December 2012 and February 2013. The results have been reported in the Table 6.4

Table 6.4 Piezometric measurements

Date	Sd1	Sd3
07/09/2012	14.32	4.48
05/12/2012	7.64	2.44
21/02/2013	6.04	3.18

GEOELECTRICAL ANALYSES

Geoelectrical tomography analyses have been carried out along two profiles called TES1 and TES2, in correspondence of the sliding zone of the Termini Nerano landslide.

In Figure 6.5 the electrical resistivity tomography sections of both profiles are drown.

In both sections, it is possible to recognize three main sub-parallel layers, characterized by different resistivity values:

TES 1

- 0.00÷10.00 m→ $\rho < 100\Omega m$
- 10.00÷12.50 m→ $506 < \rho < 1265\ \Omega m$
- 12.50÷35.00 m→ $\rho > 1265\ \Omega m$

The transition from 506 Ωm to 1265 Ωm is sharp.

TES 2

- 0.00÷6.00 m→ $\rho < 100\Omega m$
- 6.00÷7.50 m→ $100 < \rho < 1562\ \Omega m$
- 7.50÷20.00 m→ $\rho > 1562\ \Omega m$

The transition from100 Ωm to 1562 Ωm is sharp.

Following the literature (Ikhane et al. 2012) resistivity values lower than $100\Omega m$ can be associated with shale-silt lithologies, whereas resistivity values higher than $1000\Omega m$ can be associated with calcareous rocks or sandstones.

The highest resistivity values characterize the deepest parts of the investigated sections, which should be considered more stable to landslide phenomena.

By comparing these results with those obtained from stratigraphic analysis, (Fig.6.5) it was possible to verify that the resistivity variation at about 7.00 m depth corresponds to the transition from shales to shaily silts and is also in good agreement with the surface of rupture recognized in the inclinometers.

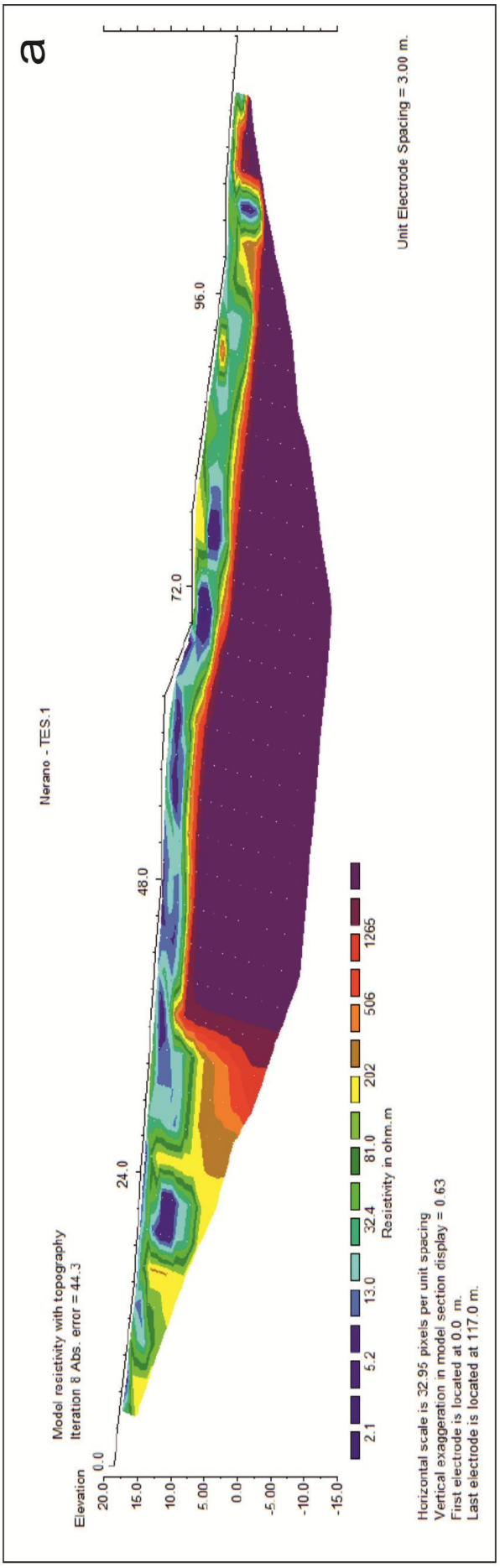

Figure 6.5 a Geoelectrical profile: TES 1.

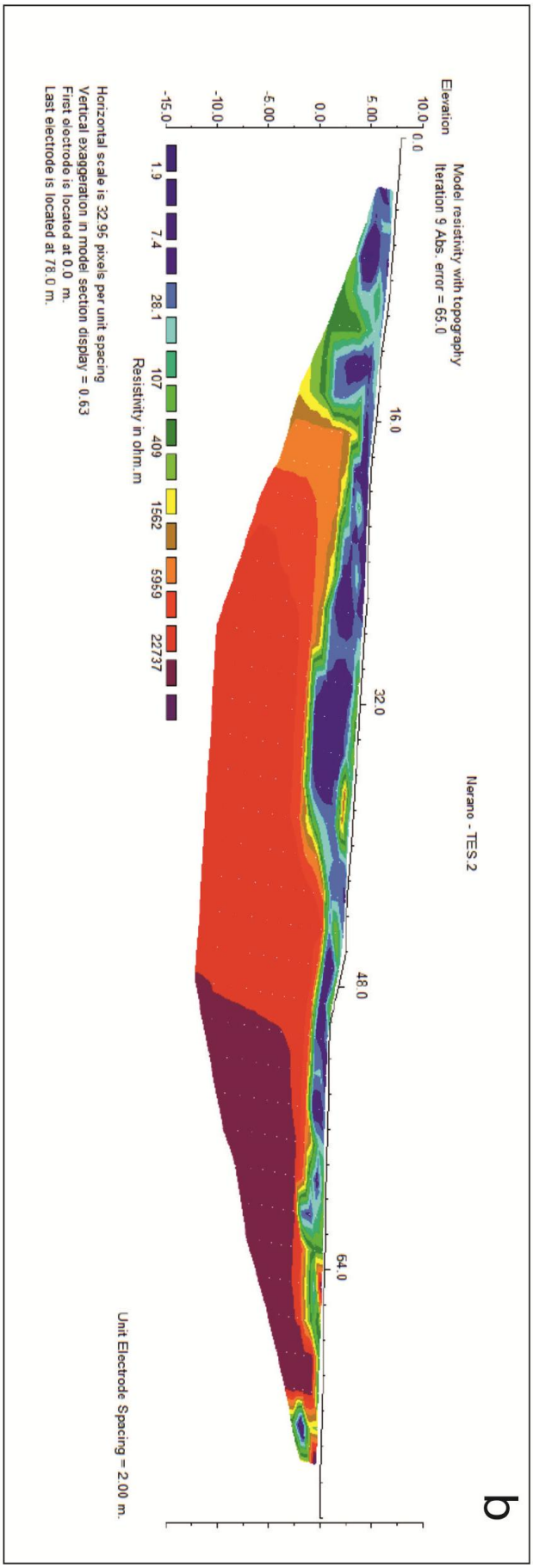

Figure 6.5 b Geoelectrical: TES 2.

AERIAL PHOTO ANALYSIS

By aerial photo analysis, it was possible to evaluate the evolution of the landslide in the period from 1955 to 2003.

The 1955 photograph reveals the presence of a wide crown zone, before the 1963 landslide event. This crown zone can be interpreted as a inherited feature of the 1940 landslide (Fig.6.6a). The landslide body stops in correspondence of the "*Strada Provinciale 138*", or "*via Rotabile di Nerano*". The absence of vegetation indicates that the landslide was active. On the eastern part of the photograph, in correspondence of minor channel other areas affected by instability can be recognized.

The 1974 photograph gives a scenario of the area affected by the 1963 landslide about ten years later (Fig.6.6b). Traces of the two landslides, occurred in the 1940 and 1963, are still visible. Features of the latter overlie those of the former, from the crown zone to the shoreline. The urbanization evidently increased, as well as the vegetation.

The 1990 photograph still allows to see the traces of the two landslide bodies (Fig. 6.7a). At the foot of the 1963 crown zone a pine forest is visible. It was created immediately after an extraordinary rainfall event, to stop the swelling phenomena of the ground.. Instability area developed on the eastern part of the crown zone is evidenced by the absence of vegetation.

In the 2003 photograph (Fig.6.7b), traces of the two landslides are only slightly visible. They are obliterated by vegetation and infrastructures. It is clear in this picture that the slope is affected by a retrogressive movement. The area located upslope of the 1963 and 1940 landslides crown zone, is light colour and no traces of vegetation are visible, which could imply that, at this time, the movement was still going on. This was also confirmed through the geological survey.

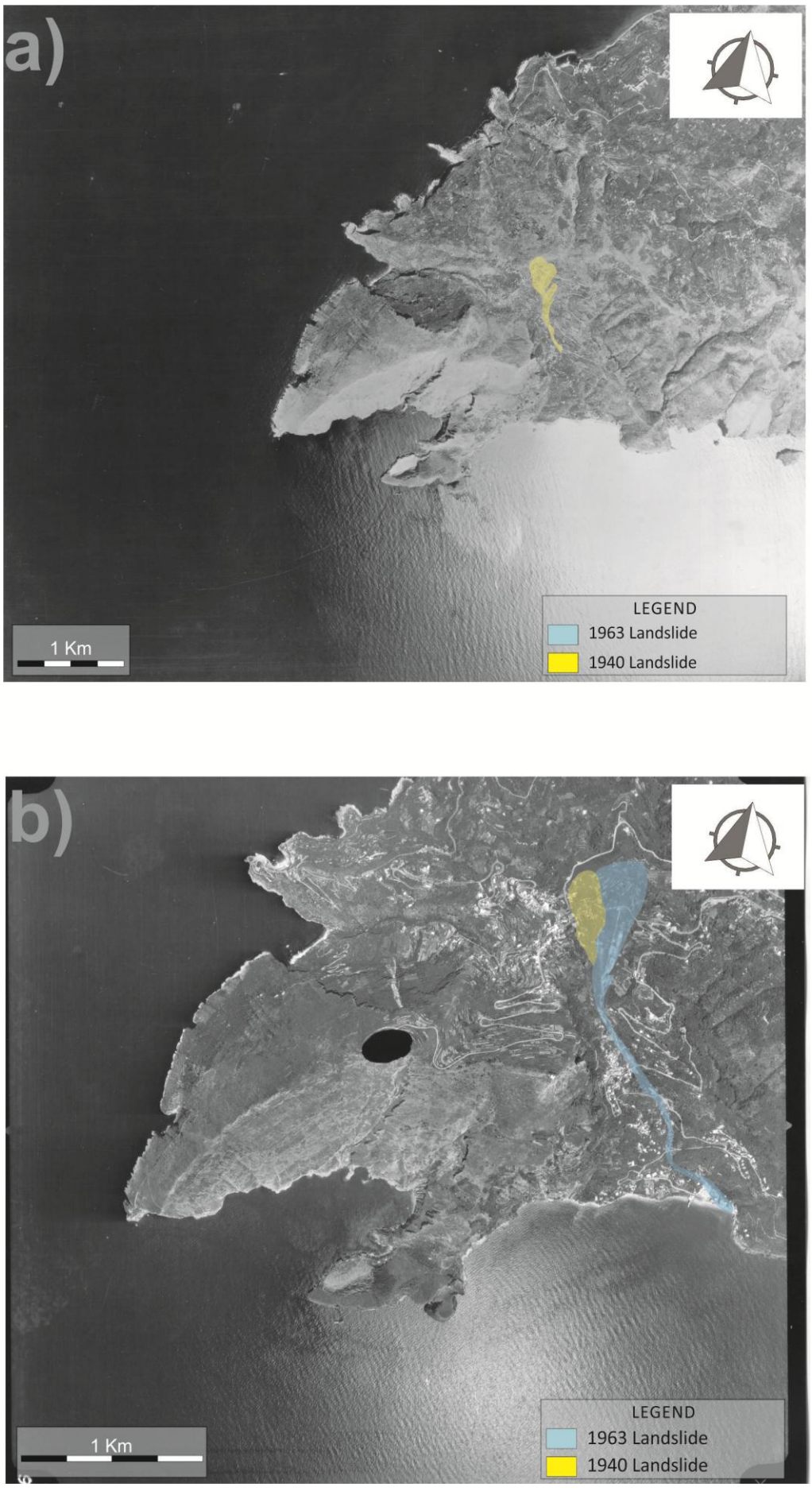

Figure 6.6 a) air-photo of 1955; b) air-photo of 1974

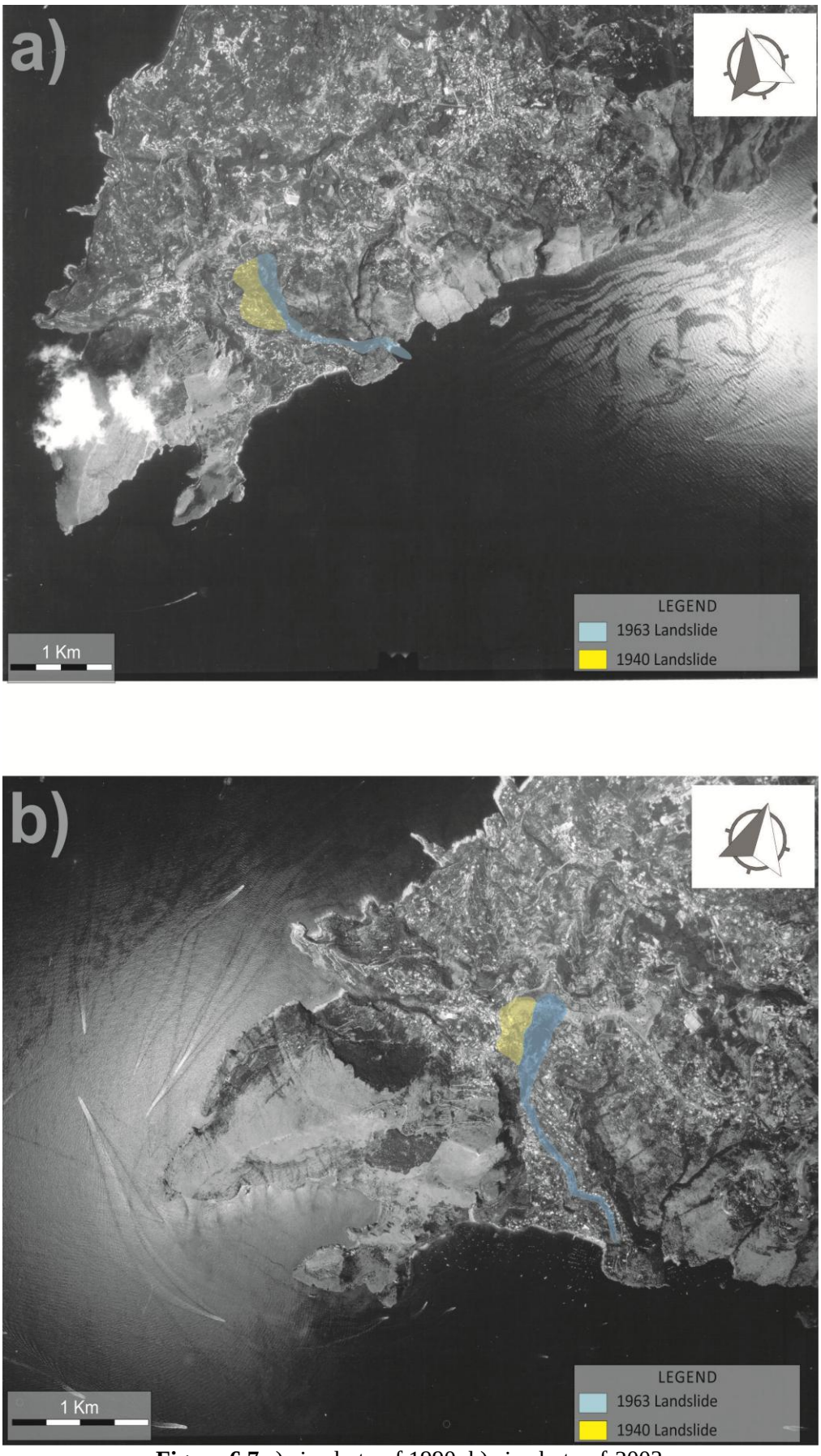

Figure 6.7 a) air-photo of 1990; b) air-photo of-2003

MINERALOGICAL CHARACTERIZATION

XRPD MINERALOGICAL ANALYSIS

The use of different methodologies for the sample preparation, did not influence the final results. By comparing patterns elaborated at DiSTAR, CNR and Indiana University, a good fitting is observed.

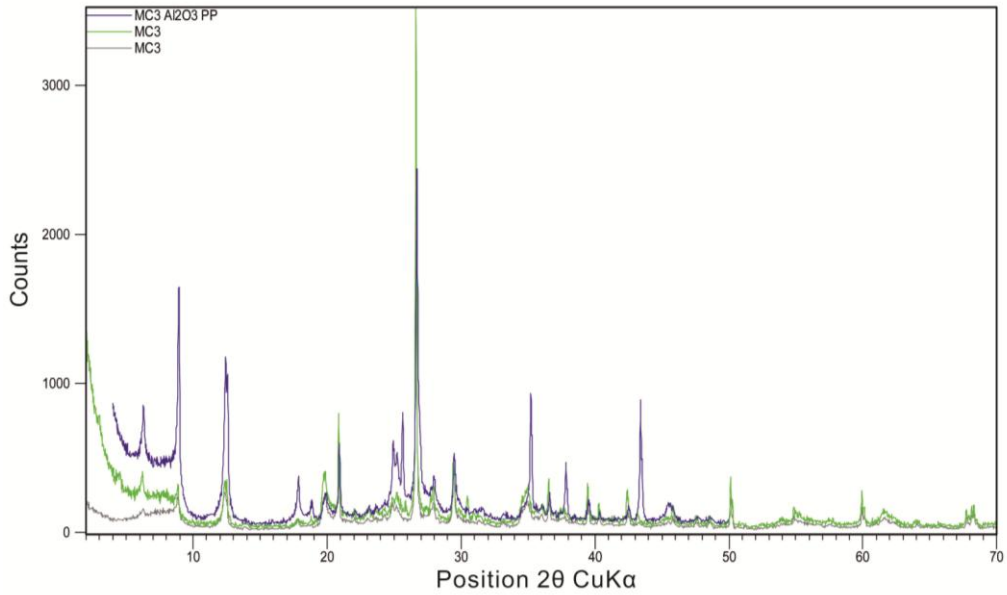

Figure 6.8 XRPD patterns of samples prepared by using different techniques: green line = sample prepared at CNR (Tito Scalo) laboratory, blue line = sample prepared at DiSTAR laboratory, gray line = sample prepared at Indiana University laboratory.

In all cases, although the analyzed materials are characterized by a great heterogeneity, the qualitative XRPD analyses showed that the samples are constituted by few types of minerals:

- Phyllosilicate minerals: chlorite, kaolinite, mica, mixed layer I/S, mixed layer Chl/S
- Quartz and feldspars (Na- and K feldspars)
- Carbonate minerals (calcite, dolomite)

In correspondence of the crown zone mixed layers I/S are the most representative mineralogical phase.

The presence of the mixed layer I/S was determined by looking the area of the XRD patterns comprised between 6°and 10° 2θ. In this area in few cases, a strong hump was evident, whereas in other cases a less intense and wider hump occurs.

For example, by looking at the PN5 sample (Fig. 6.9), there is a very intense hump between the main peaks of the two end-members illite and smectite. In the case of the PN6, PN8 and PN9 samples, this hump is still present but is located toward the illite peak.

In other samples, where smectite was not so relevant, the presence of mixed layers I/S were detected by considering the hump occurring between the chlorite and the illite peaks. Chlorite was detected into PN4, PN5, PN6, PN8 and PN9 sample differentiated from kaolinite by using the chlorite-kaolinite test.

The mixed layer Chl/S was detected by specific analysis on clay fraction.

Quartz occurs in all of the analyzed samples collected from the crown zone, as well as calcite. In these samples, dolomite was generally low. Feldspars are in most of the cases easy detectable, except for the PN5 and PN9 samples.

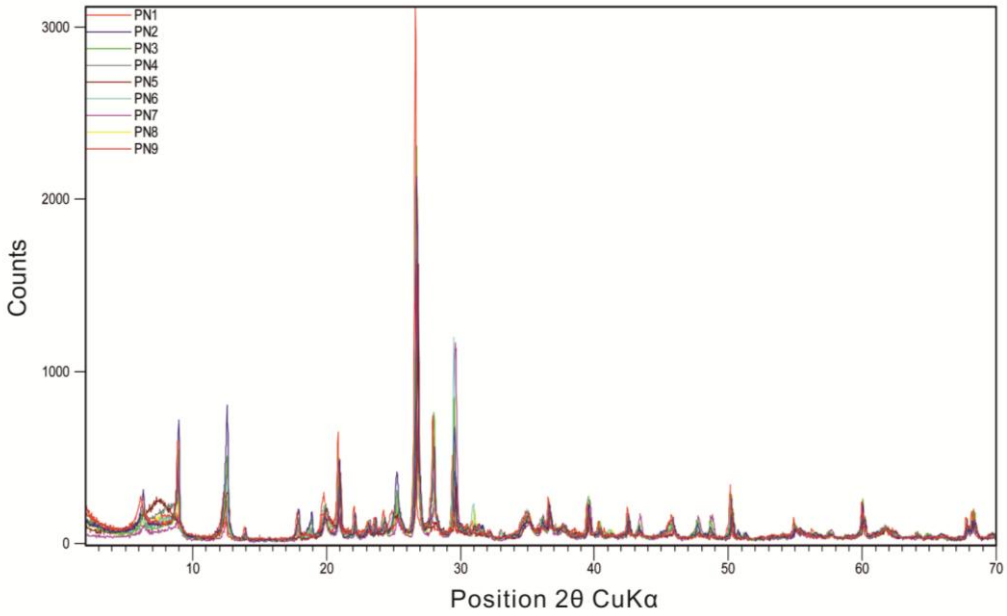

Figure 6.9 Patterns representative of samples collected from the crown zone.

Samples collected from the sliding zone (Fig.6.10) seem to be mainly characterized by quartz, feldspars (Na- and K- feldspars) and calcite, whereas the area of the pattern were clay mineral are usually well visible, is almost flat.
The hump described above, characterizing mixed layer I/S, is visible, as well as the muscovite and chlorite peaks (Fig. 6.11). The presence of clay minerals was verified by specific analyses on the clay fraction, and as in the previous case, kaolinite occurs only in a few samples (PR1, PR2 PR3, PR6), as confirmed by chlorite-kaolinite tests.

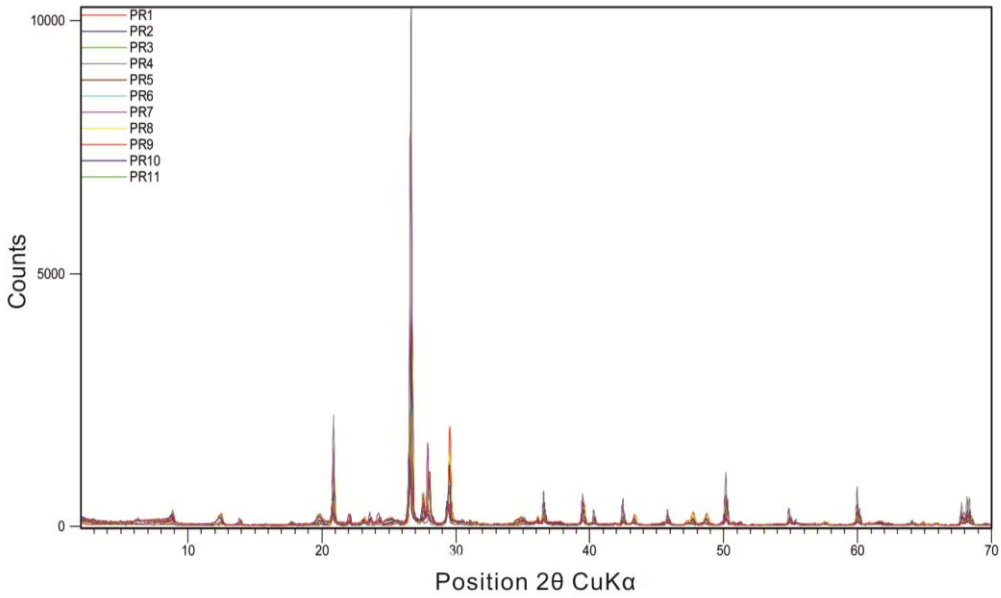

Figure 6.10 Patterns representative of samples collected from the sliding zone.

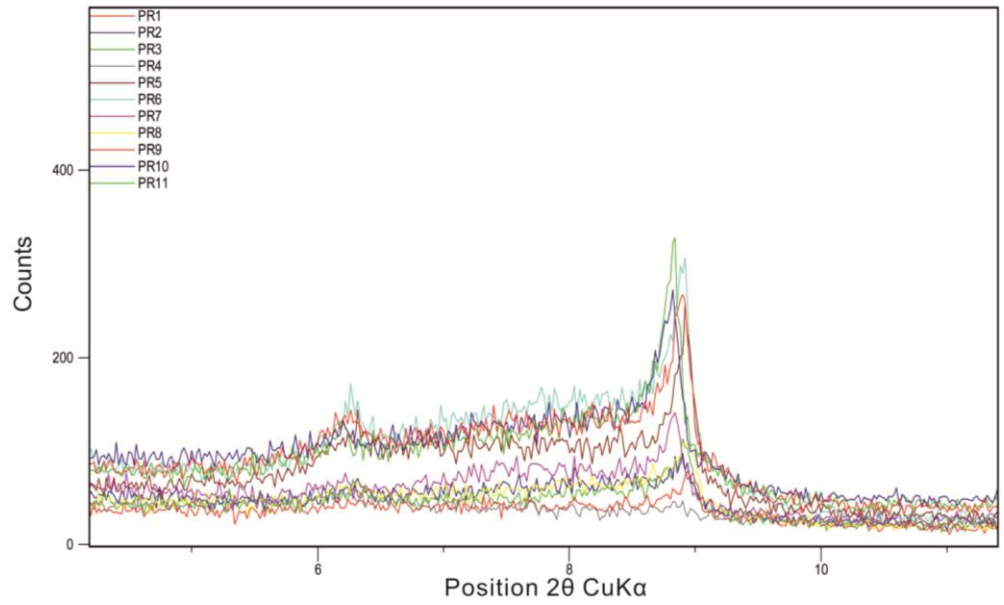

Figure 6.11 Zoom of the area between 6°2θ and 10 °2θ of patterns representative of samples collected from the sliding zone.

Samples collected from the accumulation zone are quite heterogeneous (Fig. 6.12). Specifically mixed layer I/S as well as chlorite and muscovite are well visible in all samples collected from -3.00 to -11.50 m. On the contrary, the deeper samples (from -11.50 to -30.00 m) are characterized by higher amounts of quartz, Na-feldspar, K-feldspar and calcite. Also in this case the presence of kaolinite was verified by chlorite-kaolinite tests.

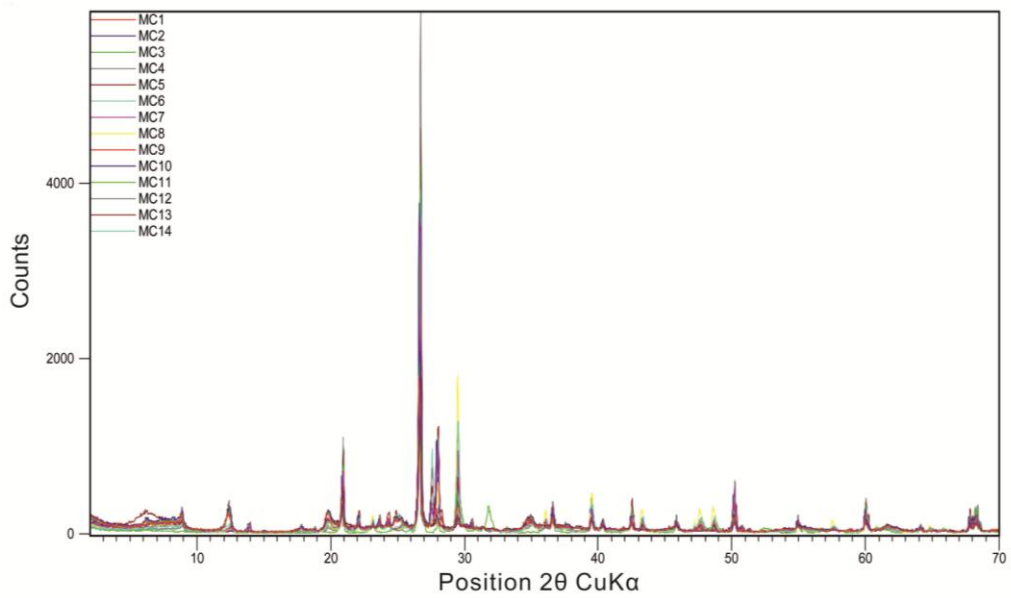

Figure 6.12 Patterns representative of samples collected from accumulation zone.

The mineralogical composition of soil used for the determination of the Atterberg limits, which is only a fraction of the whole sample material (see Methods chapter), was also evaluated. As it is possible to see in Figure 6.13, there is a good fit between the two patterns. This means that, although only a specific grain size of the whole sample was selected for the Atterberg limits evaluation, no variation in the main mineralogical composition occurred.

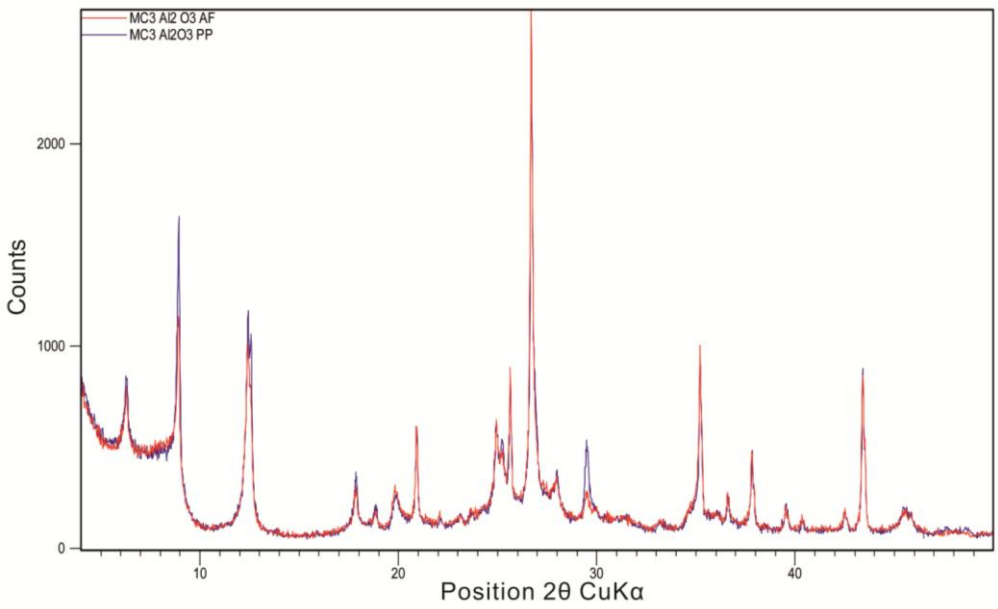

Figure 6.13 Comparison of patterns of the bulk sample (red line) and its fraction used for Atterberg limits determination (blue line).

CHLORITE-KAOLINITE TEST

As reported in the Methods chapter, chlorite-kaolinite test was carried out in order to verify the presence of kaolinite.

In detail, the presence of kaolinite has been evaluated by looking at the peak positions at 12°2θ and 25°2θ angles, between natural and heated (at 500°C) samples. When both kaolinite and chlorite are present, the peaks of the heated sample occur at higher angles than the natural sample, because of the collapse of kaolinite structure, as shown in Figure 6.14.

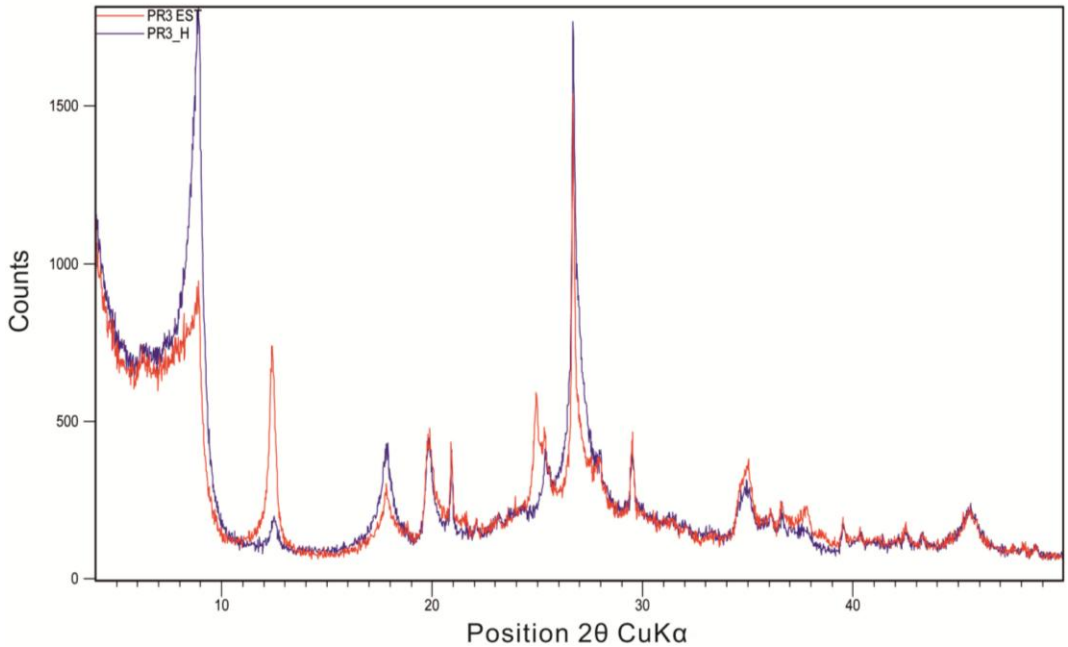

Figure 6.14 Chlorite-kaolinite test, performed on a sample where kaolinite is present

When kaolinite is absent, no change in the peak position happens, as shown in Figure 6.15.

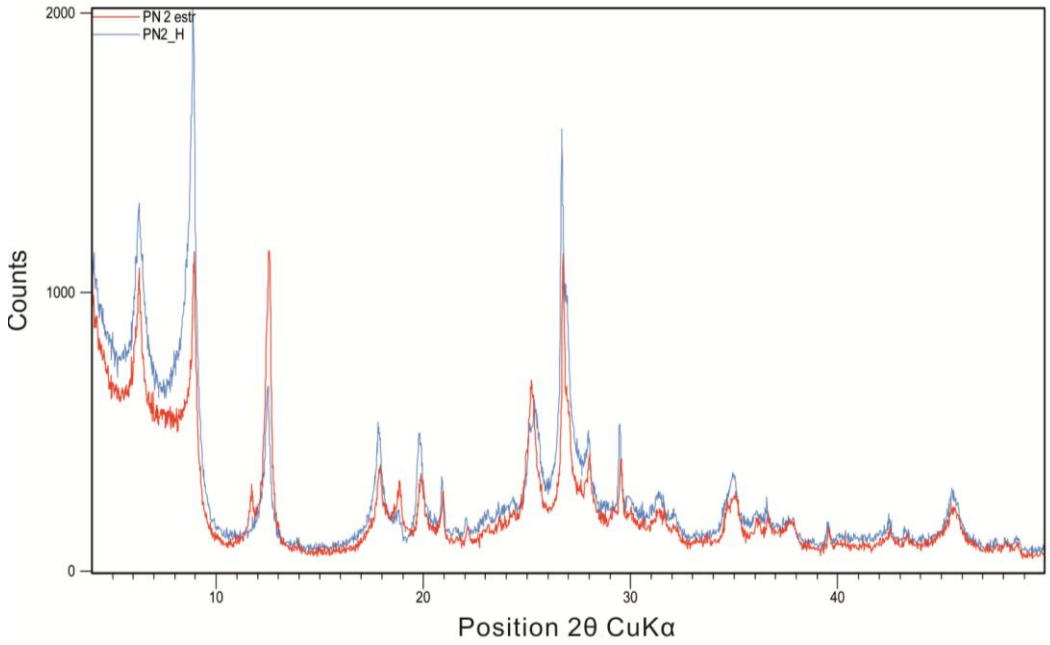

Figure 6.15 Chlorite-kaolinite Test performed on a sample where kaolinite is not present.

ORIENTED AGGREGATES

Specific analyses on the clay fraction have been carried out to obtain information about the main phyllosilicate phases, in particular mixed layer I/S and Chl/S.

Analyses have been carried out by comparing AON (normal oriented aggregate) with AOG (glycolated oriented aggregate) and AOR (heated oriented aggregate).
Also in this case, no differences are visible by comparing the AOG pattern prepared by following the CNR procedure, as well as the DiSTAR and Indiana University procedure.
The occurrence of mixed layer I/S was revealed by observing variation in the position at 6°2θ or 14 Å (AON pattern), which shifts at about 5.2°2θ or 17Å (AOG pattern) as reported by Moore & Reynolds (1997). As shown in Figure 6.16, the same peak disappear when AOR pattern is observed, due to the collapse of the smectite layers after heating.
The occurrence of mixed layer Ch/S was revealed by observing variation in the position of peak located at 11.7°2θ or 7.6 Å (AON pattern), which shift at about 11.7°2θ or 7.8Å (AOG pattern), as reported by Moore & Reynolds (1997) (Fig. 6. 16). By heating the sample (AOR pattern) the same peak shifts at 10.9°2θ or 8.0 Å.
More accurate analyses have been carried out also to evaluated the grade of ordering of the mixed layers in the analyzed samples. As reported in Moore & Reynolds (1997), the presence of a reflection at 5°2θ indicates random interstratifications (R0 ordering), whereas the presence of a reflection at 6.5 °2θ is associated to (R1 ordering).

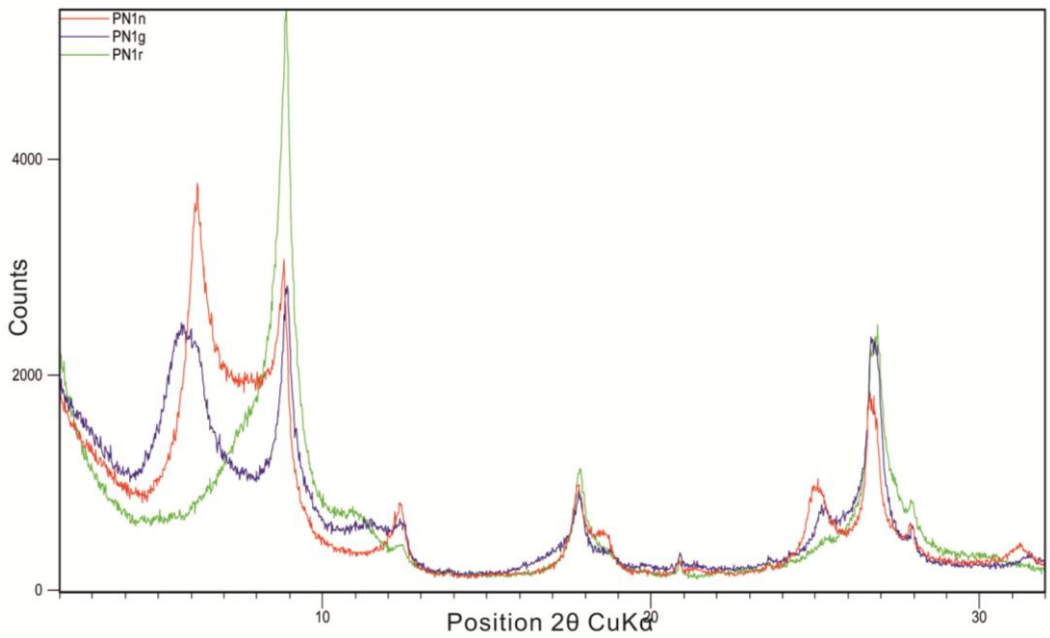

Figure 6.16 Oriented aggregate of sample characterized by mixed layer I/S and mixed layer Chl/S.

In the analyzed samples it was verified that:

- Samples collected from the Sc1 core are characterized by a grade of ordering equal to R0 with a percentage of illite ranging between 21 and 59 wt% and by a grade of ordering equal to R1, with a percentage of illite ranging 73 and 77 wt%.
- Samples collected from the Sc2 core are characterized by a grade of ordering equal to R0 ranging between 23.3 and 42.7 wt%, and by a grade of ordering equal to R1, with a percentage of illite ranging between 62.3 and 79.5 wt%
- Samples collected from the Sc3 core are characterized by a grade of ordering equal to R0 with a percentage of illite ranging between 23.3and52.7 wt% and by a grade of ordering equal to R1 with a percentage of illite ranging between 65.6 and 82.5 wt%.

As reported in Table 6.5, some samples contain both R0 and R1, and no samples show a grade of ordering equal to R3. Moreover, it is possible to see that the grade of ordering tends to change with depth without a specific trend, as shown in the diagram of Figure 6.17.

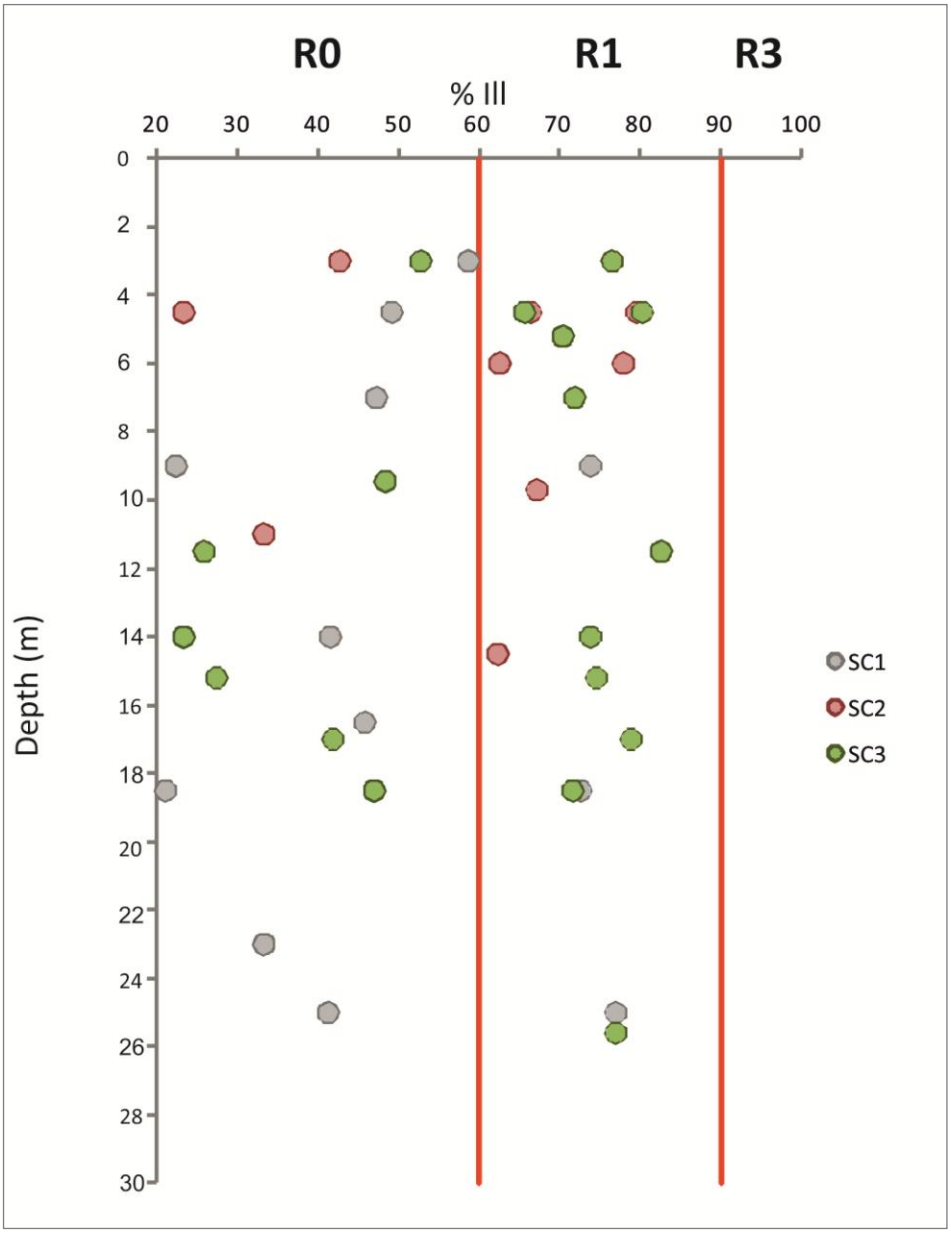

Figure 6.17 Variation grade of ordering with depth.

Table 6.5. Grade of ordering mixed layers I/S.

			001/002		002/003		
ID sample	% Illite	R*	d(Å)	2Θ	d(Å)	2Θ	Δ2Θ
PN1	58.6	R0	9.2	9.7	5.3	16.6	7.0
PN2	49.2	R0	9.0	9.9	5.4	16.5	6.6
PN3	47.2	R0	9.0	9.8	5.4	16.4	6.6
PN4	22.4	R0	8.8	10.1	5.2	15.8	5.7
PN4	73.8	R1	9.4	9.4	5.2	17	7.6
PN5	41.5	R0	9.0	9.8	5.5	16.2	6.4
PN6	45.8	R0	8.6	10.2	5.2	16.7	6.5
PN7	21.1	R0	8.9	9.9	5.7	15.6	5.7
PN7	72.6	R1	9.2	9.7	5.2	17.2	7.5
PN8	33.3	R0	8.7	10	5.5	16.1	6.1
PN9	41.3	R0	8.9	9.9	5.5	16.3	6.3
PN9	76.9	R1	9.5	9.3	5.2	17.0	7.7
PR1	42.7	R0	9	9.8	5.5	16.2	6.4
PR1	76.4	R1	9.5	9.4	5.2	17.0	7.7
PR2	23.3	R0	8.8	10	5.2	15.8	5.8
PR2	66.4	R1	9.4	9.4	5.3	16.7	7.3
PR2	79.5	R1	9.6	9.2	5.2	17.0	7.8
PR3	62.5	R1	9.1	9.6	5.3	16.7	7.1
PR3	77.9	R1	9.4	9.4	5.2	17.2	7.7
PR5	67.1	R1	9.3	9.6	5.3	16.9	7.3
PR6	33.3	R0	16.5	10	5.5	16.1	6.1
PR7	62.3	R1	9.4	9.4	5	16.5	7.1
MC1	52.7	R0	9.2	9.7	5.4	16.4	6.8
MC1	76.4	R1	9.5	9.4	5.2	17	7.7
MC2	65.6	R1	9.7	9.2	5.4	16.4	7.2
MC2	80.2	R1	9.5	9.3	5.2	17.2	7.8
MC3	70.4	R1	9.5	9.4	5.3	16.8	7.4
MC4	71.8	R1	9.4	9.4	5.3	16.9	7.5
MC5	48.3	R0	8.9	9.9	5.4	16.5	6.6
MC6	25.9	R0	8.9	9.9	5.6	15.7	5.8
MC6	82.5	R1	9.3	9.5	5.3	17.4	7.9
MC7	23.3	R0	8.6	10.3	5.4	16.0	5.8
MC7	73.8	R1	9.4	9.4	22.0	17.0	7.6
MC8	27.4	R0	8.8	10.1	5.6	15.9	5.9
MC8	74.5	R1	9.3	9.5	5.2	17.1	7.6
MC9	41.8	R0	9	9.9	5.5	16.2	6.4
MC9	78.8	R1	9.5	9.3	5.2	17.1	7.8
MC10	47.0	R0	9.3	9.5	5.5	16.1	6.5
MC10	71.6	R1	9.2	9.6	5.2	17.1	7.5
MC13	76.9	R1	9.4	9.4	5.2	17.1	7.7

Notes: R*= Reichweite. d= d spacing. Δ2Θ= distance between 001/002 and 002/003 reflections.

QUANTITATIVE ANALYSES

A quantitative evaluation of the minerals occurring in the samples was carried out by using two software: Bruker's TOPAS and Vb Affina (Cavalcanti et al., 2007; Leoni et al., 2008). Here below the results obtained by using these two techniques are shown.

Topas Software

Topas software has been used to obtain information about the quantitative amounts of minerals in the samples. The results obtained by using the Topas software are listed in Table 6.6. As shown, the mixed layer I/S is the most representative phase, followed by quartz and calcite. By using the software Topas it was not possible to evaluate the amount of mixed layer Chl/S. In fact, it was not possible to detected them in the XRD patterns of the bulk samples.

Specifically, considering the samples collected from the crown zone:

- The amount of mixed layer I/S ranges between 24 and 60.8 wt%. The lower value characterizes the PN3 sample, whereas the higher refers to the PN9 sample.
- The amount of chlorite and kaolinite ranges respectively between 1.6 and 6.9 wt% and 0 and 4.5 wt%. The amount of muscovite ranges between 0 and 16.6 wt%. The PN1, PN2 and PN3 samples contain about 16 wt% of muscovite, whereas in all other samples it ranges between 3.0 and 6.5 wt%.
- The amount of quartz ranges between 15.8 and 27.5 wt%, which indicates that it is the most representative phase after mixed layer I/S.
- The amount of Na-feldspar and K-feldspar ranges respectively between 2.9 and 16 wt%, and 2.6 and 6.3 wt%. The higher value of Na-feldspar characterized PN3 sample, whereas in case the PN5 sample the amount of Na-feldspar is lower than 5 wt%.
- The amount of calcite ranges between 4.4 and 21.1. The lower value characterizes the PN4 sample, whereas the higher characterizes the PN7.
- Dolomite occurs in trace except in case of PN8 sample, where its amount reaches 4.9 wt%.

In the samples collected from the sliding zone, it was detected that:

- The amount of mixed I/S layer ranges between 11 and 53.7 wt%. By looking at the data listed in Table 6.6, surficial samples are characterized by an average amount of I/S around 50 wt%, whereas all other samples are characterized by amounts of I/S not higher than 27 wt%.
- The amount of chlorite ranges between 1.9 and 6.4 wt%, whereas the amount of kaolinite ranges between 0 and 4.6 wt%, similarly to the samples collected from the crown zone. The amount of muscovite ranges between 0.1 and 9.6 wt%.
- The amount of quartz ranges between 15.1 and 69.9 wt%. The higher value characterizes the PR4 sample, whereas the lower value refers to the PR2 sample (<20 wt% of quartz).

- The amount of Na-feldspar and K-feldspar ranges respectively between 1.7÷20.7 wt%, and 4.0÷10.0 wt%. These values are higher than those recorded in correspondence of the crown zone.
- The amount of calcite ranges between 5.0 and 28.3. The lower value characterizes the PR7 sample, whereas the higher characterizes the PR9.
- Dolomite occurs in trace.

In the samples collected from accumulation zone, it was possible to verify that:

- The amount of mixed I/S layer ranges between 12.7 and 64.5 wt%. The higher amount of mixed layer characterizes the MC2 sample and represents the highest value recorded for all three investigated drillcores.
- The amount of chlorite and kaolinite ranges between 0.4 and 5.7 wt% and 0 and 4.5 wt%. The amount of muscovite ranges between 1.45 and 7.3 wt%.
- The amount of quartz ranges between 15.8 and 38.3 wt%. The lower value characterizes the MC2 sample, whereas the higher characterizes the MC12 sample.
- The amount of Na-feldspar ranges between 1.2 and 14 wt% whereas the amount of K-feldspar ranges between and 2.4 and 10.1 wt%.
- The amount of calcite ranges between 2.5 and 39. The lower value characterizes the MC5 sample, whereas the higher characterizes the MC6.
- Dolomite occurs in trace.

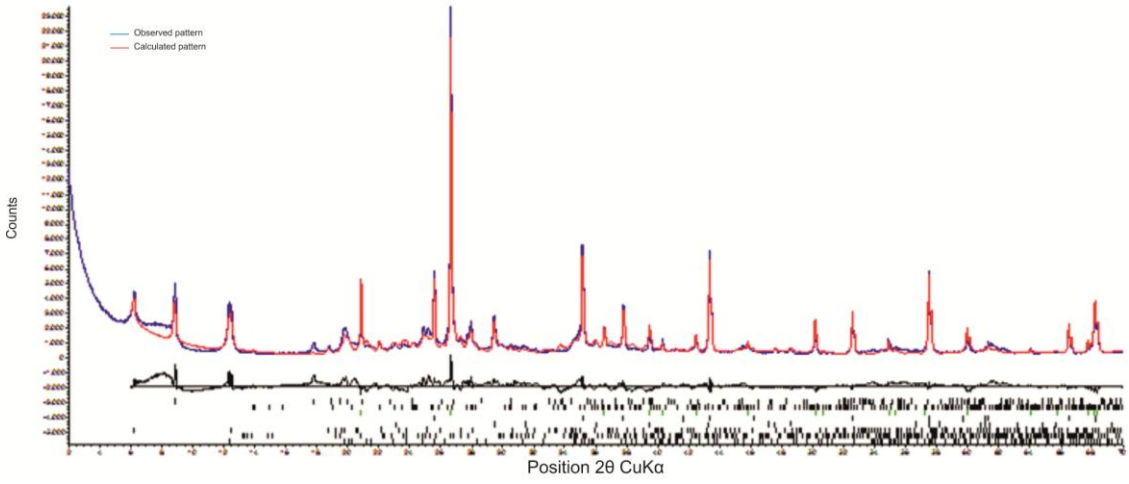

Figure 6.18 Fitting between observed and calculated patterns, by using Topas software.

By considering all these data, several doubts arise on the fact that in many cases the amount of mixed layer I/S is higher than 50 wt%, which means that the percentage of clay minerals should be almost higher than 60%. This value seems to be too high, considering that most of the analyzed samples have been classified as sandstone, and no sample have been classified as pure shale. Moreover, as mentioned in the previous chapter, the calculated and observed patterns do not fit very well in the Topas process, although corrections about the peak position and peak broadening have been conducted. In addition, the absence of mixed layer Chl/S makes the results, obtained by using only the Topas software, incomplete.

Table 6.6. XRPD quantitative analysis using Topas software.

ID sample	I/S	Ms	Na-f	Qz	Cal	Chl	Kln	K-f	Dol
				(wt %)					
PN1	31	16	15	26	4.9	2.9		4	0.4
PN2	31	16.6	11.7	21.9	10	2.2		4.3	1
PN3	24	16.2	16	27.5	9	1.6		3.7	2.3
PN4	58.7	4.6	5.7	18	4.4	3.2		4	1.4
PN5	50.4	3.1	4.3	21.7	7.7	3.2	3.2	6.3	0.2
PN6	49	6.5	7	17	6.3	6.9	0.6	4	4.5
PN7	39	3	7	16	21.1	6.6		3	3.2
PN8	39	5	8.7	22.5	10.1	4.5		2.9	4.9
PN9	60.8	3.3	3	15.8	4.7	2.1	4.6	3.3	1
PR1	51.8	5.6	8.2	19.4	6	3		5.8	0.2
PR2	53.7	6	5.5	15.1	7	6.4	4.6	5.5	0.7
PR3	45.9	9.6	7.4	21.3	5.8	3.1		6.7	0.1
PR4	11	0.1	1.7	69.9	7.8	3.8	0.2	4.4	0.9
PR5	17.6	7.7	15.3	34.3	14.18	1.9		7.6	1.4
PR6	46	0.8	11	23	6	4.1		8	
PR7	14.1	4.5	20.7	44.6	5.3	2.6		8	0.3
PR8	27	1.8	11	28.6	19.1	3.9	0.3	7	0.6
PR9	20	0.9	9	30.5	28.7	2	0.4	8	0.2
PR10	27	1.4	10	38	10.2	3.6	0.4	9	0.1
PR11	23	1.6	10	37	14.5	3.3	0.4	10	0.3
MC1	62.7	5.3	5.4	16.9	3.4	0.7		5.3	0.1
MC2	64.5	5.8	3.6	15.8	3.1	3.3	0.45	2.7	0.7
MC3	55	5	4	16	4.4	5.7	3.8	7	1.1
MC4	54.9	7.3	4.3	21.1	4.3	3.1	1.	3.6	0.4
MC5	61.1	3.1	1.2	19.3	2.5	5.7	4.5	2.4	0.4
MC6	18.3	4.1	6.5	21.9	39	2.2	1.2	5.9	0.8
MC7	36	1.9	11	26.8	9	4.9	0.3	7.3	0.7
MC8	12.7	6.4	12.3	27.9	33.1	0.4		5.	1.9
MC9	38.3	2.3	10.4	25.2	7.9	3.6	4.3	7.2	0.8
MC10	37	2.3	12	28.9	5.5	2.8	3.6	7.7	0.4
MC11	25		0.1	40	30	1.4	1	1	1.3
MC12	19.2	1.8	13.9	38.3	11.2	2.9	2	10.1	0.6
MC13	44.7	5.6	4.5	31.3	4.2	2.4		5.5	1.7
MC14	24	1.5	14.	34.7	10.4	2.9	2.2	9.3	0.6

Notes: I/S=mixed layers illite-smectite; Ms=muscovite; Na-f=Na-feldspar; Qz= quartz; Cal=calcite; Chl=chlorite; Kln=kaolinite; K-f=K-feldspar; Dol=dolomite.

Vb Affina Software

As anticipated in the Methods chapter, Vb Affina allowed to control the amount of the phases by matching chemical and mineralogical data. This procedure makes possible to obtain more accurate results.

In the Vb Affina software the data obtained by Topas were matched with chemical analyses obtained by XRF method, following the procedures described by Leoni et al. (2008), with the aim to obtain a sum of square between calculated chemical composition and experimental chemical composition close or lower than 2.00. The results are shown in Table 6.7.

As it is possible to see, the mixed layer I/S still represent the most representative phase, but the higher amount is not as high as those detected by using Topas software (52 wt% instead of 64.5 wt%). Quartz represents the second most abundant phase followed by calcite. Here below a description of the obtained data is reported.

In the case of samples collected from the crown zone:

- The amount of mixed layer I/S ranges between 26 and 52 wt%. As before, the lower value characterizes the PN3 sample whereas the higher characterizes the PN9 sample.
- The amount of Chl/S mixed layer ranges between 0 and 15 wt%. It results absent for the PN5 sample, whereas the highest amount was detected in the sample PN1.
- The amount of chlorite ranges between 6 and 17 wt%, whereas the amount of kaolinite ranges between 0 and 6 wt%. These values are not so far from those obtained by using Topas software, as well as in the case of muscovite, whose amount ranges between 4 and 16 wt%. It is also confirmed that the higher amounts of muscovite characterizes the PN1, PN2 and PN3 samples.
- The amount of quartz ranges between 13 and 20 wt%.
- The amount of Na-feldspar and microcline ranges between 3 and 9 wt%, and 1 and 5 wt% respectively. These values are slightly lower than those detected before.
- The amount of calcite ranges between 4 and 24 wt%.
- Dolomite occurs in trace except in of the sample PN8, where it reaches an amount of 6.0 wt% instead of 4.9 wt% detected by Topas.

In case of samples collected from the sliding zone

- The amount of mixed layer I/S ranges between 8 and 44 wt%. Also in this case the minimum and maximum values are lower than those detected before. By looking at data showed in Table 6.4, it is evident that from a depth of 14.00 m down to the bottom of the hole, no samples show an amount of mixed layer I/S higher than 30 wt%.
- The amount of mixed layer Chl/S ranges between 0 and 4 wt%.

- The amount of chlorite and kaolinite ranges between 1 and 11 wt% and 0 and 7 wt% respectively. Similar values have been obtained for the muscovite, whose amount ranges between 1 and 10 wt%.
- The amount of quartz ranges between 15and 66 wt%. These values are really close to those obtained by using Topas software.
- The amount of Na-feldspar ranges between 2and19 wt%, and the amount of K-feldspar ranges between and 2 and 9 wt%.
- The amount of calcite ranges between 4 and 41 wt%. As before, the higher value characterizes the PR9 sample, whereas the lower value characterizes the PR3 instead of PR7 as detected by Topas.
- Dolomite occurs in trace, except in the case of PR3 sample where it reaches 5 wt%.

In the samples collected from the accumulation zone:

- The amount of mixed layer I/S ranges between 12 and 50 wt%. The higher value characterizes the MC3 sample and the lower characterizes the MC8 sample.
- The amount of mixed Chl/S layer ranges between 0 and 4 wt%.
- The amount of chlorite and kaolinite is higher than those evaluated before ranging between 3 and 13 wt% and 0 and 12wt% respectively as in the case of muscovite whose amount ranges between 2.34 and 9 wt%.
- The amount of quartz ranges between 13 and 31 wt%.
- The amount of Na-feldspar ranges between 2 and 19 wt%, whereas the amount of K-feldspar ranges between 1 and 9 wt%.
- The amount of calcite ranges between 2 and 39. The lower value characterizes the MC2 sample instead of MC3 sample detected by Topas, whereas the higher characterizes the MC6 sample as before.
- Dolomite occurs in trace.

Table 6.7 XRPD quantitative analysis using Vb Affina software.

ID sample	I/S	Chl/ Sm	Ms	Na-f	Qtz	Cal	Chl	Kln	K-f	Dlm
					(wt%)					
PN1	33	15	16	9	15	4	6		1	1
PN2	32	4	9	7	16	9	17		3	3
PN3	26	4	10	6	18	15	14		5	2
PN4	38	4	8.5	7	14	7	10	5	4	2
PN5	47		5	3	20	8	8	6	3	1
PN6	39	4	7	9	13	8	9	5	1	5
PN7	34	4	5	9	13	24	6		1	4
PN8	39	4	7	6	15	8	9	4	2	6
PN9	52	4	4	4	13	6	10	4	1	2
PR1	34	4	9	5	19	9	8	7	2	3
PR2	44	4	1.5	2	15	13	9	6	3	2
PR3	39	4	3	6	20	4	9	7	3	5
PR4	8		1	4	66	11	5		3	2
PR5	19		10	10	27	20	7		5	2
PR6	30	4	5	9	19	15	6	5	5	2
PR7	14		5	19	40	9	7		5	1
PR8	26	4	7	7	23	10	11		9	3
PR9	22		1	5	23	41	1		2	5
PR10	24		5	10	35	16	2		6	2
PR11	22		4	8	31	25	3		5	2
MC1	43	4	9	4	16	6	8	6	1	3
MC2	46	4	4	4	16	2	12	7	3	2
MC3	50	4	3	3	13	4	12	8	2	1
MC4	43	4	8	2	15	2	13	9	3	1
MC5	48	4	7	3	13	3	8	12	1	1
MC6	15		5	5	20	39	8	4	3	1
MC7	24	4	4.5	8	24	21	4	2	6	2
MC8	12	4	7	6	19	39	4		6	3
MC9	38	4	4	8	21	14	5		3	3
MC10	31.5	4	2.3	8	29	11	6		6	2
MC12	20		4	15	31	17	3	1	7	2
MC13	17	2	5	19	31	9	5	1	9	2
MC14	24		3	13	27	16	4	1	9	3

Notes: I/S=mixed layers illite-smectite; Chl/S= mixed layer chloRite-smectite; Ms=muscovite; Na-f=Na-feldspar; Qz= quartz; Cal=calcite; Chl=chlorite; Kln=kaolinite; K-f=K-feldspar; Dol=dolomite.

CHEMICAL ANALYSES-XRF

Whole rock chemical analyses have been carried out to test and to perform the quantitative mineralogical analyses by using the experimental software Vb Affina. Specifically, in the case of samples collected from the crown zone, SiO_2 represents the most abundant oxide, with an average amount of 50.8 wt%, followed by Al_2O_3 and Fe_2O_3. These two oxides occurred in the samples with an average amount of 16.5 wt% (Al_2O_3) and 6.7 wt% (Fe_2O_3). CaO occurs with an average value of 6.2 wt%, whereas MgO with an average amount of 4.02 wt%. As shown in Table 6.8 all other oxides occur in trace.

Also in the case of samples collected from the sliding zone,

SiO2 represents the most abundant oxide, occurring with an average amount of 57.4 wt%. The amount of SiO_2 ranges between 45.3 and 76.7 wt%. The higher values characterize the calcarenitic sandstone samples, as in the case of the PR4 sample. It is followed by Al_2O_3, whose mean value is 11.9 wt%, and by CaO with an average amount of 9.4 wt%. Fe_2O_3 occurs with an average amount of 4.3 wt%. All other oxides occur in trace (Table 6.8).

In the samples collected from the accumulation zone, SiO_2 occurs with an average value of 52.7 wt%, Al_2O_3 occurs with an average amount of 14.2 wt% and CaO occurs with an average quantity of 9.3 wt%, confirming that also in this case these oxides are the most abundant for the analyzed samples. Fe_2O_3 occurs with an average amount of 5.8 wt% and all other oxides occur in trace as shown in the Table 6.8.

These chemical data do not change with depth, and do not show any trend along the cores or correlations with the stratigraphy.

Table 6.8 Whole rock chemical data of the main oxides.

SAMPLE	SiO2	TiO_2	Al_2O_3	Fe_2O_3	MnO	MgO	CaO	Na_2O	K_2O	P_2O5
					wt%					
PN1	55.7	0.8	17	6.9	0.1	5	2.4	1	0	0.1
PN2	50.6	0.7	15.4	7	0.1	5.6	5.4	1	3.1	0.1
PN3	51.2	0.7	14.7	5.8	0.1	5.1	8.3	1.1	2.9	0.1
PN4	53.6	0.9	16.8	7.5	0.1	3.5	3.9	0.7	3.3	0.1
PN6	53.1	0.9	17.5	6.8	0.1	3.1	4.3	0.9	2.1	0.2
PN6	50.6	0.8	17.9	6.	0.2	3.9	6.1	1.4	2.7	0.1
PN7	41.7	0.6	13.1	5.8	0.3	3.3	14.8	1.2	2.2	0.1
PN8	50.8	0.8	16.9	6.3	0.1	3.9	6.34	1.3	2.5	0.1
PN9	50.3	0.9	19.5	6.9	0.1	2.8	4.8	0.9	2.5	0.1
PR1	52.2	0.8	16.4	7	0.2	3.4	5.3	0.5	3.1	0.2
PR2	50.5	0.8	15.3	6.9	0.2	3.1	7.1	0.6	3.2	0.5
PR3	54.6	0.9	17.6	7.3	0.1	3.7	3.5	0.5	3.5	0.1
PR4	76.7	0.4	4.1	2.7	0.2	1.2	7.2	0.5	0.9	0.1
PR5	58.3	0.4	12.2	3.5	0.1	2.4	10.8	1.2	2.7	0.1
PR6	55.2	0.6	14.4	4.2	0.1	3.2	8.1	0.8	3.5	0.1
PR7	66.8	0.3	13	2.5	0.1	1.8	4.8	2.5	2.5	0.1
PR8	49.3	0.8	10.7	6.9	0.2	2.8	6.8	0.7	3	0.4
PR9	45.3	0.1	6.6	1.7	0.1	0.9	25.8	1.4	2.2	
PR10	63.9	0.2	10.5	2.2	0.1	1.4	9.6	1.9	2.8	0.1
PR11	58.5	0.2	9.6	2.2	0.1	1.3	14.5	1.8	2.9	0.1
MC1	52.2	1	18.5	7.8	0.2	3.5	4	0.45	3.3	0.1
MC2	54	0.9	19.5	8.3	0.3	3.4	1.6	0.4	3.6	0.1
MC3	49.9	0.9	18.2	7.6	0.2	3.4	4.4	0.5	3.2	0.1
MC4	54.2	0.9	18.7	8	0.2	3.4	1.6	0.4	3.4	0.1
MC5	53.4	1	19	8.4	0.1	2.9	1.9	0.2	2	0.2
MC6	39.8	0.6	12.5	5.1	0.4	2.3	19.9	0.6	2.2	0.1
MC7	43.5	0.5	10.8	4.8	0.3	2.2	18.6	0.4	2.2	0.1
MC8	54.	0.5	13.1	4	0.1	2	10.4	1.3	2. 8	0.1
MC9	55.4	0.7	14.8	4.9	0.1	2.7	8.8	1	3.4	0.1
MC10	60.4	0.5	13.6	4.2	0.1	2.6	6.8	1.1	3.5	0.13
MC11	359	0.3	2.5	9.3	1.9	3.4	26.1	0.2	0.1	0
MC12	61.9	0.2	10.6	2.3	0.1	1.2	10.4	2.1	2.9	0.1
MC13	63.2	0.4	14.2	2.8	0.1	1.9	5.9	2.2	3.4	0.1
MC14	60.4	0.3	12.23	2.8	0.1	1.8	10	1.9	3.3	0.1

Table 6.9 Whole rock chemical data of trace elements.

SAMPLE	Rb	Sr	Y	Zr	Nb	Ba	Cr	Ni	Sc	V	La	Ce
						(ppm)						
PN1	158.2	144.4	33.9	170.4	22	534.9	216.5	112.8	18.4	102.4	45.2	63.2
PN2	155	193	33.8	148	22.6	470.3	238.8	119.8	19.5	129.8	30.9	63
PN3	144.3	217.7	31.7	146.1	19.1	462.3	180.7	97.0	18.2	118.9	30.2	58.1
PN4	158.9	325.1	35.1	202.7	27	425.6	184.8	86.9	20.2	99.6	45.5	96.4
PN5	127.7	433.3	33.6	178.5	28	386.1	199.3	54.8	20	139.9	57.0	93
PR1	160.8	256.2	34.6	218.4	27.8	582.6	172.7	84.7	22.5	121.9	40.9	94.1
PR2	112.7	285.0	18.1	113.2	7.8	253.3	270.2	23.7	9	37.8	24.1	25.9
PR3	165.4	209.3	36.1	233.4	29.2	441.9	182.1	88.2	18.8	108.5	37.9	91.1
PR5	134.0	211.3	24.8	143.6	14.6	451.2	71.2	37.1	13.2	52.2	23.2	47.7
PR6	163.7	181.5	32.9	183.8	18.8	306.7	128.5	47.9	18.6	76.5	38.2	68.3
PR7	98.5	161.8	15.7	85.6	10.8	187.6	42.1	22.7	8.5		12.8	33.2
MC1	167.3	205.1	33.2	209.3	29.7	456.7	175.9	97.2	20.9	227.5	52.8	127.4
MC2	188.7	238.5	36.9	254.8	32.0	351.3	172.4	93.6	22.2	125.2	51.5	106.7
MC3	177.5	259.8	33.9	237.2	29.8	393.5	166.8	98.8	18.6	212.6	50.7	124.5
MC4	174.1	211.4	34	227.8	30.3	372.2	176.7	89.1	19	110.4	49.3	105.9
MC5	125.4	192.6	35	178.3	30.6	315.0	217.4	69.2	22.3	204.9	47	90.3
MC6	135.6	312.5	25.8	148.2	18.2	942.9	100.1	47.4	17.4	99	40.1	56.4
MC7	157.6	167.9	25.8	149.7	16.3	490.5	90.8	45.7	17	77.6	29.9	42.5
MC8	154.4	234.5	26.3	147.9	15	381.0	98.5	38	15.5	62.2	17	44.4
MC9	183.8	197.1	36.9	204.9	2	441.3	110.8	43	18.8	82.1	30.3	60.8
MC10	178.4	172.8	30.8	175.1	18	428.4	105.8	41.9	14	77.2	26.5	46.3
MC11	16.2	308.9	24.2	393.9	2.6	9409.8	209.3	41.3	11.5	578.6	9.7	
MC13	144.7	146.5	17.5	98.6	13.2	357.4	56	29.1	9.3	40.4	22.5	31.5

SEM ANALYSES

SEM analyses allowed to observe microtextures and morphologies of several mineral phases occurring in the samples.

Specifically, in the samples collected from the Sc1 borehole, flakes morphologies were observed; the flakes are random-oriented in the surficial samples, whereas they show a slightly sub-parallel organization more in depth. The PN1 sample also shows mineral morphologies with the characteristic sub-parallel mica structure (Figs. 6.19, 6.20, 6.21, 6.22).

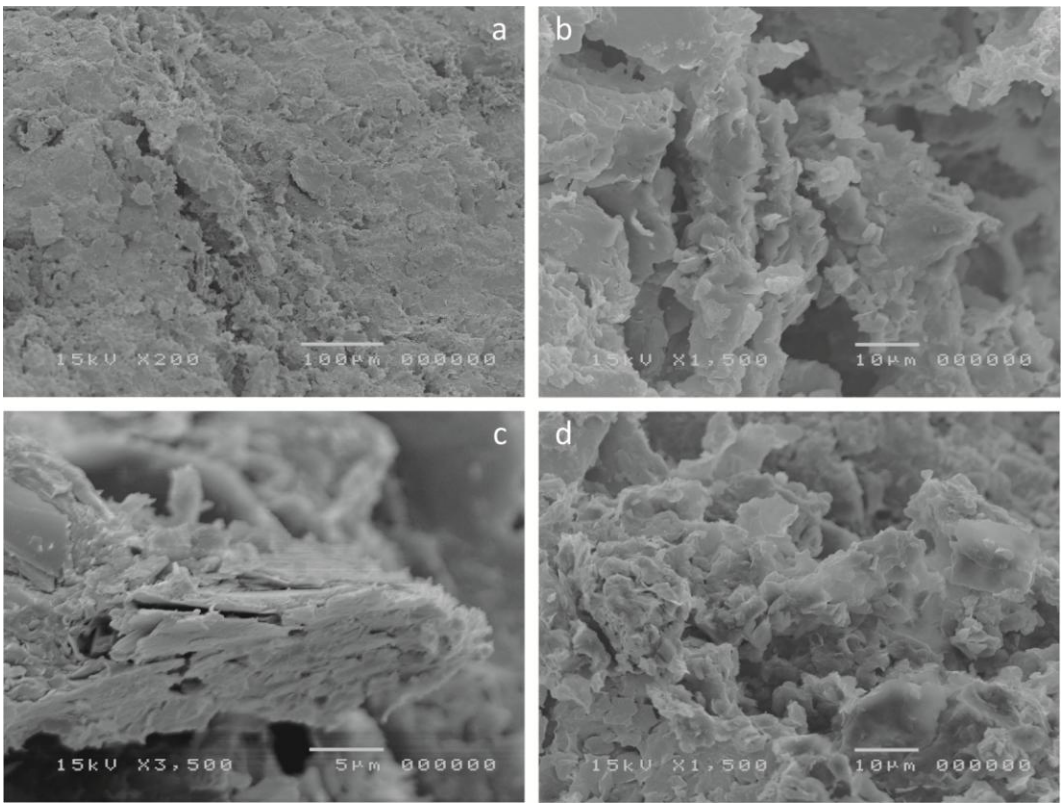

Figure 6.19 SEM images of PN1 sample: a) matrix of the sample; b) flake morphologies of clays; c) mica structure; d) flake morphologies of clays.

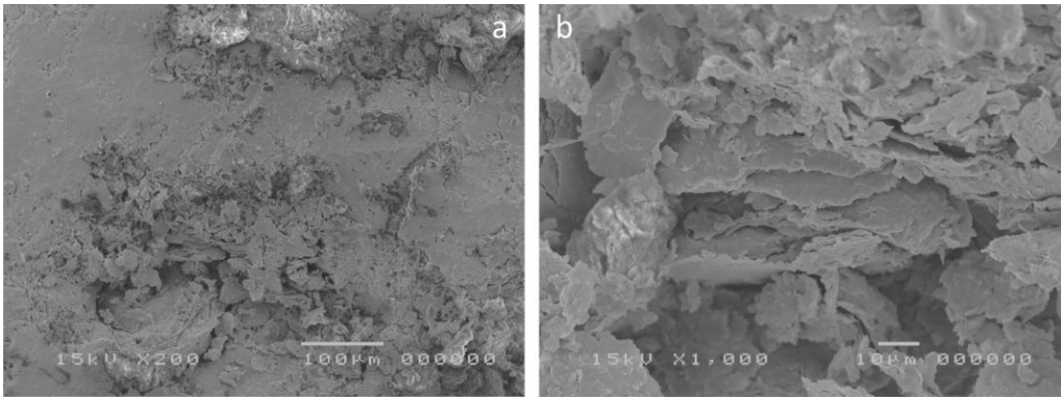

Figure 6.20 SEM images of PN5 sample: a) matrix of the sample; b) sub-parallel clay flakes.

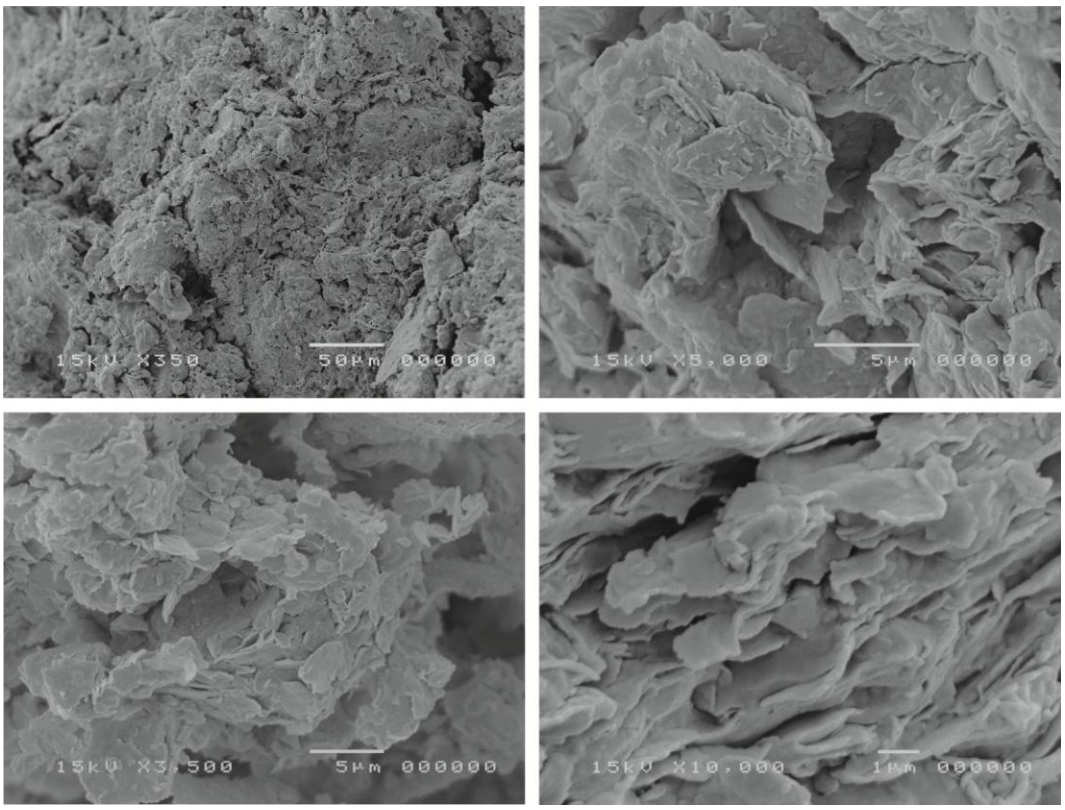

Figure 6.21 SEM images of clay flakes in the PN8 sample.

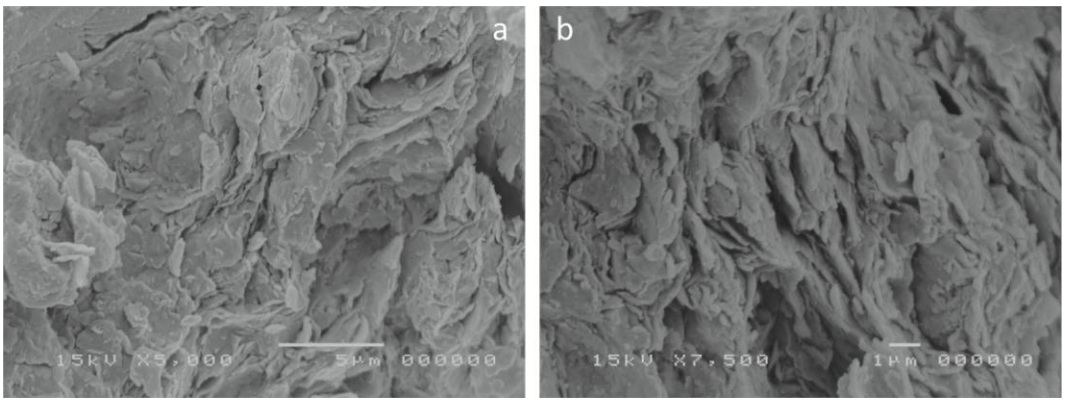

Figure 6.22 SEM images of PN9 Sample: a) clay flakes; b) enlargement of (a).

Samples collected from Sc2 core exhibit flakes, sometimes associated with quartz crystals (Figs. 6.23, 6.24, 6.25). Mica structures are also well visible in the PR11 sample (Fig. 6.26).

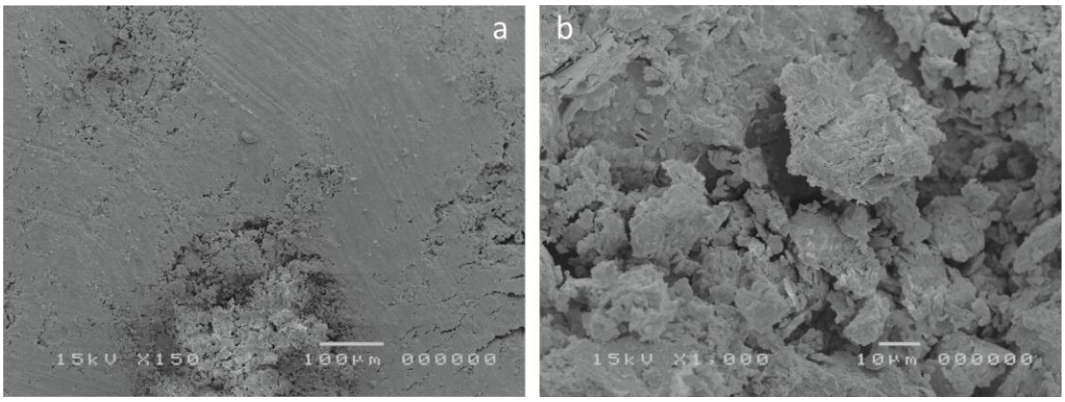

Figure 6.23 SEM images of PR1 sample: matrix.

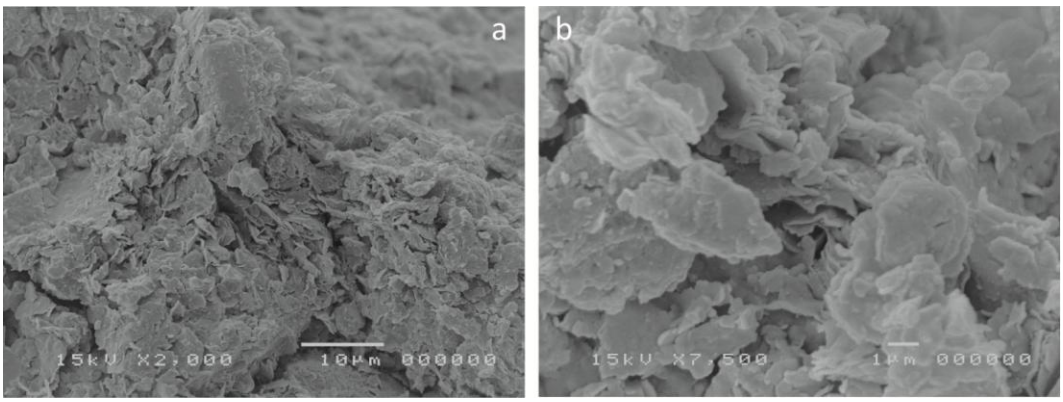

Figure 6.24 SEM images of PR5 sample: a) clay flakes; b) enlargement of (a).

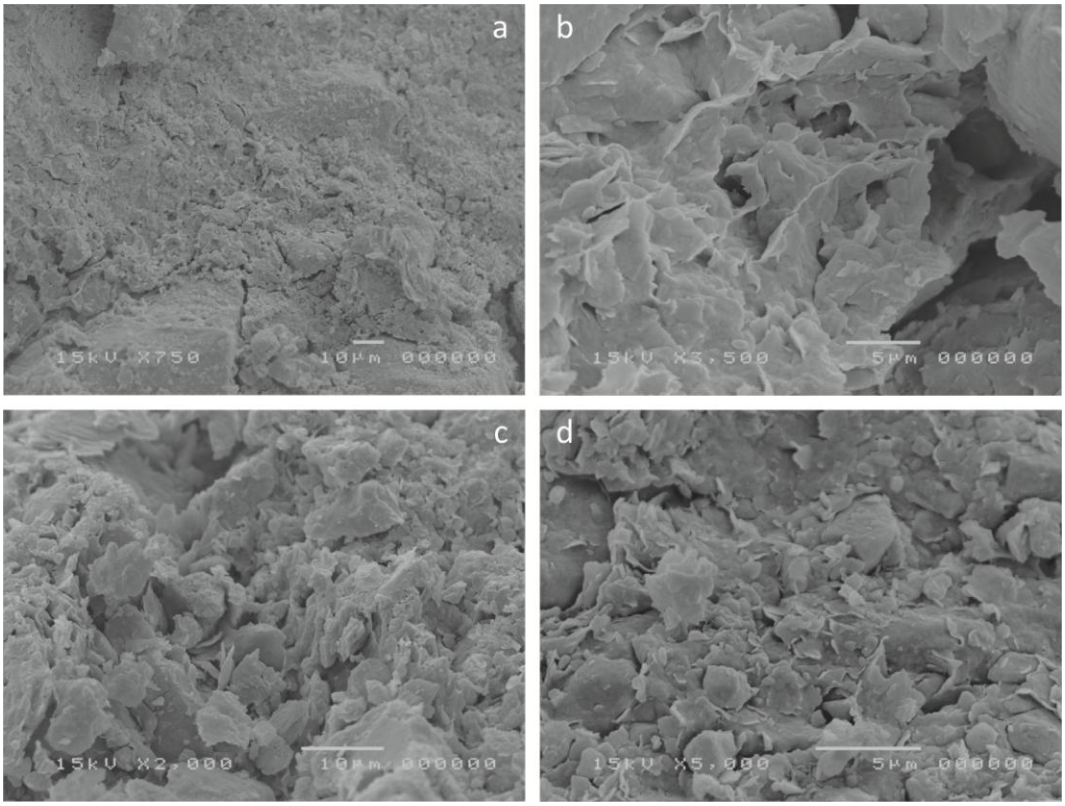

Figure 6.25 SEM images of PR7 sample: a) matrix; b) clay flakes; c) and d) clay flakes and quartz crystals.

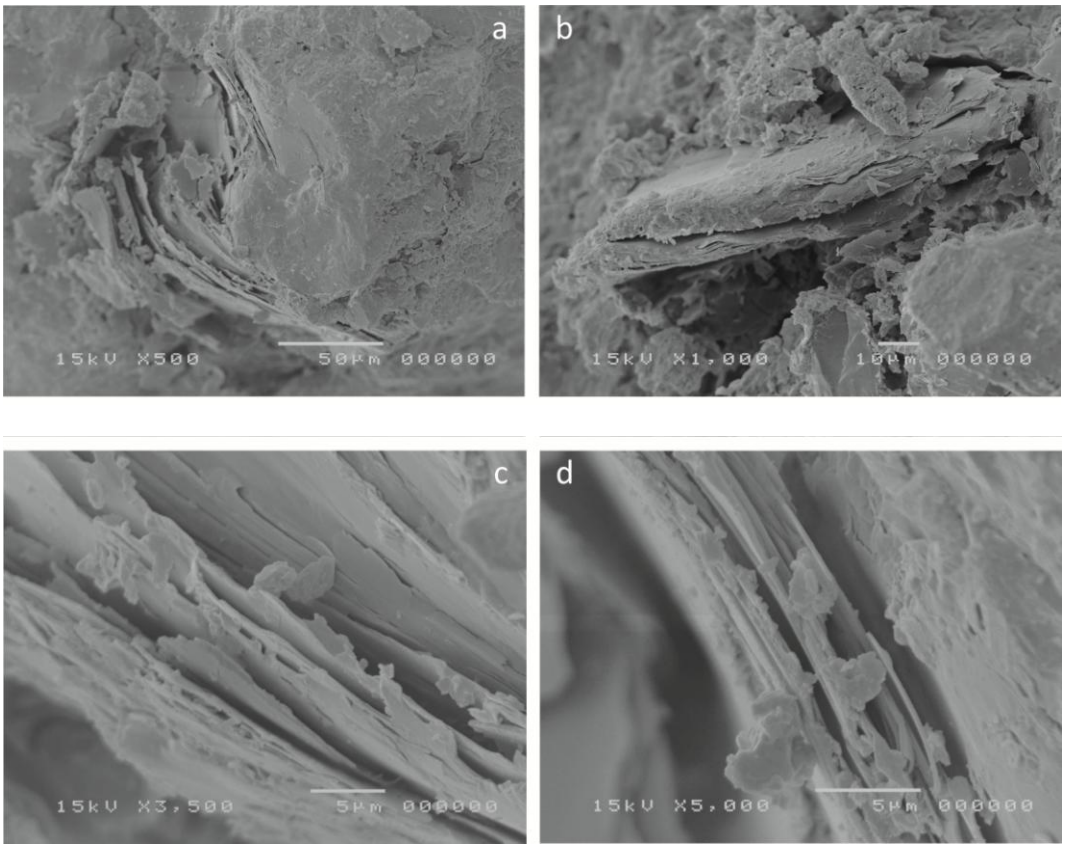

Figure 6.26 SEM images of PR11 sample: different enlargements of mica structures.

Samples collected from Sc3 core result highly heterogeneous, but also here, flakes and mica structures are detectable (Figs. 6.27, 6.28, 6.29, 6.30).

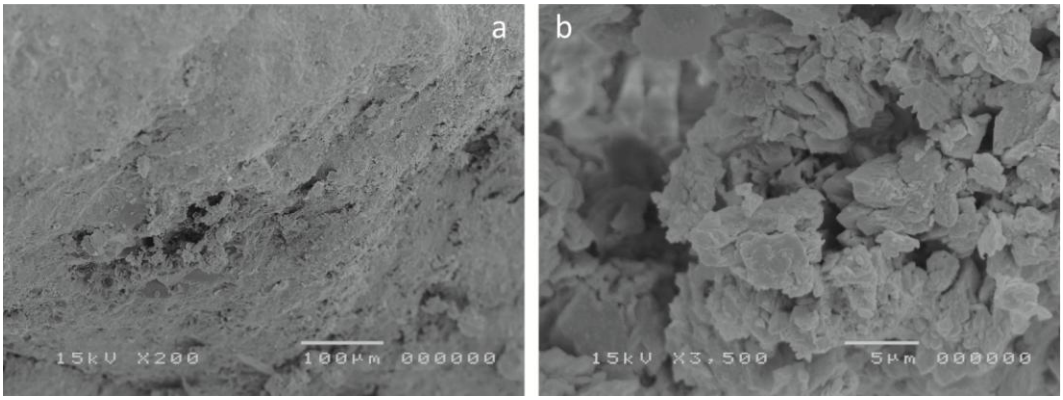

Figure 6.27 SEM images of MC1 sample a) matrix; b) enlargement of clay flakes.

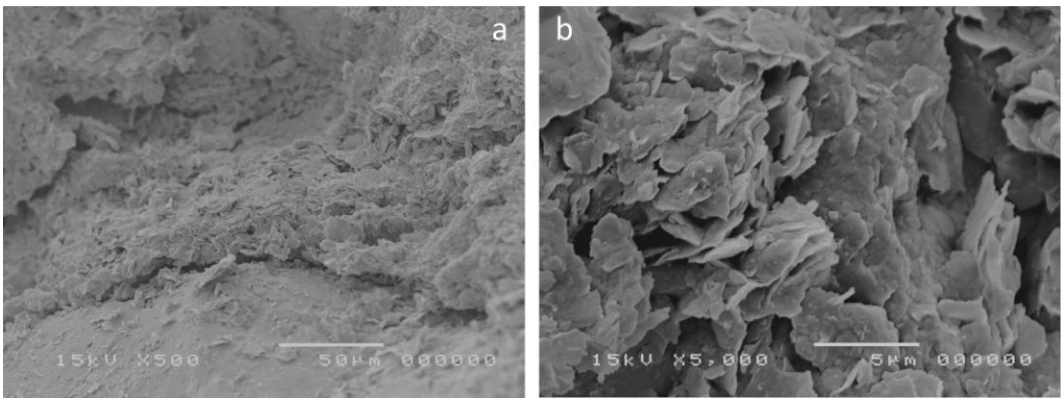

Figure 6.28 SEM images of MC5 sample a) clay flakes; b) enlargement of (a).

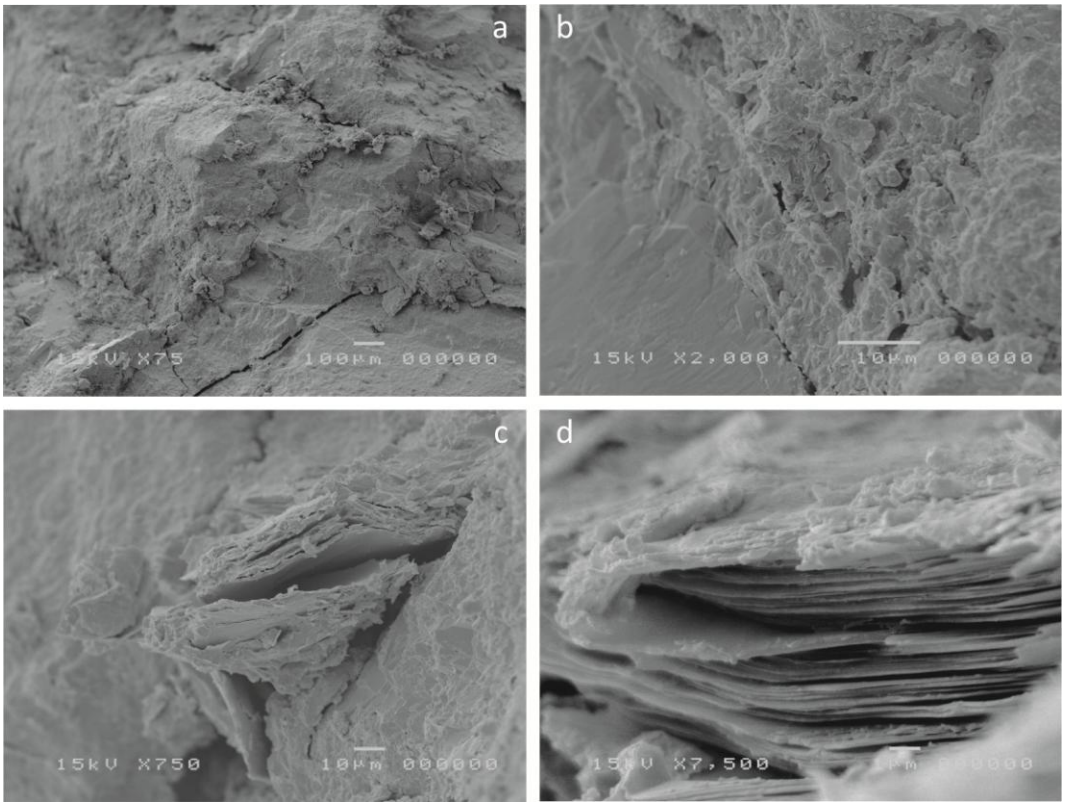

Figure 6.29 SEM images of MC7 sample: a) and b) matrix; c) and d) mica structures.

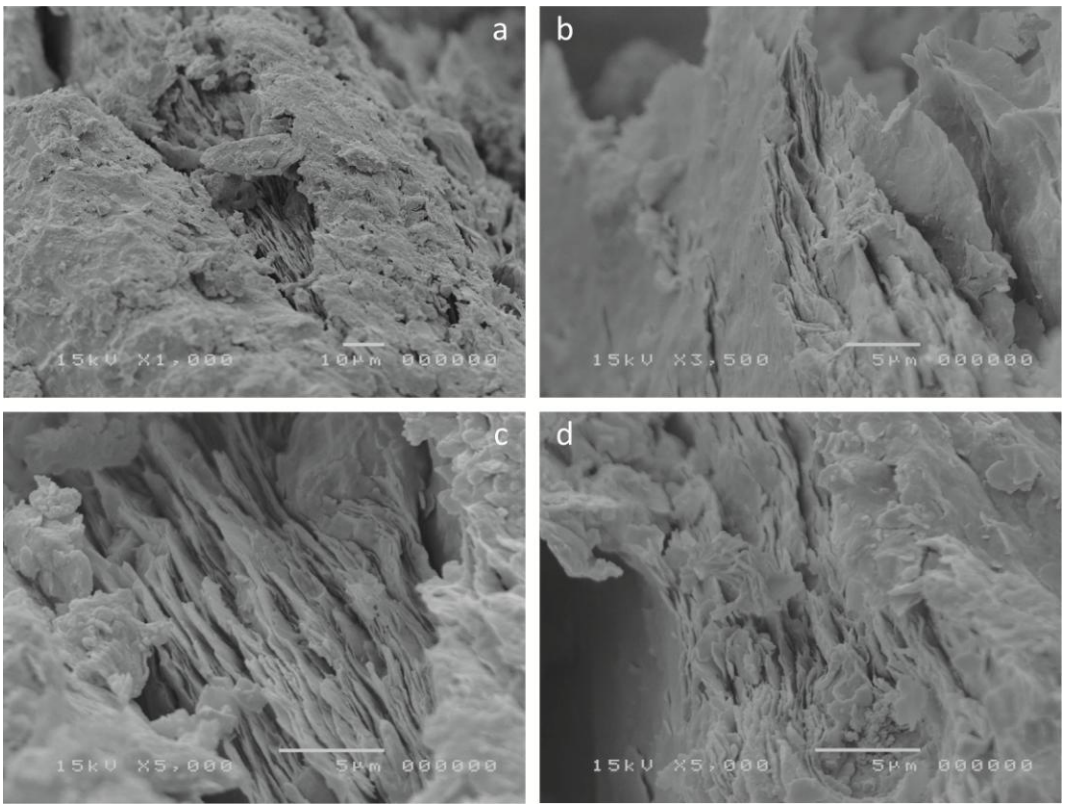

Figure 6.30 SEM images of MC12 sample: different enlargements of mica structures.

GEOTHECNICAL CHARACTERIZATION

GRAIN SIZE ANALYSES

Grain size analyses confirmed the great variability of the analyzed samples (Table.6.10). For all sample shape curve parameters have also been evaluated: uniformity coefficient (Cu) and coefficient of curvature (Cc).

Uniformity coefficient (Cu) has been evaluated by considering the following equation:

$$Cu = \frac{D_{60}}{D_{10}} \quad \text{Eq 6.1}$$

Where D_{60} is the grain diameter for which 60% of the sample is finer than D_{60} and D_{10} is the diameter for which the sample is finer than D_{10}. The larger the Cu value the wider the size distribution and vice versa.

The coefficient of curvature (Cc) has been evaluated by considering the following equation;

$$C_C = \frac{(D_{30})^2}{(D_{60} * D_{10})} \quad \text{Eq.6.2}$$

Where D_{60} is the grain diameter for which 60% of the sample is finer than D_{60}, D_{30} is the diameter for which the sample is finer than D_{30} and D_{10} is the diameter for which the sample is finer than D_{10}. A soil is well graded for coefficient of curvature ranging between 1 and 3, with Cc>4 for gravels and Cc> 6 for sands.

Specifically, in the case of samples collected from Sc1 borehole, granulometric curves (Fig.6.31) are characterized by similar patterns, except PN5 sample, which is characterized by a not gradual transition from sand to silt.

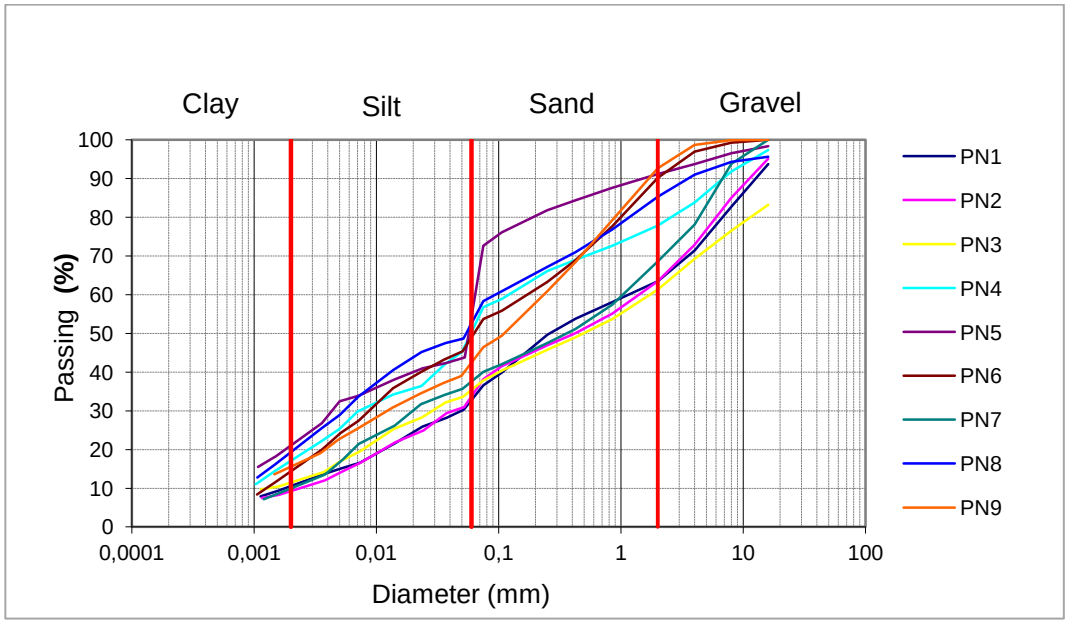

Figure 6.31 Grain size curves, samples collected from Sc1 borehole**.**

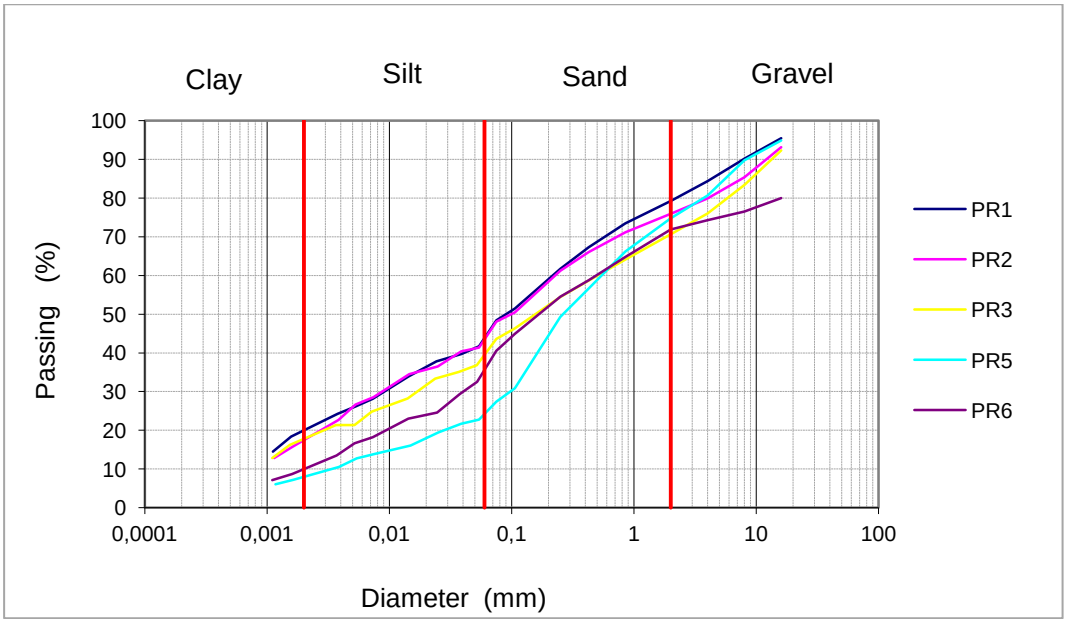

Figure 6.32 Grain size curves, samples collected from Sc2 borehole**.**

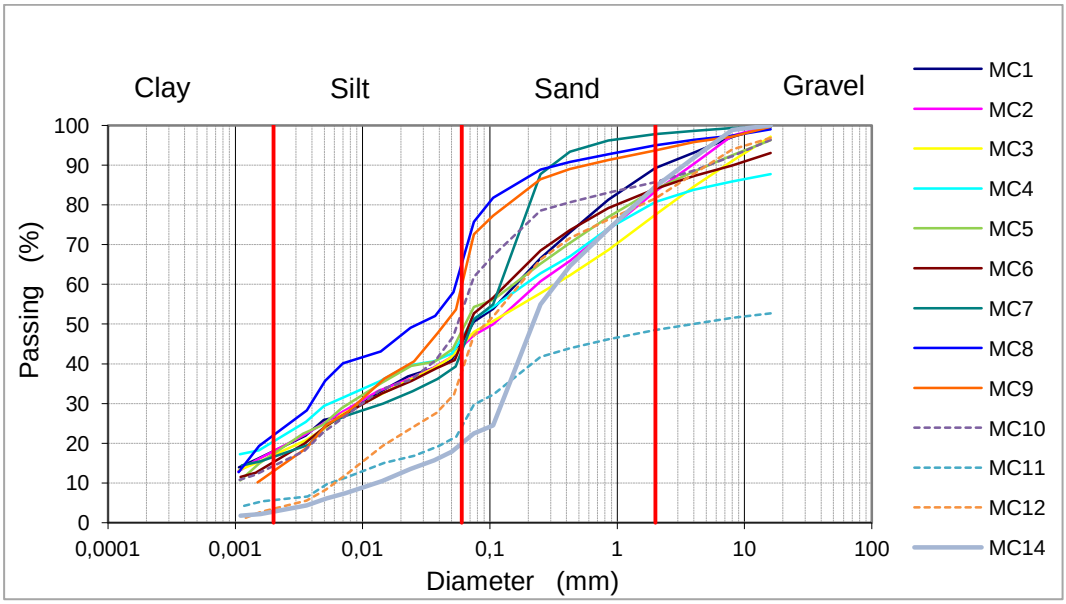

Figure 6.33 Grain size curves, samples collected from Sc3 borehole.

Looking at the data listed in Table 6.10 it is possible to see that all relative percentages tend to change without any correlation with depth.
The lowest uniformity coefficient characterizes the PN8 sample, whereas the higher one characterizes the MC4 sample.
No samples show a percentage of clay fraction higher than 22 wt%.

Table 6.10 Grain size distributions.

ID Samples	% Gravel	% Sand	% Silt	% CF	Cu	Cc
PN1	36.5	31	21.50	11	666.7	1.2
PN2	36.5	30.5	24	9	590.9	0.6
PN3	38.6	25.4	24	12	1416.6	0.4
PN4	22.1	27.9	33	17	133.3	0.5
PN5	8.8	36.2	33.5	21.5	90	0.4
PN6	9.8	40.2	37	14	150	0.4
PN7	31.4	31.1	27.5	10	500	0.2
PN8	14.7	31.3	35	19	11.6	4.2
PN9	7.3	49.7	27	16	314.3	0.9
PR1	20.7	35.8	23.5	20	262.5	0.5
PR2	24.	33	26.	17	275	0.5
PR3	29.4	31.6	22	17	555.6	0.6
PR5	25.2	51.1	15.72	8	167.7	6
PR6	28.1	35.9	26	10	240	1. 7
MC1	10.7	44.3	27	18	320	1.3
MC2	16.6	39.4	26	18	287.5	0.4
MC3	22.5	32.5	38	17	457.1	0.5
MC4	19.3	34.7	25	21	1800	1.4
MC5	16.1	35.9	30	18	150	0.3
MC6	16	38.1	30.2	15.8	162.5	1
MC7	2.18	53.82	28	16	600	7.04
MC8	4.96	30.04	42.50	22.50	510	2.98
MC9	6.32	35.68	45	13	20	0.45
MC10	14.24	31.66	40.10	14	87.50	1.79
MC11	51.51	23.49	20	5		
MC12	18.37	41.63	36	4	30	1.56
MC14	15.39	64.61	17	3	24.62	3.46

Notes:CF=clay fraction; Cu= Uniformity coefficient; Cc= curvature coefficient.

SPECIFIC GRAVITY TEST

Despite the great lithological as well as mineralogical variability of the analyzed samples, their Gs values are quite similar, ranging between 2.56 and 2.72 (kN/m^3) (Table. 6.11).

Specifically:

- Specific gravity for all samples collected from Sc1 core ranges between 26.36 and 27.44 (kN/m^3), for an average value of 26.85 (kN/m^3).

- Specific gravity for sample collected from Sc2 core ranges between 25.09 and 27.15 (kN/m3), for an average value of 26.29 (kN/m^3).

- Specific gravity for samples collected from Sc3 core ranges between 25.58 and 27.54 (kN/m3) for an average value of 26.61 (kN/m^3).

Table 6.11 G_S values.

ID Samples	GS (kN/m3)
PN1	26.75
PN2	26.56
PN3	26.66
PN4	27.34
PN5	27.44
PN6	26.85
PN7	26.46
PN8	26.36
PN9	27.24
PR1	26.07
PR2	25.09
PR3	27.05
PR5	25.58
PR6	27.15
MC1	26.85
MC2	27.24
MC3	26.95
MC4	26.66
MC5	26.85
MC6	26.26
MC7	25.68
MC8	26.85
MC9	26.07
MC10	27.54
MC11	25.58
MC12	27.05
MC14	27.44

ATTERBERG LIMITS

The W_L, W_P and I_P values (Tab.6.12), obtained by the procedures described in the "Methods" chapter range as here reported:

- Sc1→ 32.51 ÷44.52 (W_L); 18.38÷27.29 (W_P); 11.80÷17.23 (I_P)
- Sc2→ 24.18 ÷45.09 (W_L); 19.84÷28.81 (W_P); 3.28÷22.50 (I_P)
- Sc3→ 23.30 ÷49.41 (W_L); 17.18÷32.72 (W_P); 6.13÷19.69 (I_P)

Table 6.12 Atterbeerg limits values.

ID Samples	W_L	W_P	IP
PN1	35.50	21.28	14.22
PN2	32.99	19.64	13.35
PN3	33.65	18.38	15.27
PN4	38.36	24.06	14.31
PN5	44.52	27.29	17.23
PN6	32.51	18.84	13.68
PN7	35.45	20.90	14.55
PN8	39.09	23.69	15.40
PN9	35.80	24	11.80
PR1	43.40	20.90	22.50
PR2	45.09	28.81	16.28
PR3	40.44	23.31	17.13
PR5	24.18	20.90	3.28
PR6	35.21	19.84	15.37
MC1	37.89	26.74	11.15
MC2	36.57	28.85	10.72
MC3	35.85	26.13	9.72
MC4	41.29	26.56	14.73
MC5	49.41	32.72	16.69
MC6	38.10	22.34	15.76
MC7	31.02	18.44	12.58
MC8	39.64	25.60	14.04
MC9	35.12	21.09	14.03
MC10	34.19	21.16	13.03
MC12	30.95	22.08	8.87
MC14	23.30	17.18	6.13

Notes: A= activity (Skempton 1953); W_L=liquid limit; W_P=plastic limit; IP=plastic index.

These data have been plotted into the Casagrande chart, which allows to futher characterize the soils by comparing the plastic index (I_P) and the liquid limit (W_L). An empirical boundary called "A-line", whose slope is expressed by the equation:

$$I_P = 0.73(W_L - 20) \quad \text{Eq. 6.3}$$

separates inorganic clays from inorganic silts and organic soils.
Casagrande (1932) also defined the U-line which is considered the limit beyond which the plastic index data are too large for the measured liquid limit. The U-line is expressed by the equation:

$$I_P = 0.9(W_L - 8) \quad \text{Eq.6.4}$$

None of the analyzed samples is located above this line.
Further vertical subdivisions of the chart allow to distinguish other engineering properties such as compressibility, permeability and toughness (Casagrande, 1932).

The analyzed data fall in the fields of the chart assigned to *"inorganic silts and organic clay, mediumcompressibility"* and *"inorganic clays highcompressibility"*. Furthermore, one sample (PR5) is classified as "*inorganic clays, low plasticity"*, whereas the sample MC14 is classified as *"inorganic silts, low compressibility"*.

Skempton vs. Casagrande

The plastic properties of the clays are related to their ability to absorb water in the crystal structure; this aptitude depends on the mineral composition, specifically on the specific surface area (SSA) of the mineral phases. The smaller the clay particle size, the higher the SSA. The water molecules are electrostatically attracted to the surface of the clay crystal through hydrogen bonding. Consequentially the smaller the clay particle size, the higher the amount of adsorbed water. On this basis, several authors used the Atterbeg limits to obtain information about the mineralogical properties of soils, by using empirical correlations (Skempton, 1953; Holtz & Kovacs 1981; Cerato & Lutenegger, 2005):

Two tools have been used with this aim: Skempton diagram (Skempton, 1953) and Casagrande Chart (Holtz & Kovacs, 1981).

Skempton (1953) defined as "activity of a soil" the ratio between the plasticity index (Ip) and the clay fraction (CF) (Cerato & Lutenegger, 2005).

$$A = \frac{IP}{\%CF} \begin{cases} A = 1{,}25 \rightarrow Active\ clays\ (e.g. Montomorillonite \\ A = 1{,}00 \rightarrow Normal\ clays\ (e.g. Illite) \\ A = 0{,}75 \rightarrow Inactive\ clays\ (e.g. Kaolinite) \end{cases} \qquad \text{Eq. 6.6}$$

On the basis of their Activity (A), clays have been subdivided into three groups*:* *Inactive*, *Normal and Active* (Eq. 6.6). Each category is related to specific types of mineral phases, which are characterized by a specific SSA (Fig. 6.34).

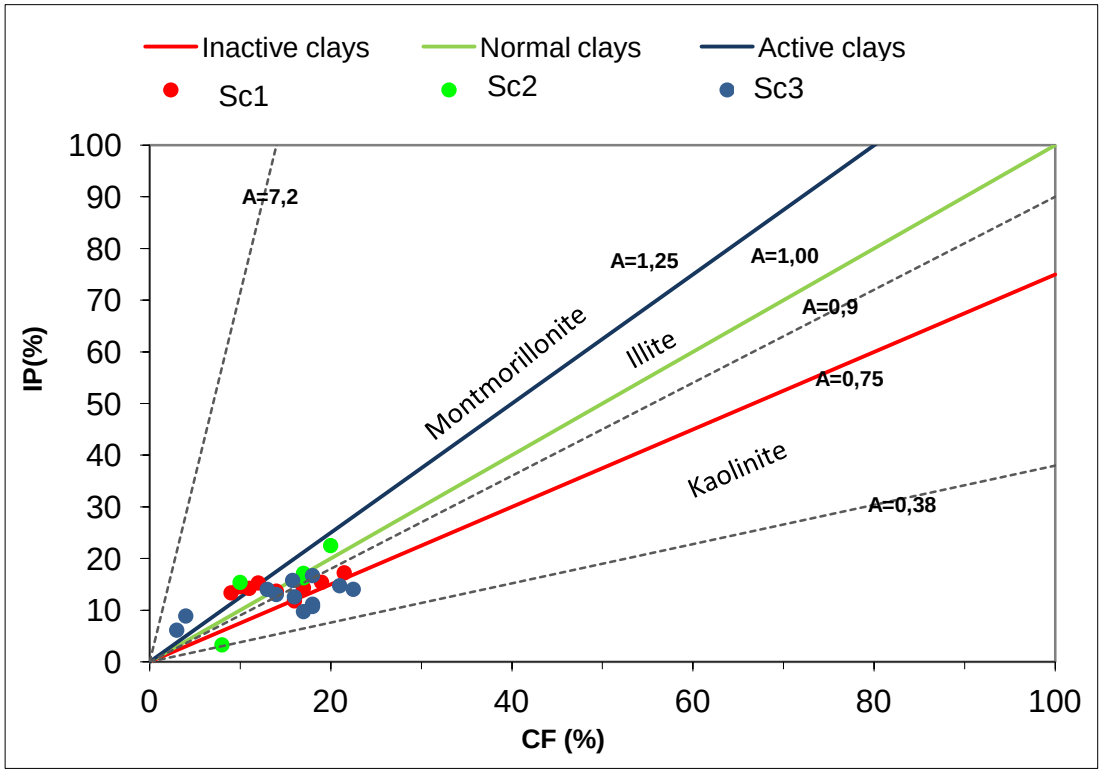

Figure 6.34 Skempton diagram.

As regards the Casagrande chart, Holtz & Kovacs (1981) have shown the correlation between the liquid limit and the plastic index (Fig.6.35), and the mineralogical properties. For example samples located above the A-line, near the U-line, should contain great amount of montmorillonite. Samples located below the A-line should be mainly characterized by the presence of kaolinite. Finally illite should be the most representative mineral phase for all samples placed above the A-line.

By plotting the Termini-Nerano samples in the Skempton diagram (Fig.6.34) as well as in the Casagrande chart (Fig.6.35), it is possible to see that most of them are characterized by illite and kaolinite, and only a few samples should contain montmorillonite as main phase.

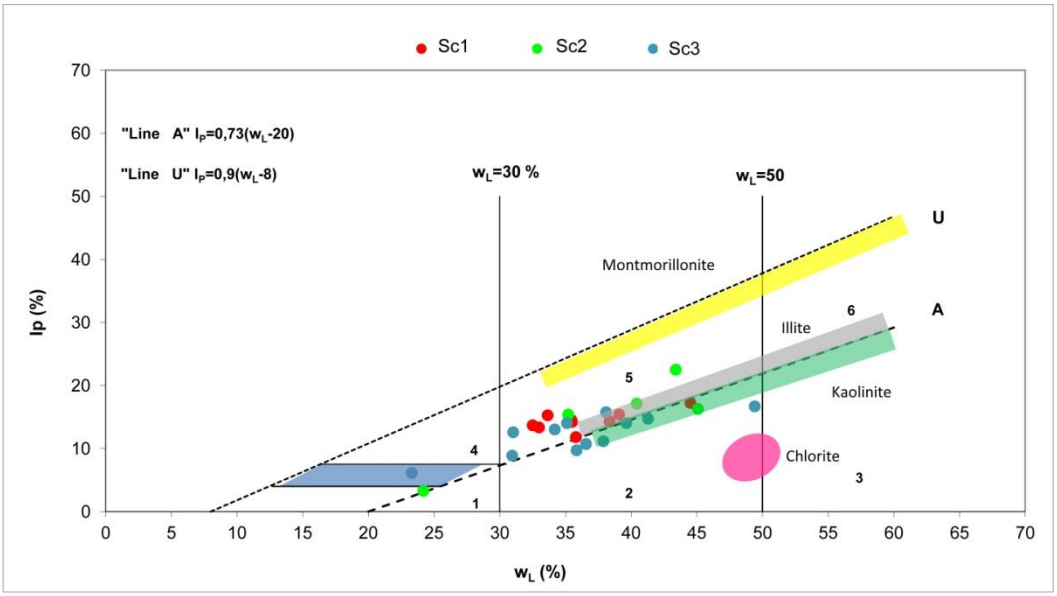

Figure 6.35 Casagrande chart: 1) Inorganic silts, low compressibility; 2) Inorganic silts and organic clays, medium compressibility;3) Inorganic silts and organic clays high compressibility; 4)Inorganic clays, low plasticity; 5) Inorganic clays, medium plasticity; 6) Inorganic clays, high plasticity.

Moreover, there is not perfect match between the two diagrams, as it is possible to verify by looking at data listed in Table 6.12. For example, the sample PN1 is characterized by active clays (montmorillonite) in the Skempton chart, but at the same time, it falls in the field of the Casagrande chart assigned to illite. The same happens to the PN7 and MC12 samples. The last sample contains only 4 wt% of clay fraction, suggesting that the relative activity is not reliable.

In a few cases, samples considered to be constituted by normal clays (e.g. illite), are mainly characterized by kaolinite (e.g. PN5 and MC5 samples).

All other samples are characterized by a good correlation between Casagrande chart and Skempton diagram.

Further correlations between geotechnical and mineralogical parameters are reported in the "Discussion" chapter.

USCS CLASSIFICATION

In the engineering and geology disciplines the most used soil classification method is the "Unified Soil Classification System" which allows to describe the

texture and the grain size of a soil. USCS can be applied to the unconsolidated materials (Fig. 6.36).

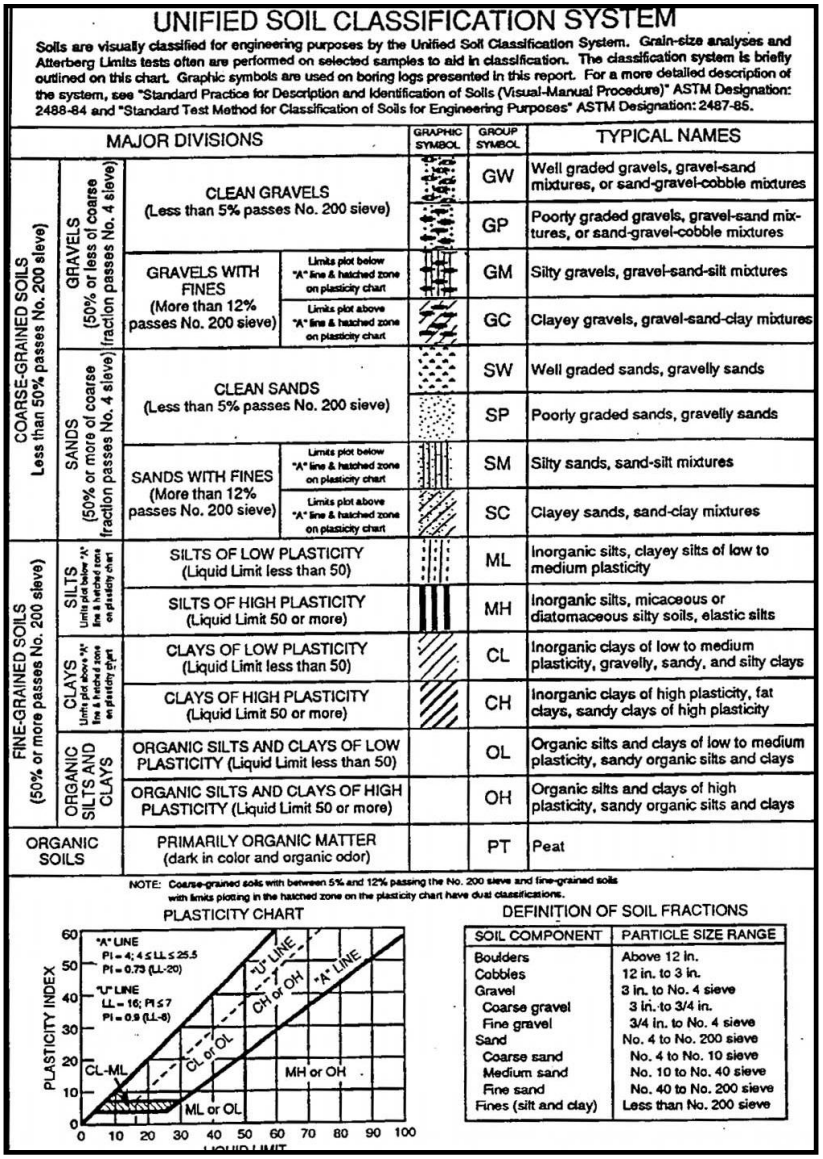

Figure 6.36 USCS classification

The USCS classification allows to subdivide soils in three major groups (Bhargavi & Jyothi, 2009), on the basis of the major geotechnical properties described above:

- Coarse grained soil (e.g. sands and gravels)
- Fine grained soils (e.g. silts and clays)
- Highly organic soils

The analyzed samples have been classified as follow (Table.6.13).

Table 6.13 Skempton data vs. Casagrande data.

ID Samples	Activity	Skempton mineralogical classification	Casagrande mineralogical classification
PN1	1.29	Active clay	Ilt
PN2	1.48	Active clay	Ilt-Mnt
PN3	1.27	Active clay	Ilt-Mnt
PN4	0.84	Normal clay	Ilt
PN5	0.80	Normal clay	Kln
PN6	0.98	Normal clay	Ilt-Mnt
PN7	1.45	Active clay	Ilt
PN8	0.81	Normal clay	Ilt
PN9	0.74	Inctive clay	Ilt-Kln
PR1	1.13	Normal clay	Ilt-Mnt
PR2	0.96	Normal clay	Ilt-kln
PR3	1.01	Normal clay	Ilt
PR5	0.41	Inactive clay	Ilt-Mnt
PR6	1.54	Active clay	Ilt-Mnt
MC1	0.62	Inactive clay	Kln
MC2	0.60	Inactive clay	Kln
MC3	0.57	Inactive clay	Kln
MC4	0.70	Inactive clay	Kln
MC5	0.93	Normal clay	Kln
MC6	1	Normal clay	Ill
MC7	0.79	Normal clay	Ilt-Mnt
MC8	0.62	Inactive clay	Ilt-kln
MC9	1.08	Normal cla	Ilt
MC10	0.93	Normal clay	Ilt
MC12	2.22	Active clay	Ilt
MC14	2.80	Active clay	N.I.

Notes: Active clay e.g. montmorillonite (Mnt); Normal clay e.g. illite (Ilt); Inactive clay e.g. Kaolinite (Kln);

DIRECT SHEAR TEST

Shear tests have been carried out to evaluated peak and residual shear strength of the collected undisturbed samples (Tab. 5.4).

Possible explanation of the obtained results will be shown in the next chapters. As shown in Figure 6.37, the cohesion for SC1 is null, whereas the shear strength as well as the friction angle decreases passing from peak to residual data (Fig. 6.37).

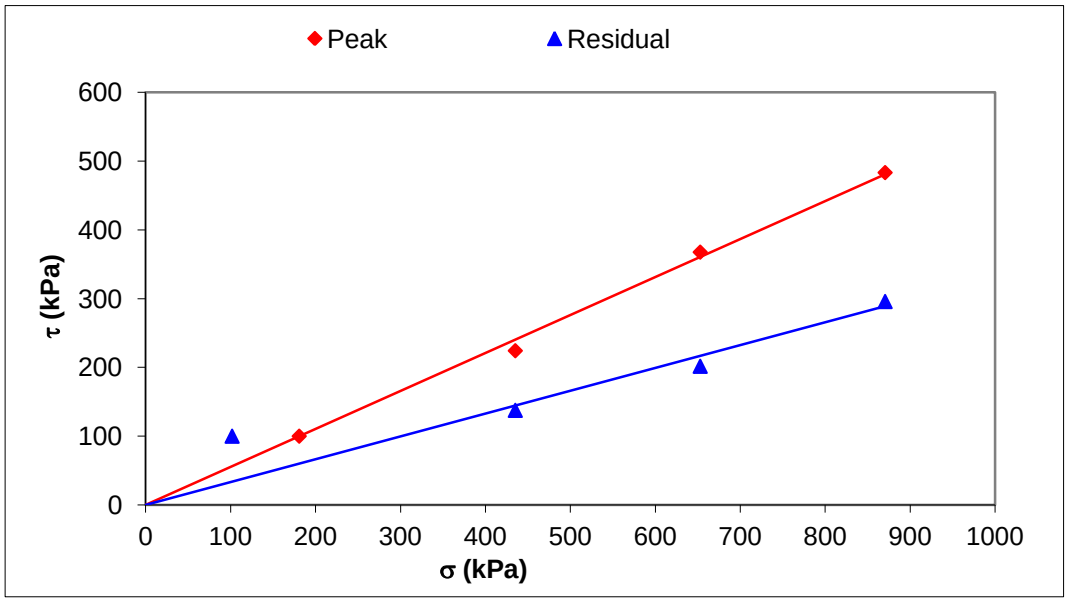

Figure 6.37 Shear test diagram SC1 sample.

In the case of the SC2 sample (Fig. 6.38), the transition from peak to residual values is characterized by the increase of the cohesion and the shear strength, whereas the friction angles remains stable.

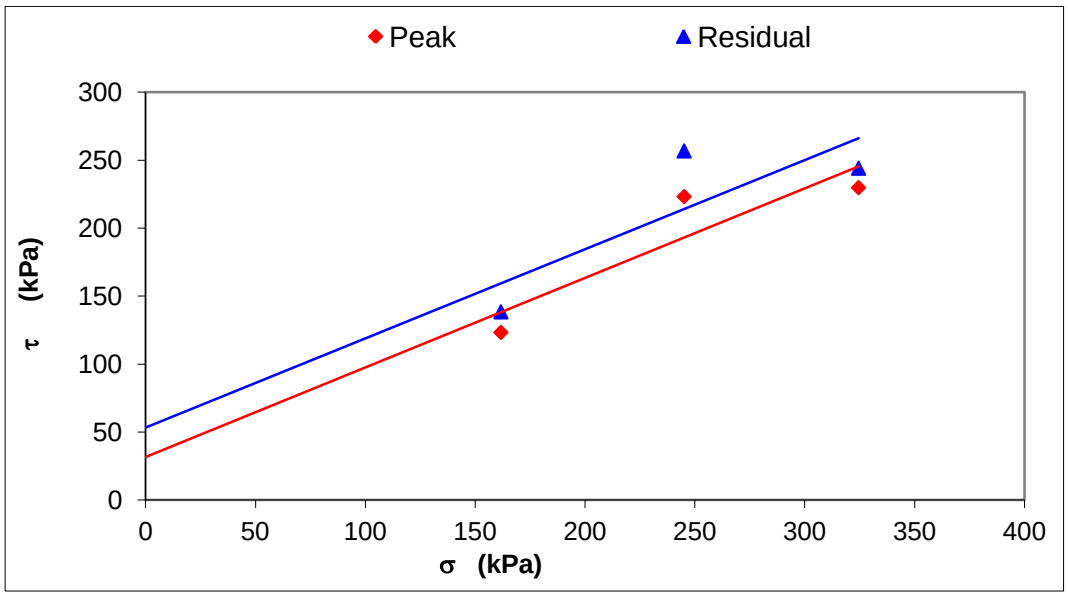

Figure 6.38 Shear test diagram SC2 sample.

Table 6.14 Shear test peak data

ID sample	φ_R	c'_R (kPa)	τ_R(kPa)
SC1	20	0	158.3
SC2	33	32.4	139.7

Table 6.15 Shear test residual data

ID sample	φ_P	c'_P (kPa)	τ_P(kPa)
SC1	31	0	259.1
SC2	33	32.4	139.7

These data will be explained in the *Discussion and Conclusions*.

The data obtained from direct shear strength tests have been used to evaluate another parameter called *"Brittleness Index"* (Bishop, 1967) useful to verify the existence of retrogressive movement (Cruden & Varnes, 1996):

$$I_B = \frac{(\tau_P - \tau_R)}{\tau_P} * 100 \quad \text{Eq.6.7}$$

Where I_B represents the brittleness index, τ_P is the peak shear strength and τ_R is the residual shear strength.

- for I_B <30% retrogression does not exist
- for I_B >70% retrogression exists

The Brittleness Index has been evaluated for the SC1 sample, because the SC2 was characterized by residual strength higher than peak strength. The obtained value (38.9%) indicates an area where a retrogressive movement is active, as it was also confirmed by the field survey.

FLOW BEHAVIOUR CHARACTERIZATION

RHEOLOGICAL ANALYSES

Rheological analyses have been carried out on a set of 17 specimens, selected on the basis of their mineralogical properties, as well as their relative depth.

As reported in the previous chapter, two experiments have been carried out, by changing the amount of water added at the samples.

By considering all samples together, it is possible to verify that they are characterized by pseudo-plastic behaviour, with a yield point (Schramm,1998). By changing the amount of water it was possible to verify that, although the behaviour of the soils is the same, the lower the amount of water the higher the yield point position, because the viscosity of material is higher. Specifically by considering the samples collected from Sc1 borehole, it is possible to see that the

flow curves of most of samples show a similar pattern except PN2 and PN3 that exhibit a more fluid behaviour.

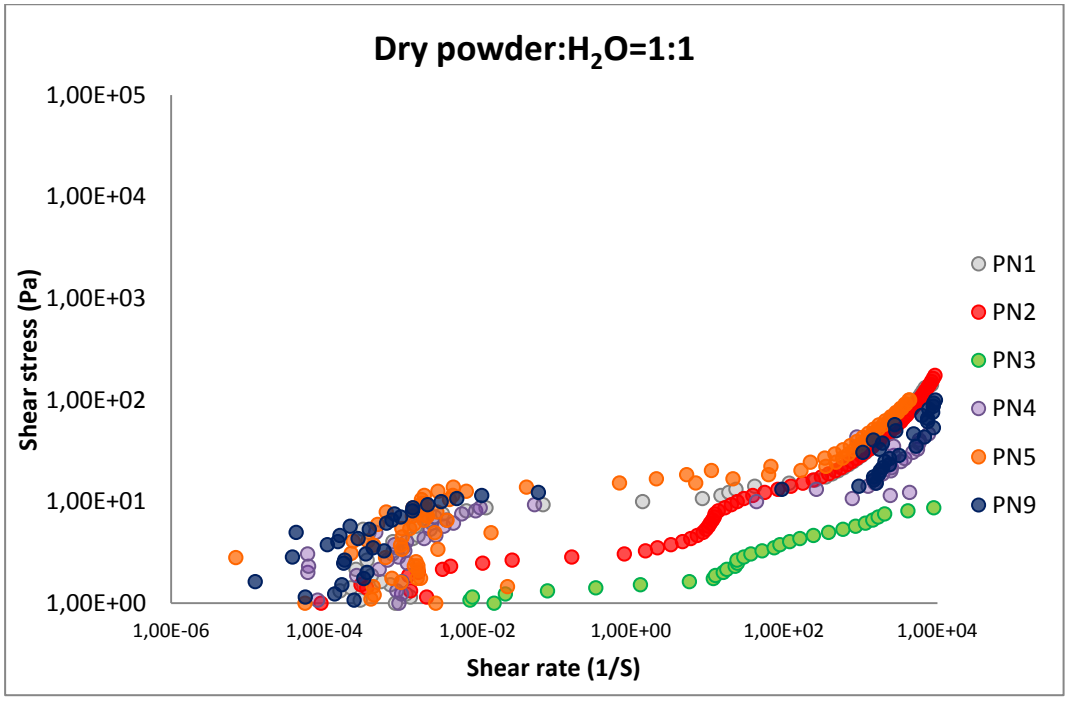

Figure 6.39 Rheological analysis diagram, by considering the same amount of water and specimens, performed on samples collected from the crown zone.

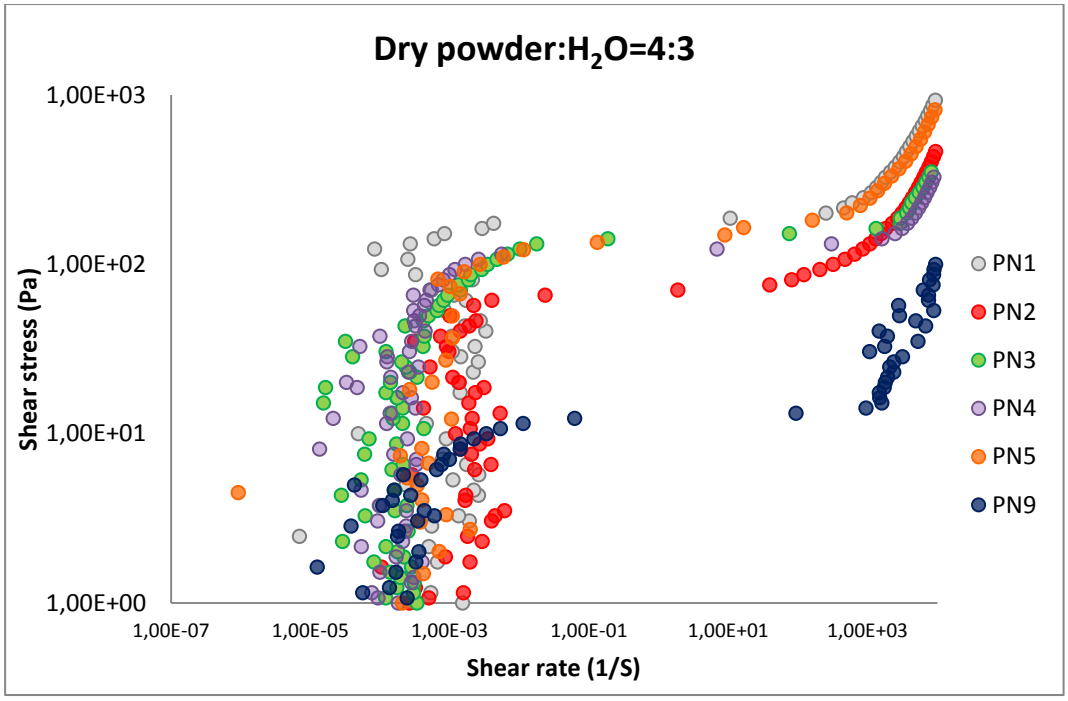

Figure 6.40 Rheological analysis diagram considering the amount of water lower than the amount of specimens, performed on samples collected from the crown zone.

The flow curves characteristic of samples collected from the SC2 borehole show the same shape, although the yield points are not coincident. Only the PR5 sample exhibits similar flow behaviour. Its yield point is not well visible.

By reducing the amount of water, the flow curves of the samples assume a similar pattern.

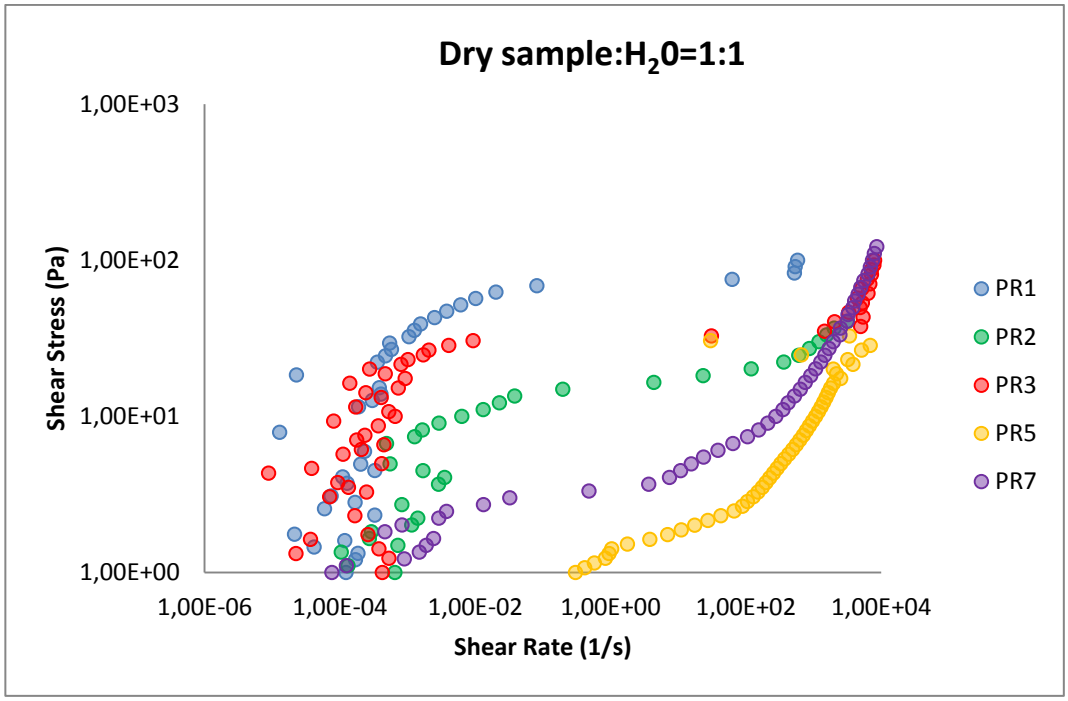

Figure 6.41 Rheological analysis diagram, by considering the same amount of water and specimens, performed on samples collected from the sliding zone.

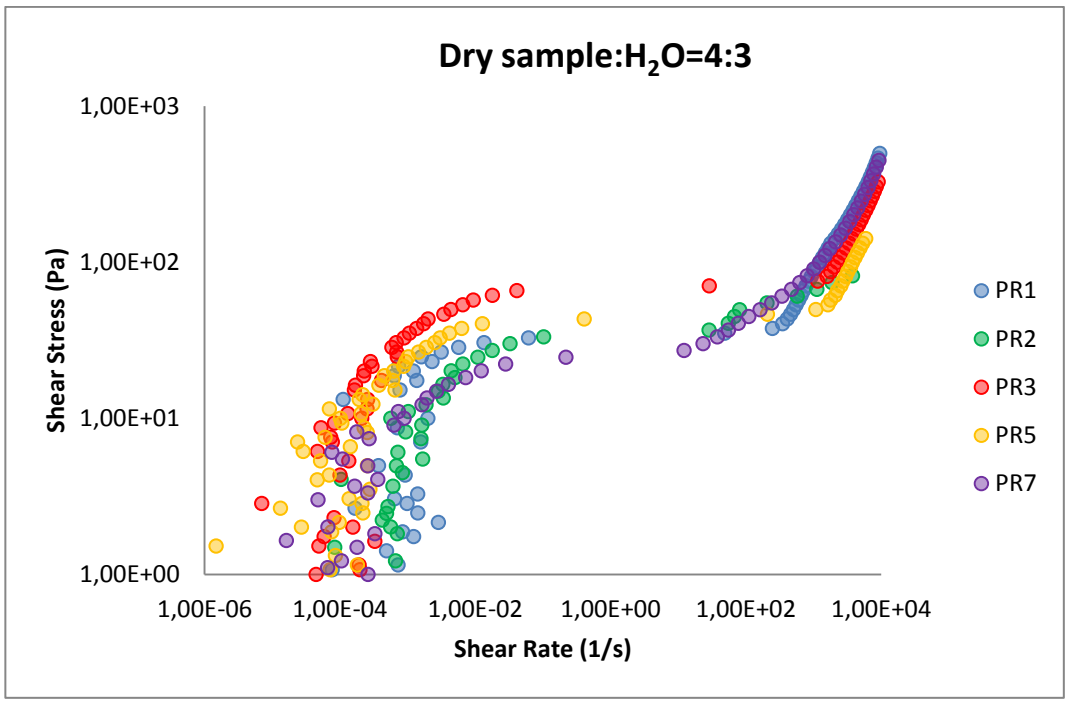

Figure 6.42 Rheological analysis diagram considering the amount of water lower than the amount of specimens, performed on samples collected from the sliding zone.

The samples collected from the SC3 borehole exhibit a non-homogeneous flow trend. Also in this case, a reduction of the water amount corresponds to the increase of material viscosity and consequently to higher positions of the yield point.

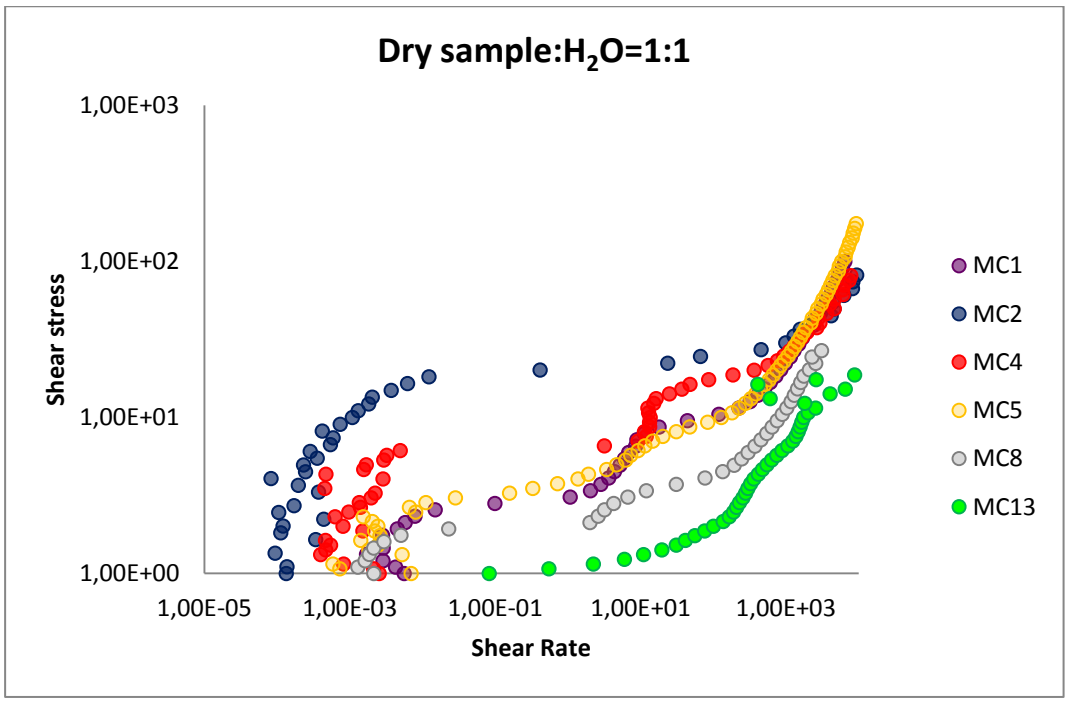

Figure 6.43 Rheological analysis diagram considering the amount of water lower than the amount of specimens, performed on samples collected from the accumulation zone.

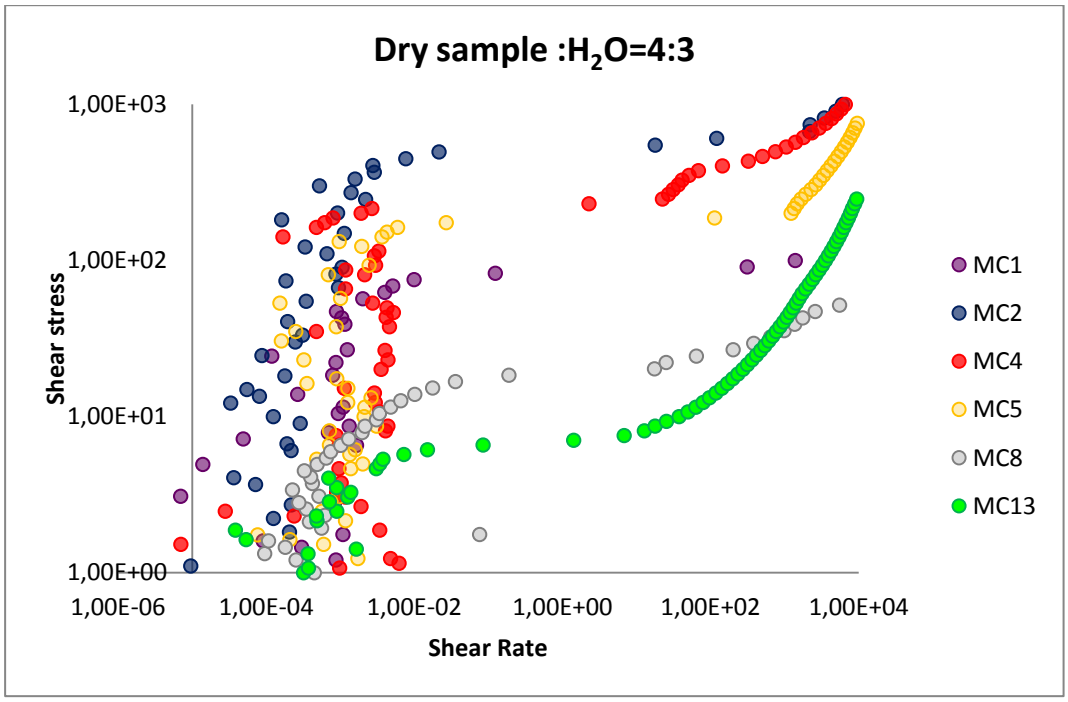

Figure 6.44 Rheological analysis diagram considering the amount of water lower than the amount of specimens, performed on samples collected from the accumulation zone.

CHAPTER 7

DISCUSSION AND CONCLUIONS

Slow-moving landslides are down-slope movements of soils, characterized by low rates of displacement (from few mm per year up to 1/2 m per year). External phenomena, as long-duration rainfalls or earthquakes, can trigger paroxysmal events, increasing the velocity of landslides up to some m/day, and consequently making them very dangerous. Slow-moving landslides are usually associated with different types of flysch formation Units typical of southern Apennine (Italy), which are collectively called "Structurally complex formations". The aim of this research was to study the Termini Nerano landslide (municipality of Massalubrense, southern Italy), to improve the knowledge on slow-moving landslides, and to verify whether their occurrence is associated with more weathered lithologies.

A multidisciplinary approach, based upon combined mineralogical and geotechnical analyses, was adopted, to investigate possible relationships between the different clay minerals properties and geotechnical parameters of materials involved in landslides. In fact, it is generally assumed that expandable clays should be present in higher amounts in highly weathered soils, and that there is a relationship between the content of expandable clays and the decrease of the shear strength of a rock material. The presence of these clay types (e.g. smectite) should favor the water absorption in the rock and the consequent decrease of its shear strength.

Mineralogical analyses on the material involved in the Termini Nerano landslide, allowed to integrate the information reported by Cotecchia & Melidoro (1966), who reported the presence of illite and quartz, evaluated by XRPD, as the main phases characterizing the slid rock material.

In this research, a higher number of phases have been detected:

- several phyllosilicates (mixed layers, chlorite, kaolinite, muscovite)
- quartz and feldspars
- carbonate minerals (calcite and dolomite).

Quantitative analyses were carried out by using two software Topas and Vb Affina. The second software was particularly adapt to solve the problems related to the presence of poorly crystalline phases (e.g. mixed layers I/S) in the samples.

In the analyzed samples, phyllosilicates (mixed layers I/S and Chl/S, chlorite, kaolinite, muscovite) represent the most abundant minerals, exceeding in most of the cases 50 wt%, whereas quartz plus feldspars occurs with an average of about 30 wt%, and carbonate minerals (calcite and dolomite) show an average amount of 8 wt%.

Mineralogical analyses on the clay fraction of the analyzed materials allowed to obtain specific and peculiar information about mixed layers I/S.

According to literature (Uneno et al., 2008) the percentage of smectite in mixed layers I/S should play a role in the landslide development. Moreover, physico-

chemical weathering is usually considered to promote formation in the soil of alteration zones as those detected, for example, by Calcaterra et al. (2007) in the soil material involved in the Agnone landslide. In this case, three different weathering zones were detected on the basis of mineralogical and geotechnical analyses.

In the studied Termini Nerano area, the smectite amount (in mixed layers I/S) (Fig. 7.1), is not regularly distributed along the vertical section of the soil. Moreover, a variable distribution of mixed layers I/S grade of ordering has been also observed (Fig. 6.17).

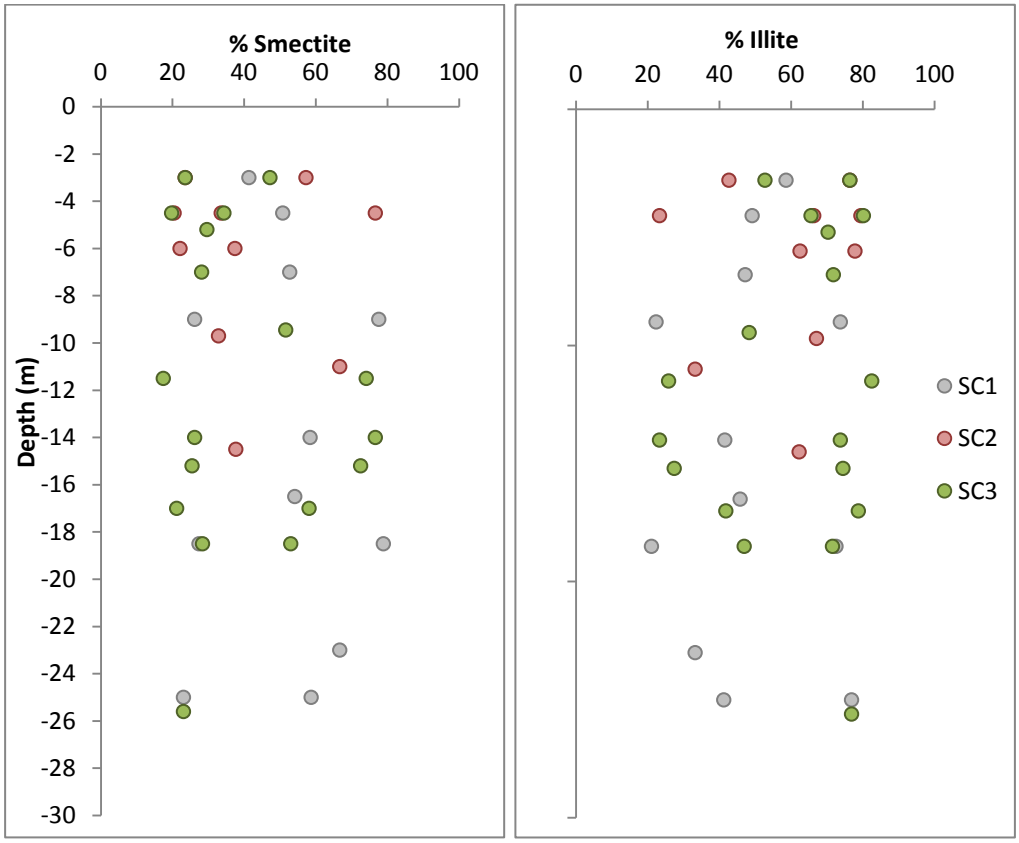

Figure 7.1 Illite and smectite distribution, evaluate by using the Moore & Reynolds method (see chapter 5).

These facts indicate that the studied soils do not comprehend typical weathering zones, as observed in the Agnone landslide, and that the clays cannot be considered a typical product of a weathering. The heterogeneous distribution of mixed layers I/S is instead probably related to the consolidation processes associated with the burial diagenesis of the sedimentary lithologies, occurred in the Miocene age, after their deposition. As reported in the 2nd chapter, Velde (1995) considered that burial diagenesis represents the most common type of diagenesis for silicates. In fact, as sedimentation proceeds in a basin, an increase of temperature occurs, producing diagenesis processes. Pollastro (1993) affirmed, "*changes in the proportion of illite, smectite and ordering of I/S, correlate with changes in temperature due to burial diagenesis*". Starting from this assumption, several models have been created with the aim to use mixed layers I/S as geothermometer, e.g. the *Hoffman & Hower model* (1979) and *short-life*

geothermal model (Jennings & Thompson, 1986). As shown in Table 7.1, the former considers that transition from R0 to R1 and can occur at temperatures comprised between 60-100°C, whereas the latter considers that transition between R0 to R1 can occur at temperatures comprised between 120°-140°C. In both cases, the transition from R1 to R3 occurs at about 170°-180°C.

Table 7.1 Approximate temperatures for changes in mixed layer I/S in Hoffman and Hower and Short-life geothermal I/S geothermometry models (after Pollastro,1993).

Change in I/S	Hoffman and Hower model (5.300 m.y.)	Short life geo-thermal model (<3 m.y.)
Smectite to R= I/S	50°-60°C	variable
R=0 to R=1	100°-110°C	120°-140°C
R=1 to R=3	170°-180°C	170°-180°C

The *Hoffman & Hower model* (1979) is widely used for the Tertiary and Late Mesozoic basinal rocks. For example, Cavalcante et al. (2007) used this model to date siliciclastic sediments in the Southern Apennine. Specifically, in that case, by using a detailed powder X-ray diffraction study of mixed layers I/S, clay mineralogy was used as a tool to study the emplacement of thrust sheets. The same data were also used to obtain information about the main processes occurred during sedimentation of the analyzed rocks. For example, in the case of material belonging to Sicilide successions the presence of mixed layer I/S with high illite content and ordered I/S *R*1 and *R*3, %I=60-95, indicates that this succession experienced a strong tectonic load (Cavalcante et al., 2007).

In the case of the material involved in the Termini Nerano landslide, this type of correlation appears to be slightly more complicated. After Pollastro (1993), the use of mixed layers I/S as geothermometer is strictly related to the possibility to know the mineralogy of the material from which mixed layers have been originated. In case of the analyzed material, although the grade of ordering equal to R0 and R1 makes possible to suppose that the illitization process occurred at about 100°C, the great heterogeneity of the grade of ordering distribution in the same samples is typical of sedimentary rocks affected by several cycles of burial diagenesis (Pollastro, 1993). For this reason it is not possible to obtain information about the mineralogical composition of the parent material.

Geotechnical analyses were carried out on samples, to verify possible relationships between the mechanical behaviour of the soil and its mineralogical composition.
Considering the Casagrande chart, the analyzed samples were categorized as "*medium plasticity silt, inorganic silt"* and *"medium plasticity inorganic clays"*, on the basis of their Atterberg parameters, W_L and IP, according to the results obtained from specific gravity tests.

Several authors use the Atterberg limits to obtain information on the mineralogy of a soil, by using empirical correlations, as those depicted in the Casagrande chart and the Skempton diagram (Calcaterra et al., 2007, 2008). In this study the mineralogical compositions, evaluated by using the Casagrande chart and the Skempton diagram, were compared with the mineralogy obtained by XRPD quantitative analysis (Table 6.7, Table 6.13).
From the Casagrande chart and the Skempton diagram, the analyzed samples should be mostly constituted by illite and kaolinite. The mixed layers I/S, detected by XRPD analyses, were not revealed by these correlations. Moreover, other peculiarities were also evidenced. For example, considering the Casagrande chart and the XRPD analyses, the PN1 sample appears to be mainly characterized by illite. Looking instead at the Skempton diagram, the same sample is (wrongly) classified as an *Active clay*, constituted by smectite. The PN5 sample results a kaolinite in the Casagrande chart, whilst only 7 wt% kaolinite has been effectively measured by XRPD analysis. The same sample, although has been classified as *Normal clay* (mainly constituted by illite) by using the Skempton diagram, has an absolute grade of activity quite close to that corresponding to the inactive clay (i.e. kaolinite) (Table 6.13).
In addition, some samples (e.g. MC12 and MC14 samples) are not classifiable by using both the Casagrande chart and Skempton diagram, because they contain less than 5 wt% of clay fraction. This probably depends, as shown in the *Results* chapter, by the fact that, in most cases, grain size distribution analyses underestimated the amount of clay fraction, due to the high grade of compaction of particles at microscale. In fact, coarse grains could be constituted by strongly aggregated small particles, which are subjected to important chemical-physical particle interactions (Mitchell, 1993).
Although direct shear tests were also performed on undisturbed samples from the landslide area, it was not possible to compare the obtained data to the mineralogical compositions, for two reasons: firstly, because these tests were carried out only on two samples, which cannot be considered representative for the whole investigated area; secondly, because these two samples are not comparable, considering mineralogical and geotechnical data obtained for samples located above and below the undisturbed samples, and also considering their stratigraphical characterization (see chapter 6).
Only the results obtained for the SC1 sample can be considered satisfactory. In this case, the transition from peak to residual data is characterized by a reduction of shear strength, and friction angle. The absence of cohesion is due to the wrong positioning of sample into the shear box, which was probably loaded with cleavage parallel to the shear plane. In the case of SC2 sample, better results could be reached carrying out a greater number of analyses on the same material.

Rheological analyses confirmed that the rate of movement of this landslide is variable. The flow behavior of the material involved in the landslide is pseudo-plastic with yield point. This means that, according to literature, the first stage of movement is connected to slow plastic deformation, and that, after the yiald point, the same material starts to flow, because of a viscosity decrease. In fact it results

that the lower the viscosity, the higher the rate of movement. These data agree with the main feature of the slow-moving landslides, which usually start to flow after triggering events.

Environmental samples were also collected to obtain information about the microbial community characterizing material involved in the Termini-Nerano landslide. In 2008, Alekseeva et al. demonstrated that in the case of clay minerals, alkaline cyanobacterial communities promote the intensification of the exchange bases removal and the dissolution of silicates, whereas the presence of alkaliphilic cynobacterial is associated with an increasing amount of iron oxides.
The analyses have been carried out at the Department of Biology (Federico II University of Naples), by Professor Marco Guida's research group, by culture-independent method, based on DNA analysis. As reported in Guida et al. (2014), the study shows that the bacterial and fungal communities occurring in the samples (i.e. *Leptothrix cholodnii Trichocomaceae, Fusarium* and *Nectria*) can contribute to the degradation processes leading to soil properties change. The obtained results have been considered as an initial attempt for evaluating the relationship between bacterial and fungal community and landslide occurrence.

In conclusion, the material involved in the Termini Nerano landslide can be considered *a structurally complex formation* of the highly heterogeneous type. In fact it was not possible to correlate neither stratigraphic nor mineralogical features between drillcores, although all analyzed samples belong to the same Unit (*Membro delle Arenarie di Nerano*-Iannace et al., in press.). The presence of mixed layer I/S with different grade of ordering not continuously varying with depth indicates that the considered material is highly overconsolidated and then it cannot be associated with a weathering profile. The heterogeneous distribution of mixed layers grade of ordering probably derives from consolidation processes associated with regional tectonic events of the area.
Combining laboratory tests with field activity, it was possible to verify that the Termini Nerano landslide is still active. A slow retrogressive movement affects the 1963 crown zone, and involves a great amount of material. No deep detachment surface has been identified from the investigated samples, and consequently it is not possible to predict the amount of material which really will be involved in a possible paroxysmal reactivation of the landslide.

This research also highlighted the major limits in the use of empirical geotechnical relationships for clay-type determination.
Several features explain why there are differences in the mineralogical evaluation of the samples by using the Casagrande chart and Skempton diagram and the XRPD analyses. First of all, the coexistence of different mineralogical phases with different SSA (Specific Surface Area) probably invalidates the use of Casagrande chart and Skempton diagram. This parameter varies greatly between soils, on the basis of differences in mineralogy, organic composition and particle sizes distribution (Cerato & Lutenegger, 2005). In fact, in soils mostly constituted

by clays, Atterberg limits and direct mineralogical analyses produce more coherent and comparable results (Skempton, 1953; Holtz & Kovacs, 1981).
Secondly, the high consolidation of the analyzed material produces a strong aggregation between the particles, and reduces the fraction of loose material in the rocks. Consequently, grain size distribution analyses underestimate the amount of clay fraction relatively to the direct XRPD mineralogical analyses, making difficult to obtain accurate values of the grade of activity of the analyzed material.
Finally, it is necessary to remember that a difference, which has plagued several authors in the past (Guggenheim & Martin, 1995), exists between the concepts of "clay minerals" and "clay size". Clay minerals are phyllosilicates, characterized by a peculiar mineralogical composition and a particles size below 2 μm. Clay size is a term referred to those particles of a grained loose soil, which are smaller than 0.002 mm (2 μm), independently by their mineralogical composition, e.g. these small particles can be constituted not only by clay minerals, but also by feldspar, quartz or other minerals.
In definitive, when studying this type of geomaterials, it is necessary to kindly use the empirical geotechnical relationships for mineralogical characterization and clay amount evaluation.

ACKNOWLEDGEMENTS

Above all, I thank my supervisors Prof. Piergiulio Cappelletti, Prof. Domenico Calcaterra, Prof. Pantaleone De Vita, Prof. Massimo Ramondini, Dott. Saverio Fiore and Prof. Maurizio De Gennaro.
Prof. Piergiulio Cappelletti introduced me to the Clay Mineralogy world and gave me numerous scientific and academic opportunities during these three years, which greatly improved my capacities and knowledges. I thank him to have thrust in me and accepted me as his PhD student. Prof. Domenico Calcaterra is thanked to have managed many parts of the project, and to have guided me in these years. Prof. Piergiulio Cappelletti and Prof. Domenico Calcaterra are greatly thanked for the complete revision of the thesis.
Prof. Maurizio De Gennaro is thanked to be our scientific father.
Prof. Massimo Ramondini is thanked for the help in the field and laboratory activity. Dott. Saverio Fiore introduced me to the CNR of Tito Scalo and allowed me to collaborate with his research group.
A special thank to Prof. Pantaleone De Vita to have proposed me the "PhD idea", after the Master thesis.

I thank Doctor David L. Bish to have hosted me at the Indiana University. I thank him for the different kinds of supports and helps during my staying in Bloomington, and also to have showed me an unexpected and pleasant way to live the science.

I thank Claudia Belviso and Francesco Cavalcante for the huge support during the analytical work at CNR of Tito Scalo. Claudia is specially thanked for her friendship.

Thanks are also due to E. Di Clemente (*Università di Napoli*) for helping with the geotechnical analyses, R. de' Gennaro (*Università di Napoli*) for the help with SEM analysis, Luigi Franciosi (*Università di Napoli*) and Mauro Pallara (*Università di Bari*) for the XRF analyses, M. Guida (*Università di Napoli*) for the environmental analyses.
I also thank all the colleagues, met during these years in Naples (Giovanni, Gianmarco, Claudia, Abner, Fabio, Tina, Mariano, and many others).
A special thank to the friends met in Bloomington, because they were very friendly with me when I was (as a perfect Italian) very sad: Abhy, Kriss, Hongjige, Josh, thank you for all the funny moments there, especially to have joked with me about my English. You all, together with David and Karen made me feel at home.

I thank my family: my father and my mother, who have believed and invested in me, and survived the fear to "send" me in America, my sisters (Idana and Francesca) for being them.
All my friend (especially Marcella) are thanked for the support and encouragements, and for various different reasons.

I thank "my almost-husband" Nicola, simply to be with me.

REFERENCES

Alt JC., Honnorez J., Emmermann R. (1986)- *Hydrothermal alteration of a 1 km section through the upper oceanic crust. Deep Sea Drilling Project Hole 504B: mineralogy hemistry, and evolution of seawater- basalt interaction.* J Geophys Res 91: pp.10309-10335.

ASTM D2217-85 (Reapproved 1998)- *Standard Practice for Wet Preparation of Soil Samples for Particle-Size Analysis and Determination of Soil Cnstans.* Annual (2000) Book of ASTM Standards, American Society of Testing and Materials, Philadelfia, Pennsylvania, Vol. 04,08, p.10-16.

ASTM Standard (1999)- *D3080-98 Standard test Method for Direct Shear Test of Soil Under Consolidated Drained Conditions.* Annual Book of ASTM Standard, ASTM. West Conshohocken, PA.

ASTM Standard (1999)- *D854-92 Specific gravity of soil.* Annual Book of ASTM Standard, ASTM. West Conshohocken, PA.

Bailey S.W. (1980b)- *Structures of layer silicates.* In Brindley G.W. and Brown G., editor, Crystal structures of clay minerals and their X-ray Identification, Monograph No 5. Mineral society of London, pp. 1-123.

Bauluz B. (2007)- *Illitization processes: Series of dioctahedral clays and mechanisms of formation*. In: Nieto F. and Jiménez-Millán J., eds. (2007). Diagenesis and Low-Temperature Metamorphism. Theory, Methods and Regional Aspects. 31-39. Seminarios de la Sociedad Española de Mineralogía, 3, Sociedad Española de Mineralogía, ISSN 1698-5478.

Bettison-Varga L.A. & Mackinnon IDR. (1997)- *The role of randomly mixed-layered chlorite/ smectite in the transformation of smectite to chlorite*. Clays Clay Miner. Vol. 44, pp.506-516

Bettison-Varga L.A. & Schiffman P. (1988)- *Compositional and structural variation of phyllosilicates from the Pint Sal ophiolite, California.* Am. Miner. Vol. 73, pp. 62-76.

Bevins RE. Robinson D., Rowbotham G. (1991)- *Compositional variation in mafic phyllosilicated from regional low grade matabasites an application of the chlorite geothermometer.* J. Metamorphica Geol. Vol. 9, pp. 711-721.

Bhargavi P, & Jyothi S. (2009)- *Applying Naive Bayes data mining technique for classification of agricultural land soils*. International journal of computer science and network security, Vol. 9(8), pp. 117-122.

Bish D. & Chipera S.J.(1988)- *Problems and solution in quantitative analysis of complex mixture by X-ray powder diffraction.* Adv. Xray Anal. Vol. 31, pp. 295-307.

Bishop A. W. (1967)- *Discussione nella 2° sessione << Shear strenght of stiff clay*>>- Atti Geotechnical Conference, Oslo, Vol. 2, pp. 142-150.

Bizjak K. Fifer & Zupančič A. (2007)- *Rheological investigation for the landslide Slano Blato near Ajdovščina (Slovenia).* Geologija Vol.50/1, pp.121-129.

Bonardi G., Ciarcia S., Di Nocera S., Matano F., Sgrosso I., Torre M., (2009)- *Carta delle principali unità cinematiche dell'Appennino meridionale*. Nota illustrativa. Bollettino della Società Geologica Italiana. Vol. 128, pp. 47-60.

Bonzanigo L., Tornaghi M., Oppizzi P., Uggeri A. (2006)- *Hydrodynamics and rheology: Key Factors in Mechanisms of Large Landslides.* Engineering Conferences International, 14 p.

Bragg W.L. (1913)- *The Diffraction of Short Electromagnetic Waves by a Crystal.* Proceedings of the Cambridge Philosophical Society, Vol.17, pp. 43-57.

British Standard 1377 (1975)- *Methods of testing soils for civil engineering purpose*. (British Standards Institute: London)

Brown P. J. & Downing M. C. (2001)- *Discussion of Fall Cone Penetration and Water Content Relationship of Clays*. Geotechnique Vol. 51, No.2, pp.181-187.

Calcaterra D., Calò F., Cappelletti P., de' Gennaro M., Di Martire D., Parise M., Ramondini M. (2007)- *Mineralogical and geotechnical characterization of alarge earthflow in weathered structurally complex terrains of the Molise region, Italy*- Geophysical Research Abstracts, Vol. 9.

Calcaterra D., Croce C., de Luca Tupputi Schinosa F., Di Martire D., Parise P., Ramondini M., Borrelli E., Salzano M., Serricchio A. (2006)- *The Colle Lapponi-Piano Ovetta landslide (Agnone, Molise, Italy), an example of rainfall-induced reactivation in weathered structurally complex materials*. Geophysical Research Abstracts, Vol. 8. European Geosciences Union.

Calcaterra D., Di Martire D., Ramondini M., Calò F., Parise M. (2008)- *Geotechnical analisys of a complex slope movement in sedimentary sucession of the Southern Apennines (Molise).* Chapter 25, pp. 299-305.Taylor & Francis Group, London, ISBN 978-0-415-41196-725.

Calò F. (2009)- *Analysis of slow-moving landslides in Southern Apennines by integrating ground monitoring and Remote Sensing techniques.* Phd thesis, Federico II, Naples, Italy.

Carrara A., Agnesi V., Macaluso T., Monteleone S. , Pipitone G. (1986)- *Slope movement induced by the southern Italy earthquake of November 1980.* Geol. Appl. Indrogeol. Vol. 21 (2), pp. 237-250.

Casagrande A. (1932)-.*Research on the Atterberg Limits ofSoils*. Public Roads, Vol 13. No 8, pp 121-136

Cascini L., Bonnard C., Corominas J, Jibson R., Montero-Olarte J. (2005)- *Landslide hazard and risk zoning for urban planning and development.* State of the Art Report. Proceedings of the International conference on Landslide Risk Menagment. Taylor and Francis, London, pp.199-235.

Cavalcante F., Fiore S., Lettino A., Piccaretti G., Tateo F. (2007)- *Illite-Smectite mixed layers in sicilide shales and piggy-back deposits of the Gorgoglione Formation (Southern Apennines): geological inferences.* Boll. Soc. Geol.It (Ital. J. Geosci.), Vol. 126, No. pp. 241-254.

Cerato, A. B. & Lutenegger, A.J., (2005)- *Activity, Relative Activity and Specific Surface Area of Fine- Grained Soils*. Proceedings of the 16th International Conference on Soil Mechanics and Foundation Engineering, Vol. 2, pp. 325-328.

Cotecchia V. (1986)- *Earthquake-prone Environments.* In Anderson M.G. and Richars K.S. (Eds), Slope Stability, John Wiley and Sons, pp. 287-329.

Cotecchia V. (1986)- *Ground deformation and slope instability produced by the earthquake of 23 November 1980 in Campania and Basilicata*. Geol. App. and Idrogeol., Vol. 21 (5), pp.31-100.

Cotecchia V & Del Prete M. (1984)- *The reactivation of large flows in the part of the southern Italy affected by the earthquake of November 1980, with reference to the evolution mechanism.* IV International Symposium on Landslides, Toronto (Canada).

Cotecchia V., Melidoro G. (1966)- *Geologia e Frana di Termini Nerano (Penisola Sorrentina)*- Geologia Applicata e Idrogeologia, Vol. 1, pp. 93-126.

Cruden D.M. & Varnes D.J. (1996)- *Landslides Types and Processes.* In: Turner, A.K., Schusteer, R.J. (Eds.), Landslides: Investigation and Mitigation, Special Report 247. Transportation Research Board, National Academy Press, Washington, DC, pp. 36-75.

Cruden D.M. (1991)- *A simple definition of Landslide*-Bulletin of International Association of Engineering Geology. No 43, pp. 27-29.

Cruden D.M., Thomson S., Hoffman B.A.(1991)- *Observation of Graben Geometry in Landslides* –In Slope Stability Engineering-Development and Applications: Proc., International Conference on Slope Stability, Isle of Wight, 15-18 April (R.J. Chandler, ed.), Thomsd Telford Ltd., London, pp. 33-36.

Cuadros J, Delgado A, Cardenete A, Reyes E, Linares J. (1994)- *Kaolinite/montmorillonite resembles beidellite*. Clays Clay Miner. Vol.42, pp. 643-51.

Cullity B.D. (1978)- *Element of X-ray diffraction, Second edition*-Addison-Wesley publishing company, Inc.

D'argenio B., Pescatore T. & Scandone P. (1973) - *Schema geologico dell'Appennino meridionale (Campania e Lucania)*. Atti del Conv. Moderne vedute sulla geologia dell'Appennino. Acc. Nazion. Lincei, Vol 182, pp. 49-72.

D'argenio B., Pescatore T. & Scandone P. (1975)- *Structural pattern of the Campania-Lucania Apennines*. In: Ogniben L., Parotto M. & Praturlon A. (Ed.), Structural model of Italy, Quaderni de «La ricerca scientifica», Vol. 90, pp. 313-327, C.N.R. Roma.

Delvaux B, Herbillon AJ,Vielvoye L, Mestdagh MM. (1990)- *Surface properties and clay mineralogy of hydrated halloysitic soil clays*. II. Evidence for the presence of halloysite/smectite (H/Sm) mixed-layer clays. Clay Miner.Vol. 25, pp. 141–60

Di Maio C & Onorati R (2000a)- *Swelling behaviour of active clays: the case of an overconsolidated, marine origin clay*. In: Proceedings, Eighth International Symposium on Landslide, Cardiff, UK, pp.469- 474.

Di Maio C & Onorati R (2000b)- *Osmotic softening of overconsolidated clays*. In: Proceedings, International Conference on Geotechnical and Geological Engineering, Melbourne, Australia, 6 p.

Di Matteo L. (2012)-*Liquid limit of low to medium plasticity soils: comparison between Casagrande cup and cone penetrometer test.* Bul. Engin. Geol. Environ, Vol.71, pp. 79-85

Di Nocera S., Fenelli G.B., Iaccarino G., Pellegrino A., Oescatire T.S., Picarelli L., Urcioli G. (1995)-*An example on the geotechnical implication of geological history*.Proc. XI ECSMFE, Vol.8, pp. 39-48.

Dragoni W., Prosperini N., Vinti G. (2008)- S*ome observations on the procedures for the determination of the liquid limit: an application on plio-pleistocenic clave soils from Umbria region (Italy). DOI: 10.4408/IJEGE.2008-01.S-12*

Esu F., (1977)-*Behaviour of slopes in structurally complex formations. In: Proceedings of International Symposium on the Geotechnics of Structurally Complex Formations* – International Symposium, the Geotechnics of Structurally Complex Formations, Vol. 1, pp. 292-303.

Fenelli G.B. & Picarelli L. (1990)- *The pore pressure field built up in a rapidly eroded soil mass.* Canad. Geotechn. Journ., Vol. 27, No 3,pp. 387-392.

Fiorillo F., Parise M., Wasowski J. (2006)-*Slope instability in the Bisaccia area (Southern Apennines, Italy).* Landslides, Senneset (ed.). pp. 965-971.

Guggenheim S. & Martin R.T. (1995)-*Definition of clay mineral: joint report of the AIPEA nomenclature and CMS nomenclature committees.* Clays and clay Minerals, Vol. 43, pp. 255-256.

Guida M., Cannavacciuolo P.L. Cesarano M., Borra M., Biffali E., De Mieri G., D'Alessandro R., De Felice B.(2014)- *Microbial diversity of landslide soils*

assessed by RFLP and SSCP fingerprints : Microbial fingerprint of landslide soil. Journal of Applied Genetics Volume 55, Issue 3, pp 403-415

Hendron A.J. & Patton F.D. (1985)-The Vajont slide, a geotechnical analysis based on new geologic observations of the failure surface. US Army Corps of Engineers Technical Report GL-85-5 (2 volumes).

Highland L.M.& Bobrowsky, P. (2008)- *The landslide handbook—A guide to understanding landslides: Reston, Virginia, U.S.* Geological Survey Circular 1325, 129 p.

Hogentogler, C.A & Terzaghi, K. (1929)-*Interrelationship of load, road and subgrade*. Public Roads: pp.37–64

Hoffman J. & Hower, J. (1979)- *Clay mineral assemblages as low grade metamorphic geothermometers: Application to the thrust faulted disturbed belt of Montana*. In Aspects ofDiagenesis, P. A. Scholle and P. S. Schluger, eds., SEPM Spec. Publ. Vol. 26, pp. 55-79.

Holtz R. D & Kovacs W. D. (1981)- *An Introduction to Geotechnical Engineering*: Englewood Cliffs, New Jersey, Prentice-Hall, 733 p.

Hower J., Esligenger E.V., Hower M.N., Perry E.A. (1976)-*Mechanism of burial metamorphism of argillaceous sediment: Mineralogical and chemical evidence.*Geol. Soc.Amer. Bull. Vol. 87, pp.725-737.

Hughes RE, Moore DM, Reynolds RC Jr. (1993)-. *The nature, detection, occurrence, and originof kaolinite/smectite.* In *Kaolin Genesis and Utilization*, ed. H Murray, W Bundy, C Harvey,pp. 291-323. Boulder, CO: Clay Mineral. Soc.

Hungr O., Evans S.G., Bovis M., Hutchinson J.N. (2001)-*Review of the classification of landslides of the flow type.* Environmental and Engineering Geoscience, Vol. 7, pp.221-238.

Hutchinson J.N (1973).- *The response of London Clay cliffs to differing rates of toe erosion.* Geologia Applicata e Idrogeologia, Vol. 8, pp. 221-239.

Hutchinson J.N. (1988)- *Morphological and geotechnical parameters of landslides in relation to geology and hydrogeology.* General Report. 5th international Symposium on Landslides, Lausanne, Vol.1, pp. 3-35.

Iannace A., Merola D., Perrone V., Amato A., Cinque A. (in press.)- *Note illustrative Della Carta geologica d'Italia Alla scala 1:50.000 Foglio 466* Sorrento.Servizio Geologico d'Italia, ISPRA.

Ikhane P.R., Omosanya K.O., Akinmosin A.A., Odugbesan A.B. (2012)- *Electrical resistivity Imaging (ERI) of slope deposits and structures in some parts of eastern Dahomey Basin.* Journal of Applied Sciences, Vol. 12, pp. 716-726.

Inoue A. (1987)- *Conversion of smectite to by hydrothermal and diagenetic alterations, Hokuroku Kuroko mineralization area, northeast Japan*. Proc. Int. Clay Conf., Denver, 1985, pp. 158-64.

Inoue A. (1995)- *Formation of clay minerals in hydrothermal environment.* In Velde B. (Ed.) Origin and Mineralogy of Clays: Clays and Environment. Springer, Berlin, pp. 268-329.

Inoue A. & Utada M. (1991)- *Smectite-to-chlorite transformation in thermally metamorphosed volcanoclastic rocks in the Kamikita area, northern Honshu, Japan*. Am Miner Vol.76, pp. 628- 640.

Inoue AM, Utada M, Negata H, Watanabe T. (1984)- *Conversion of trioctahedral smectite to interstratified chlorite/ smectite in Pliocene acidic pyroclastic sediments of the Ohyu district, Akita Prefecture, Japan.* Clay Sci Soc Jpn 6:

Jennings S. and Thompson G.R. (1986)- *Diagenesis of Plio- Pliocene sediments of the Colorado River della, southern California*. J. Sed. Petrol. Vol. 56, pp. 89-98.

Jeong S.W. (2010)- *Grain size dependent rheology on the mobility of debris flows.* Geosciences Journal, Vol. 14, pp. 359-369.

Kilburn C.R.J. & Petley D.N. (2003)- *Forecasting giant, catastrophic slope collapse: lesson form Vajont, Northern Italy*- Geomorphology Vol. 54, pp. 21-32.

Klug H.P. & Aexander L.E. (1974)- *X-Ray Diffraction procedures or polycrystalline and amorphous materials.* J. Wiley and Sons (eds.), New York.

Krahn J.& Morgenstern *N.R. (*1979*)- The ultimate frictional resistance of rock discontinuities*. Int. J. Rock Mech. Min. Sci. & Geomech. Abstr., Vol. 16 pp. 127-133.

Leoni L., Lezzerini M., Saitta M. (2008)- *Calcolo computerizzatodell'analisi mineralogica quantitative di rocce e sedimenti argillosi basato sulla compinazione dei dati chimici e diffrattometrci*. Atti Soc. tosc. Sci. nat., Mem., Serie A, 113, Pag. 63-69.

Macht F., Eusterheus K., Pronk G.J., Tossche K. U. (2011)- *Specific surface area if clay minerals: Comparison between atomic force microscopy measurements and bulk gas (N_2) and liquid (EGME) adsorption methods.* Applied Clay Science Vol. 53, pp. 20-26.

Maggiò (2003)- *Influenza della composizione del liquido interstiziale sulla resistenza dei terreni argillosi a struttura complessa.* Phd thesis in Dottorato di Ricerca in Ingegneria Geotecnica, University of Naples Federico II.

Maggiò F. & Pellegrino A. (2002)- *Sperimentazione in sito sul miglioramento dell resistenza di un'argilla attiva con modifica della composizione chimica del liquido interstiziale.* Incontro Annuale dei Ricercatori di Geotecnica IARG, pp.1-4.

Malet J.-P, Maquaire O., Locat J., Remaitre A. (2004)- *Assessing debris flow hazards associated with slow moving landslides: methodology and numerical analyses.* Landslides Vol. 1, pp. 83-90.

Malet J.-P., Remaitre A., Maquaire O. (2003)- *Flow susceptibility of heterogeneous marly formations: implications for torrent hazard control in the Barcelonnette Basin (Alpes-de-Haute-Provence, France).* Debris Flow Hazards Mitigation: Mechanics, Prediction, and Assessement, Rickenmann & Chen (eds.), Millipress, Rotterdam, ISBN, pp.351-362.

Mansour M.F. & Morgenstern N.R. Martin C.D. (2011)- *Expected damage from displacement of slow moving slides.* Landslide Vol. 8, pp. 117-131.

Martino S. & Scarascia Mugnozza G. (2005)– *The role of the seismic trigger in the Calitri landslide (Italy): historical reconstruction and dynamic analysis*. Soil Dynamic Earthquake engineering, Vol. 25, pp. 933-950.

Mazzoli S., D'Errico M., Aldega L., Corrado S., Invernizzi C., Shinner P., Zattin M. (2008)-*Tectonic burial and young (<10 Ma) exhumation in the southern Apennines fold and thrust belt (Italy)*-Geology Vol.36, pp. 243-246.

Mitchel J.K. & Soga K. (2005*)-Foundamental of Soil behavior*, 3rd Edition, Wiley.

Moore D.M. & Reynolds R.C.J$_R$ (1997)- X-*ray diffraction and the identification and analysis of clay minerals*. Second edition. Oxford University Press, Oxford and New York, 378 p.

Mostardini F. & Merlini S. (1986) - *Appennino centro meridionale.Sezioni geologiche e proposta di modello strutturale*. Mem. Soc.Geol. It., Vol. 35, pp. 177-202.

Ogniben L. (1969) - *Schema introduttivo alla geologia del confine calabro-lucano*. Mem. Soc. Geol. It., Vol. 8, pp. 453-763.

Parise M.& Wasowski J. (1999)- *Landslide Activity maps for Landslide Hazard Evaluation: three case studies from Southern Italy*. Natural Hazard Vol. 20, pp. 159-183.

Patacca E., & Scandone P. (2007)-*Geology of Southern Apennines*.- CROP-04 (ed. By Mazzotti A., Patacca E. & Scandone P.) Bollettino della Società Geologica Italiana,Spec. Issue, Vol.7, pp. 75-119.

Pearson T. C. & Costa, J. E. (1987)- A *rheological classification of subaerial sediment-water flow*s. In: Debris Flow/Avalanches: Process, Recognition and Mitigation (Eds: Costa, J. E. & Wieczorek, G. F.). Reviews in Engineering Geology Volume VII, 1-12. Boulder, CO: Geological Society of America.

Pescatore T., Renda P., Schiattarella M., Tramutoli M. (1999)- *Stratigraphic and structural relatinships between Meso-Ceozoic Lagonegro basin and coeval carbonate platforms in southern Apennines, Italy*- Tectonophysics Vol. 315, pp. 269-286.

Picarelli L.& Russo C.(2004)- *Remarks on the mechanisms of slow active landslides and the interaction with man-made works.* In Lacerda W. et al. (Ed.)

Proceedings of the IX International Symposium on Landslide Rio de Janeiro, Brazil, Vol. 2, pp. 1141-1176.

Picarelli L. & Urcioli G. (1993)- *Effetti dell'erosione in argillite di alta plasticità*. Rivista Italiana di Geotecnica, Vol. 17, pp. 29-49.

Pollastro R.M. (1993)- *Consideration and Applications of the Illite-Smectite geothemometer in Hydrocarbon-Bearing Rocks of Miocene to Mississipian Age.* Clays and Clay Minerals. Vol 41, No.2, pp. 119-133.

Rankka K., Andersson Sköld Y.., Hultén C., Leroux V., Dahlin T. (2004)- *Quick clay in Sweden*. Swedish Geotechnical institute. Report No 65, 145 p.

Rashid A. S. B. A. (2005)- *Determination of Plastic Limit of Soil using Modified Cone Penetration Method*. M.Sc. Thesis, Univ. of Malaysia.

Ray R.G. (1960)-*Aerial photographs in geologic interpretation and mapping-U.S.* Geol. Survey Prof. Paper 237 p.

Reynolds J.M.(1997)- *An Introduction to Applied and Environmental Geophysics*. John Wiley and Sons Ltd, Chichester, 796 p., first edition.

Reynolds Jr. R.C. (1980): *Interstratified clay minerals.* In Crystal Structures of Clay Minerals and Their X-ray Identification, Brindley G.W. and Brown G. eds. Mineralogical Society, London, pp. 249-303.

Reza Emami Azadi M. & Monfared S.R. (2012)- *Fall cone test Parameters and their effects on the Liquid and Plastic Limits of homogeneous and non Homogeneous soil samples.* EJGE, Vol 17, pp.1615-1646.

Robinson D & Wright VP. (1987)- *Ordered illitesmectite and kaolinite-smectite: pedogenic minerals in a Lower Carboniferous paleosol sequence, SouthWales*. Clay Miner. Vol. 22, pp.109-18.

Sassa K. (1985)- The *geotechnical classification of landslides.* Landslides news, Vol. 3, pp. 21-24.

Scandone P. (1967) - *Studi di geologia lucana: la serie calcareo-silicomarnosa e suoi rapporti con l'Appennino calcareo*. Boll. Soc. Nat. in Napoli, Vol. 76, pp. 1-175

Schiffman P & Staudigel H. (1995)- *The smectite to chlorite transition in a fossil seamount hydrothermal system: The basement complex of La Palma, Canary Islands*. J Metamorphic Geol Vol., 13, pp. 487-498.

Schramm G. (1998)- *A pratical Approach to Rheology and Rheometry, 2nd edition*- Gebrueder HAAKE GmbH, Karlsuruhe, Federal Republic of Germany.

Selli R. (1962) - *Il Paleogene nel quadro della geologia dell'Italia meridionale*. Mem. Soc. Geol. It., Vol. 3, pp.737-790.

Sgrosso I. (1988) - *Nuovi elementi per un più articolato modello paleogeografico nell'Appennino centro-meridionale.* Mem. Soc. Geol. It., Vol. 41, pp.225-252.

Sgrosso I. (1996) - *I rapporti tra i depositi del massiccio del Matese e quelli del bacino molisano.* Mem. Soc. Geol. It., Vol. 51, pp. 263-272.

Sgrosso I. (1998) - *Possibile evoluzione cinematica miocenica nell'orogene centro-sud appenninico.* Boll. Soc. Geol. It., Vol 117, pp. 679-724.

Shau YH & Peacor D. (1992)- *Phyllosilicates in hydrothermally altered basalts from DSDP hole 504B, leg 83-A TEM and AEM study*. Contrib. Mineral. Petrol., Vol 112, pp. 119-133.

Skempton A.W. (1953)- *The Colloidal Activity of Clays*-3rd.International Conference Soil Mech found Eng. Switzerland, Vol. 1, pp. 57-60.

Skempton A.W. (1970)- *First time slides in over-consolidated clays.* Geotechnique, London, England, Vol. 20(3), pp. 320-324.

Snyder R.L. & Bish D.L. (1989)- *Quantitative analysis by X-Ray powder diffraction.* In Modern Powder Diffraction (Bish D.L. as Post J.E. Eds.), Vol. 20, pp. 101-145.

Środoń J. & Eberl D.D. (1984)- *Illite.* In Micas, Reviews in Mineralogy 13. Bailey S. W. ed. Mineralogical Society of America, Washington D.C. pp. 495-544.

Środoń J. (1999)- *Nature and of Mixed Layer Clays and Mechanism of their Formation and Alteration.* Annu. Rev. Earth Planet. Sci. Vol. 27, pp. 19-53.

Summa V., Tateo F., Giannossi M.L., Bonelli C.G. (2010)- *Influence of clay mineralogy on the stability of a landslide in Plio Pleistocene sediments near Grassano (Southern Italy)*- Catena Vol. 80 , pp.75-85.

Taylor K.R.& Cripps J.C. (1987)- *Weathering Effects: Slopes in mudrocks and Over Consolidated Calys*-Cap 13 of Slope Stability, Edited by M.G. Anderson and K.S.Richards, pp. 405-445.

Taylor R.K. & Spears D.A. (1981): *The breakdown of British coal measure rocks.* Int. J. Rock Mech. Mining Sci., Vol. 7, pp. 481-501.

Telford W.M., Geldart L.P., Sheriff R.A. (1990)- *Applied geophysics*.2nd edition: Cambridge Univ. Press.

Terzaghi K. (1943)- *Theoretical Soil Mehanics*, John Wiley & Sons, New York, USA.510 p.

Thornton C. & Zhang L. (2003)- *Numerical simulations of the Direct Shear Test*- Chem. Eng. Technol. Vol. 26, pp. 153-156.

Uneno H., Jige M., Sakamoto T., Balce G.R., Deguchi I. (2008)- *Geology and clay mineralogy of the landslides area in Guisaugon, southern Leyte Island, Philippines*. University Bulletin of Chiba Institue of Schenze, No 1, 9p.

Varnes D.J. (1978)- *Slope movement types and processes.* In Shuster & Krizek (eds.), Landslides, Analysis, and Control: Transportation Research Board, National Academy of Sciences, Washington, DC., Special Report Vol. 176, pp.11-33.

Velde B. (1995)- *Origin and Mineralogy of Clays. Clays and the Environment.* Berlin, Heidelberg, New York, Barcelona, Budapest, Hong Kong, London, Milan, Paris, Tokyo: Springer-Verlag. xv + 334 p.

Vitale S., Ciarcia S., Mazzoli S., Iannace A., Torre M. (2010)- *Structural analysis of the Internal Units of Cilento, Italy: New costrains on the Miocene tectonic evolution of the southern Apennine accretionary wedge*- C.R. Geoscience Vol. 342, pp. 474-482.

Wood D. M. & Worth C. P. (1978) -*The use of Cone Penetrometer to Determine the Plastic Limit of Soils.* J. of Ground Eng., Vol.11, No. 3, 37 p.

WP/WLI (1993). *A suggested method for describing the activity of a landslide*. Bulletin International Association for Engineering Geology, Vol. 47, pp. 53-57.

APPENDIX 1: XRPD PATTERNS

PN1

BULK SAMPLE

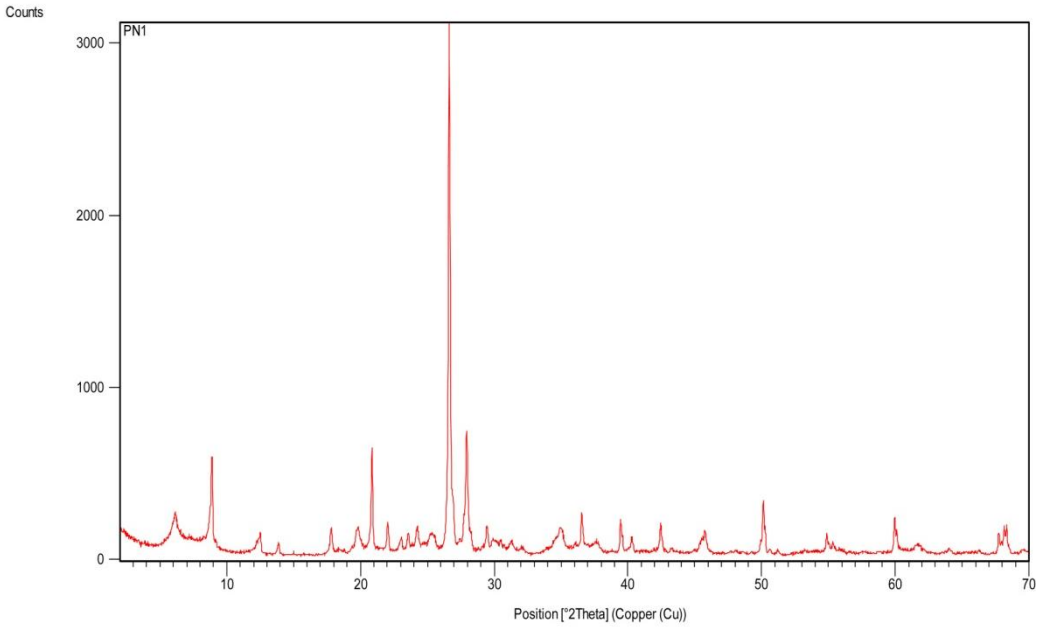

ORIENTED AGGREGATES

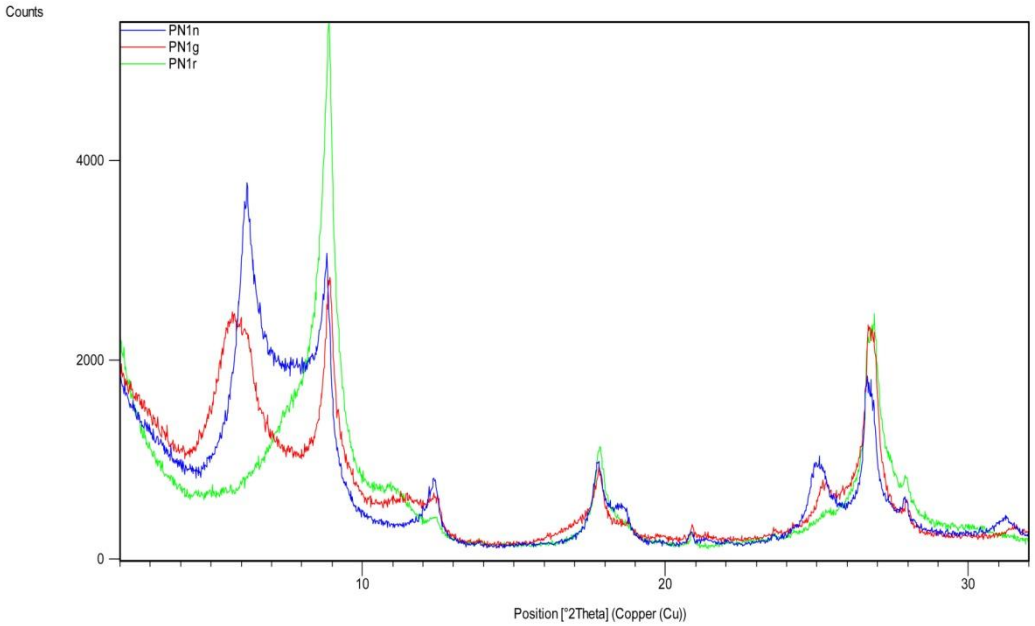

Mineralogy: mixed layer illite/smectite, mixed layer chlorite/smectite, chlorite, muscovite, Na-feldspar, K-feldspar, quartz, calcite, dolomite.

PN2

BULK SAMPLE

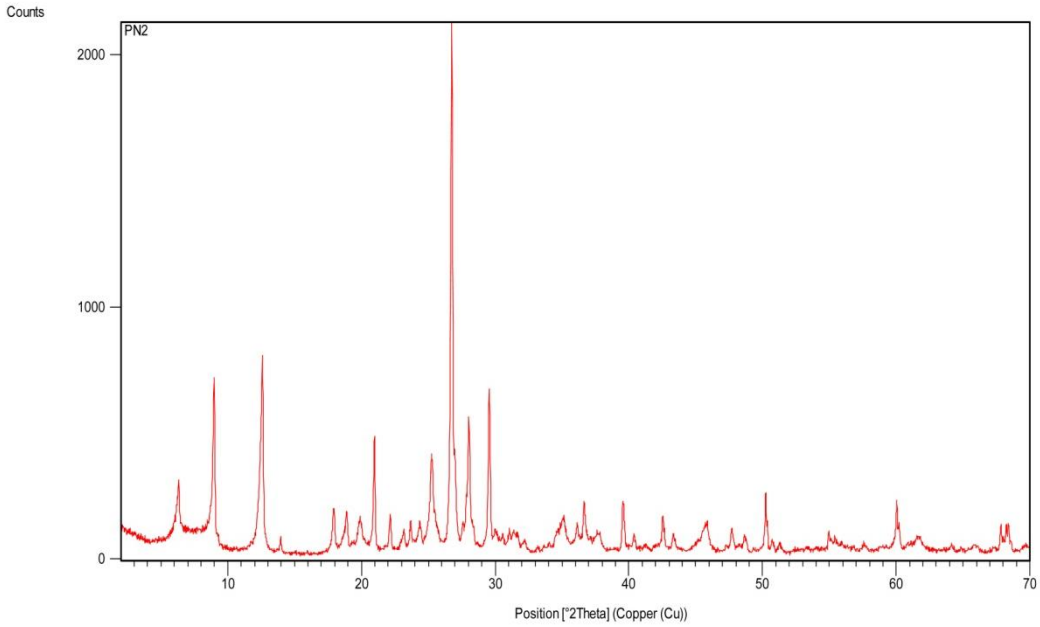

ORIENTED AGGREGATES

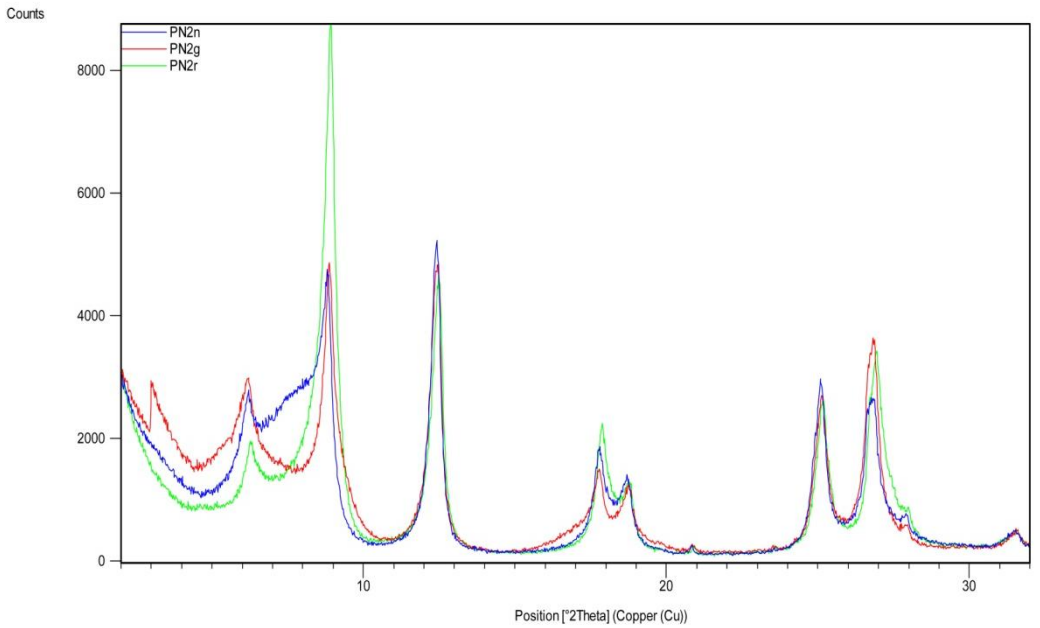

Mineralogy: mixed layer illite/smectite, mixed layer chlorite/ smectite, chlorite, muscovite, Na-feldspar, K-feldspar, quartz, calcite, dolomite.

PN3

ROW MATERIAL

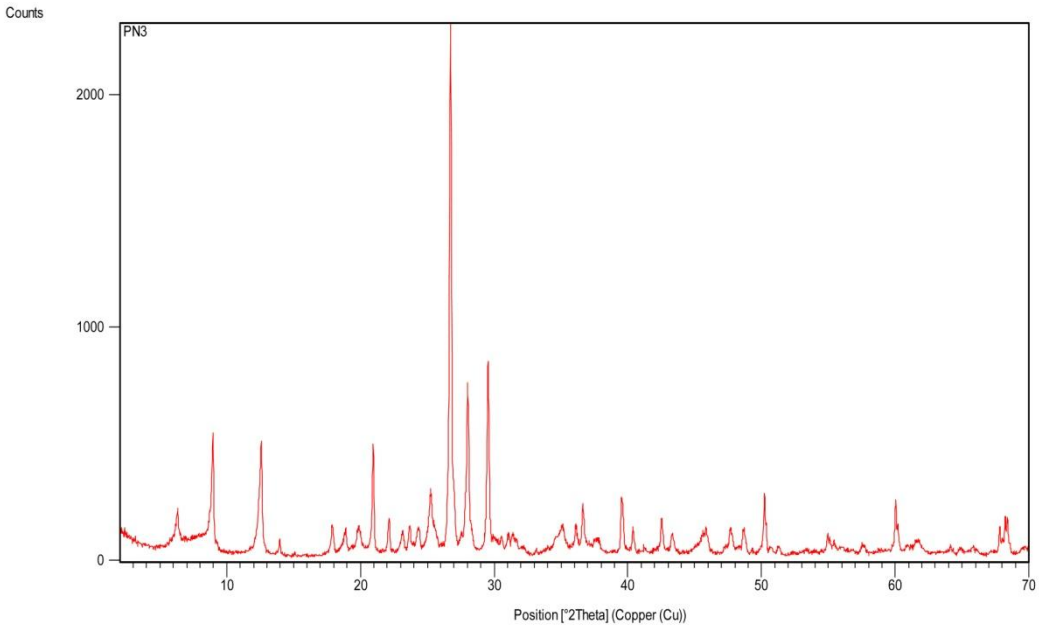

ORIENTED AGGREGATES

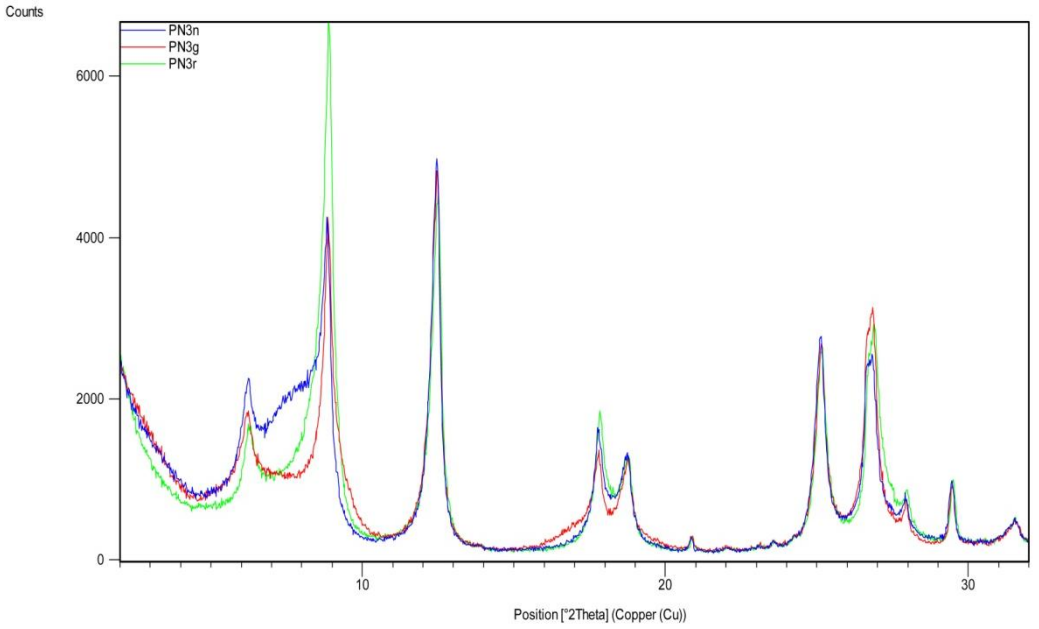

Mineralogy: mixed layer illite/smectite, mixed layer chlorite/smectite, chlorite, muscovite, Na-feldspar, K-feldspar, quartz, calcite, dolomite.

PN4

BULK SAMPLE

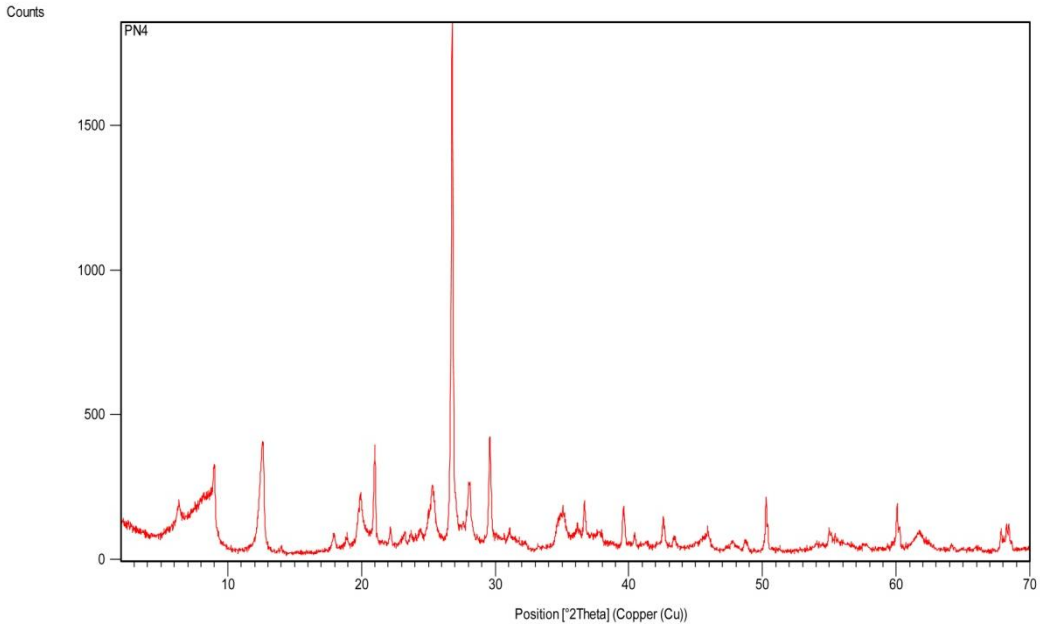

ORIENTED AGGREGATES

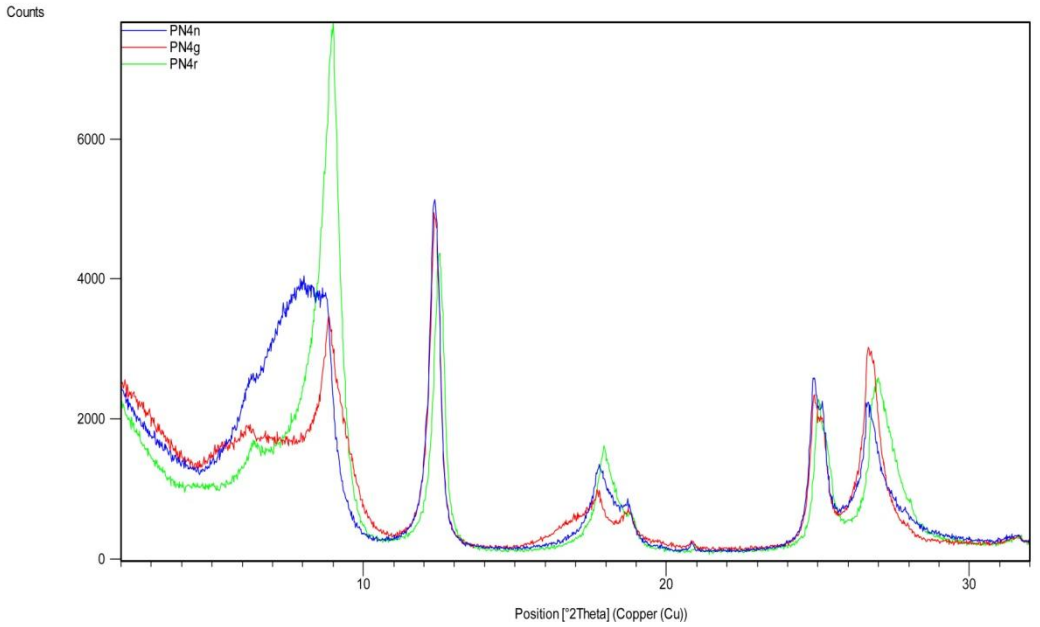

Mineralogy: mixed layer illite/smectite, mixed layer chlorite/smectite, chlorite, kaolinite, muscovite, Na-feldspar, K-feldspar, quartz, calcite, dolomite.

PN5

BULK SAMPLE

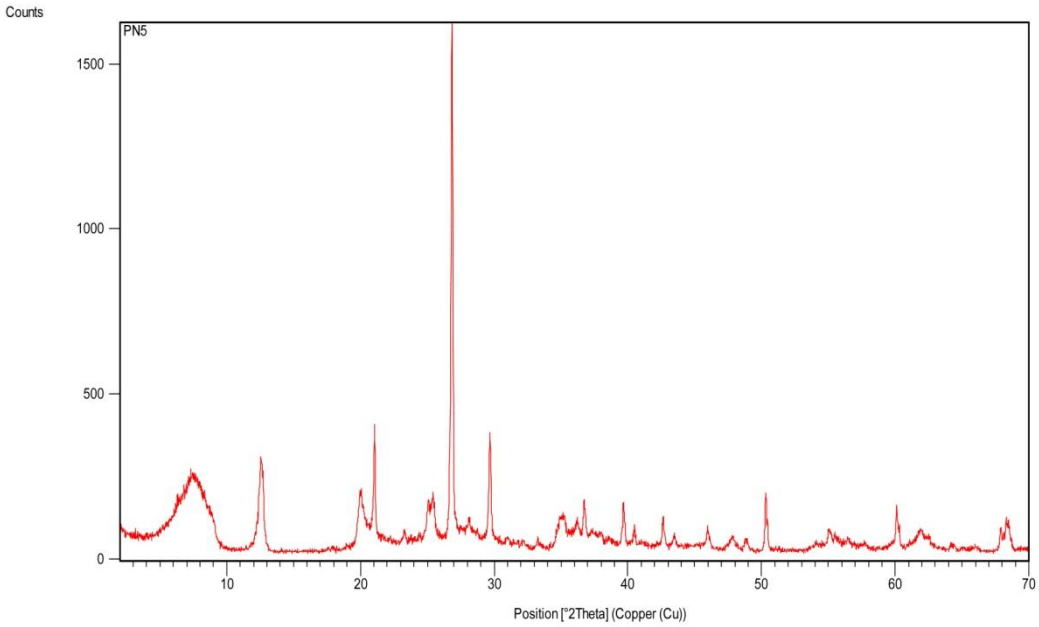

ORIENTED AGGREGATES

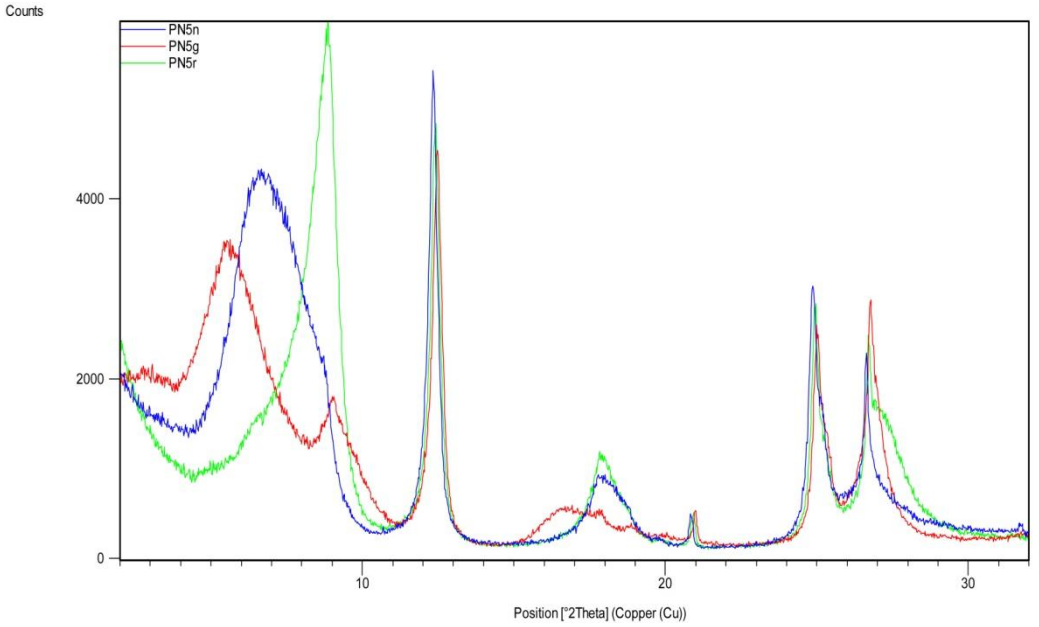

Mineralogy: mixed layer illite/smectite, chlorite, kaolinite, muscovite, Na-feldspar, K-feldspar, quartz, calcite, dolomite.

PN6

BULK SAMPLE

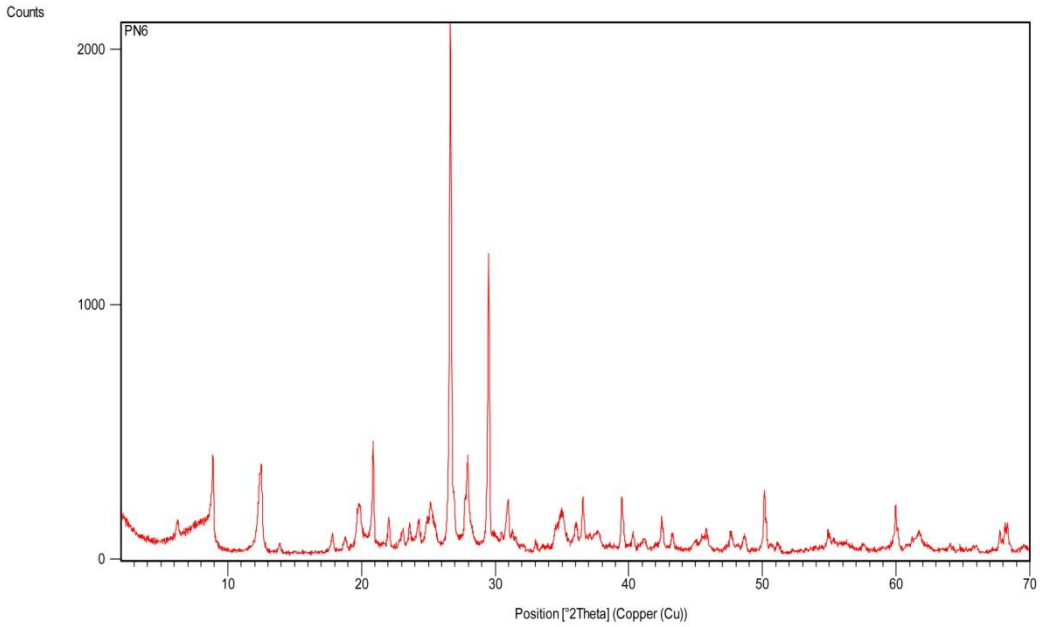

ORIENTED AGGREGATES

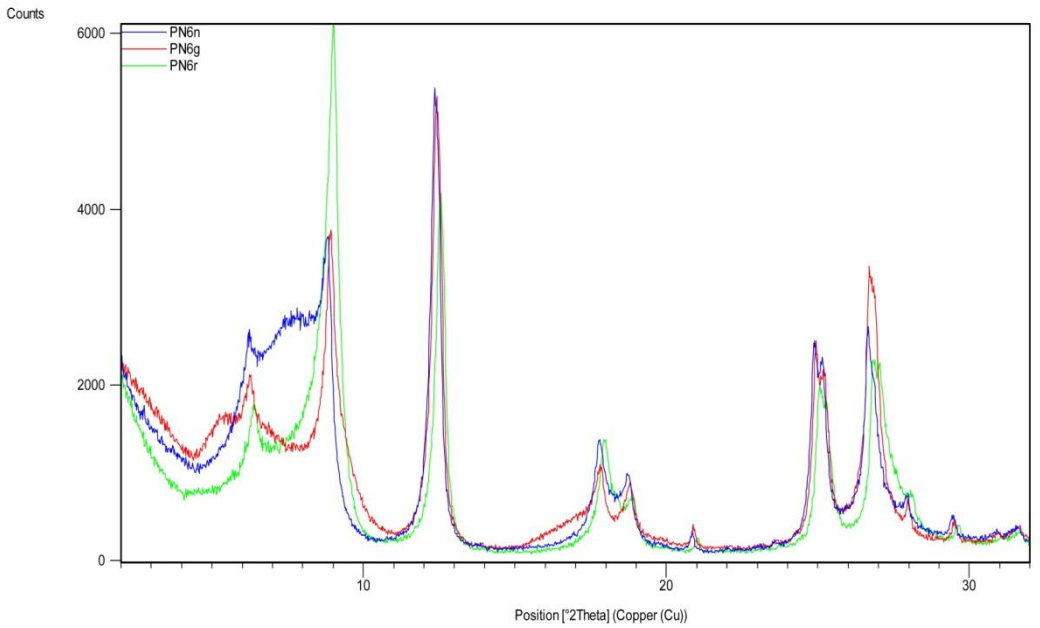

Mineralogy: mixed layer illite/smectite, mixed layer chlorite/smectite, chlorite, kaolinite, muscovite, Na-feldspar, K-feldspar, quartz, calcite, dolomite.

PN7

BULK SAMPLE

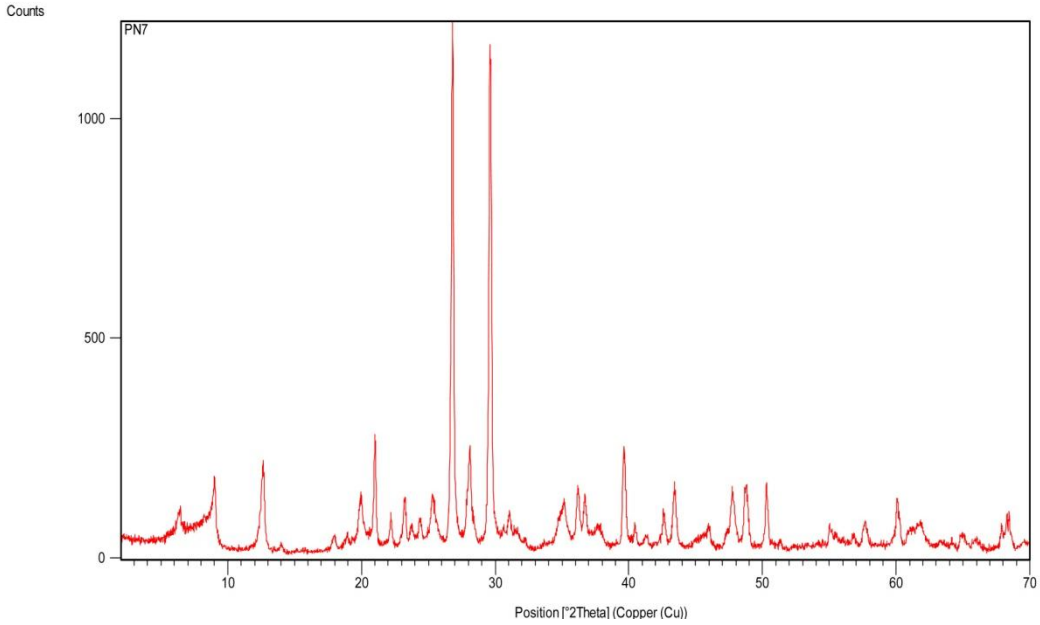

ORIENTED AGGREGATES

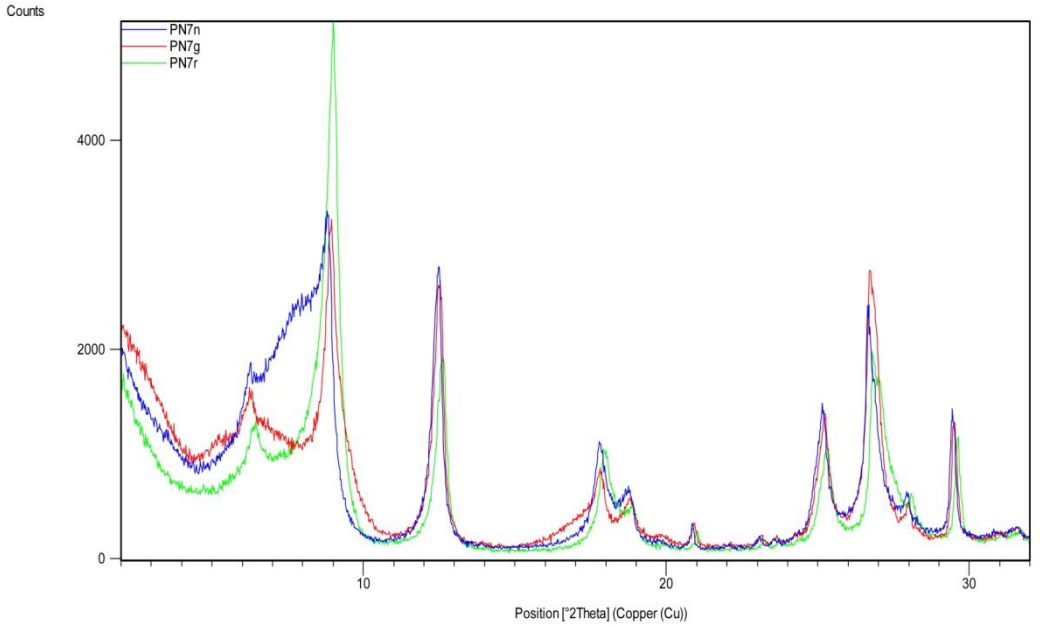

Mineralogy: mixed layer illite/smectite, mixed layer chlorite/smectite, chlorite, muscovite, Na-feldspar, K-feldspar, quartz, calcite, dolomite.

PN8

BULK SAMPLE

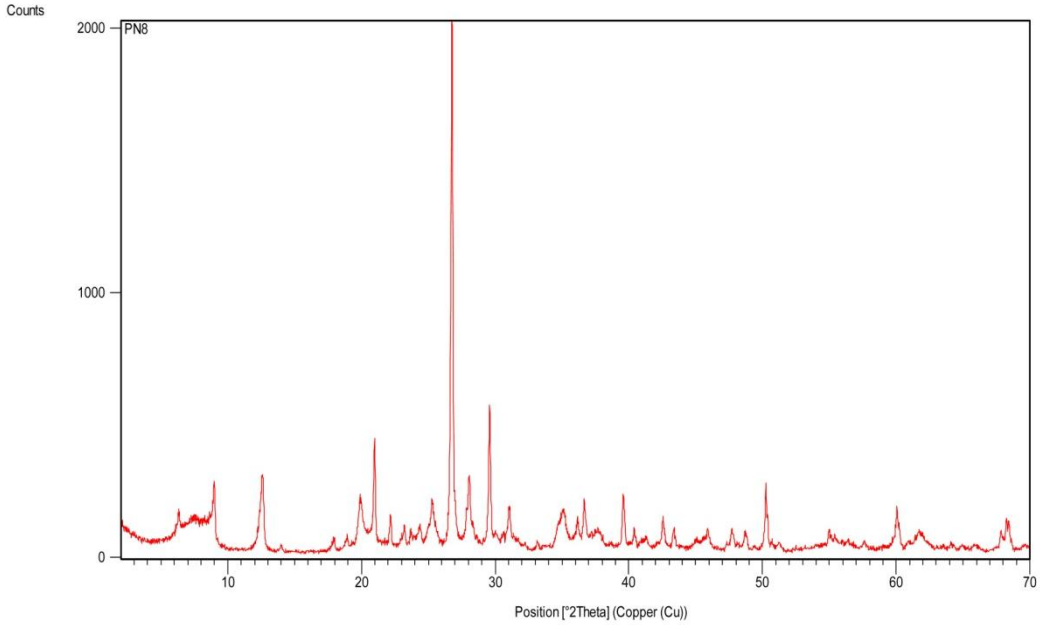

ORIENTED AGGREGATES

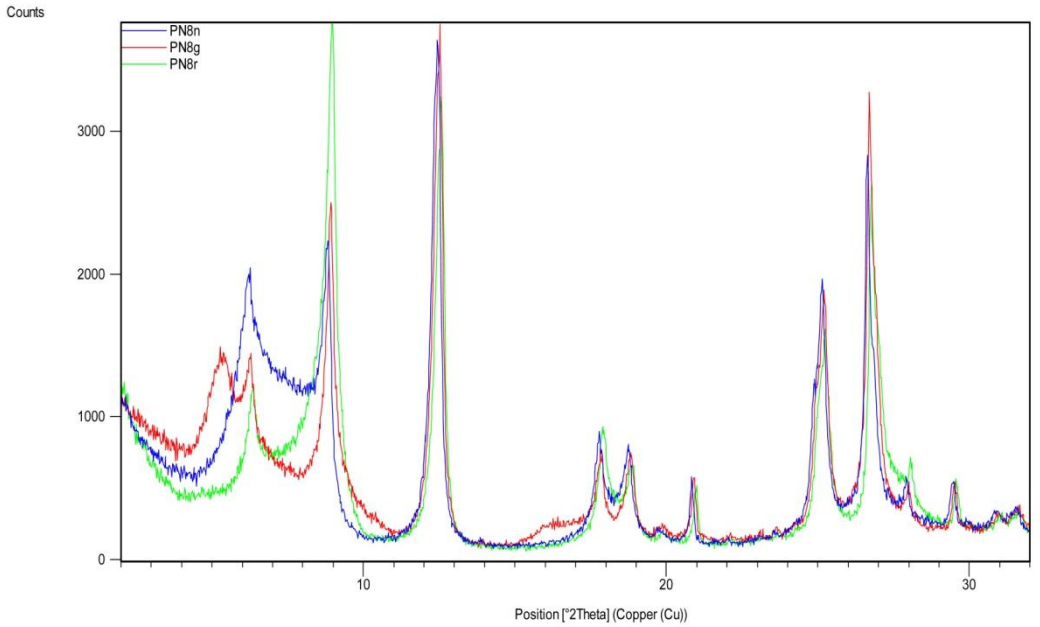

Mineralogy: mixed layer illite/smectite, mixed layer chlorite/smectite, chlorite, kaolinite, muscovite, Na-feldspar, K-feldspar, quartz, calcite, dolomite.

PN9

BULK SAMPLE

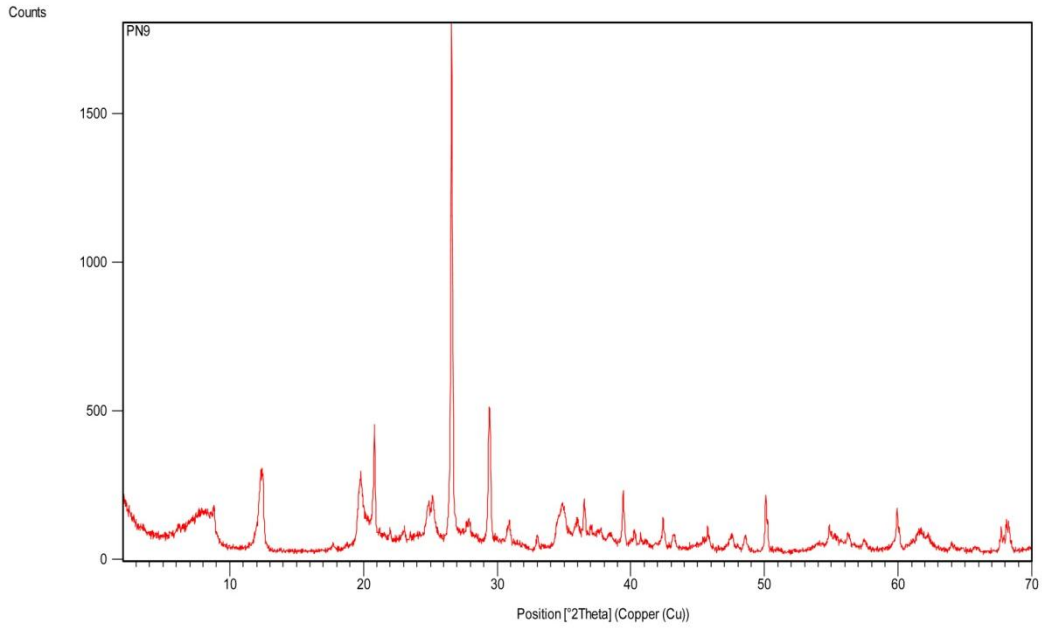

ORIENTED AGGREGATES

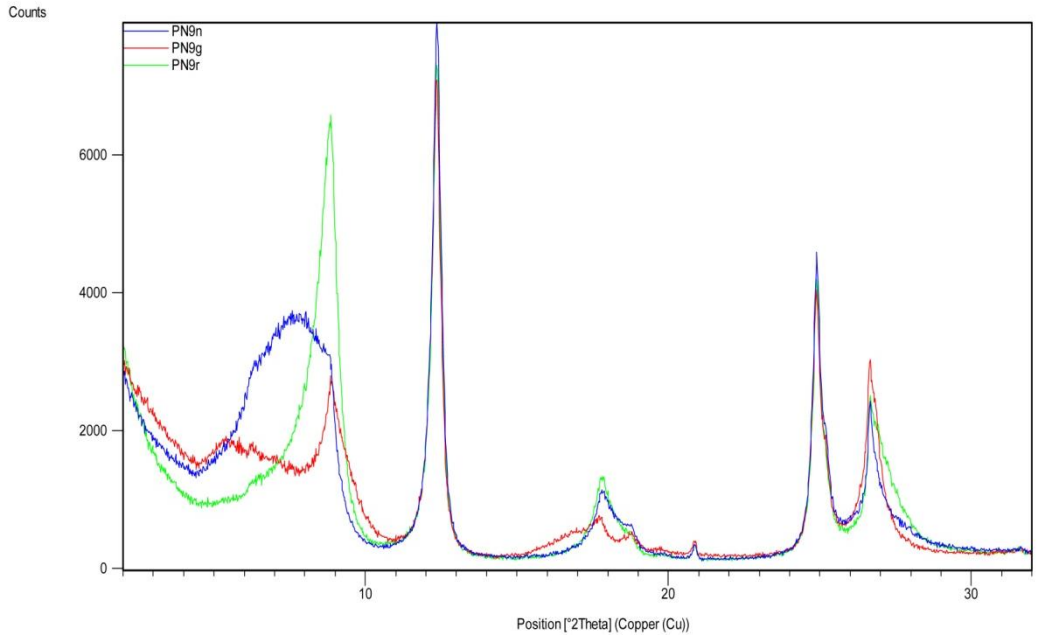

Mineralogy: mixed layer illite/smectite, mixed layer chlorite/smectite, chlorite, kaolinite, muscovite, Na-feldspar, K-feldspar, quartz, calcite, dolomite.

PR1

BULK SAMPLE

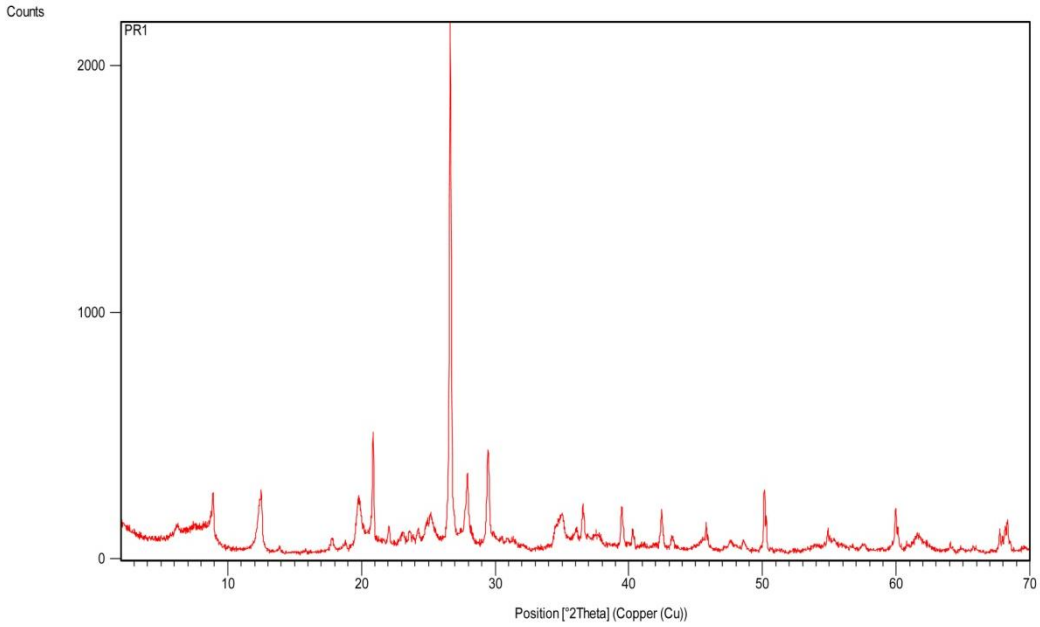

ORIENTED AGGREGATES

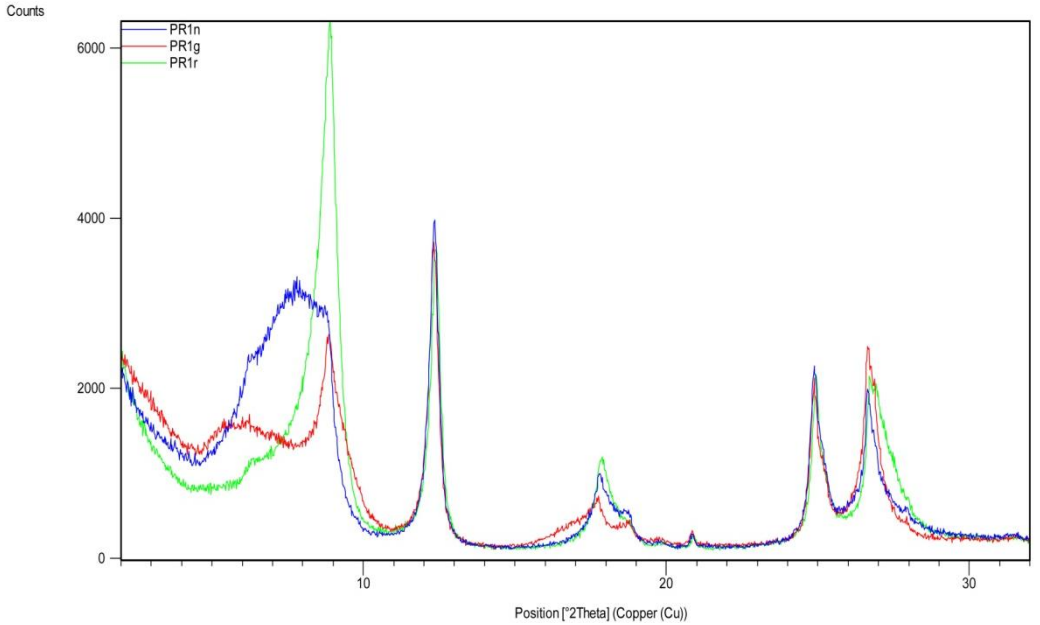

Mineralogy: mixed layer illite/smectite, mixed layer chlorite/smectite, chlorite, kaolinite, muscovite, Na-feldspar, K-feldspar, quartz, calcite, dolomite.

PR2

BULK SAMPLE

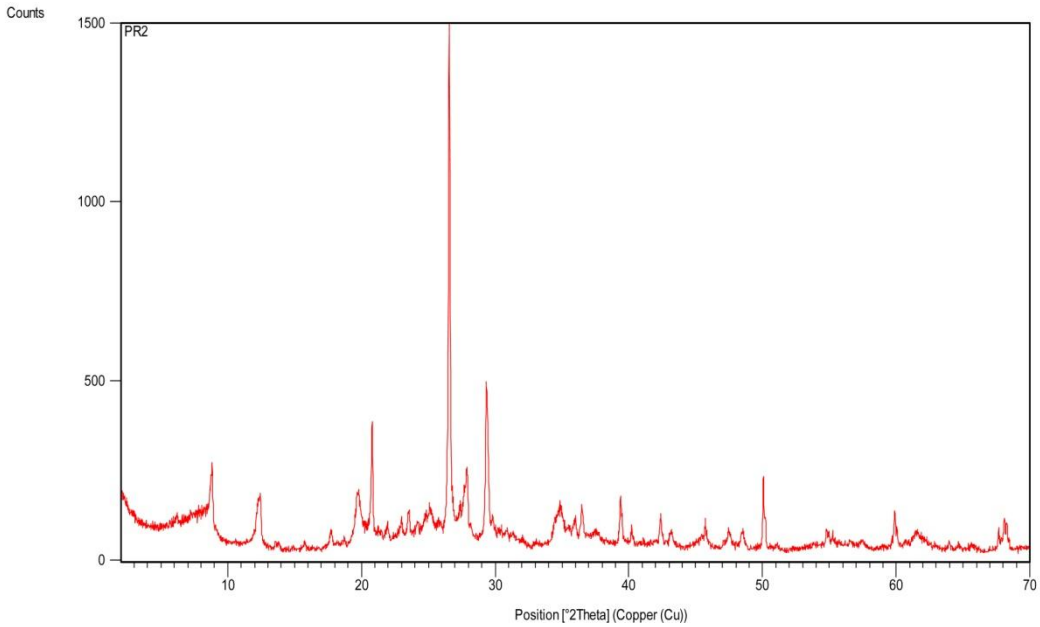

ORIENTED AGGREGATES

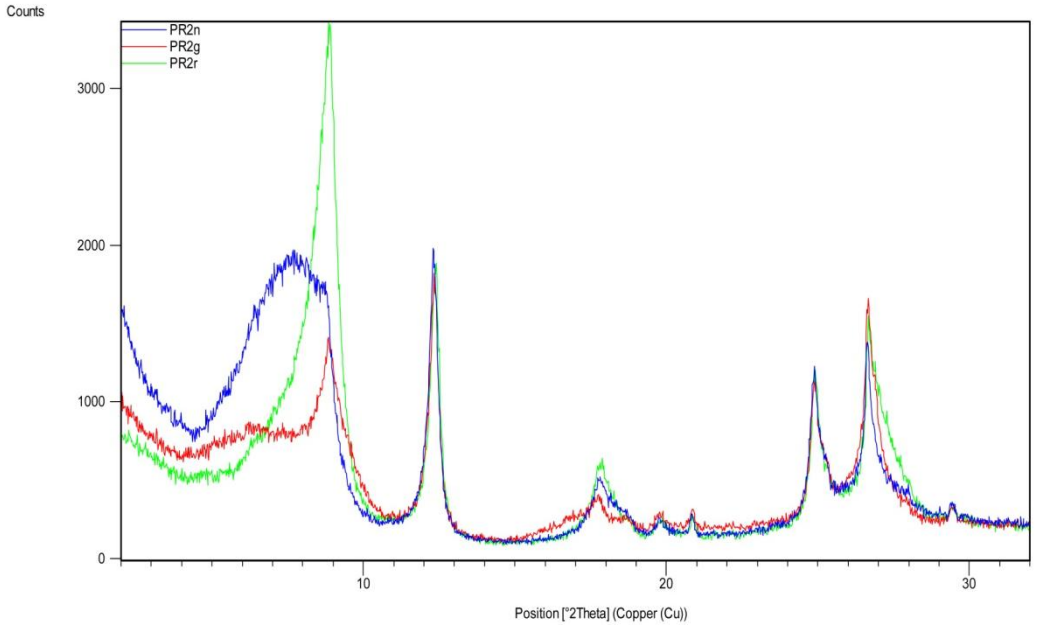

Mineralogy: mixed layer illite/smectite, mixed layer chlorite/ smectite, chlorite, kaolinite, muscovite, Na-feldspar, K-feldspar, quartz, calcite, dolomite.

PR3

BULK SAMPLE

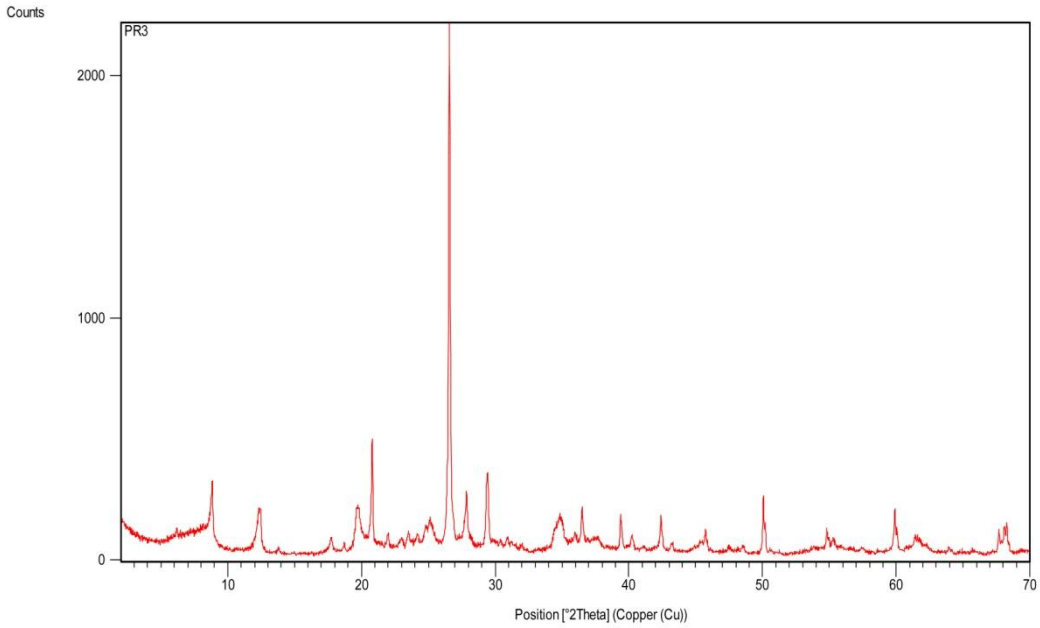

ORIENTED AGGREGATES

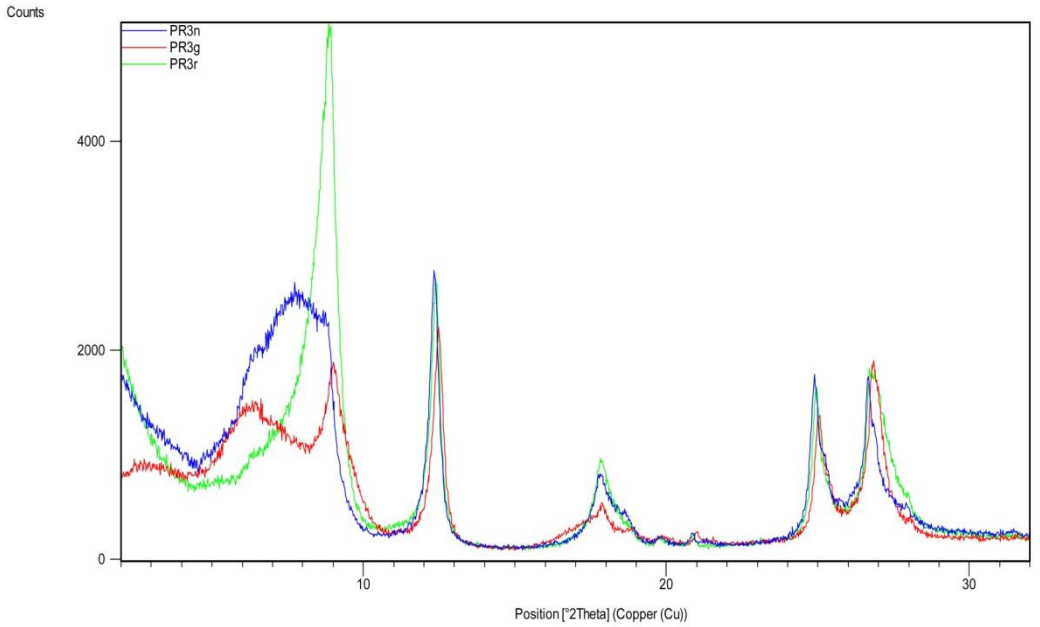

Mineralogy: mixed layer illite/smectite, mixed layer chlorite/smectite , chlorite, kaolinite, muscovite, Na-feldspar, K-feldspar, quartz, calcite, dolomite.

PR4

BULK SAMPLE

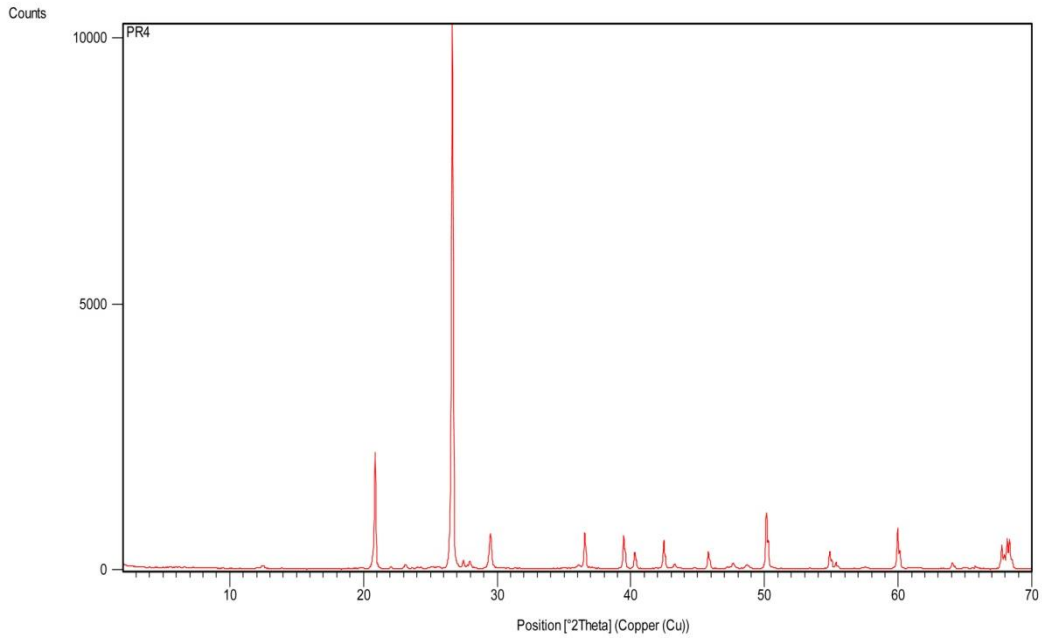

Mineralogy: mixed layer illite/smectite, chlorite, muscovite, Na-feldspar, K-feldspar, quartz, calcite, dolomite.

PR5

BULK SAMPLE

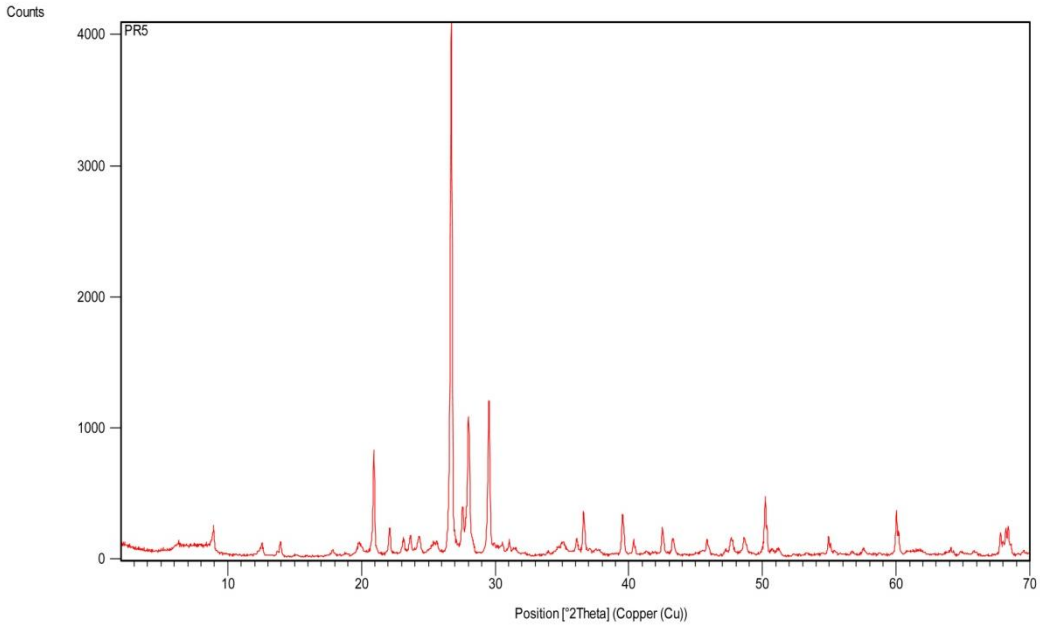

ORIENTED AGGREGATES

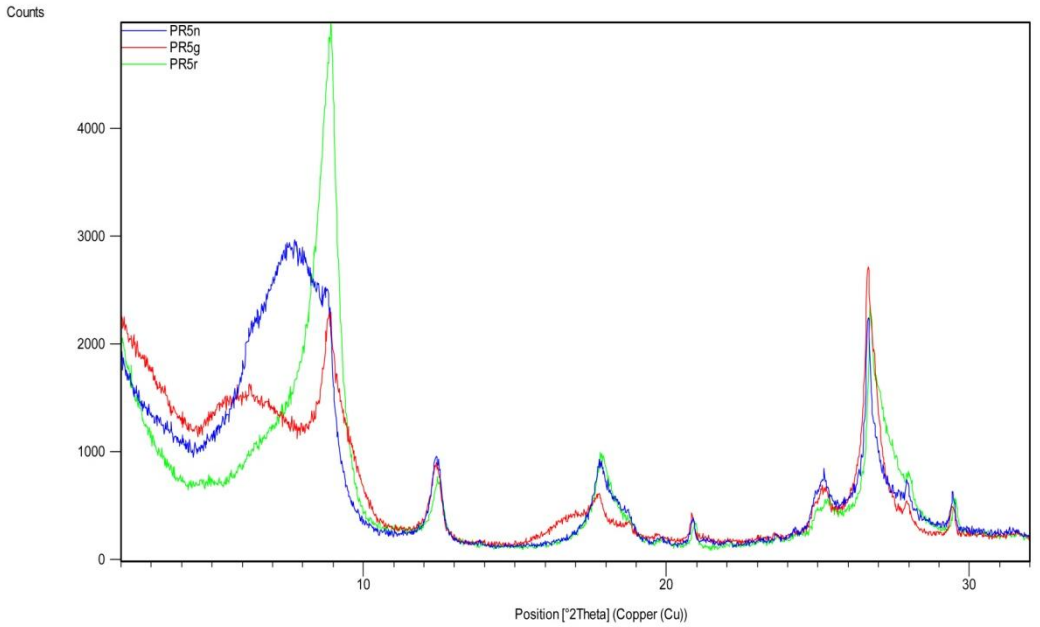

Mineralogy: mixed layer illite/smectite, chlorite, muscovite, Na-feldspar, K-feldspar, quartz, calcite, dolomite.

PR6

BULK SAMPLE

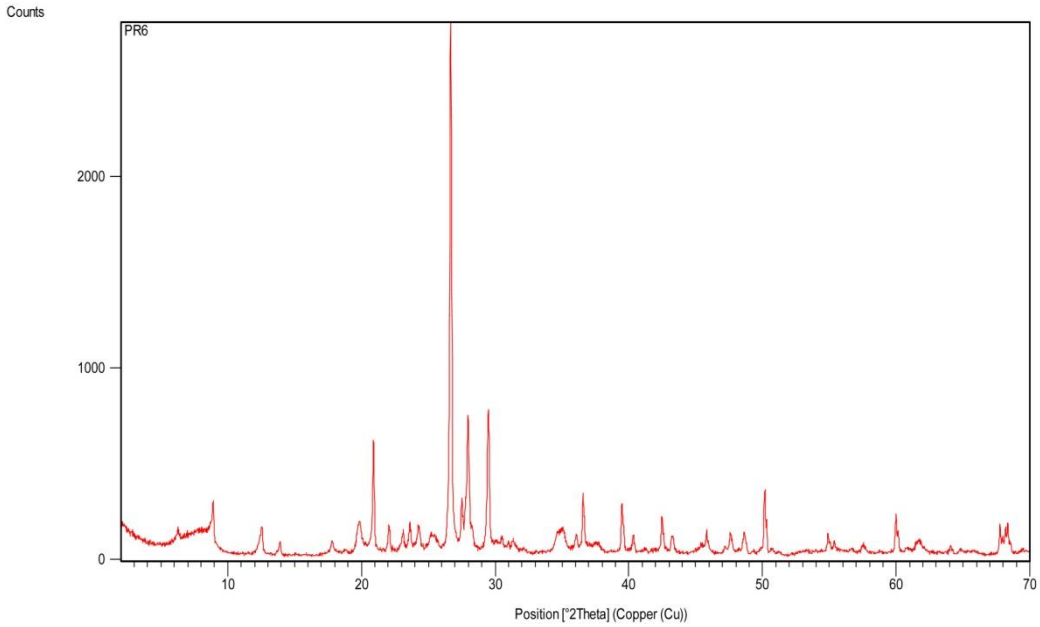

ORIENTED AGGREGATES

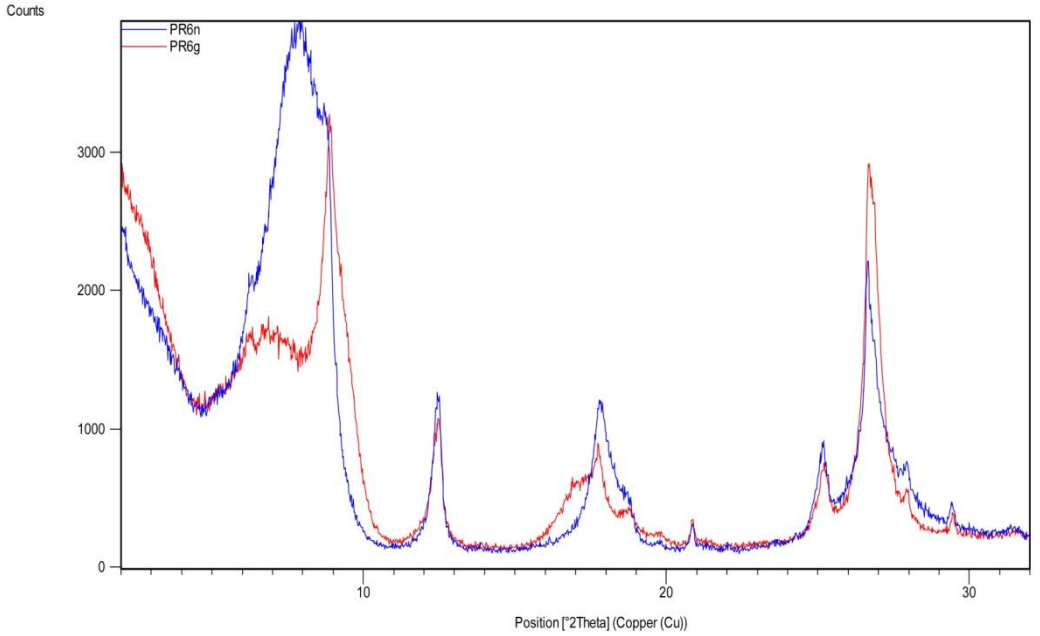

Mineralogy: mixed layer illite/smectite, mixed layer chlorite/smectite, chlorite, kaolinite, muscovite, Na-feldspar, K-feldspar, quartz, calcite, dolomite.

PR7

BULK SAMPLE

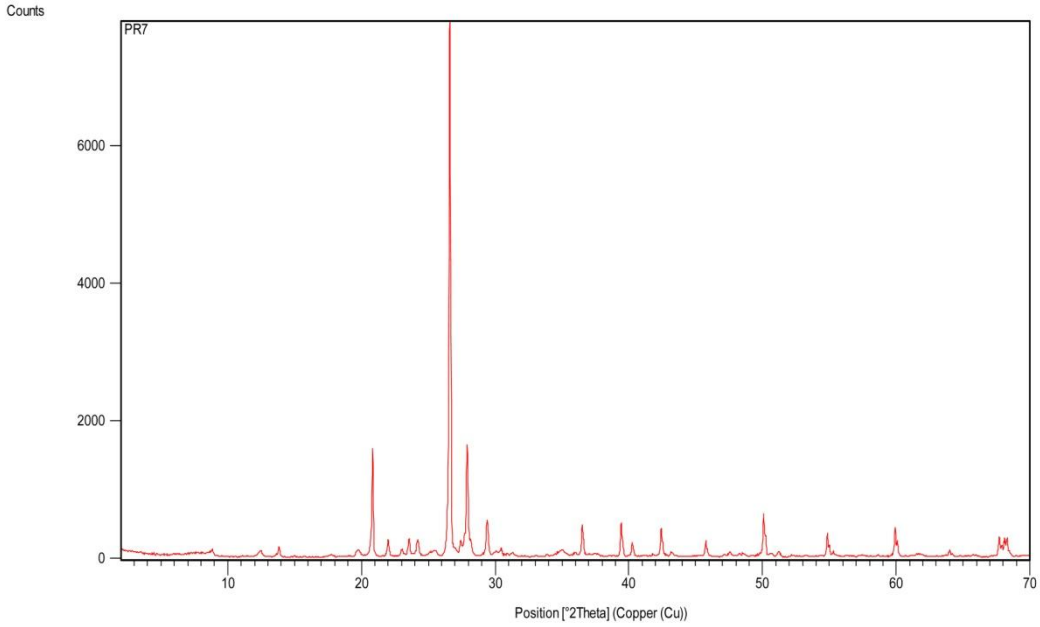

ORIENTED AGGREGATES

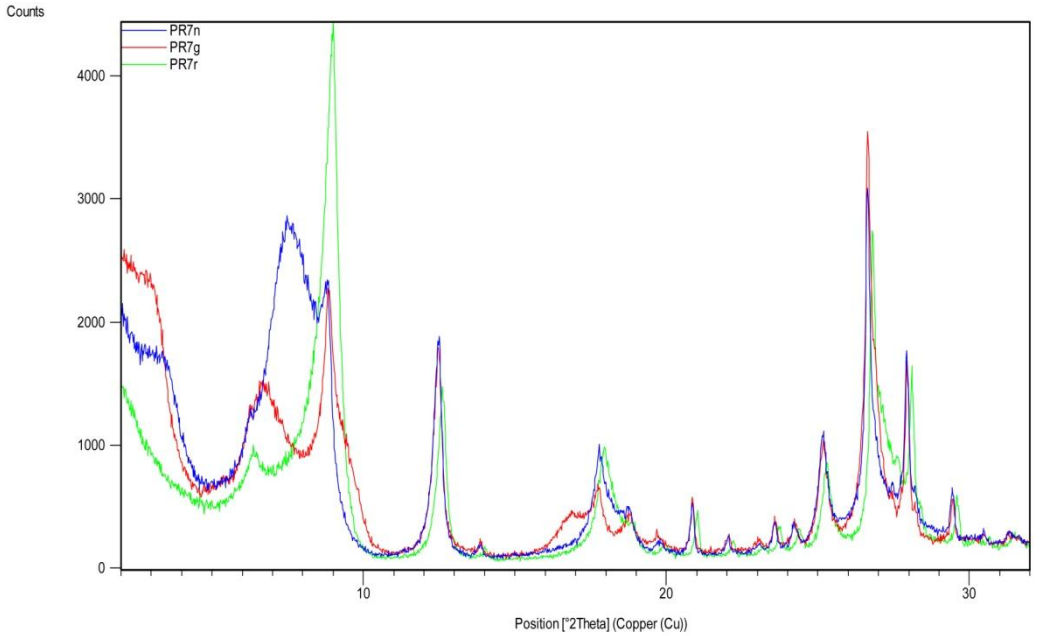

Mineralogy: mixed layer illite/smectite, chlorite, muscovite, Na-feldspar, K-feldspar, quartz, calcite, dolomite.

PR8

BULK SAMPLE

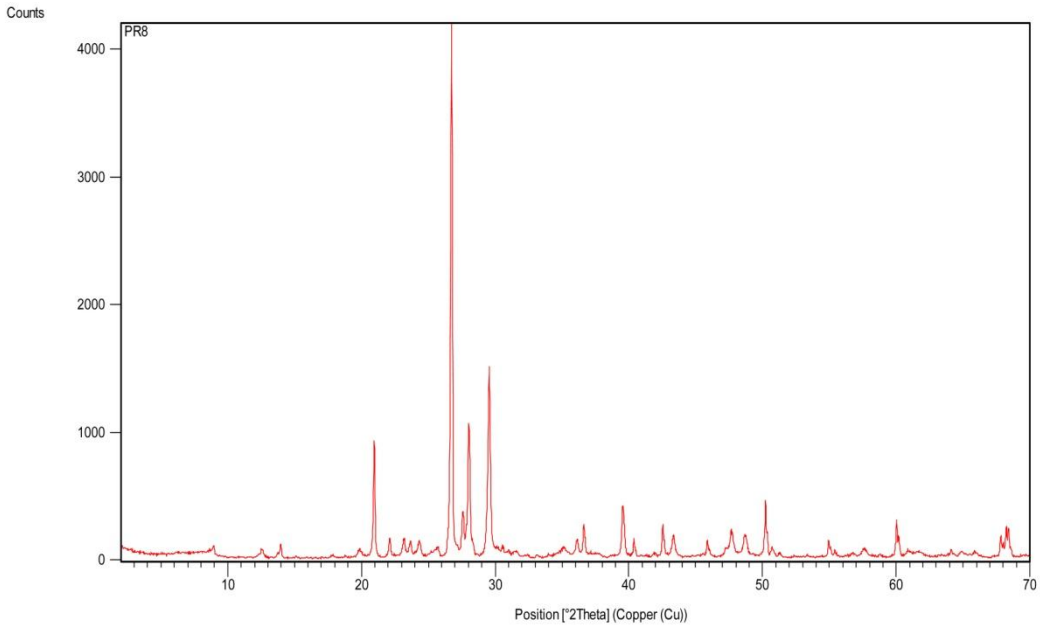

Mineralogy: mixed layer illite/smectite, mixed layer chlorite/smectite, chlorite, muscovite, Na-feldspar, K-feldspar, quartz, calcite, dolomite.

PR9

BULK SAMPLE

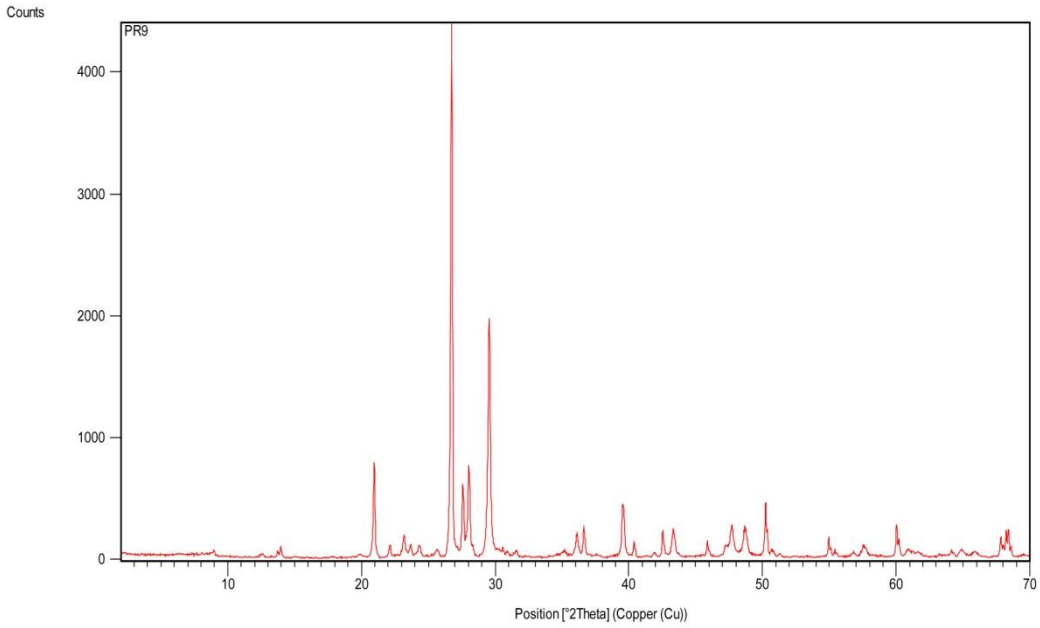

Mineralogy: mixed layer illite/smectite, chlorite, muscovite, Na-feldspar, K-feldspar, quartz, calcite, dolomite.

PR10

BULK SAMPLE

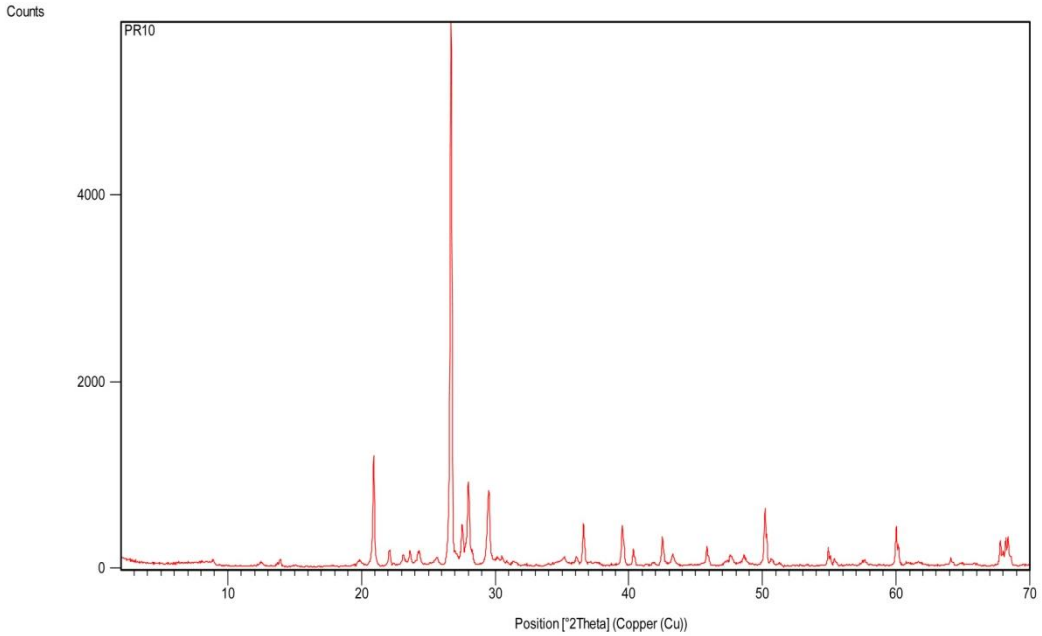

Mineralogy: mixed layer illite/smectite, chlorite, muscovite, Na-feldspar, K-feldspar, quartz, calcite, dolomite.

PR11

BULK SAMPLE

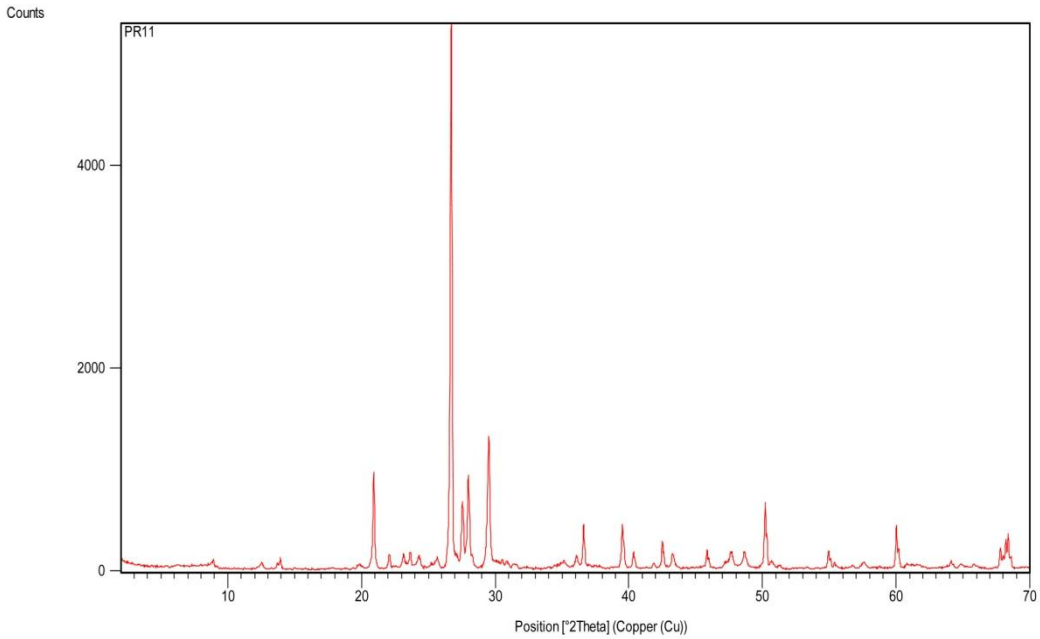

Mineralogy: mixed layer illite/smectite, chlorite, muscovite, Na-feldspar, K-feldspar, quartz, calcite, dolomite.

MC1

BULK SAMPLE

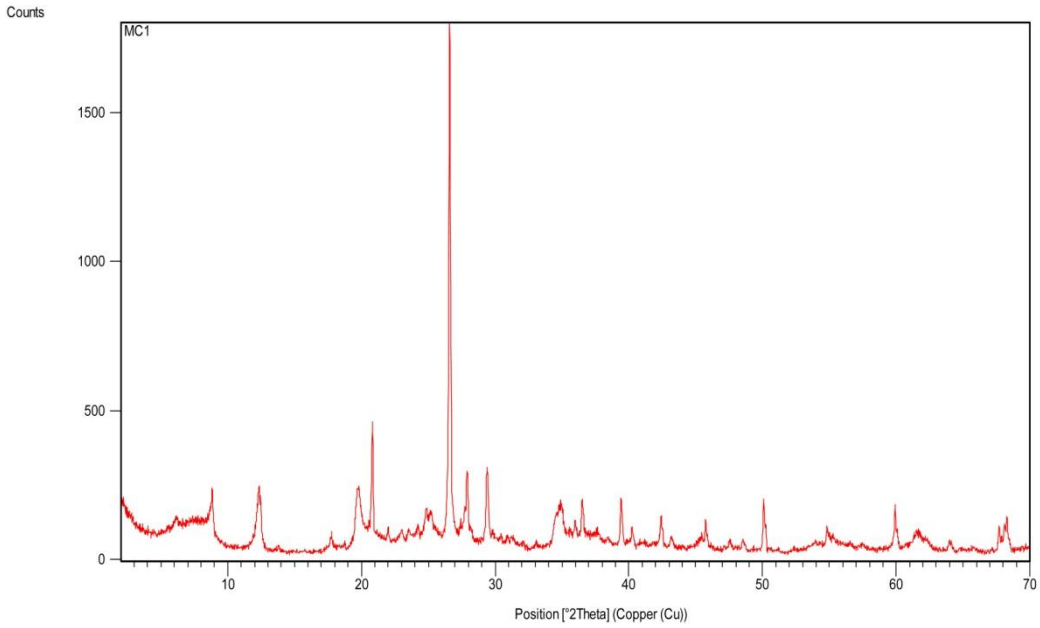

ORIENTED AGGREGATES

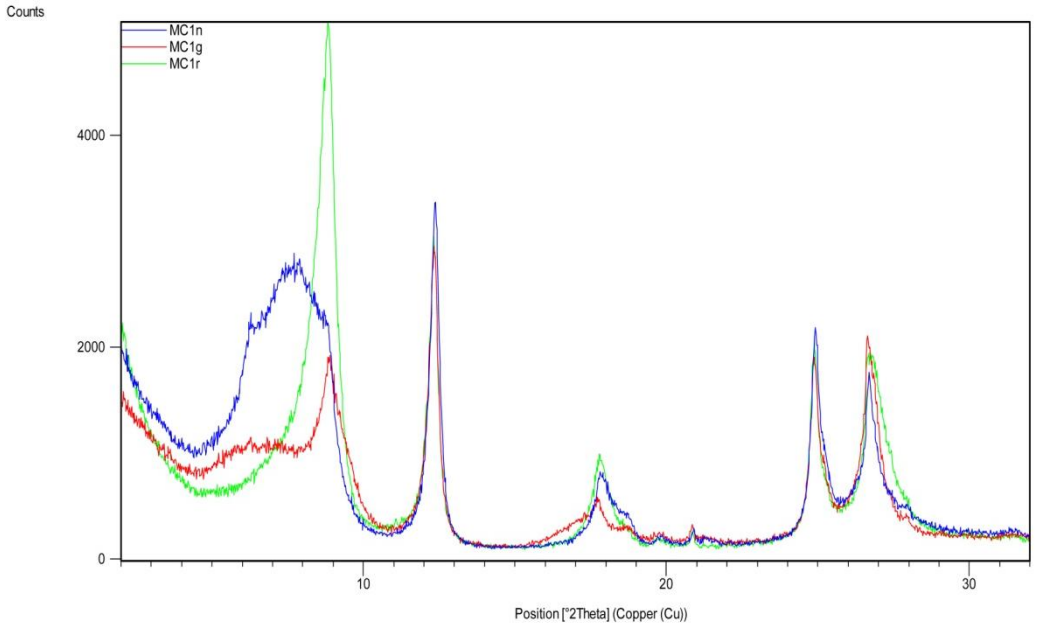

Mineralogy: mixed layer illite/smectite, mixed layer chlorite/smectite, chlorite, kaolinite, muscovite, Na-feldspar, K-feldspar, quartz, calcite, dolomite.

MC2

BULK SAMPLE

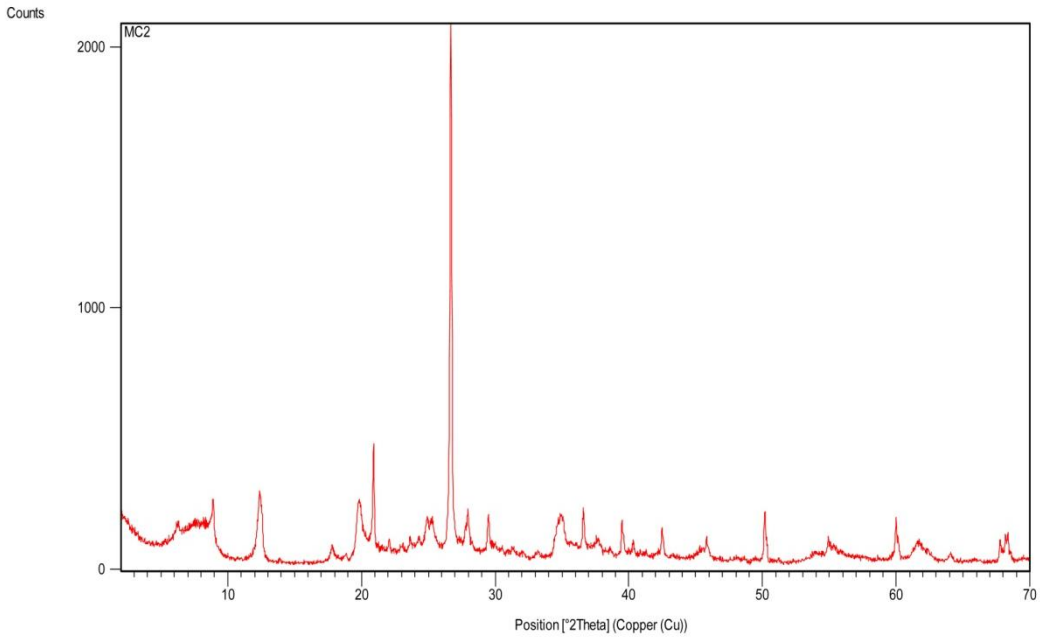

ORIENTED AGGREGATES

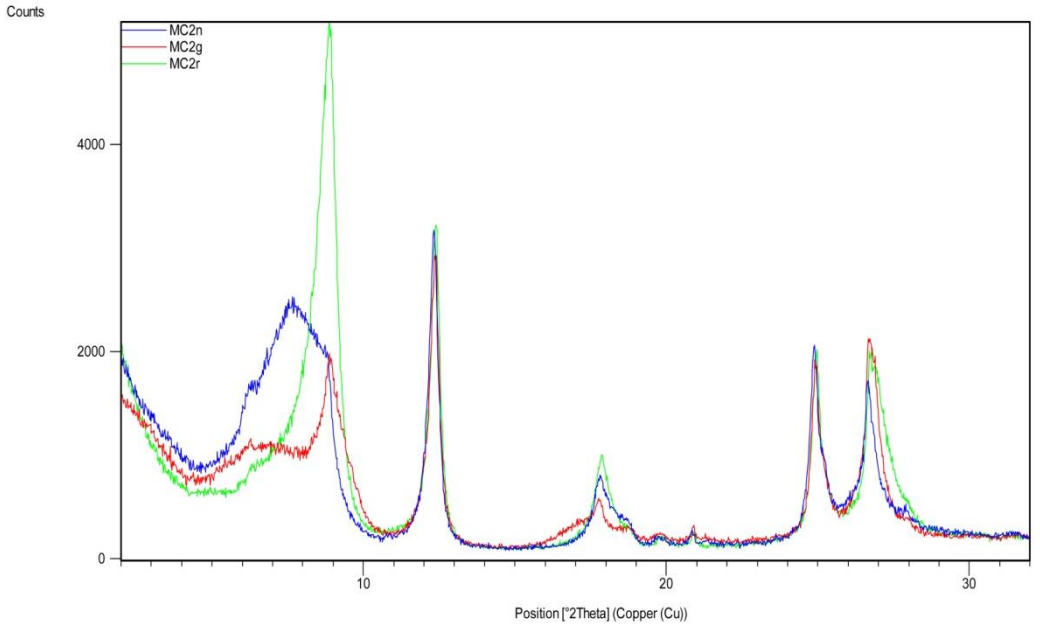

Mineralogy: mixed layer illite/smectite, mixed layer chlorite/smectite, chlorite, kaolinite, muscovite, Na-feldspar, K-feldspar, quartz, calcite, dolomite.

MC3

BULK SAMPLE

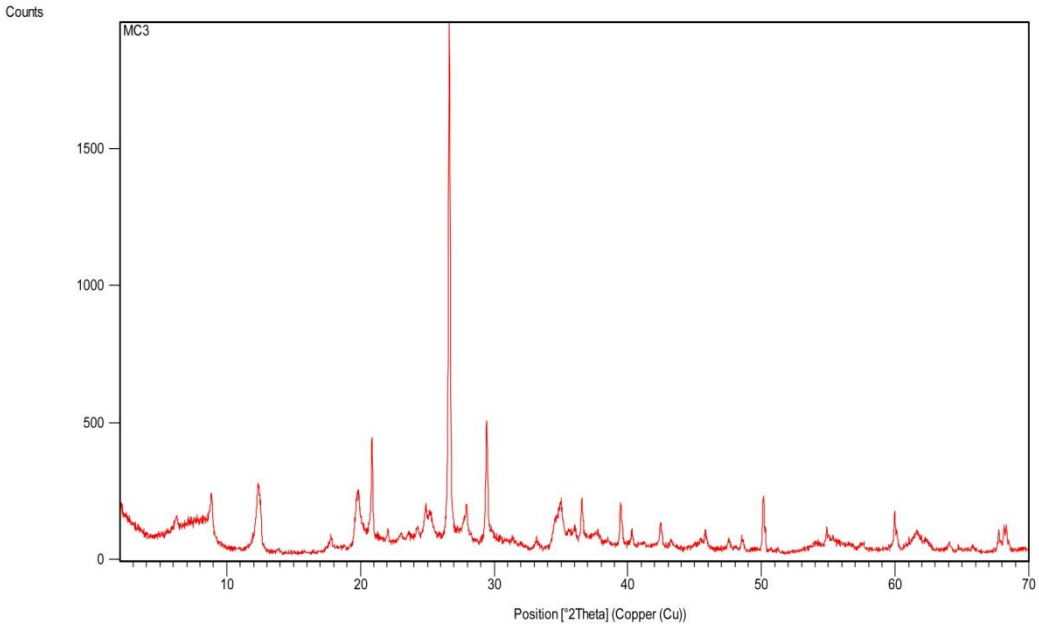

ORIENTED AGGREGATES

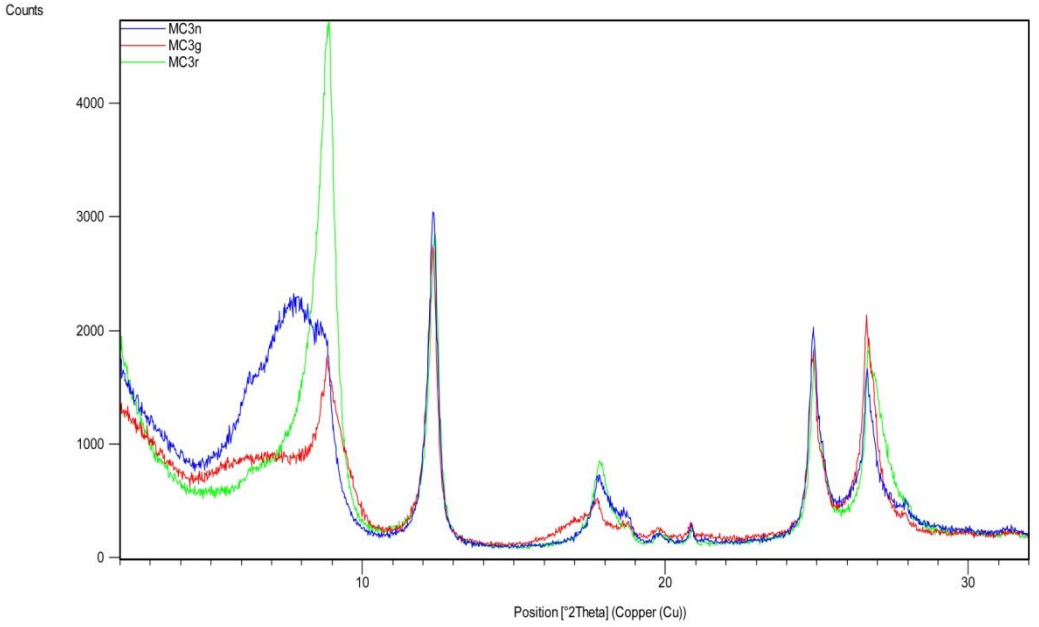

Mineralogy: mixed layer illite/smectite, mixed layer chlorite/smectite, chlorite, kaolinite, muscovite, Na-feldspar, K-feldspar, quartz, calcite, dolomite.

MC4

BULK SAMPLE

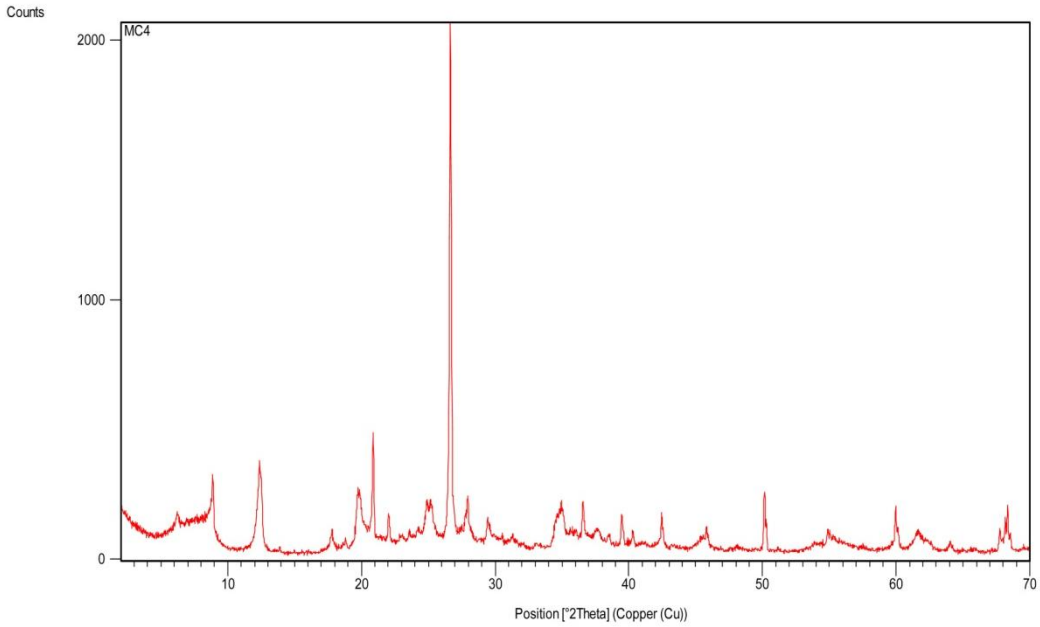

ORIENTED AGGREGATES

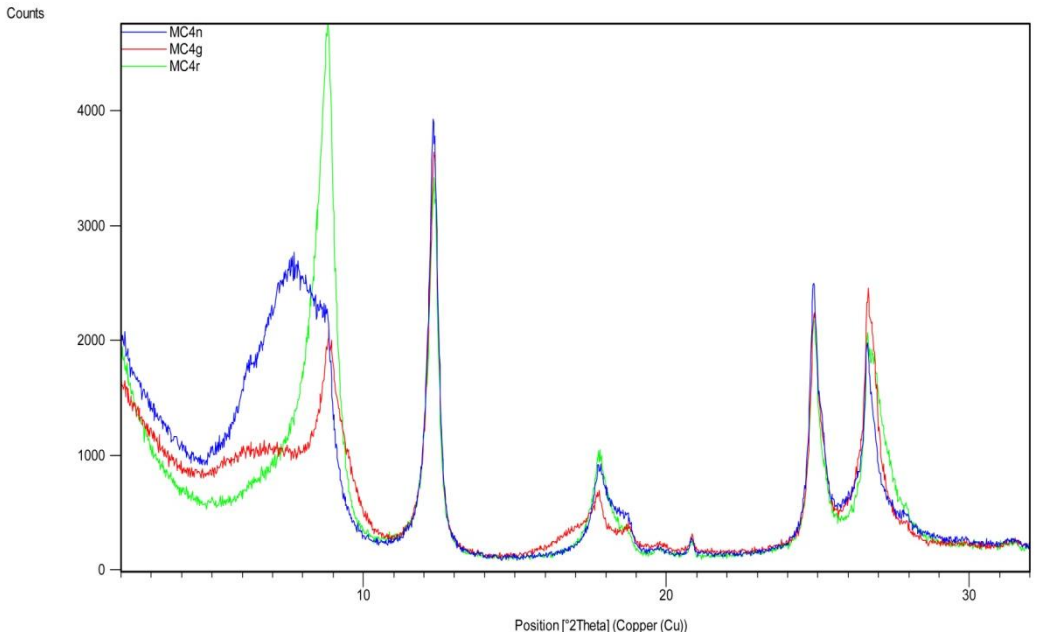

Mineralogy: mixed layer illite/smectite, mixed layer chlorite/smectite, chlorite, kaolinite, muscovite, Na-feldspar, K-feldspar, quartz, calcite, dolomite.

MC5

BULK SAMPLE

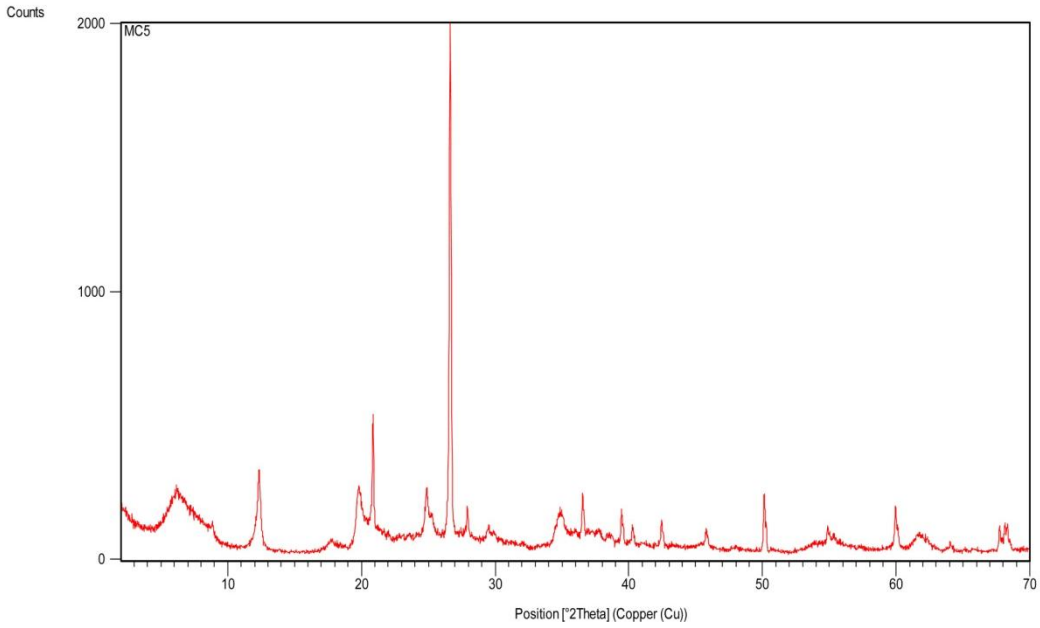

ORIENTED AGGREGATES

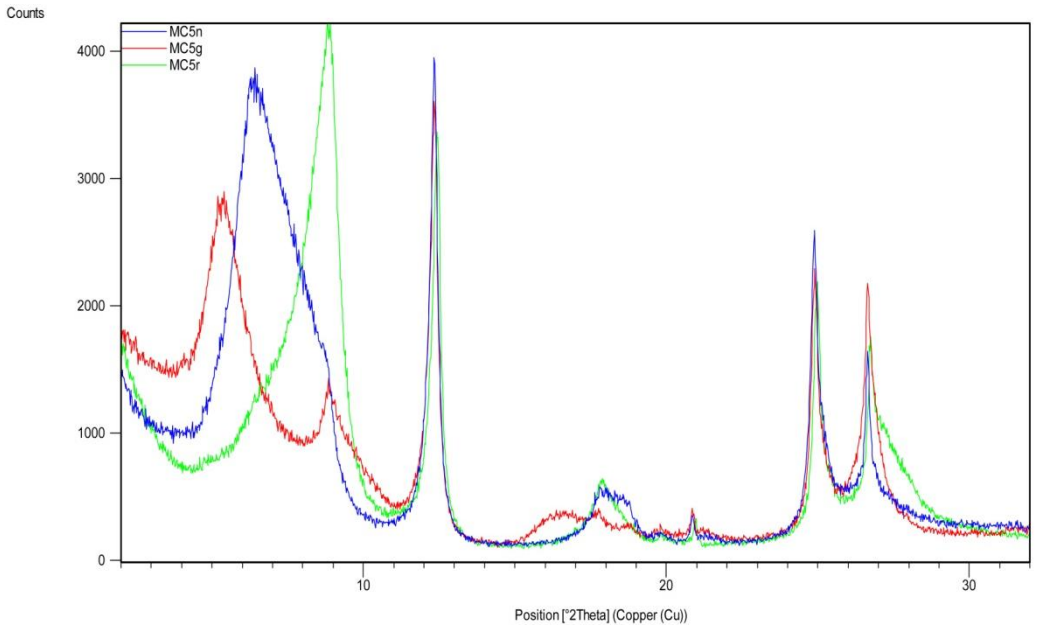

Mineralogy: mixed layer illite/smectite, mixed layer chlorite/smectite, chlorite, kaolinite, muscovite, Na-feldspar, K-feldspar, quartz, calcite, dolomite.

MC6

BULK SAMPLE

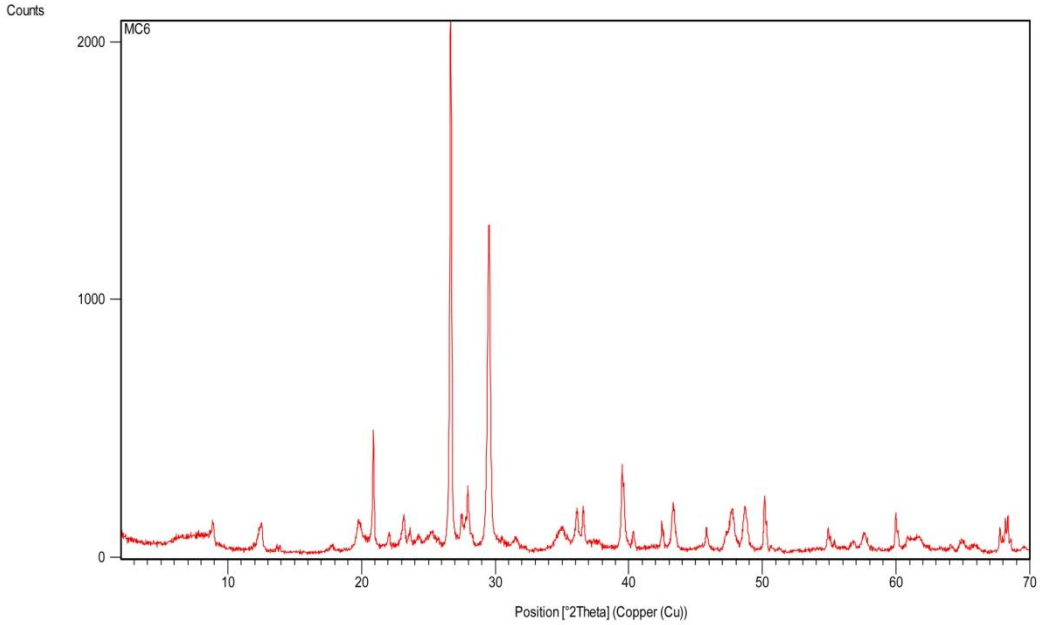

ORIENTED AGGREGATES

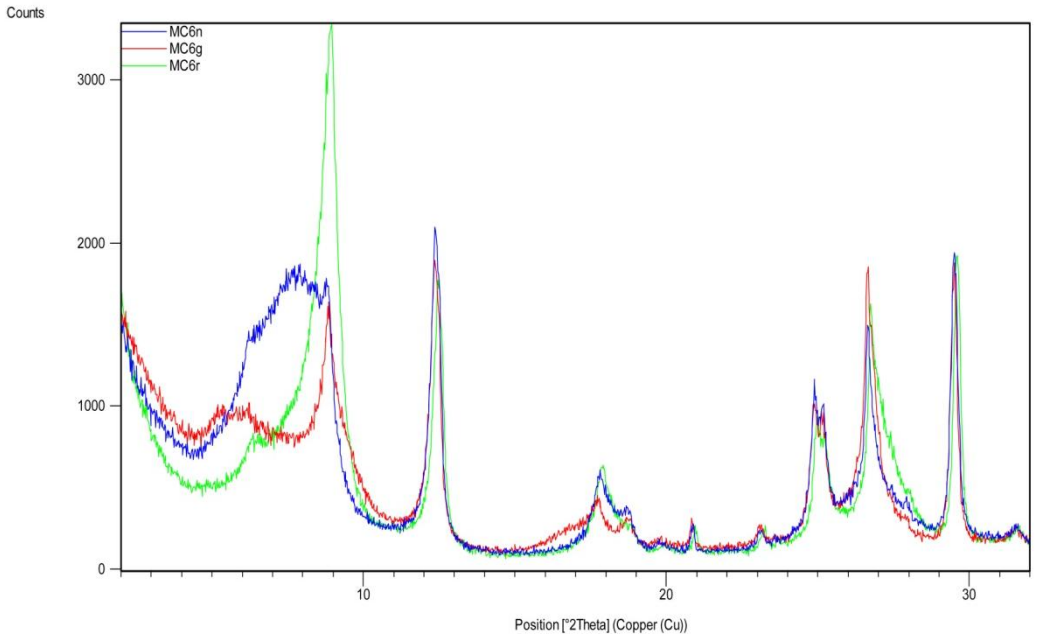

Mineralogy: mixed layer illite/smectite, chlorite, kaolinite, muscovite, Na-feldspar, K-feldspar, quartz, calcite, dolomite.

MC7

BULK SAMPLE

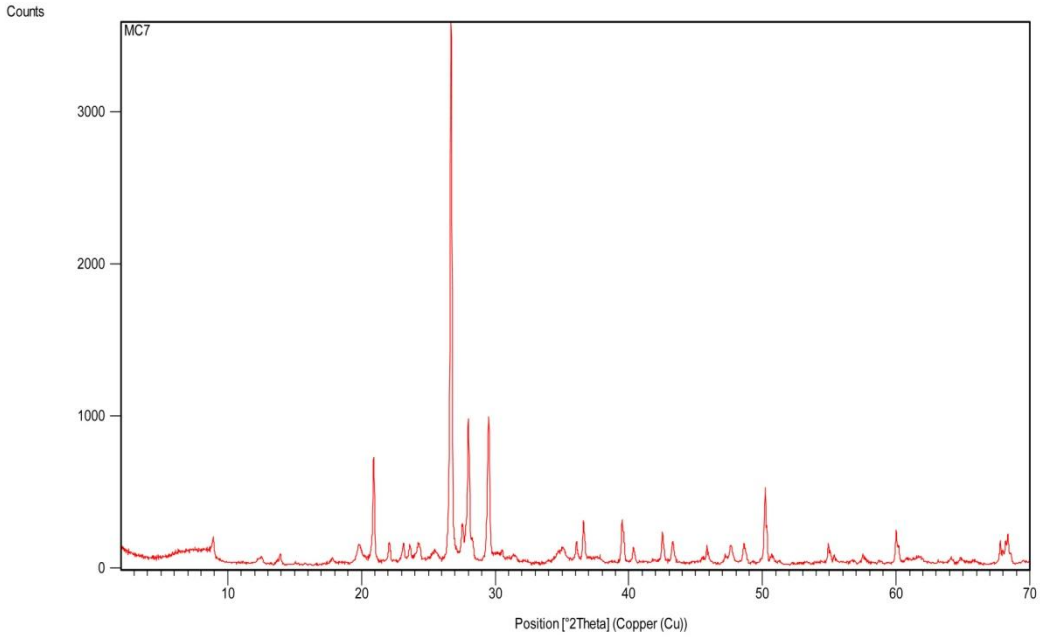

ORIENTED AGGREGATES

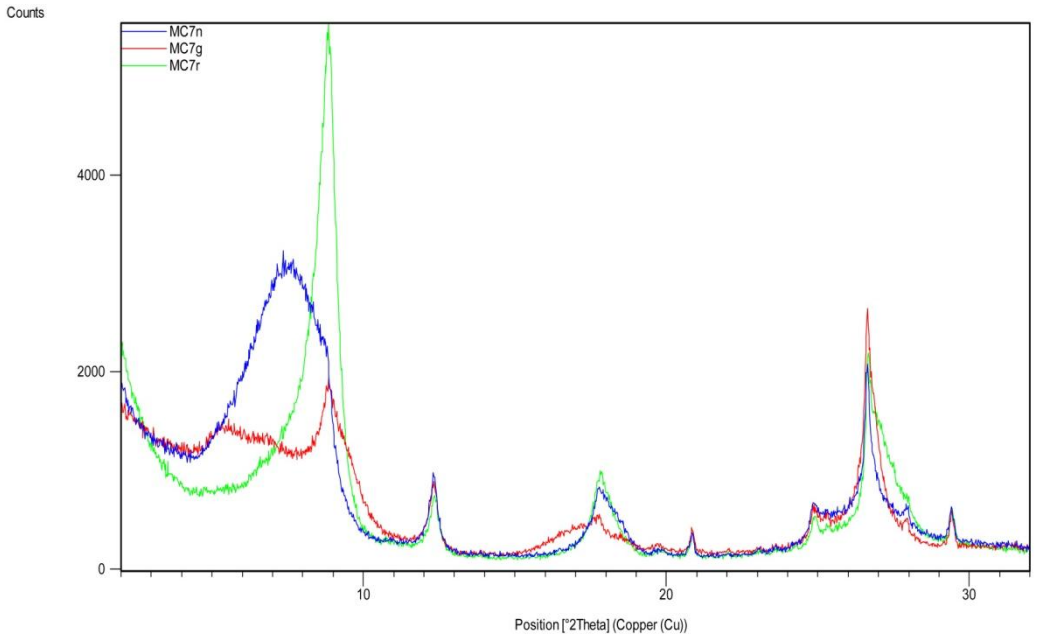

Mineralogy: mixed layer illite/smectite, mixed layer chlorite/smectite, chlorite, kaolinite, muscovite, Na-feldspar, K-feldspar, quartz, calcite, dolomite.

MC8

BULK SAMPLE

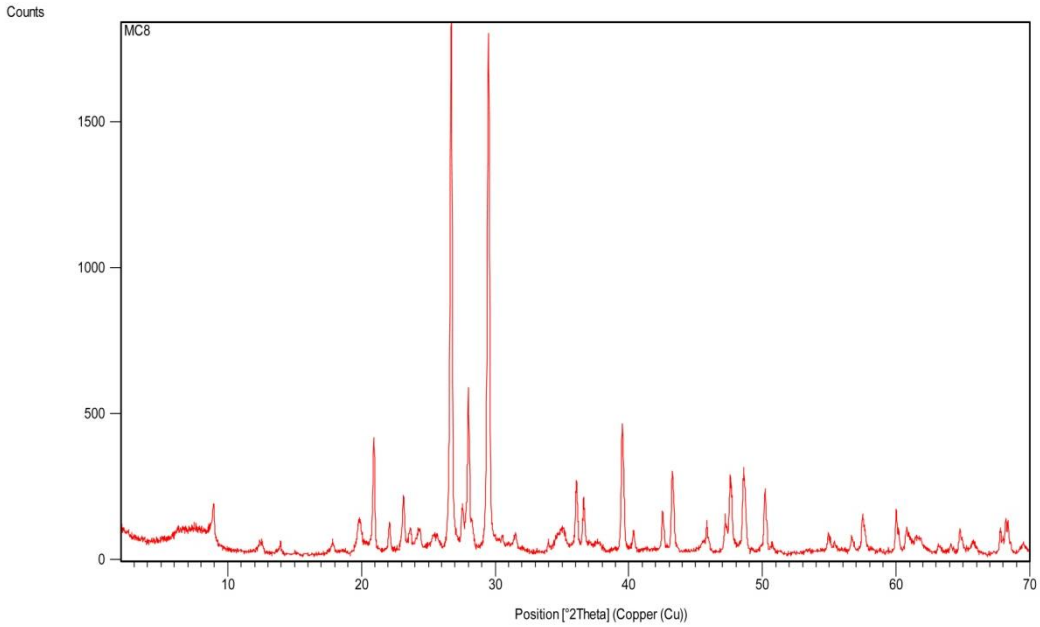

ORIENTED AGGREGATES

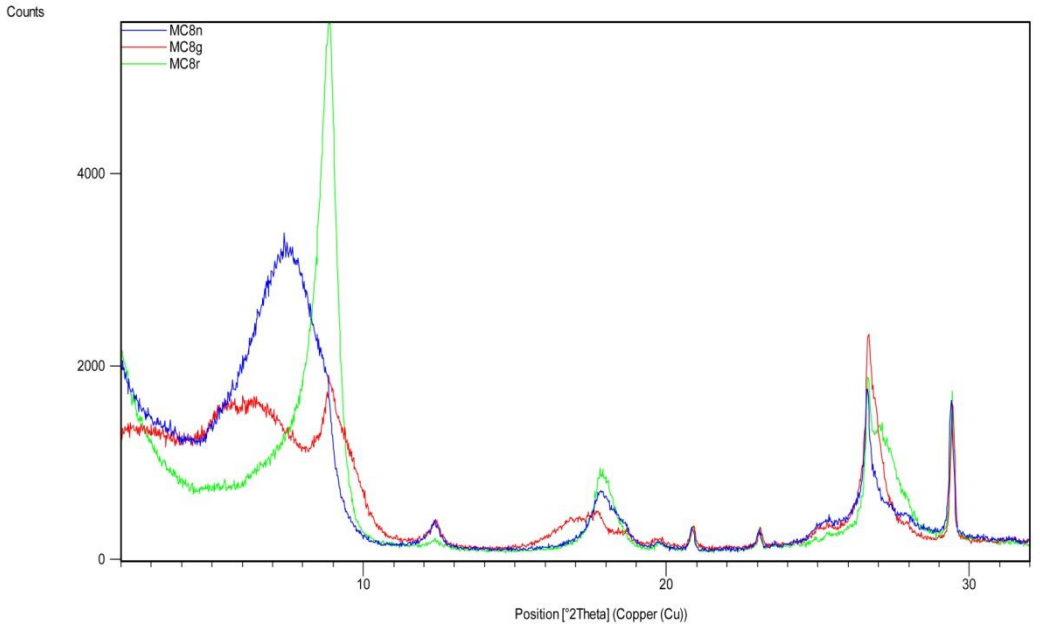

Mineralogy: mixed layer illite/smectite, mixed layer chlorite/smectite, chlorite, muscovite, Na-feldspar, K-feldspar, quartz, calcite, dolomite.

MC9

BULK SAMPLE

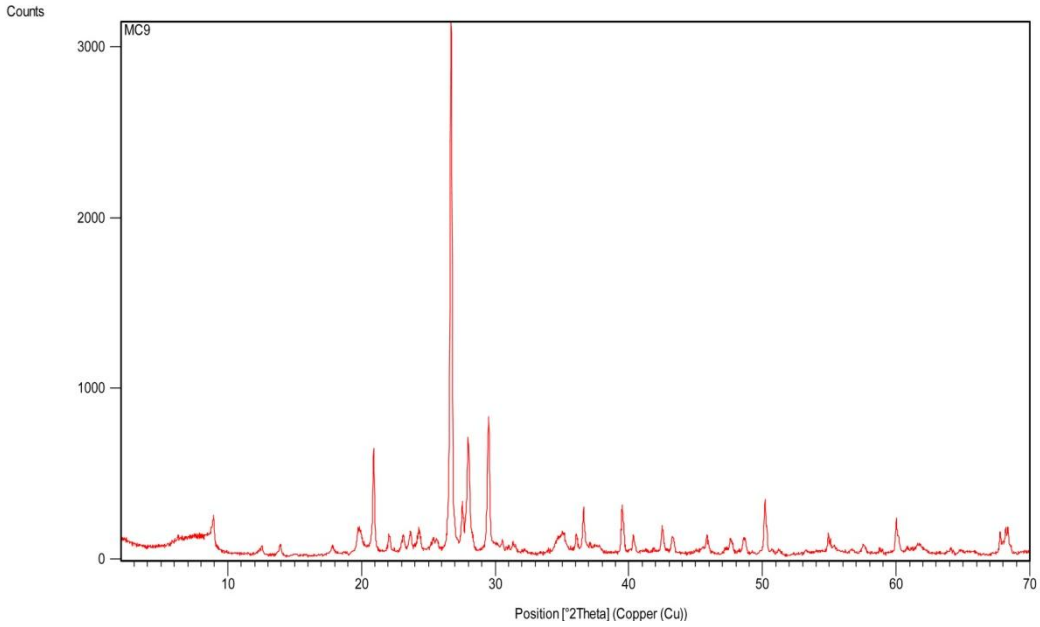

ORIENTED AGGREGATES

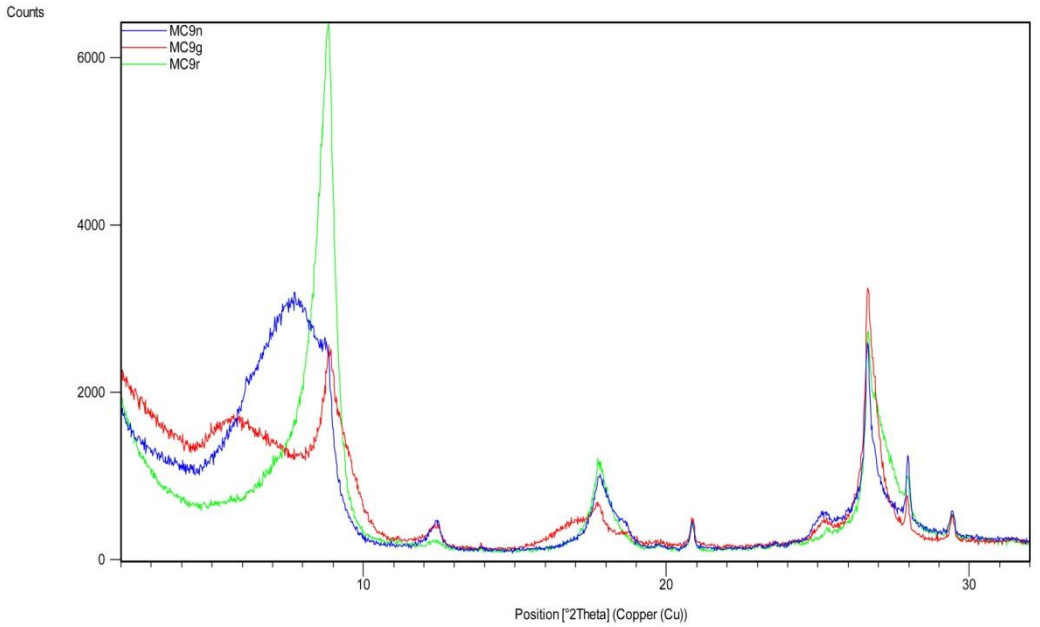

Mineralogy: mixed layer illite/smectite, mixed layer chlorite/smectite, chlorite, muscovite, Na-feldspar, K-feldspar, quartz, calcite, dolomite.

MC10

BULK SAMPLE

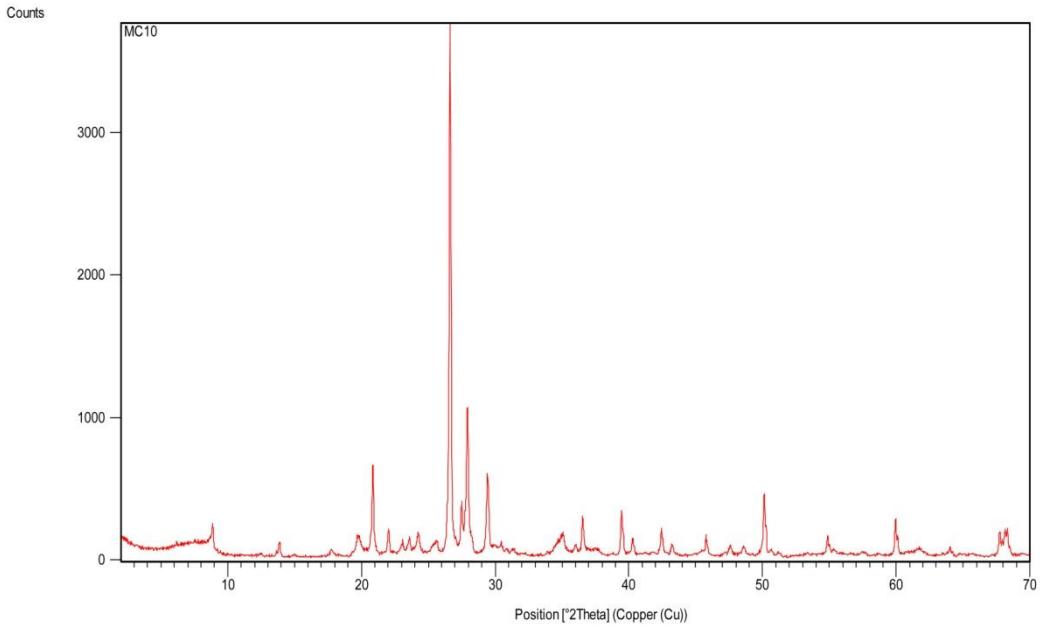

ORIENTED AGGREGATES

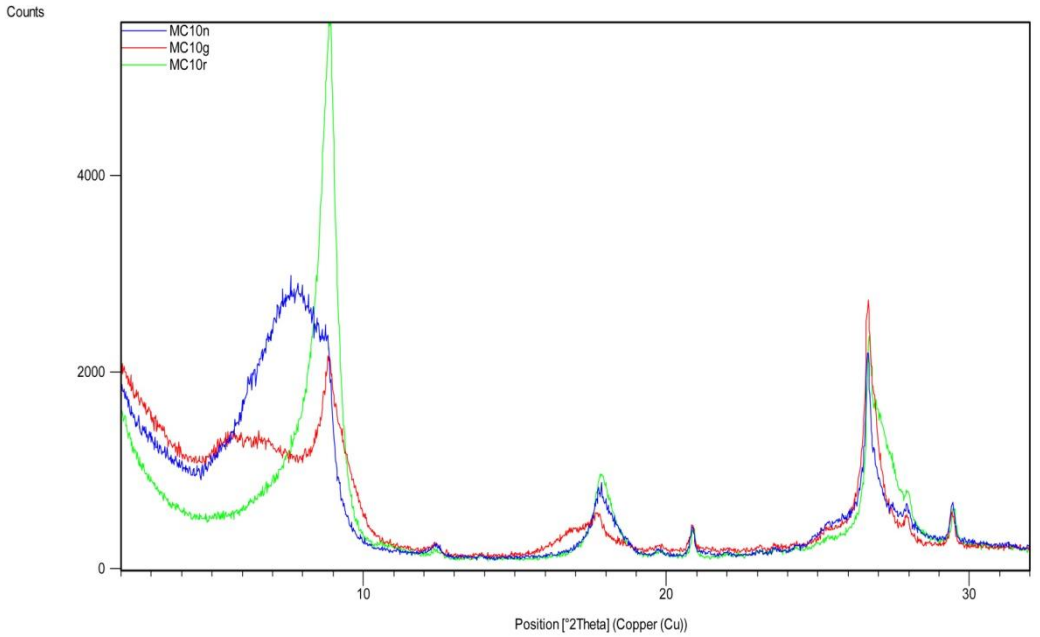

Mineralogy: mixed layer illite/smectite, mixed layer chlorite/smectite, chlorite, muscovite, Na-feldspar, K-feldspar, quartz, calcite, dolomite.

MC11

BULK SAMPLE

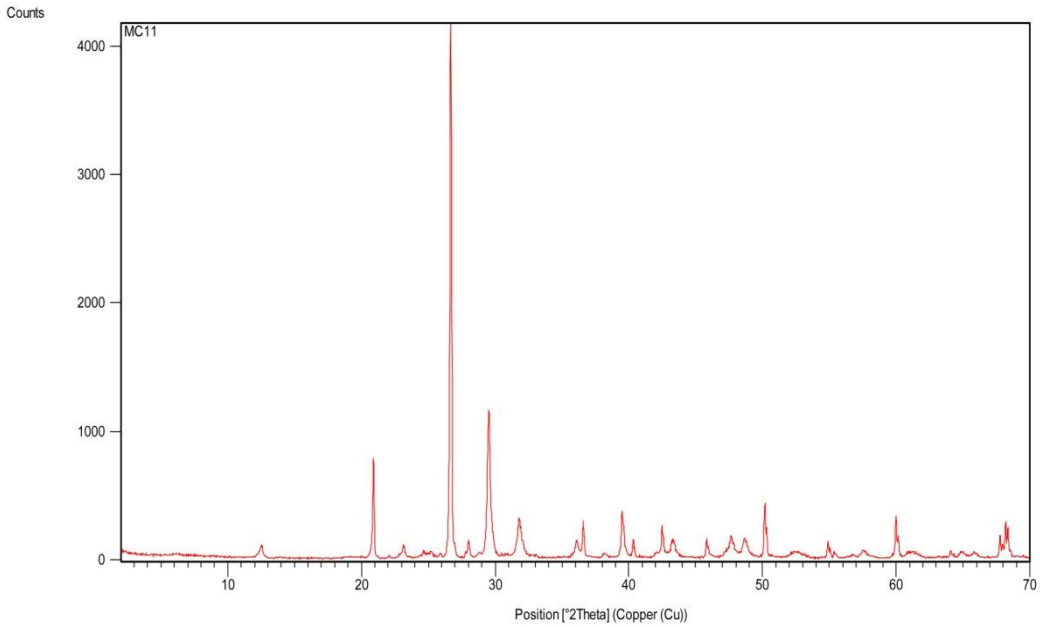

Mineralogy: mixed layer illite/smectite, chlorite, kaolinite, muscovite, Na feldspar, K-feldspar, quartz, calcite, dolomite.

MC12

BULK SAMPLE

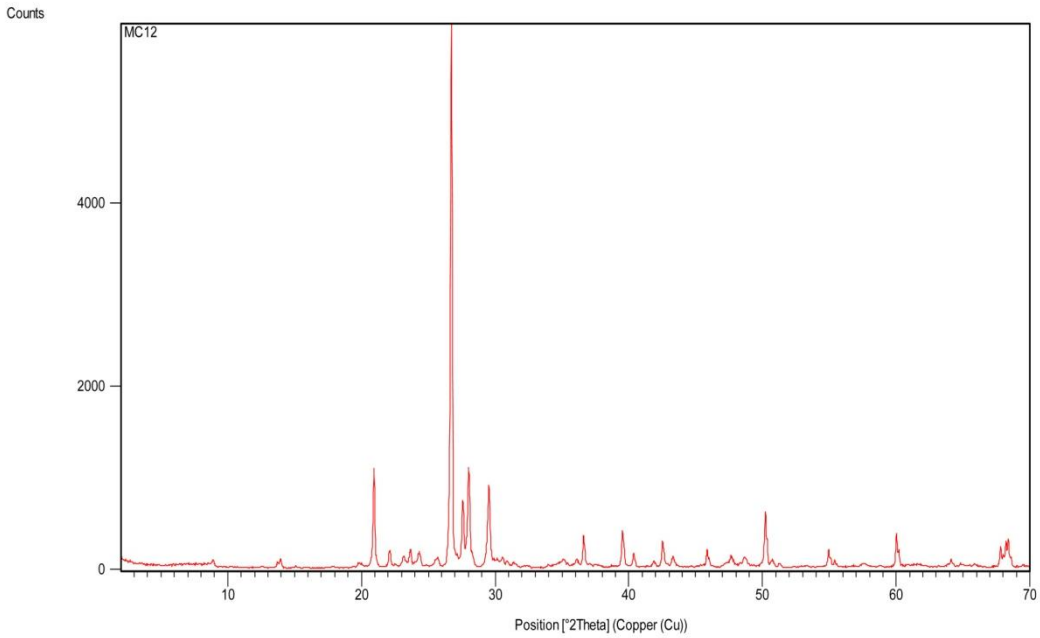

Mineralogy: mixed layer illite/smectite, chlorite, kaolinite, muscovite, Na-feldspar, K-feldspar, quartz, calcite, dolomite.

MC13

BULK SAMPLE

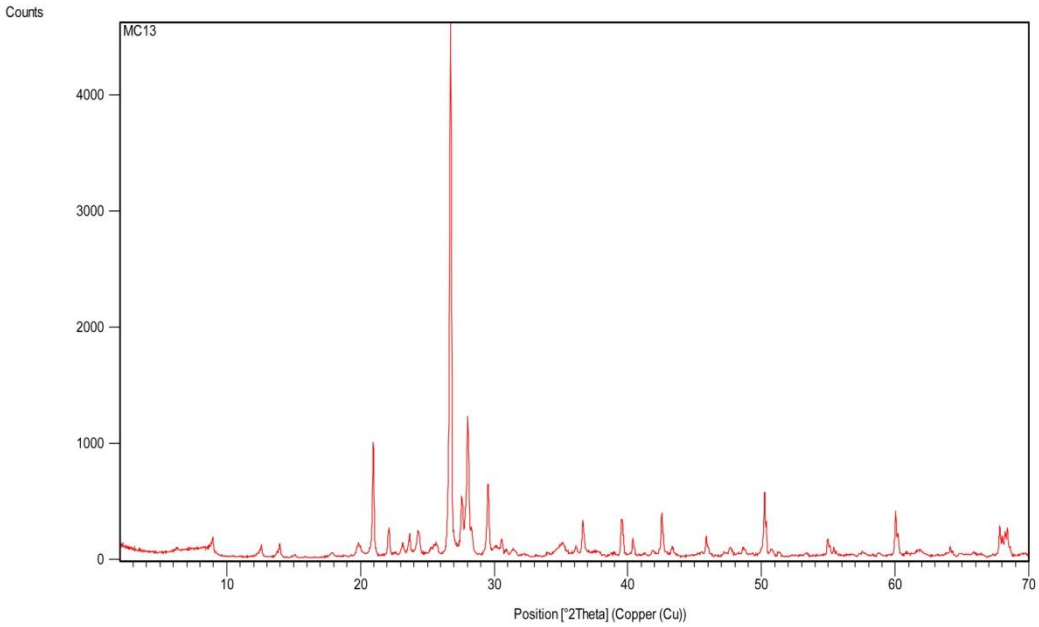

ORIENTED AGGREGATES

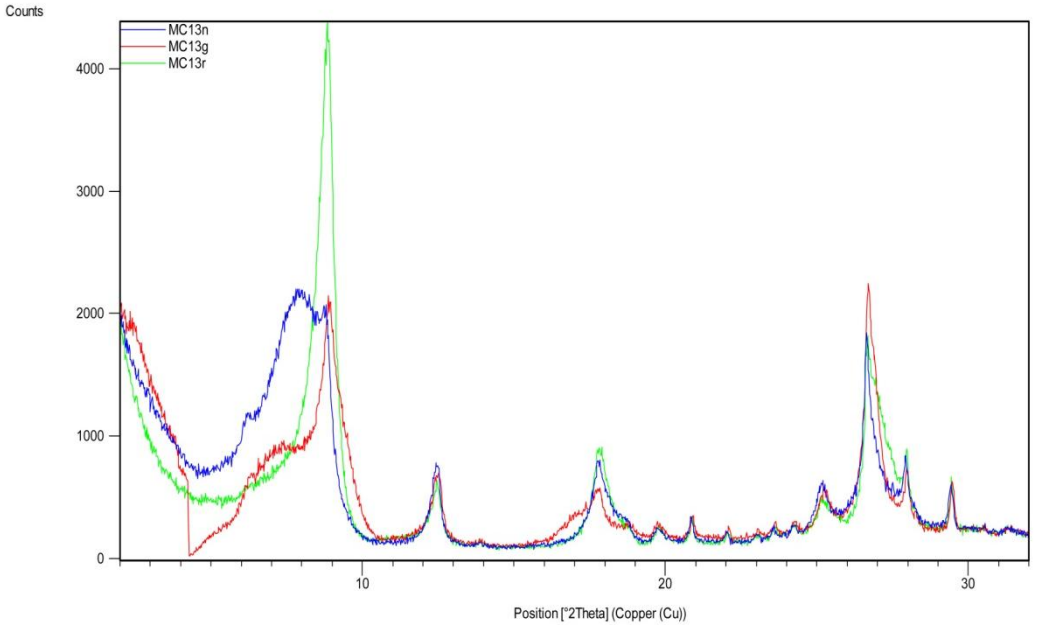

Mineralogy: mixed layer illite/smectite, mixed layer chlorite/smectite, chlorite, kaolinite, muscovite, Na feldspar, K-feldspar, quartz, calcite, dolomite.

MC14

BULK SAMPLE

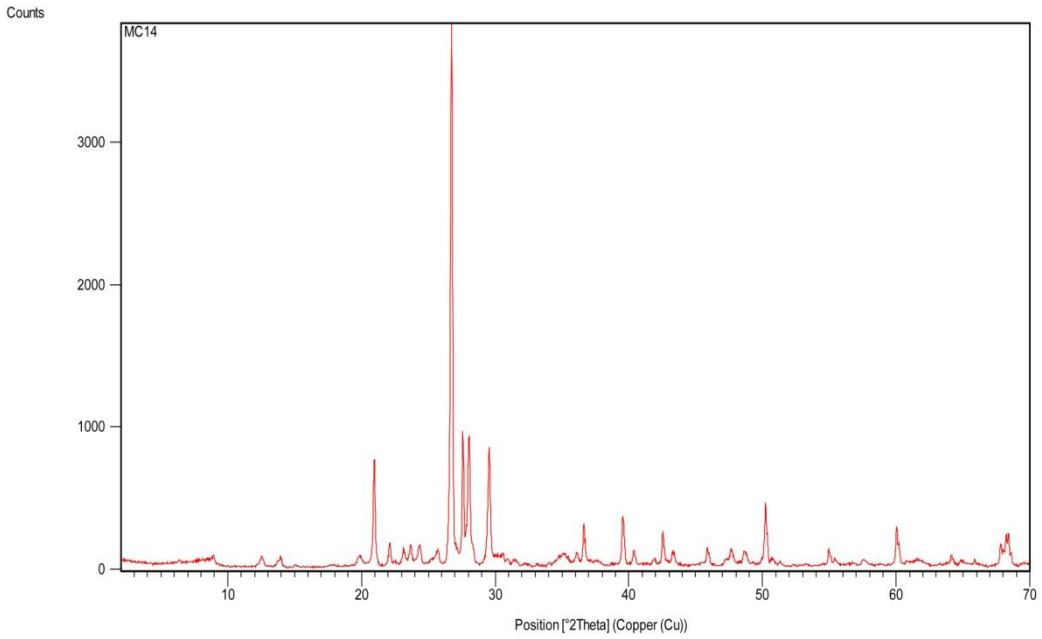

Mineralogy: mixed layer illite/smectite, chlorite, kaolinite, muscovite, Na feldspar, K-feldspar, quartz, calcite, dolomite.